SHRP-H-672

Development of Ground-Penetrating Radar Equipment for Detecting Pavement Condition for Preventive Maintenance

Stanley S. Smith
Geophysical Survey Systems, Inc.
North Salem, New Hampshire 0373

Thomas Scullion
Texas Transportation Institute
College Station, Texas 77843

Strategic Highway Research Program
National Research Council
Washington, DC 1993

SHRP–H-672
Contract H-104A
Product Code: 3018

Program Manager: *Don M. Harriott*
Project Manager: *Brian Cox*
Production Editor: *Marsha Barrett*
Program Area Secretary: *Francine Burgess*

October 1993

key words:
GPR
ground penetrating radar (GPR)
nondestructive technology

Strategic Highway Research Program
National Academy of Sciences
2101 Constitution Avenue N.W.
Washington, DC 20418

(202) 334-3774

350/NAP/1093

Acknowledgments

The research described herein was supported by the Strategic Highway Research Program (SHRP). SHRP is a unit of the National Research Council that was authorized by section 128 of the Surface Transportation and Uniform Relocation Assistance Act of 1987.

The authors would like to thank the group of individuals whose efforts made this research possible. Our gratitude is extended to the supporting staff at Geophysical Survey Systems, Inc. and Texas Transportation Institute.

The Engineering staff and Production personnel worked many long, hard hours to produce the equipment used in this research within an extremely limited timeframe. Special thanks should be extended to engineers Leo Galvinovsky, Jim Godfrey, Jack Howley, Rick Moreau and John Rudy.

John Ragsdale, Chun Lok Lau and Yiqing Chen of TTI assisted in all phases of data collection and processing.

Rex Morey of Morey Research acted as a consultant on the antenna development and the computer modellings. All his efforts are appreciated; as are those of Jim Tovey, contract engineer for the antenna trailer.

The diligent performance of the SHRP staff should be acknowledged. Brian Cox was the project manager. Don Harriott and Shashikant Shah were always supportive.

The ETG provided an essential perspective to the application of this technology to highway maintenance problems. Mike Markow and Ken Maser were consultants to SHRP. Mike Markow kept the project focused on providing useful solutions to pavement defect location, not just extending the state of the art of GPR. Ken Maser's experience and advice provided valuable technological assistance.

Kirsten Vargas assisted in completing the reports throughout this project.

Finally, all the efforts of Texas DOT and Georgia DOT in aiding us to conduct field tests are acknowledged. Special thanks to Wouter Gulden of the Georgia DOT and Sally Wegmann of the Houston Residency.

Contents

Acknowledgments iii

List of Figures vii

List of Tables xi

Abstract 1

Executive Summary 3

1 **Introduction** 5
- 1.1 Problem Statement 5
- 1.2 Research Approach 6
- 1.3 Criteria for Detecting Pavement Problems 8
- 1.4 Proposed Operational Constraints 9

2 **Ground-Penetrating Radar Theory** 13
- 2.1 Basic GPR Theory 13
- 2.2 Layer Thickness Determination 17
- 2.3 Void Detection 20
- 2.4 Moisture Content Assessment 20

3 **Prediction of Radar Response to Pavement Condition** 25
- 3.1 Modeling 25
- 3.2 Moisture in Asphalt 28
- 3.3 Moisture in Base Layer 33
- 3.4 Voids under Concrete Slab 39
- 3.5 Overlay Delaminations 46

4 **Equipment Description** 57
- 4.1 1.0- and 2.5-GHz Antennas 57
- 4.2 Digital Acquisition System 58

5 **Equipment Development** 59
5.1 Breadboard System 59
5.2 First-Generation Prototype 62
5.3 Second-Generation Prototype 65
6 **Interpretation Software Development** 71
6.1 Forward Modeling 71
6.2 Neural Network Applications 80
6.3 Signal-Processing System 98

7 **Laboratory and Field Test Program** 105
7.1 Specifications Testing 105
7.2 Laboratory Test 110
7.3 Pilot Scale Field Test Results 119

8 **Field Tests** 124
8.1 Plan 124
8.2 Site-Selection Plan 124
8.3 Testing Sequence 129
8.4 Observations during Testing 129

9 **Results of Field Tests** 135
9.1 Neural Network Results 135
9.2 TTI Software Results 147

10 **Conclusions and Recommendations** 169
10.1 Conclusions 169
10.2 Recommendations for Future Research 170
10.3 Recommendations for Implementation in State DOTs 171

Appendix: Software Development 173

References 176

List of Figures

2.1. Reflections off the interfaces in pavement section 14
2.2. Radar scan that results from pavement section in figure 2.1 15
2.3. Effect of a void on radar trace. 20
3.1. Plots of the real and imaginary parts of the dielectric constant versus the moisture content of asphalt 27
3.2. Synthetic radar scan from an asphalt pavement with a base moisture content of 0%. 29
3.3. Synthetic radar scan from an asphalt pavement with a base moisture content of 1%. 30
3.4. Synthetic radar scan from an asphalt pavement with a base moisture content of 4%. 31
3.5. Synthetic radar scan from an asphalt pavement with a base moisture content of 8%. 32
3.6. Synthetic radar scan from a concrete pavement with a base moisture content of 8%. 34
3.7. Synthetic radar scan from a concrete pavement with a base moisture content of 10%. 35
3.8. Synthetic radar scan from a concrete pavement with a base moisture content of 14%. 36
3.9. Synthetic radar scan from a concrete pavement with a base moisture content of 22%. 37
3.10. Plot of the reflection coefficient of the concrete-base interface versus the moisture content of the base layer. 38
3.11. Reflection at the concrete-base interface with no void introduced. 40
3.12. Reflection at the concrete-base interface with a 0.1-cm void introduced. 41
3.13. Reflection at the concrete-base interface with a 0.2-cm void introduced. 42
3.14. Reflection at the concrete-base interface with a 0.6-cm void introduced. 43
3.15. Reflection at the concrete-base interface with a 2-cm void introduced. 44
3.16. Plot of the reflection coefficient of the concrete-base interface versus the air void thickness. 45
3.17. Reflection due to an air-filled delamination in asphalt—gap thickness, 0.1 cm. 47
3.18. Reflection due to an air-filled delamination in asphalt—gap thickness, 0.2 cm. 48

3.19. Reflection due to an air-filled delamination in asphalt—gap thickness, 0.6 cm. . . . 49
3.20. Reflection due to an air-filled delamination in asphalt—gap thickness, 2 cm. . . . 50
3.21. Plot of the reflection coefficient due to a air-filled delamination in asphalt versus the gap thickness . . . 51
3.22. Reflection due to an water-filled delamination in asphalt—gap thickness, 0.02 cm . . . 52
3.23. Reflection due to an water-filled delamination in asphalt—gap thickness, 0.05 cm. . . . 53
3.24. Reflection due to an water-filled delamination in asphalt—gap thickness, 0.2 cm. . . . 54
3.25. Reflection due to an water-filled delamination in asphalt—gap thickness, 0.6 cm. . . . 55
3.26. Plot of the reflection coefficient due to a water-filled delamination in asphalt versus the gap thickness . . . 56
5.1. Block diagram of breadboard prototype . . . 61
5.2. Block diagram of first-generation prototype . . . 63
5.3. SIR-10 used to control the 1.0- and 2.5-GHz antennas and store the digital data for later analysis . . . 64
5.4. Antenna trailer carrying four sets of TEM horns. . . . 66
5.5. Block diagram of second-generation prototype . . . 67
6.1. Example of a radar scan acquired with the SIR-10 and the 2.5-GHz antennas . . . 73
6.2. Example of model data overlaying a measured radar scan for 25 cm of asphalt . . . 74
6.3. Example of model scan in which random noise and clutter have been added . . . 75
6.4. Simulated radar profile (1.0-GHz) for 15 cm of PCC pavement over three voids . . . 76
6.5. Neural network output showing the three voids (see figure 6.4) under 6 in. of pavement . . . 77
6.6. Simulated radar profile (2.5-GHz) for 15 cm of asphalt pavement over 15 cm of base material . . . 78
6.7. Neural network output for the input profile in figure 6.6 . . . 79
6.8. Block diagram of neural network processing . . . 80
6.9. Example of neural network architecture . . . 82
6.10. Original model data trace and resulting neural network input . . . 84
6.11. Model and real data for 15 cm thickness . . . 85
6.12. Model data for various pavement thicknesses . . . 86
6.13. Scans of 15 cm (6 in.) pavement thickness from 1.0- and 2.5-GHz antennas . . . 88
6.14. Real and model scans for 15 cm asphalt pavement thickness . . . 88
6.15. Model scans of 5 cm and 15 cm pavement thickness . . . 89
6.16. Clean and noisy data . . . 90
6.17. Superimposed clean and noisy data for a 1.3 cm void . . . 91
6.18. Air and water voids . . . 96

6.19. Hilbert transforms of scans with varying moisture content 96
6.20. Hilbert transforms of clean and noisy data—moisture content, 6% 97
6.21. Hilbert transforms of clean and noisy data—moisture content, 11% 97
6.22. Example of layer thickness calculation procedure. 99
6.23. Graphical display from TTI data-processing system 104
7.1. Metal plate reflection from 1.0 GHz antenna 108
7.2. Metal plate reflection from 2.5-GHz antenna 109
7.3. Air void study 111
7.4. Air void test results 112
7.5. Moisture-filled void study 113
7.6. Base moisture test results—granular base alone 116
7.7. Base moisture test results—asphalt slab over granular base 117
7.8. Base moisture test results—PCC slab over granular base 118
7.9. Ground-penetrating radar traces from asphalt control test sections 1 and 2 . . 121
7.10. Ground-penetrating radar traces from asphalt control test sections 3 and 4 . . 122
7.11 Ground-penetrating radar waveforms from concrete test slab 123
8.1. Riverwatch Parkway, Georgia—moisture seeping through construction joint . 126
8.2. FM 2920, Tomball, Texas—moisture seeping through surface crack 127
8.3. IH 20, Near Augusta, Georgia 128
8.4. GSSI trailer with 1.0-GHz and 2.5-GHz antennas 131
8.5. Dry augering of base samples 132
8.6. Drilling dry hole for epoxy core test 133
9.1. Asphalt thickness of IH 45 138
9.2. Pavement thickness of IH 45 138
9.3. Severity of stripping on IH 45 138
9.4. Sample laboratory and field traces 139
9.5. Pavement thickness of Riverwatch Parkway 144
9.6. Moisture content of Riverwatch Parkway 144
9.7. Neural network results from a section of Georgia IH 20, Georgia 146
9.8. Ground-penetrating radar traces from U.S. 41, Georgia 148
9.9. U.S. 41, Georgia 149
9.10. Extracted core—macadam layer at bottom of core 149
9.11. Radar trace and ground truth core 8, which contains no stripping 151
9.12 Radar trace and ground truth core 5, which contains a stripped layer 152
9.13. Radar trace and ground truth core 4, which contains stripping 153
9.14. Radar trace and ground truth core 3, which contains stripping 154
9.15. Radar trace and ground truth core 1, which contains stripping 155
9.16. Ground-penetrating radar traces (1.0-GHz) from Riverwatch Parkway, Georgia 157
9.17. Extracted core hole 6 from Riverwatch Parkway, Georgia 158
9.18. IH 20, near Augusta, Georgia—jointed concrete pavement suspected of having voids and trapped moisture at joints 162
9.19. GSSI 1.0-GHz reflected waveform from IH 20 Georgia—moisture-filled void location 163
9.20. GSSI 1.0-GHz reflected waveform from IH 20, Georgia—no-void location . 164
9.21 Core taken from IH 20, Georgia, after epoxy core test. 165

9.22. Amplitude of reflection from beneath the slab for eight joints on IH 20, Georgia. 166
9.23. Color-coded display of ground-penetrating radar data collected on IH 20, Georgia 167

List of Tables

2.1 Effect of Changes in Pavement Maintenance Condition on Radar Signal 16
2.2 Measured Dielectric Constants of Pavement-Related Materials 19
5.1 System Performance Comparison between the SIR-10 and the New SIR-10A. 68
6.1 Results from Neural Network Trained on Model Thickness Data 87
6.2 Output File for Neural Network Trained to Detect Voids 92
6.3 Output File for Neural Network Trained to Detect Moisture Content 93
6.4 Neural Network Output with Both Thickness and Moisture Content Varying . . 94
6.5 Neural Network Output Identifying Air and Moisture Voids 95
7.1 Results of Specification Test of the Second-Generation Prototype 107
7.2 Results from Signal Processing of Base Moisture Test Results 115
7.3 Results of TTI Software on Test Section with Varying Asphalt Thickness 120
7.4 Results of TTI Software on Test Section with Asphalt Stripping 120
9.1 Radar Files Used for Neural Network 136
9.2 Output from Trained Neural Network 136
9.3 Files Used for Neural Network 140
9.4 Sample Output of Texas Network 141
9.5 Files Used for Training and Testing Georgia Neural Network 141
9.6 Sample Output of Trained Neural Network 142
9.7 Results from Combined Neural Network 143
9.8 Results of IH 20 Void Testing 145

9.9 Typical Results from Seven Core Holes 156
9.10 Typical Results for Six Core Holes 161

Abstract

This report documents the development of a ground-penetrating radar (GPR) system for locating potential maintenance problems in highway pavements. We developed the system to identify sections of pavement with conditions, such as voids, that could be effectively treated with maintenance measures.

The report illustrates how GPR has the potential to detect four defects in pavements:

1. Stripping in an asphalt layer
2. Moisture in base layer
3. Voids or loss of support under rigid pavements
4. Overlay delamination

We designed, fabricated, and tested two generations of prototype systems in the development cycles of our research. This process produced a GPR system that could acquire radar signals with higher resolution than previously possible and interpret the data by automatic signal-processing techniques. We tested the complete prototype GPR in the laboratory on specially constructed test blocks with simulated pavement defects. We then tested in-service pavements in Texas and Georgia.

The report describes the results of tests on the second-generation prototype and the correlation between the radar results and ground truth. Finally, the report presents recommendations for further testing and development together with recommendations for incorporating a GPR system into typical pavement maintenance and rehabilitation operations.

Executive Summary

Billions of dollars are spent annually in the United States to maintain and rehabilitate the highway system. If problems are detected early, appropriate maintenance can be applied rather than the more expensive rehabilitation or reconstruction. Currently, there are few, if any, test procedures to help engineers answer the key questions they face daily, which include the following:

1. Given early detection of a localized problem (for example, debonding), how widespread is that condition throughout the project?
2. How effective was the maintenance treatment?
3. Do voids exist beneath the slab?
4. Is the asphalt layer sound, or is stripping present?

Strategic Highway Research Program Project H-104A, "Fabrication and Testing of Maintenance Measuring Equipment," is focused on evaluating whether ground-penetrating radar (GPR) can be used as a network or project-level tool for assisting with maintenance.

This final report on the development efforts of the study illustrates our approach to using GPR to detect pavements problems while they can still be treated by preventive maintenance. The research team identified the quantitative changes in pavements associated with some of the distresses of interest to the maintenance engineer. The first effort was to identify the conditions to which the radar would be most sensitive. The best results were obtained in the laboratory and on the pilot scale. The system appeared capable of detecting moisture in the base and both air-filled and moisture-filled voids. The results from field testing on in-service pavements were mixed. Moisture-filled voids were detected in Georgia. The pavement sections selected for measurements of moisture in the base showed no significant differences between the GPR data and ground truth testing, even though water was observed around localized cracks in the surface. More work is needed on detecting both stripping and overlay delaminations. The 1.0-GHz system could accurately measure both surface and base thicknesses. More work was needed to improve the quality of the signal from the 2.5-GHz system; the return signal contains significant clutter.

Once the conditions of interest were defined, computer modeling was performed. The research team used computer-generated radar waveforms to illustrate the effect of the

variation in the pavement condition. From this analysis we concluded that GPR has the potential to help in identifying many problems.

This report describes the development of a dual antenna system featuring both 1.0- and 2.5-GHz air-launched horn antennas. This system can be used at close to highway speed with the antenna suspended about 30 cm (12 in.) above the pavement. The GPR system captures waveforms reflected from the pavement layer interfaces and discontinuities. The system is capable of collecting waveforms at speeds up to 80 kph (50 mph); this provides a measurement up to every 20 cm (8 in.) along the pavement. Post processing of these waveforms is achieved by using of automatic-interpretation signal- processing algorithms.

The ability of the newly developed equipment to identify problems early has been evaluated in a series of laboratory, pilot-scale and full-scale tests in Texas and Georgia.

The overall performance of the system was good, and the system showed potential for providing useful information to the maintenance engineer. The analysis of the data showed that the system could detect the degree of stripping in asphalt layers in Texas and Georgia and measure the moisture content of the base layer beneath asphalt. The system could detect voids under concrete pavements easily in the laboratory, but detection was more difficult in the field. Water-filled voids were successfully detected in Georgia.

We suggest that the system, as it exists at the time of this report, needs further development. The most important aspect would be continued testing and correlation with ground truth in a wider variety of in-service pavements. These efforts would be used to improve the GPR system and interpretation software; thus, a production system would be made available to highway departments so that maintenance engineers would have useful information for making better maintenance treatment decisions.

1

Introduction

The Highway Operation Program of Strategic Highway Research Program (SHRP) Project H-103 set as one of its goals to define pavement conditions that relate to maintenance effectiveness (Maser and Markow 1989). The objective is a result of the growing understanding that preventive maintenance is more effective than damage repair. So, this project, H-104 was established to develop instrumentation to measure pavement conditions that are important to maintenance engineers.

It is important that the instrumentation be capable of detecting and interpreting those pavement conditions. If the instrumentation provides an interpretation along with the measurement, maintenance engineers can better evaluate and select appropriate treatments. In addition, the instrumentation could be used to monitor the effectiveness of treatment in preventing pavement deterioration.

SHRP chose ground-penetrating radar (GPR) as a nondestructive technology for providing information on various subsurface conditions, including moisture in the pavement and voids or loss of support. This study was performed by a research team composed of Geophysical Survey Systems, Inc. (GSSI), and Texas Transportation Institute (TTI). The following report documents this research effort.

1.1 Problem Statement

The objectives of SHRP Project H-104, as described in the Request for Proposal, were as follows:

1. To specify, test, and evaluate pavement measurement technologies that can do the following:
   a. Yield information (before maintenance) on whether maintenance is needed and help identify the appropriate type and location of maintenance treatment

b. Yield information after maintenance on whether the problem treated was in fact correct
c. Yield information during consecutive maintenance cycles to verify and calibrate the effectiveness models under development in SHRP Project H-101

2. To develop, fabricate, test, and demonstrate prototype equipment that meets objective 1.
3. On the basis of prototype testing and demonstration, to complete specifications for eventual production, cost estimates, recommendations for use, and training guides and manuals. The specification for production units would include the following:
   a. Exactly what precursors to distress are to be measured
   b. Proposed measurement range and required accuracy and precision
   c. Appropriate measurement procedure
   d. Necessary ambient conditions
   e. Anticipated cost range

The research team believed that the following five pavement characteristics were good candidates for radar evaluation:

1. Moisture in the surface asphalt layer as a precursor to stripping
2. Density of the asphalt layer (or intermediate layer) as an indicator of an existing stripped layer
3. Moisture in the base as a precursor to structural damage such as alligator cracking
4. Voids or loss of support beneath slabs as a precursor to joint failure
5. Overlay delamination as a precursor to overlay bonding failure

One of the goals of this project was to study the parameters measured by radar—the layer electrical properties (dielectric constants) and thicknesses—as indicators of these pavement conditions. Each of these conditions can be addressed by maintenance treatments but if left untreated or undetected, can lead to major structural problems in the pavement. GPR could provide the maintenance engineer with valuable information for making decisions. However, as with all new technologies, the outputs must be presented in a format that the engineer can interpret and act on. In this report, we have tried to identify trigger levels and reporting requirements appropriate for maintenance personnel.

1.2 Research Approach

The project was divided into the following three phases:

Phase I comprised three tasks. The first dealt with specifications of the pavement measurements to be made with GPR. Efforts were made to define typical pavement deteriorating cycles and to identify what changes in pavement characteristics indicated the need for preventive maintenance. Tentative criteria were proposed as critical or intervention levels in terms of changes in equilibrium moisture content or void size. The second task concerned the development of a measurement concept. The system proposed by the research team had a dual bistatic antenna composed of 1.0-GHz and 2.5-GHz antennas. The 1.0-GHz unit was for relatively deep penetrations up to 60 cm (24 in.); the high frequency, 2.5-GHz unit was for high-precision evaluation of the upper layers of the pavement. The third task was to evaluate the system in the laboratory and develop recommendations for a first-generation prototype for phase II. The findings of each task were reported to SHRP in interim reports.

Phase II was the design and construction of a first-generation prototype. Major modifications were made to all system components, including the system sampler and pulsing units. The GSSI digital data acquisition system, the Subsurface Interface Radar System-10, was redesigned to handle both 1.0- and 2.5-GHz systems simultaneously collecting data at close to highway speed. A series of laboratory and pilot-scale field measurements was made on highways in Texas. The results appeared promising, so SHRP gave GSSI permission to design and construct the full-scale field unit. This unit was planned to be a trailer-mounted system capable of testing both wheel paths with both 1.0- and 2.5-GHz systems at close to highway speed.

Phase III was the third and final stage of this study. The results from phase III are presented in this report. The activities to be described include the following:

1. Construction of a unit to meet the performance specification developed in phase II.
2. A series of laboratory and field tests on the final GPR system. This test program included several components:
    a. Specification testing to ensure that the system met the operational requirements for signal stability and system noise.
    b. Laboratory testing of specially constructed samples, typically 90 x 90 x 30 cm (36 x 36 x 12 ins.) with simulated voids and wet base conditions.
    c. Pilot-scale testing of test pavements at Texas A&M University Research Annex. Test pavements of varying layer thickness, and pavements containing voids and other defects were specially constructed for this study.
    d. Full- scale testing, including ground truth testing, on in-service pavements in Texas and Georgia.

1.3 Criteria for Detecting Pavement Problems

One major issue addressed in the phase I report was what amount of change in a pavement condition indicates that maintenance is needed and therefore should be of concern to maintenance personnel. The phase I report proposed the following criteria for identifying maintenance problems:

1. Stripping in asphalt

    a. Locations where the volumetric moisture content is 3.0% (approximately 1.3% by weight) higher than the equilibrium moisture content. These are locations in the asphalt layer where moisture may be trapped.
    b. Locations where the moisture content of the asphalt is greater than 3% by weight.

2. Moisture in base

    a. Locations where the volumetric moisture content is 2.0% (approximately 1.0% by weight) higher than the equilibrium moisture content. These are localized wet spots in the base.
    b. Locations where the moisture content of the base is above 8% by weight.

3. Loss of support beneath rigid pavement joints

    a. Comparison of the moisture content beneath a joint with that measured at center slab. Highlight areas showing a difference of more than 2% of weight.
    b. Areas where moisture problems extend at least 36 cm (14 in.) from the joint.
    c. Air-filled voids of 0.5 cm (0.2 in.) or larger, moisture-filled voids of 0.25 cm (0.1 in.) or larger.

4. Delaminations or debonding

    Areas where thickness of debonding is greater than 0.25 cm (0.1 in.) and gap is moisture-filled.

Subsequent work in phases II and III has expanded the criteria for use in detecting stripping. In practice, it was very difficult to validate the criterion of moisture in the asphalt. Furthermore, a major interest of the maintenance engineer is to detect buried layers of stripping. These layers often manifest themselves as thin, low-density layers that disintegrate during coring. Often the key issue is how much of the section has stripping and at what depth the stripping is located. Small localized areas can be repaired with patching; larger areas need total removal and replacement. Too often, stripping layers go undetected; maintenance engineers place thin overlays to address

surface cracking, only to see the cracking rapidly reappear. In conversations, Department of Transportation (DOT) personnel indicated that it was important that the GPR system be able to detect stripped layers.

To achieve this capability, an additional criterion is now proposed: significant reductions in density of subsurface asphalt layers.

No criteria for the size of the reduction are available yet. How to relate these criteria to the GPR measurements is discussed in section 6.

1.4 Proposed Operational Constraints

The radar system developed by GSSI should be inside a vehicle where the following environmental conditions exist:

Temperature:	Zero to 30°C (32°F to 86°F)
Relative humidity:	Less than 95% (noncondensing)

The accompanying radar antennas are mounted outside the vehicle on a trailer.

Surveys shall not be conducted in the rain or on highways with standing water. Surveys should also not be conducted within 48 hours of significant rainfall (greater than 0.25 cm [0.1 in.] per day) to ensure that no transient flow conditions are in effect and that the pavement is in moisture equilibrium. The pavement temperature must be above freezing.

Proposed Measurement Range

To be of benefit to maintenance personnel, the radar system should primarily be used to obtain information from the top two layers in the pavement system. This includes estimation of moisture content in either layer and detection of interface problems or anomalies within layers. The key benefit of radar is that it can take a large number of readings per section and therefore define how widespread a particular problem is.

Typical layer thicknesses for asphalt surfacings are 8 to 20 cm (3 to 8 in.), and for flexible bases, 15 to 45 cm (6 to 18 in.). For concrete pavements, slab thicknesses typically range from 15 to 33 cm (6 to 13 in.). The proposed radar system should have adequate power to penetrate these thicknesses of pavements and provide adequate return signals.

To obtain the information from the returned radar signals, the system must be sensitive to changes in the pavement. The following tentative ranges and accuracies are proposed as guidelines for maintenance engineers:

1. Moisture in asphalt
   Range: 0 to 10% by volume
   Accuracy: 1% by volume
   Acquisition speed: $\leq$ 80 kph (50 mph)

2. Moisture in base course:
   Range: 0 to 30% by volume
   Accuracy: 2% by volume
   Acquisition speed: $\leq$ 80 kph (50 mph)

3. Loss of support under rigid pavement joints
   Range: air-filled 0.5 cm (0.2 in.) or larger
   Loss of accuracy: Moisture content to nearest 1%; length of loss of support to nearest 5 cm (2 in.).
   Acquisition speed: 16 kph (10 mph)

4. Overlay delamination:
   Range: air-filled 0.5 cm (0.2 in.) or larger; minimum depth below surface 5 cm (2 in.)
   Range: water-filled 0.25 cm (0.1 in.) or larger; minimum depth below surface 5 cm (2 in.)
   Accuracy: length of delamination to nearest 5 cm (2 in.)
   Acquisition speed: 16 kph (10 mph)

The vehicle speed for performing measurements would depend on the application. For example, for moisture content determination in surface or base layers, highway speeds $\geq$ 80 kph would be possible. At this speed, the system would provide data at intervals of 0.5 to 2 m (1.6 to 6.6 ft) as it travels down the highway. In most cases, this will still be too much information for the maintenance engineer, and the data would need to be summarized into significant reporting units (e.g., 30-m [100-ft] lengths).

For measuring loss of support or delamination, the speed of travel would be dictated by the pulse repetition rate of the radar system (50 readings per second per channel) and specified resolution required. At the required specification, detecting the length of loss of support to $\pm$ 5 cm (2 in.), the vehicle would need to travel at approximately 16 kph (10 mph) to adequately test each joint.

Traffic Control

For high-speed measurements, little traffic control would be needed. The measurements needed would depend on the state's requirement for traffic control for a moving operation. A truck with an arrow signboard might be needed, for example. Control for low-speed measurements would be more elaborate because of the low speed of the radar vehicle. It is anticipated that the traffic control systems currently used for deflection

systems (falling-weight deflectometer, Dynaflect, or Beam measurements) would be adequate for radar testing.

Spatial Distribution

Traditionally, radar systems are employed by moving the transducer along a straight path along which the system produces a profile. Additional, parallel runs would be used to cover each lane of the highway, if required. Using more than one antenna at a time would reduce the time spent acquiring data. For example, using two transducers would reduce acquisition time by a factor of two. Reducing time spent on the highway improves safety.

The standard setup proposed in this study involves simultaneous testing of both wheel paths of the lane. The wheel paths are the locations where most deterioration occurs. GSSI has developed a four-antenna system for this project. The antennas have been mounted on a trailer with both a low- and a high-frequency unit in each wheel path.

In some cases, it might be necessary to make measurements outside the wheel paths; for example:

1. To detect loss of support at the edge of a concrete pavement, two parallel runs would be required; one at center slab, the other at the edge.
2. To detect drainage problems in asphalt pavements, testing on the crown of the pavement should give the minimum base moisture conditions. Repeat parallel runs could be used to detect the transverse distribution of moisture.

Skill of Operator

It is anticipated that the radar system would be run by a technician with a skill level similar to that required to operate other nondestructive testing equipment, such as the falling-weight deflectometer. A 1-week training program would be required. In addition, training manuals and an operator's videotape would be needed for periodic review.

Cost of Operation

At the time of this writing, the initial cost of the equipment is estimated to be $125,000. This price is for a four-antenna system including two high-frequency antennas (2.5 GHz) for detecting near-surface problems and two lower-frequency antennas (1.0 GHz) for deeper investigations. By configuring one antenna of each frequency in each wheel path, a lane could be investigated in one pass of the survey vehicle. Assuming 5-year amortization, the yearly cost should be approximately $25,000. With 100 days of surveying per year, the operating cost would be $250 per day. At a conservative estimate

of 4 hours of surveying per day at 16 kph (10 mph), 64 km (40 miles) could be covered per day. The operating cost per measurement would be less than 0.5 cents per meter (0.15 cents per foot). Note that these figures exclude other operating costs, such as vehicle and operator costs.

2

Ground-Penetrating Radar Theory

The technology employed by the research team is known as ground penetrating radar (GPR). This system transmits and receives pulses of radio energy. The signals reflected from interfaces in the pavement give information about subsurface conditions.

2.1 Basic GPR Theory

GPR functions on the principle that when a pulse of radio energy encounters a point where the electrical properties of the subsurface changes, some of the energy is reflected off the discontinuity, while the rest passes through. To record these events, the system emits a pulse and "listens" for returns. The returned signals are processed by using a sampling technique that converts the radio frequencies to audio frequencies, thus allowing simple data-processing and recording techniques.

Traditionally, the returned signals are combined to produce a profile, that observers then interpret. These profiles can be complicated and difficult to analyze, so different observers can have different interpretations. The research team has used modeling and artificial intelligence to enable the system to interpret the GPR data for maintenance personnel.

Of the electrical properties of interest for interpretation, the dielectric constant (or permittivity) provides the most information. When the radio energy passes from one layer to another with a different dielectric constant, a portion of the energy is reflected and part is transmitted. The amplitude of the reflections, or echos, provides information on the dielectric properties. How to extract the information is covered later in this report. In pavements, the parameter that influences the dielectric constant of any layer is the moisture content of the layer.

First, a discussion of the principles involved is appropriate. The discussion is focused on the pavement system. Pavement is made up of several layers (figure 2.1): the surface layer could be asphalt or concrete, the next layer is the base course, and the final layer is

subgrade. If electrical properties (moisture content) change from one layer to the next, there will be reflections from each interface (figure 2.2). The timing and amplitude of these reflections provide information on the properties of these layers.

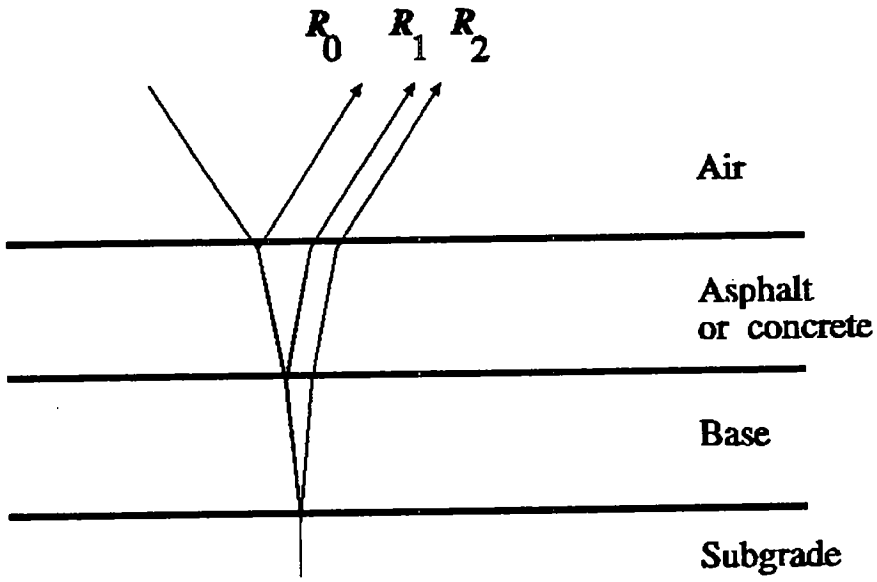

Figure 2.1. Reflections off the interfaces in pavement section

In figure 2.2, the radar waveform parameters are as follows:

A_0 = Amplitude of surface echo (R_0) (volts)
A_1 = Amplitude of echo from asphalt-base interface (R_1) (volts)
A_2 = Amplitude of echo from base-subgrade interface (R_2) (volts)
Δt_1 = Time for the pulse to travel through surface layer and back, or $t_1 - t_0$
Δt_2 = Time for the pulse to travel through base layer and back, or $t_2 - t_1$

A_0 can be used to calculate the dielectric constant of the surface layer, and Δt_1 to calculate the layer thickness. Similarly A_1 and Δt_2 can be used to calculate the dielectric constant and thickness of the second layer. Finally, A_2 can provide the dielectric constant of the third layer.

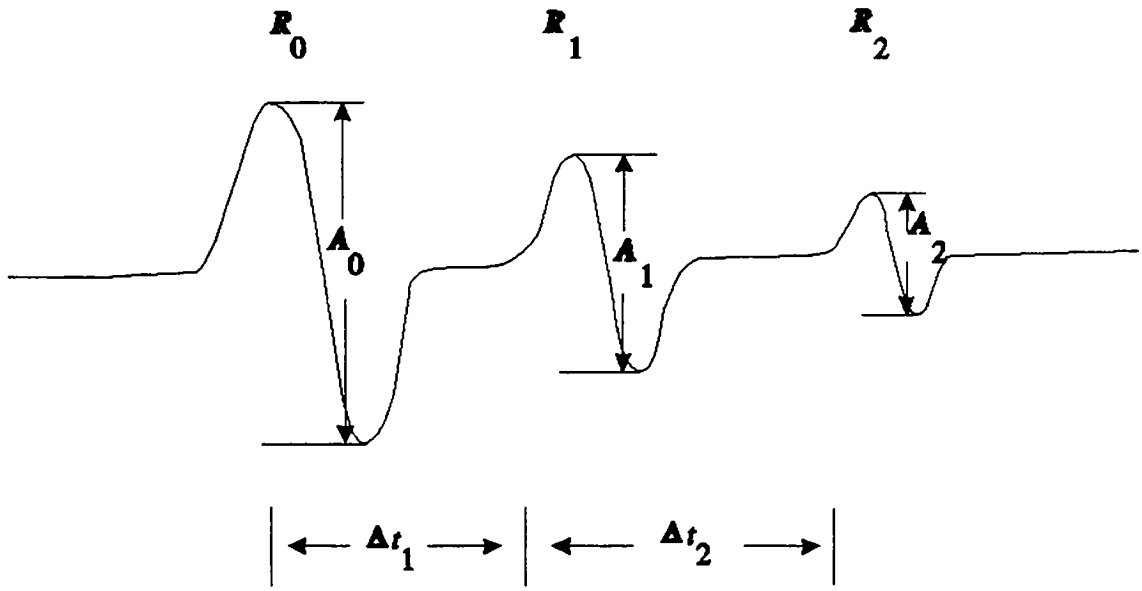

Figure 2.2. Radar scan that results from pavement section in figure 2.1

Table 2.1 shows the anticipated changes in radar return signal that correspond to various pavement conditions. An up arrow indicates an increase in that parameter, and a down arrow a decrease. For example, an increase in base moisture content would be expected to increase A_1 and Δt_2 and decrease A_2. The table was useful in interpreting the field data collected in this study. Typically, when data were collected in a visually undistressed pavement section, the table was used to get a preliminary indication of changing pavement conditions as the radar traveled along the highway.

Table 2.1
Effect of Changes in Pavement Maintenance Condition on Radar Signal

Maintenance Condition	Effect on Radar Signal				
	A_0	A_1	A_2	Δt_1	Δt_2
Increase in base moisture	-	↑	↓	-	↑
Increase in subgrade moisture	-	-	↑	-	-
Increase in moisture below slab joint	-	↑	↓	-	-
Moisture in surface layer					
a. Layer completely wet	↑	↓	↓	↑	-
b. Large wet area	-	↑	↓	↓	↓
Buried low-density stripped layer	Negative peak between A_0 and A_1				
Air voids or loss of support	Distortion of peak A_1				
Overlay delamination	Multiple small peaks between A_0 and A_1				

To calculate the dielectric constant from the reflection amplitude, the reflection coefficient (R) is employed. The equation for this coefficient is:

$$R = \frac{\left(\sqrt{\epsilon_{r1}} - \sqrt{\epsilon_{r2}}\right)}{\left(\sqrt{\epsilon_{r1}} + \sqrt{\epsilon_{r2}}\right)} \qquad (1)$$

where

ϵ_{r1} = Dielectric constant of the upper layer
ϵ_{r2} = Dielectric constant of the lower layer

So, if R and ϵ_{r1} are known, ϵ_{r2} can be computed.

The radar system does not supply the dielectric constant directly, but, it can be derived from the reflection coefficient. R can be obtained by comparing the surface reflection with that of a perfect reflector, such as a large metal plate.

For the reflection off the surface of the pavement, ϵ_{r2} can be calculated from R. R is the peak-to-peak amplitude of A_0, normalized to a metal plate reflection. The value of ϵ_{r1}, the dielectric constant of air, is 1. Solving for the dielectric constant of the surface layer in terms of the reflection coefficient, the following relationship is obtained:

$$\epsilon_r = \left(\frac{1 + R}{1 - R}\right)^2 \quad (2)$$

Some issues involved in employing this method are covered in section 6. For example, when thin overlays exist, the surface reflection may not be representative of the dielectric constant of the entire asphalt layer, particularly when low-density wearing courses are applied.

2.2 Layer Thickness Determination

To calculate the layer thickness the dielectric constant, ϵ_r is used. This parameter governs the velocity of the pulse in the layer. The formula for the velocity (v) is:

$$v = \frac{c}{\sqrt{\epsilon_r}} \quad (3)$$

where

c = Speed of light, 30 cm/nsec (11.8 in./nsec)

If the dielectric constant of the layer is known, the velocity can be determined. This information can be used with the two-way travel time to calculate the thickness of the layer. The equation for the thickness (h_1) is

$$h_1 = \frac{c\ \Delta t_1}{2\sqrt{\epsilon_1}} \quad (4)$$

where

h_1 = Thickness of layer
c = Speed of light in air
Δt_1 = Time delay between peaks (nanoseconds)
ϵ_1 = Dielectric constant of layer

In practice, the c value is often slightly different from the theoretical value because of drift in the electronics of the system. The value of c is determined experimentally by collecting GPR traces with the antenna mounted at two different heights above a metal plate. The difference in height in air is related to the difference in travel time recorded by the system, and a calibration value of c is calculated (see figure 2.2).

In addition to the dielectric constant, our research efforts have been concerned with conductivity. Conductivity is the reciprocal of resistivity. Conductivity contributes to the attenuation of the radar signal as it propagates through a layer. Increased layer conductivity increases signal attenuation. The low conductivity of fresh water allows

penetration to approximately 10 to 20 m (30 to 60 ft) at low frequency (i.e., 100 MHz). In contrast, salt water, because it is much more conductive, allows penetration to only 1 to 2 m (3 to 6 ft). The research team has taken conductivity into account when predicting or evaluating the performance of the radar system. This consideration is particularly important when comparing how GPR performs on asphalt and concrete layers, since concrete is more conductive than asphalt.

The electrical properties of the media to be investigated are important and are shown in table 2.2. These values were used to estimate the response of the radar to the pavement system. In the following table, ϵ', is the real part of dielectric constant, and ϵ'', is the loss term, the imaginary part of the dielectric constant.

Table 2.2
Measured Dielectric Constants of Pavement-Related Materials

Material	Temperature(°C)		Frequency (Hz)						
			10^5	10^6	10^7	$3x10^8$	$3x10^9$	10^{10}	124-180
Clay soil (dry)[1]	25	ϵ'_r	2.79	2.57	2.44	2.38	2.27	2.16	-
		$10^4\ \epsilon''_r$	2800	1700	980	480	340	280	
Loamy soil (dry)[1]	25	ϵ'_r	2.60	2.53	2.48	2.47	2.44	2.44	-
		$10^4\ \epsilon''_r$	780	460	360	160	27	34	
Sandy soil (dry)	25	ϵ'_r	2.65	2.59	2.55	2.55	2.55	2.53	-
		$10^4\ \epsilon''_r$	530	440	410	250	160	92	
Conoco* asphalt cement[2]	room temp.	ϵ'_r	-	-	-	-	-	-	2.64
		$10^4\ \epsilon''_r$							111.8
Witco* asphalt cement[2]	room temp.	ϵ'_r	-	-	-	-	-	-	2.68
		$10^4\ \epsilon''_r$							90.98
Shamrock* asphalt cement$_2$	room temp.	ϵ'_r	-	-	-	-	-	-	2.67
		$10^4\ \epsilon''_r$							87.78
Limestone* aggregate[2]	room temp.	ϵ'_r	-	-	-	-	-	-	4.23
		$10^4\ \epsilon''_r$							318.3
Gravel aggregate[2]	room temp.	ϵ'_r	-	-	-	-	-	-	3.20
		$10^4\ \epsilon''_r$							346.8
Asphalt concrete[2]	room temp.	ϵ'_r	-	-	-	-	-	-	4.682
		$10^4\ \epsilon''_r$							251.40
Asphalt concrete with 5.77% moisture	room temp.	ϵ'_r	-	-	-	-	-	-	5.431
		$10^4\ \epsilon''_r$							560.60
Limestone ($CaCO_3$)	20	ϵ_r'	-	6.14	-	-	-	-	-
Water	1.5	ϵ'_r	87.0	87.0	87	87	86.5	80.5	38
		$10^4\ \epsilon''_r$	165000	16500	1700	6100	28000	250000	390000
	25	ϵ'_r	78.2	78.2	78.2	78	77.5	76.7	55
		$10^4\ \epsilon''_r$	310000	31000	3600	3900	12500	120000	300000
	85	ϵ'_r	58	58	58	58	57	56.5	56
		$10^4\ \epsilon''_r$	720000	72000	7300	1800	4200	310000	140000

* = Supplier's brand name
[1] = "Tables of Dielectric Materials, Vol. 4, MIT, Research Laboratory on Insulation, Technical Report.
[2] = I. L. Al-Qadi, "Detection of Moisture in Asphaltic Concrete by Microwave Measurements, Pennsylvania State University, May, 1990.
ϵ'_r = Real part of the complex dielectric constant
ϵ''_r = Imaginary part of the complex dielectric constant

2.3 Void Detection

Typically, voids occur directly beneath rigid pavements. How do voids affect the radar signal? A void is a gap, which appears to the radar as two reflectors close together, the concrete-air and air-base interfaces. If the reflections overlap (figure 2.3), it is difficult to calculate the separation between the two interfaces. Section 3 illustrates the effect of various void thicknesses on the resultant radar traces, as well as the effect of water in the void.

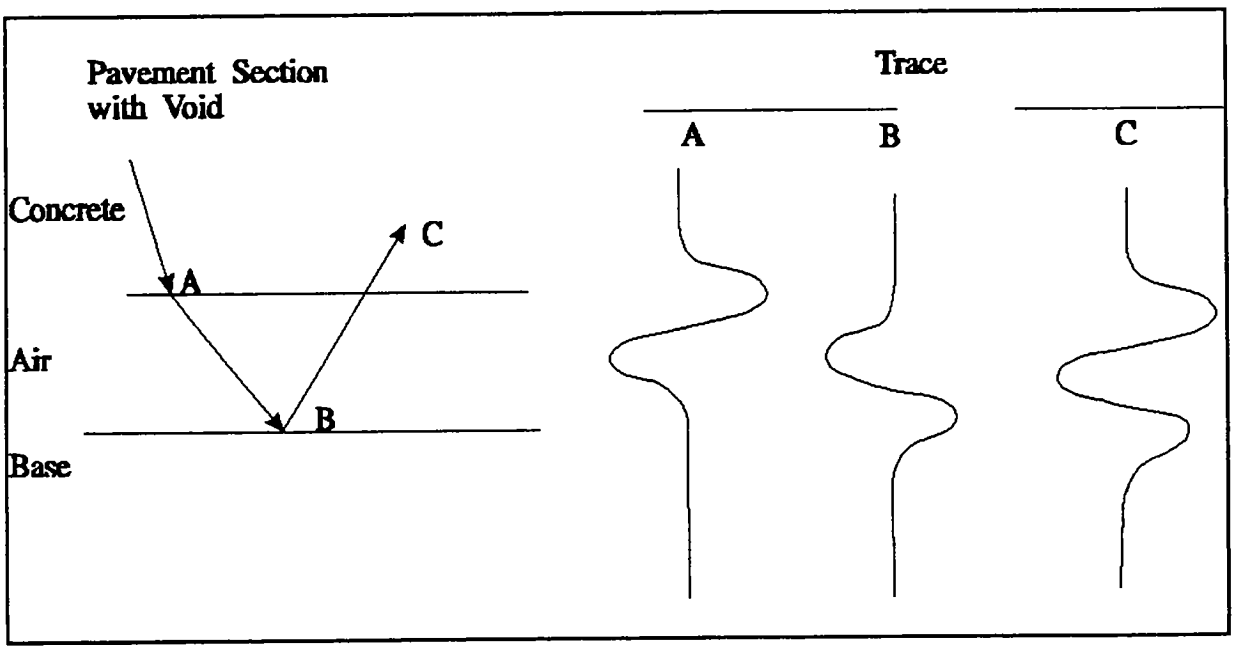

Figure 2.3. Effect of a void on radar trace. The figure at the left diagrams a rigid pavement section with a void underneath. Trace A is the reflection from the concrete-air interface, trace B is from the air-base interface, and trace C is the sum of A and B, which is the signal the radar will detect. The reflection coefficients of A and B are out of phase. As the gap widens, the reflections separate in time, and the resulting changes in trace C indicate the thickness of the gap.

Steinway et al, (1981) and Bomar et al, (1988) employ a similar method to model voids beneath pavements. Methods for deriving the gap thicknesses have inherent problems. The research team believes that comparing the radar signal from the center slab with the signal from near the joints will be useful in detecting voids.

2.4 Moisture Content Assessment

The Texas Transportation Institute (TTI) signal-processing software processes individual GPR traces and calculates layer properties such as thickness and dielectric constant (see section 6.3 for details). In many flexible pavements, one parameter of interest is the

moisture content of the base. In this section, equations will be developed that relate the dielectric constant of a layer to the moisture content of the layer, using the example of moisture in a granular base. The initial derivations were proposed by Dr. Robert L. Lytton of Texas A&M University. The first step involves proposing a constitutive model that relates the measured layer dielectric to that of the component materials. The next step is to use standard weight-volume relationships to simplify the equations.

For granular base material, the following Complex Refractive Index Model (CRIM) constitutive model has been proposed:

$$\sqrt{\epsilon_b} = \theta_s\sqrt{\epsilon_s} + \theta_w\sqrt{\epsilon_w} + \theta_a\sqrt{\epsilon_a} \tag{5}$$

where

ϵ_b = dielectric constant of the base calculated from field measurements
θ_s, θ_w, θ_a = volumetric concentrations of solid, water, and air, respectively, in the base course
ϵ_s, ϵ_w, ϵ_a = dielectric constants of the solids (typically 4 to 8), water (81), and air (1), respectively

This equation can therefore be simplified as

$$\sqrt{\epsilon_b} = \theta_s\sqrt{\epsilon_s} + 9\theta_w + \theta_a \tag{6}$$

The standard weight-volume relationships for a unit volume are shown below:

	Volumetric Concentration	Weight
Air	θ_a	0
Water γ_w	θ_w	W_w
Solid $\gamma_s = G_s\gamma_w$	θ_s	W_s
1		W_t

where

W_w, W_s = weights of water and solids, respectively, in the base layer
γ_w, γ_s = unit weights of water and solids, respectively
G_s = specific gravity of solids
W_t = weight of unit volume of base material

The gravimetric moisture content is defined as

$$w = \frac{w_t \text{ water}}{w_t \text{ solids}} = \frac{W_w}{W_s} \tag{7}$$

The volumetric moisture (V_m) content is defined as

$$V_w = \frac{volume\ water}{total\ volume} = \theta_w \tag{8}$$

The volume of air in the unit volume is therefore

$$\theta_a = 1 - \theta_w - \theta_s \tag{9}$$

By substitution,

$$\theta_a = 1 - \frac{W_s w}{\gamma_w} - \frac{W_s}{\gamma_s} \tag{10}$$

Equation (6) then becomes

$$\sqrt{\epsilon_b} = \frac{W_s}{\gamma_s}\sqrt{\epsilon_s} + 9\,\frac{W_s w}{\gamma_w} + \left(1 - \frac{W_s w}{\gamma_w} - \frac{W_s}{\gamma_s}\right) \tag{11}$$

Replacing γ_w with γ_s/G_s and collecting terms,

$$\sqrt{\epsilon_b} = \frac{W_s}{\gamma_s}\left(\sqrt{\epsilon_s} - 1\right) + 8\,w\,\frac{W_s G_s}{\gamma_s} + 1 \tag{12}$$

$$w = \frac{\left(\sqrt{\epsilon_b} - 1\right) - \frac{W_s}{\gamma_s}\left(\sqrt{\epsilon_s} - 1\right)}{8\,G_s\,\frac{W_s}{\gamma_s}} \tag{13}$$

The volumetric moisture content then becomes

$$V_w = \frac{\left(\sqrt{\epsilon_b} - 1\right) - \frac{W_s}{\gamma_s}\left(\sqrt{\epsilon_s} - 1\right)}{8} \tag{14}$$

The above equations are based on the square-root dielectric model, equation 5. In practice, ϵ_s can be assumed, and ϵ_b can be estimated from the GPR trace. Another model, which may be more appropriate for granular materials, is the linear model, shown

in equation 15. (With equation 5 the dielectric constant of the base must be less than 9.0, which from the field is not always the case.)

$$\epsilon_b = \theta_s \epsilon_s + \theta_w \epsilon_w + \theta_a \epsilon_a \tag{15}$$

Using this model, equations 16 and 17 become

$$w = \frac{\epsilon_b - 1 - \frac{W_s}{\gamma_s}(\epsilon_s - 1)}{80 G_s \frac{W_s}{\gamma_s}} \tag{16}$$

$$V_w = \frac{\epsilon_b - 1 - \frac{W_s}{\gamma_s}(\epsilon_s - 1)}{80} \tag{17}$$

Reasonable estimates can be made about the unknowns in equations 16 and 17 (W_s, γ_s, ϵ_s, G_s). For typical aggregates γ_s = 165 lb/ft^3, G_s = 2.64, ϵ_s = 5. The only unknown is W_s, which is the weight of the solids in a unit volume of base. In practice this is best achieved by making a calibration measurement of base dielectric at a single location and then taking samples from the same location to obtain the in situ moisture content in the laboratory. The terms ϵ_b and w will be known, and the unknown ratio can be calculated from the information for that location.

This study uses equations 16 and 17. Their application is discussed in section 6. The above derivations are based on the following assumptions:

1. The dielectric constant of the aggregates used is constant.
2. The density of the base is constant along a project.
3. The moisture content of the base does not vary with depth.

Assumption 2 is clearly violated in most granular base courses. However, it is not thought to have a major impact on the resulting moisture content calculations. Large increases in base dielectric constant can be attributed only to significant changes in base moisture content. If assumption 3 is violated, the moisture content estimate will be for the top of the base layer.

3

Prediction of Radar Response to Pavement Condition

This section explains and illustrates the research team's approach to using ground-penetrating radar (GPR) to detect pavement problems while they can still be treated by preventive maintenance. The research team evaluated the response of the radar to differences in the pavements and described a concept for detecting pavement conditions.

The pavement conditions can be modeled so that the changes in the radar signal can be examined. The research team generated by computer many radar waveforms that illustrate the effect of the variation in the pavement condition.

In actual practice, the relationships described previously can be processed quantitatively by a computer. From known relations in physics, the computer can be used to solve for the moisture content in asphalt or subgrade, or the degree of void or loss of support, as Texas Transportation Institute (TTI) found with their interpretation technique.

Thus a GPR system can give pavement engineers information on the subsurface condition of the pavements. This information will be reliable enough to allow constructive preventive maintenance decisions.

3.1 Modeling

A key to our application of GPR is modeling. According to The Encyclopedic Dictionary of Exploration Geophysics, a model is "a concept from which one can deduce effects which can then be compared to observations; used to understand the significance of observations" (Sheriff 1973, 143). The research team's concept is that the condition of the pavements can be expressed quantitatively. Once this is accomplished, the computer can be employed to solve the problem. This process is *inversion*, or *back-calculation*. Inversion is reverse modeling. That is, the predicted model can be used to derive the condition that would cause the resultant radar trace.

As a result of task 1, the detrimental pavement conditions are expressed quantitatively. This allows the response of the radar signal to the pavement to be modeled. As the equations in section 2 of this report illustrate, the amplitudes and timing can be calculated. The important parameter in this calculation is the dielectric constant. Given a set of pavement components, the dielectric constant can be estimated by using a mixture model.

A theoretical model that describes how the pulse travels in the pavement layer system and reflects at each interface, has been derived by Dr. Robert Lytton of TTI. To simplify our discussion, this model incorporates a linear-mixture model, which states that the dielectric constant of a mixture is the summation of the dielectric constants of its constituents weighted by the corresponding volumetric ratios.

An asphalt pavement has only a few components, which include aggregate, asphalt, air, and possibly moisture. The dielectric constant of the asphalt mixture (ϵ_{ac}) can be expressed as follows:

$$\epsilon_{ac} = \epsilon_s V_s + \epsilon_{as} V_{as} + \epsilon_a V_a \qquad (18)$$

where

ϵ_{ac}	=	Dielectric constant of the asphalt mixture
ϵ_s, ϵ_{as}, ϵ_a	=	Dielectric constants of the aggregate, asphalt, and air, respectively
V_s, V_{as}, V_a	=	Volumetric ratios of aggregate, asphalt, and air, respectively

Assuming layer thicknesses and dielectric constants, the radar traces are modeled to simulate the radar response to the pavement distresses of interest to the maintenance engineers.

The research team has compiled several model traces to illustrate the effects of some pavement conditions. The mixture equation can be adjusted to predict changes in the dielectric constant caused by adding water. Water has a dielectric constant of approximately 80 and will greatly affect the radar trace. Figure 3.1 shows the change in the dielectric constant of asphalt as a function of moisture.

As the equations in section 2 show, changes in the dielectric constant affect both the amplitude and the timing of the reflected signals. By employing this relationship, we can generate synthetic or modeled waveforms. This is called forward modeling. The model traces that follow are generated with computer simulation by using a wave shape much like the one our system employs.

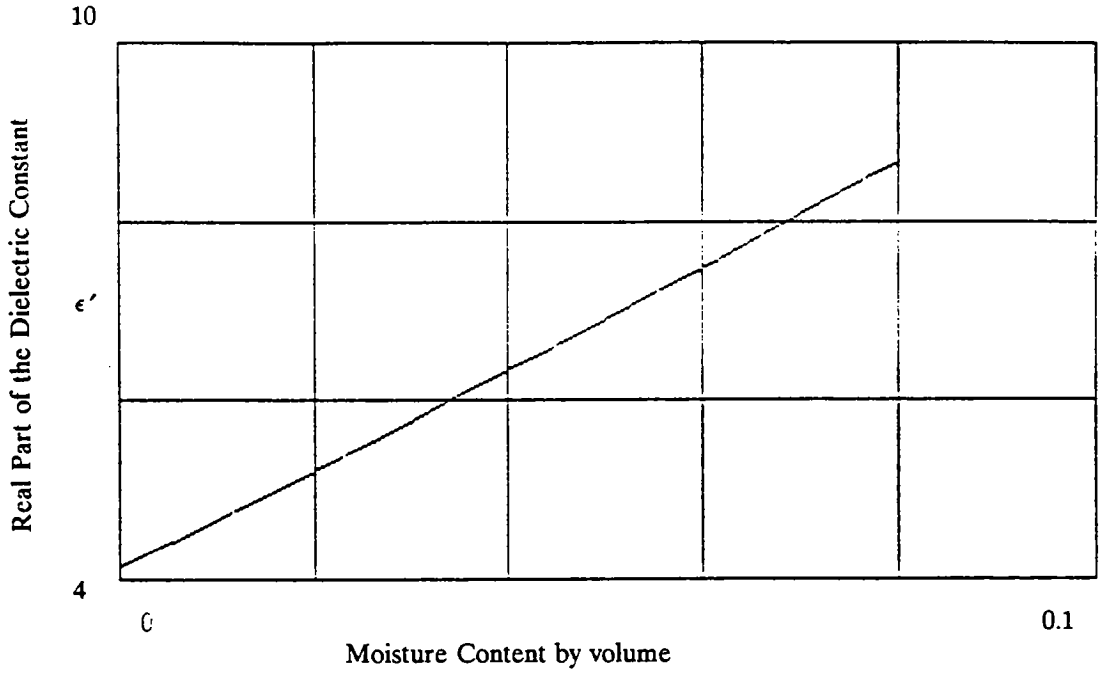

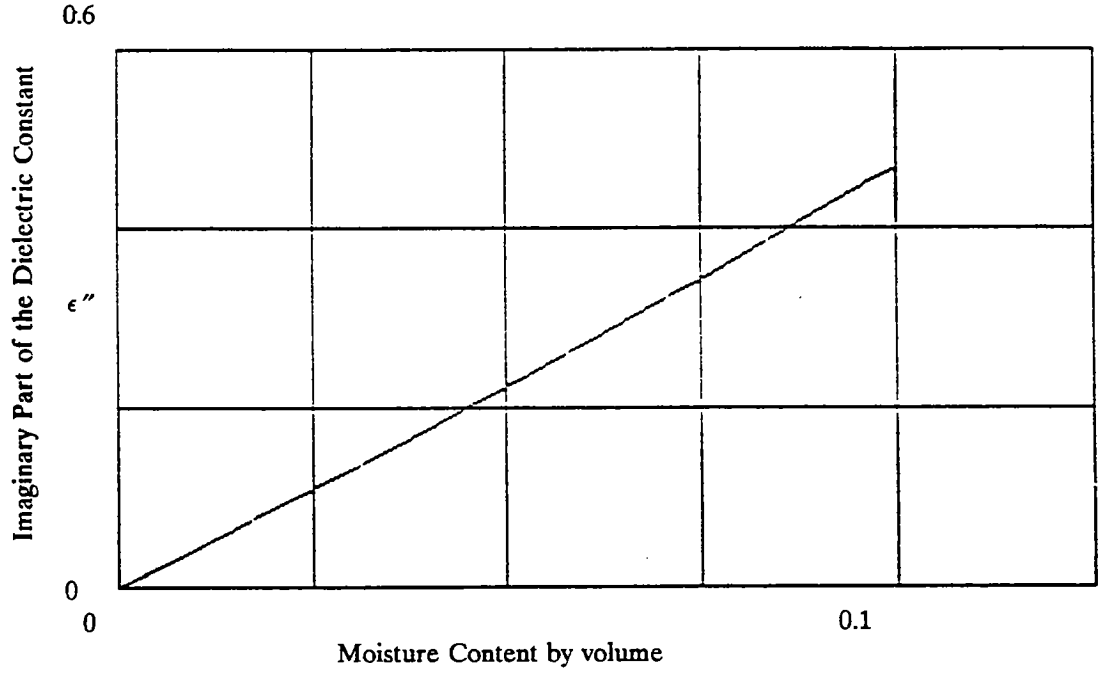

f	=	2.5×10^3	Center frequency of wavelet spectrum (megahertz)
T	=	30	Temperature (celsius)
S	=	0.2	Water salinity (parts/thousand)
$\epsilon(f)$	=	$75.584 - 8.248i$	Dielectric constant of pore water
ϵ_2	=	$4.5 - 1 \times 10\, i$	Dielectric constant of solid asphalt

Figure 3.1. Plots of the real and imaginary parts of the dielectric constant versus the moisture content of asphalt

Figure 3.1 shows plots of the real and imaginary parts of the dielectric constant versus the moisture content of asphalt. The asphalt model employed had a volumetric pore space content of 8%. Note that both parts of the dielectric constant increase with increasing moisture content.

It is important to explain why we are employing complex modeling techniques. Signals like those used in GPR systems actually contain a broad range of frequencies, and are therefore referred to as broad-band width signals. The losses at high frequencies are greater than the losses at low frequencies, and this phenomenon causes dispersion in the data. The result is an apparent broadening of the signal (i.e., it will appear to have a lower frequency).

In terms of our measurement concept, we will perform certain analyses in the frequency domain. Doing so permits the team to take dispersion into account, so that we can use the best modeling available. Many previous efforts to apply radar to pavement problems have had shortcomings. We hope that our approach is a truer representation of the radar's response to pavement distresses.

3.2 Moisture in Asphalt

Figures 3.2 through 3.5 show how moisture in asphalt affects the GPR signal. Note that as the moisture is increased, the amplitude of the surface reflection increases. For the second reflection, the reflection time increases and its amplitude decreases. The decrease in the amplitude is due the decrease in to the dielectric contrast (i.e., the dielectric constants of the asphalt and the base becoming equal).

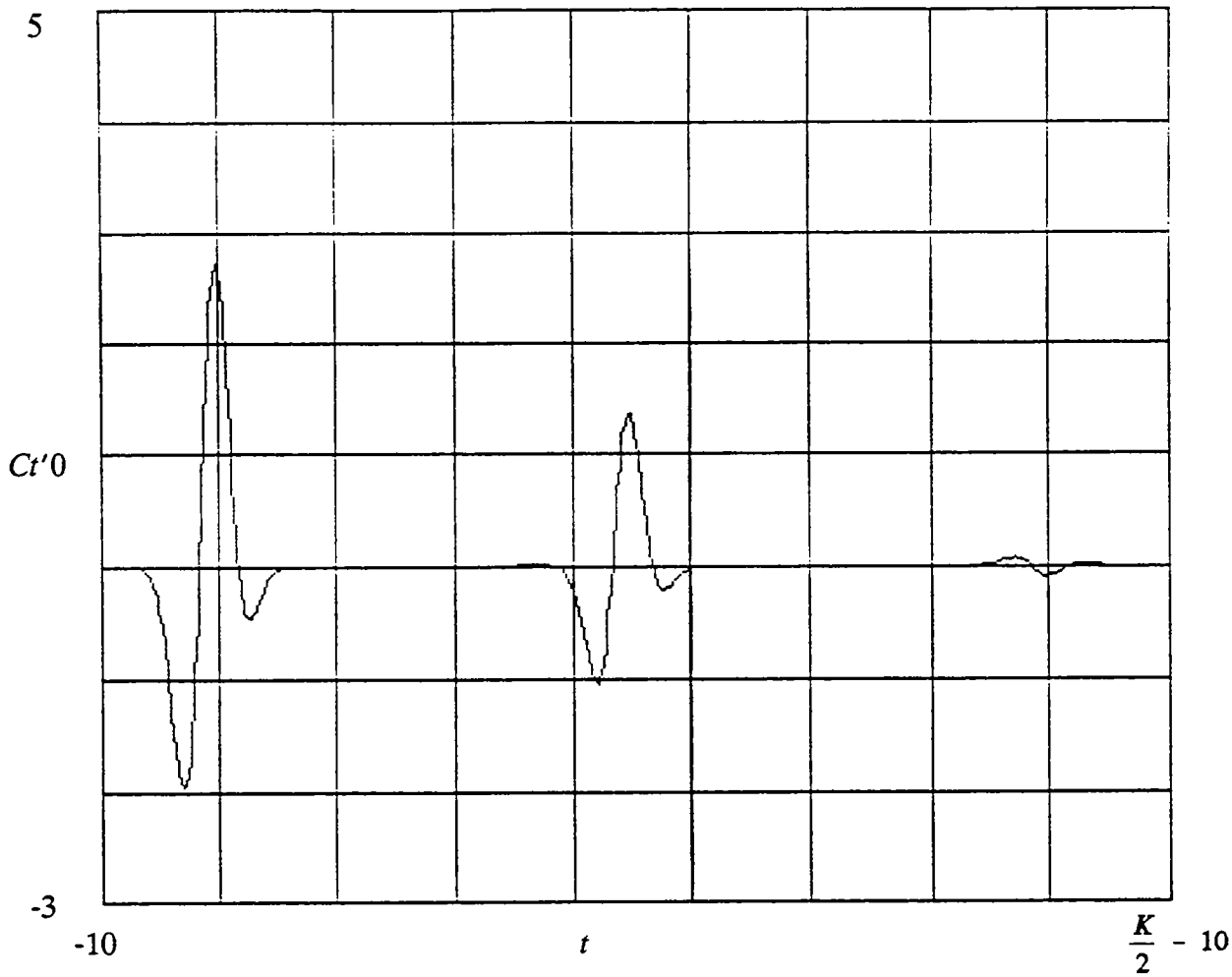

Time (nanoseconds, 0.5 nsec/division)

ϵ_2	= 4.06 + 9 x $10^{-4}i$	Asphalt layer: porosity = 10%, thickness = 13 cm
ϵ_3	= 8.97 + 0.55i	Base layer: porosity = 25%, moisture content = 10%
R	= 0.337	Surface reflection coefficient

Figure 3.2. Synthetic radar scan from an asphalt pavement with a base moisture content of 0%. The pulse on the left is the surface reflection. The reflection in the middle is from the asphalt-base boundary. The rightmost event is a small multiple.

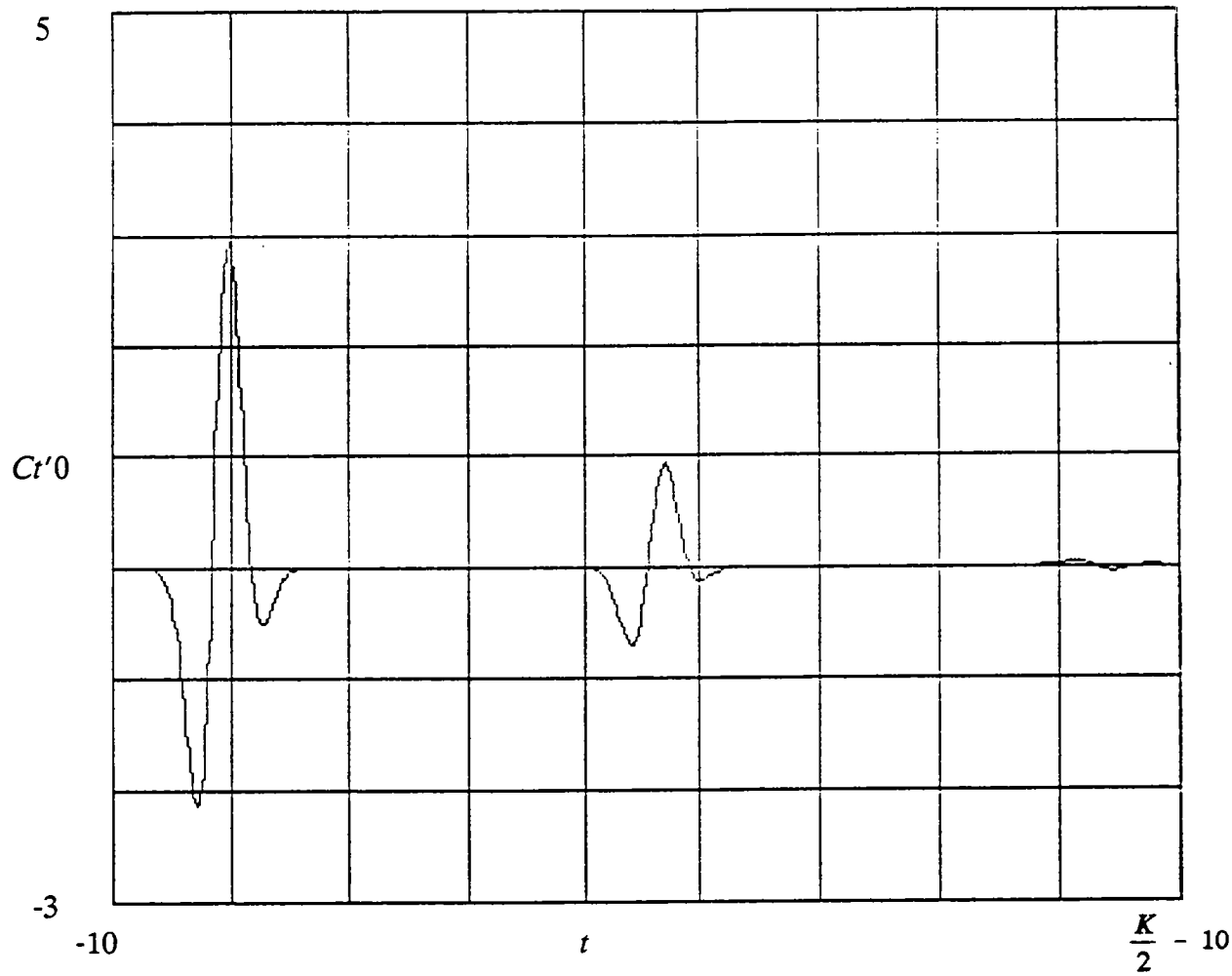

Time (nanoseconds, 0.5 nsec/division)

ϵ_2	= 4.59 + 0.055i	Asphalt layer: porosity = 10%, thickness = 13 cm
ϵ_3	= 8.97 + 0.55i	Base layer: porosity = 25%, moisture content = 10%
R	= 0.365	Surface reflection coefficient

Figure 3.3. Synthetic radar scan from an asphalt pavement with a base moisture content of 1%. Note that the amplitude of the surface reflection is increased relative to figure 3.2.

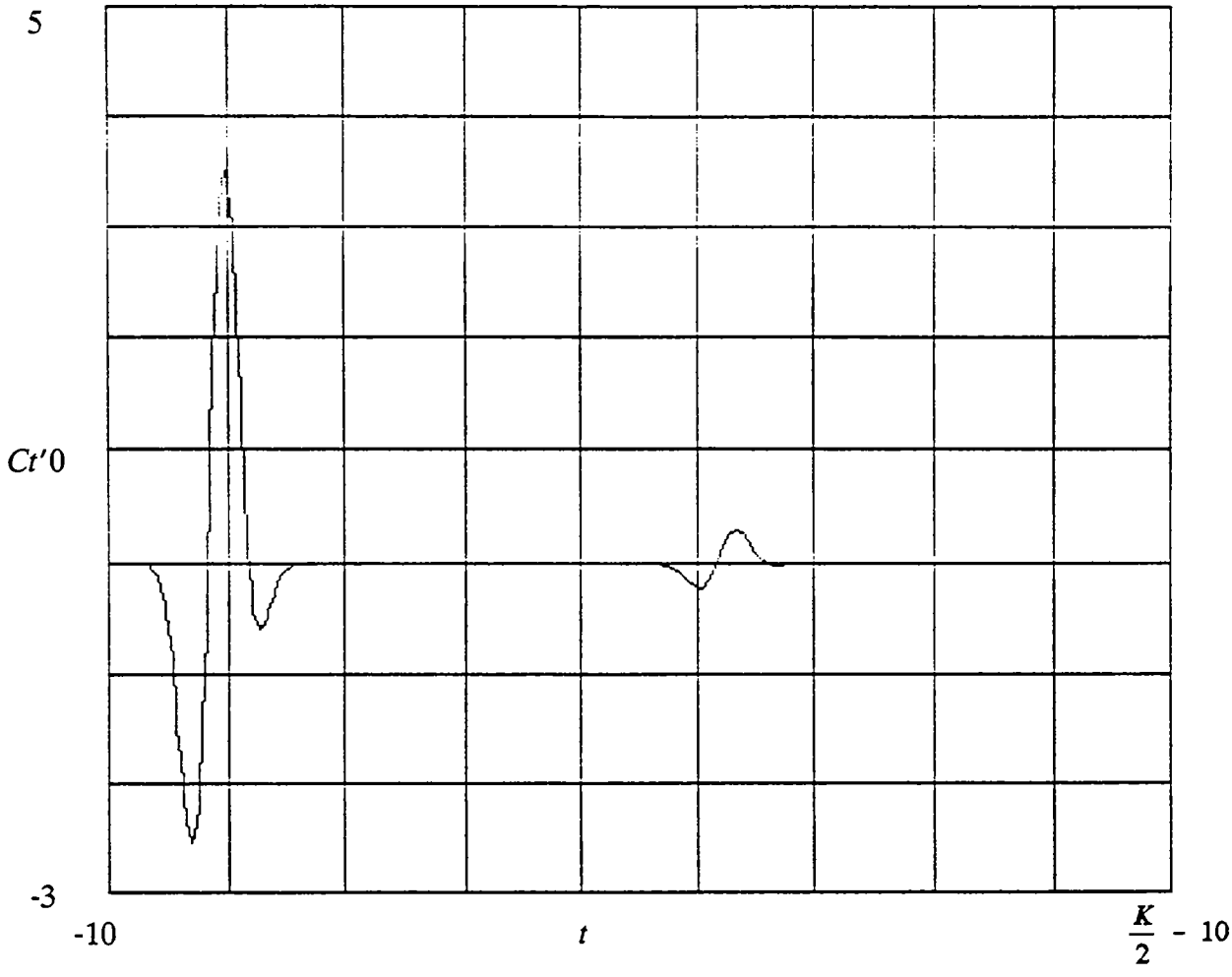

Time (nanoseconds, 0.5 nsec/division)

ϵ_2	= 6.23 + 0.22i	Asphalt layer: porosity = 10%, thickness = 13 cm
ϵ_3	= 8.97 + 0.55i	Base layer: porosity = 25%, moisture content = 10%
R	= 0.432	Surface reflection coefficient

Figure 3.4. Synthetic radar scan from an asphalt pavement with a base moisture content of 4%. Note that the amplitude of the surface reflection is increased relative to figure 3.3.

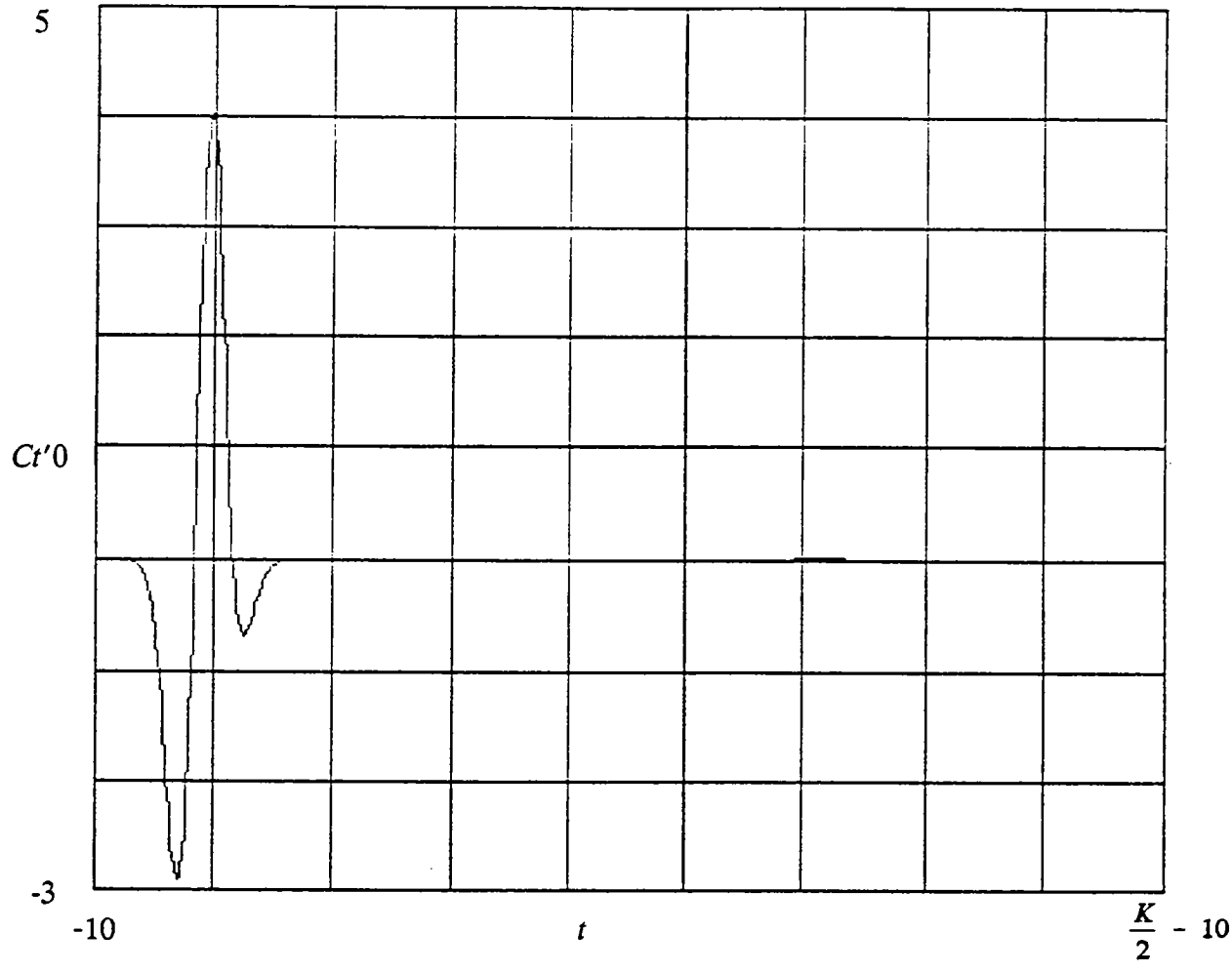

Time (nanoseconds, 0.5 nsec/division)

ϵ_2	= 8.55 + 0.46i	Asphalt layer: porosity = 10%, thickness = 13 cm
ϵ_3	= 8.97 + 0.55i	Base layer: porosity = 25%, moisture content = 10%
R	= 0.497	Surface reflection coefficient

Figure 3.5. Synthetic radar scan from an asphalt pavement with a base moisture content of 8%. Note that the amplitude of the asphalt-base reflection is decreased slightly relative to figure 3.4.

3.3 Moisture in Base Layer

The modeled traces for the moisture in the base layer were created by using a concrete pavement system. Figures 3.6 through 3.9 show the reflections from the surface and from the concrete-base interface. Note that the concrete-base reflection increases predictably. Figure 3.10 is a plot of the reflection coefficient versus the moisture content of the base layer.

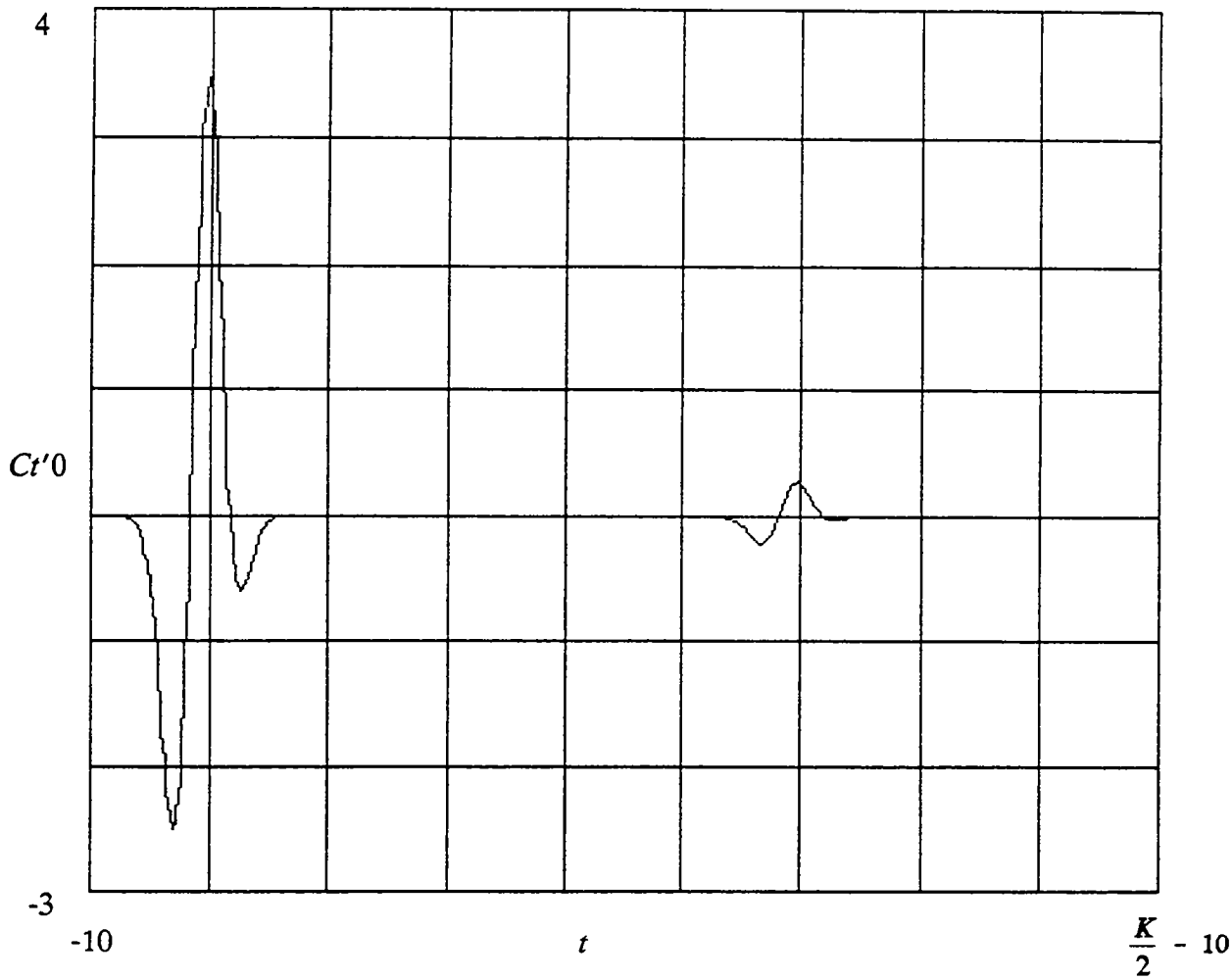

Time (nanoseconds, 0.5 nsec/division)

ϵ_2	= 6.14 + 0.1i	Portland cement concrete (PCC): thickness = 13 cm
ϵ_3	= 7.8 + 0.43i	Base layer: porosity = 25%, moisture content = 8%
R	= 0.427	Surface reflection coefficient
R_2	= 0.042	PCC-base reflection coefficient

Figure 3.6. Synthetic radar scan from a concrete pavement with a base moisture content of 8%. The pulse on the left is the surface reflection. The reflection on the right is from the concrete-base boundary.

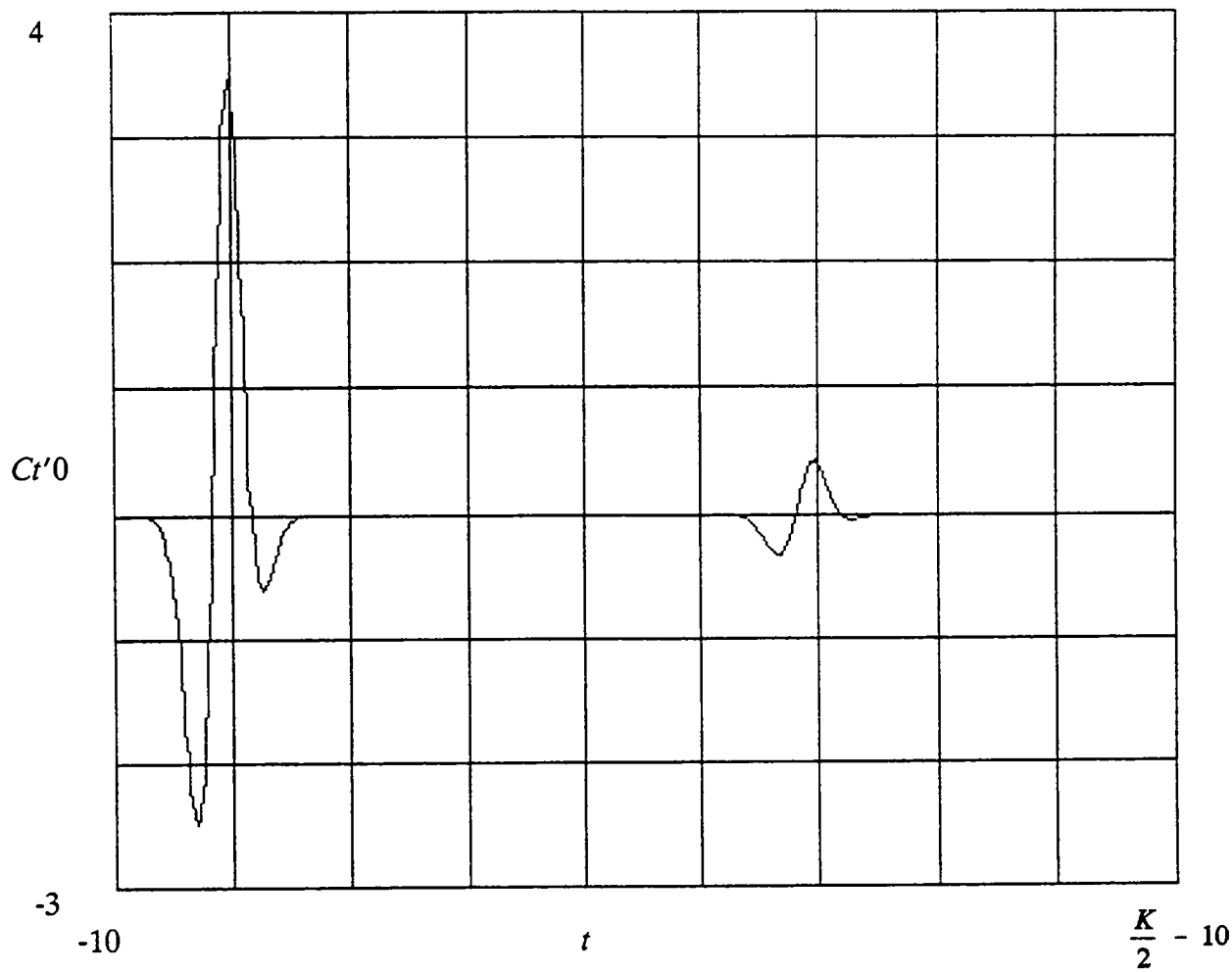

Time (nanoseconds, 0.5 nsec/division)

ϵ_2	= 6.14 + 0.1i	Portland cement concrete (PCC): thickness = 15 cm
ϵ_3	= 8.97 + 0.55i	Base layer: porosity = 25%, moisture content = 10%
R	= 0.427	Surface reflection coefficient
R_2	= 0.065	PCC-base reflection coefficient

Figure 3.7. Synthetic radar scan from a concrete pavement with a base moisture content of 10%. Note that the amplitude of the concrete-base reflection is increased relative to figure 3.6.

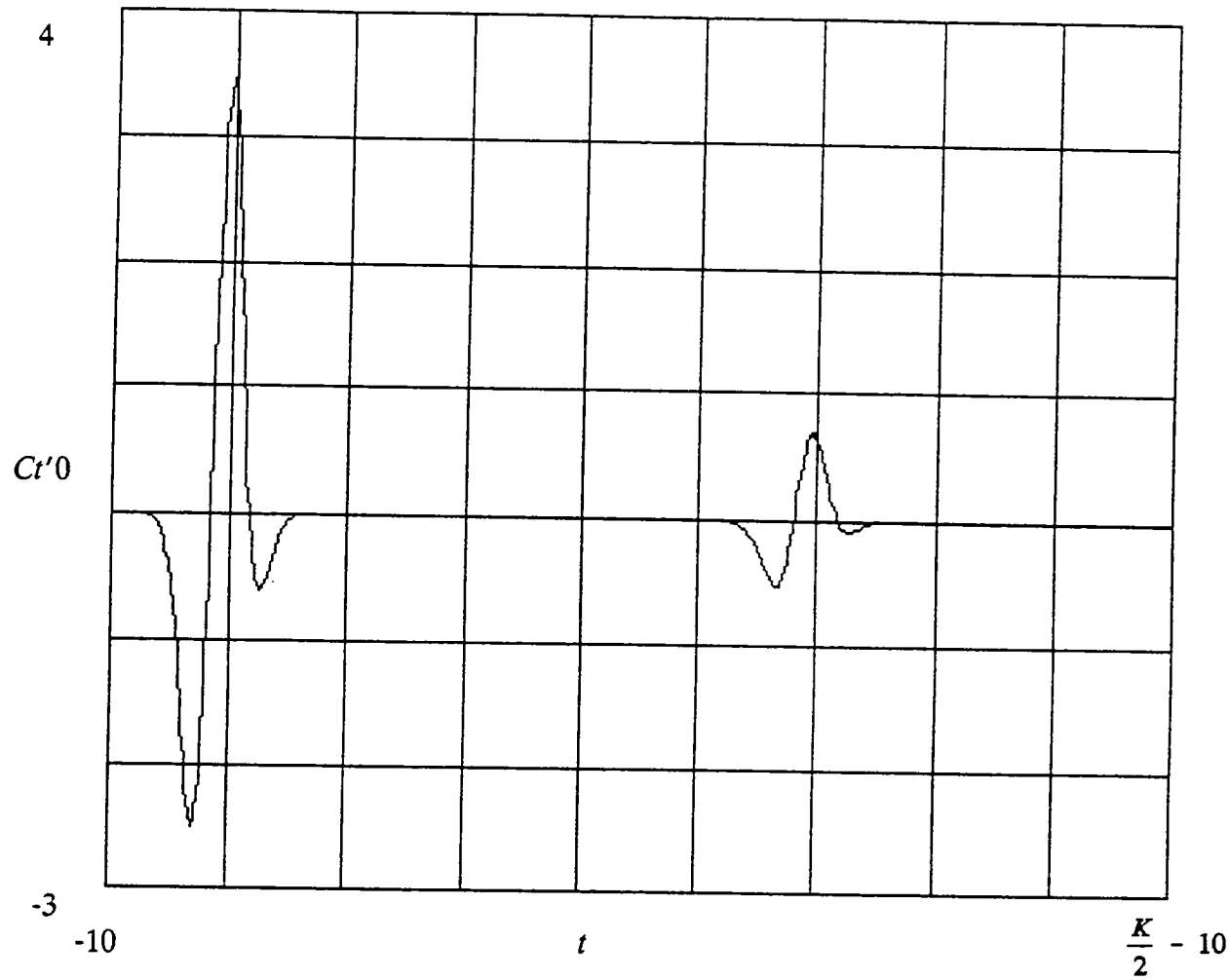

Time (nanoseconds, 0.5 nsec/division)

ϵ_2	= 6.14 + 0.1i	Portland cement concrete (PCC): thickness = 15 cm
ϵ_3	= 11.41 + 0.8i	Base layer: porosity = 25%, moisture content = 14%
R	= 0.427	Surface reflection coefficient
R_2	= 0.105	PCC-base reflection coefficient

Figure 3.8. Synthetic radar scan from a concrete pavement with a base moisture content of 14%. Note that the amplitude of the concrete-base reflection is increased relative to figure 3.7.

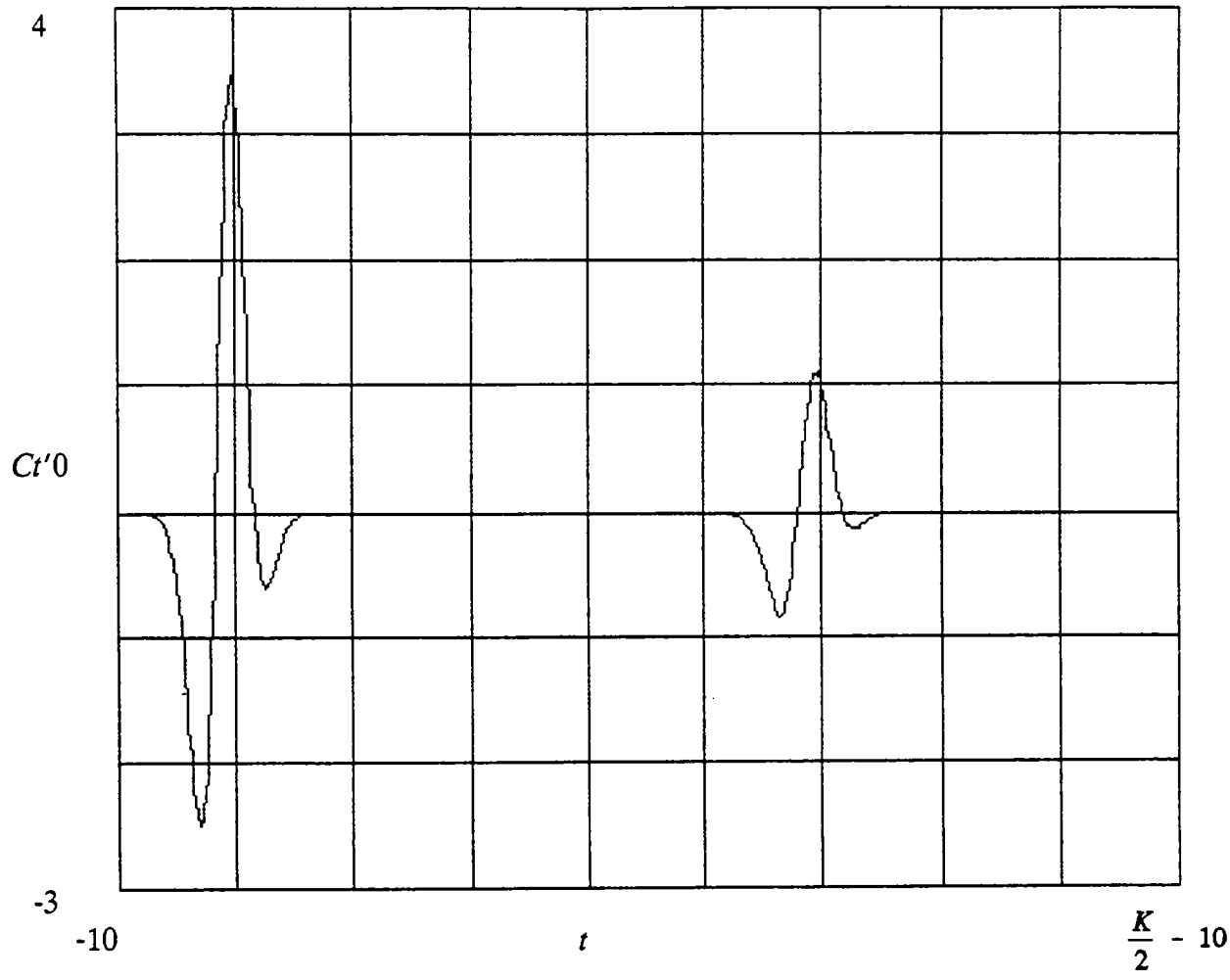

Time (nanoseconds, 0.5 nsec/division)

ϵ_2	= 6.14 + 0.1i	Portland cement concrete (PCC): thickness = 15 cm
ϵ_3	= 16.72 + 1.35i	Base layer: porosity = 25%, moisture content = 22%
R	= 0.427	Surface reflection coefficient
R_2	= 0.168	PCC-base reflection coefficient

Figure 3.9. Synthetic radar scan from a concrete pavement with a base moisture content of 22%. Note that the amplitude of the concrete-base reflection is increased relative to figure 3.8.

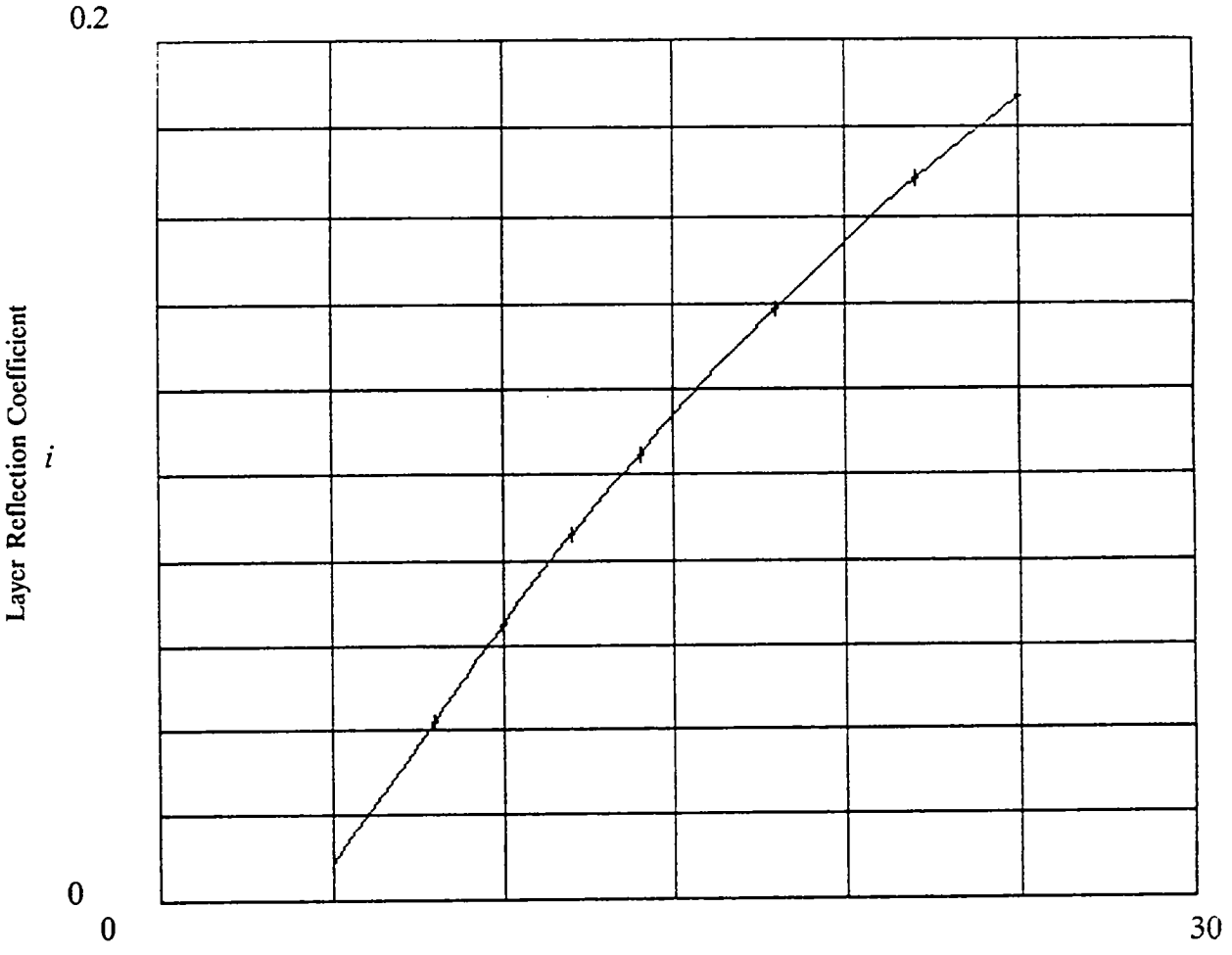

PCC pavements: Thickness = 15 cm
Base layer: porosity = 25%

Figure 3.10. Plot of the reflection coefficient of the concrete-base interface versus the moisture content of the base layer. The reflection is normalized to a metal plate reflector at the surface.

3.4 Voids under Concrete Slab

Figures 3.11 through 3.15 illustrate the change in the reflection from the concrete-base interface as a void is introduced. Figure 3.11 shows the reflection when there is no air gap. Figure 3.12 shows the reflection with a 0.1-cm (0.04-in.) air gap. The gap is then increased to a maximum of 2 cm. (0.4 in.), shown in Figure 3.15. Note that the phase of the reflection changes as the gap is increased. Figure 3.16 shows the plot of the reflection coefficient versus the gap thickness.

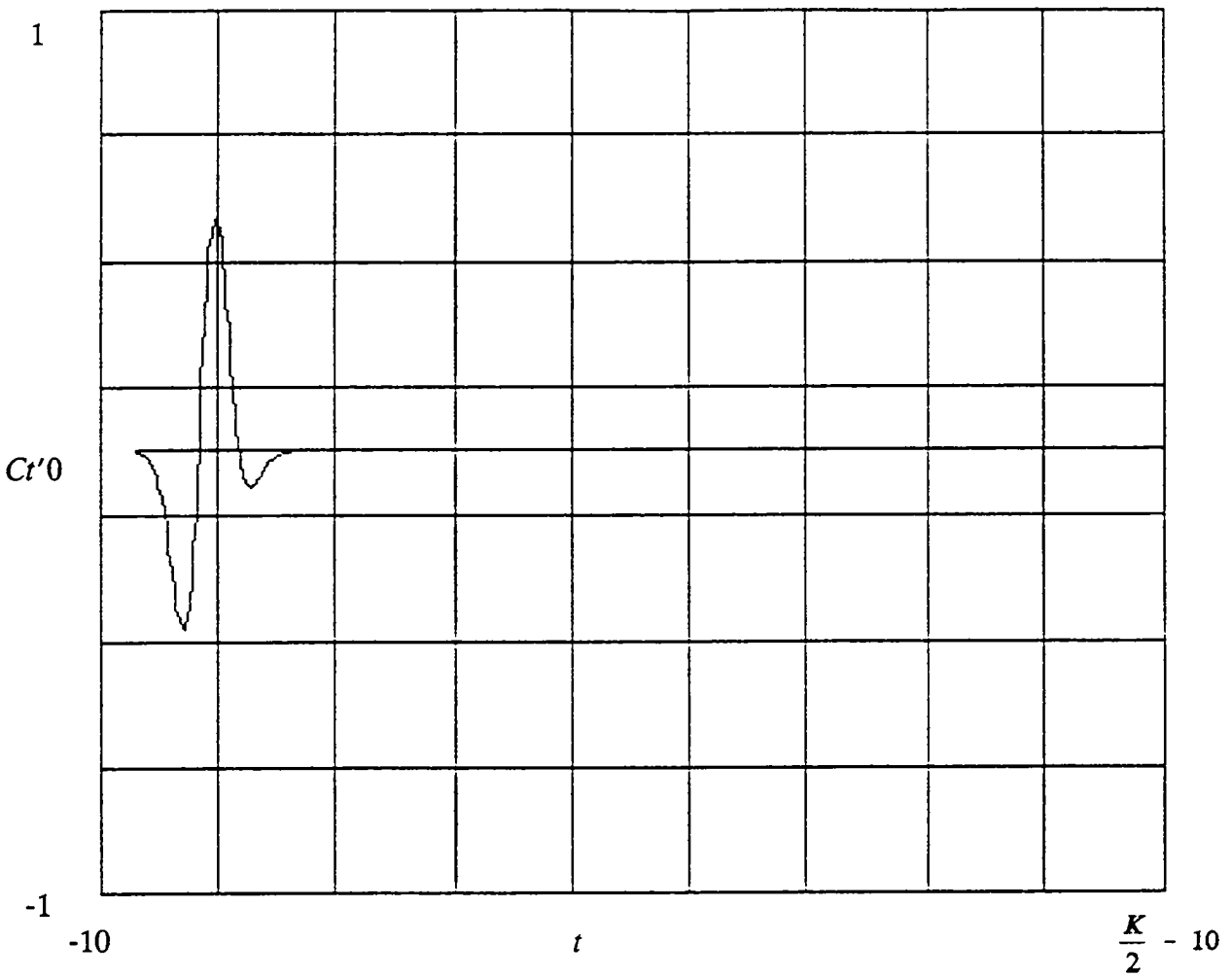

Time (nanoseconds, 0.5 nsec/division)

ϵ_1	= 6.14 + 0.1i	Portland cement concrete (PCC): thickness = 15 cm
ϵ_2	= 1	Air gap thickness = d_2 = 0 cm
ϵ_3	= 7.8 + 0.43i	Base layer: porosity = 25%, moisture content = 8%
R	= 0.066	Thin layer reflection coefficient
R_2	= 0.042	PCC-air gap-base reflection coefficient

Figure 3.11. Reflection at the concrete-base interface with no void introduced. This is an enlarged display of the rightmost reflection in figure 3.7.

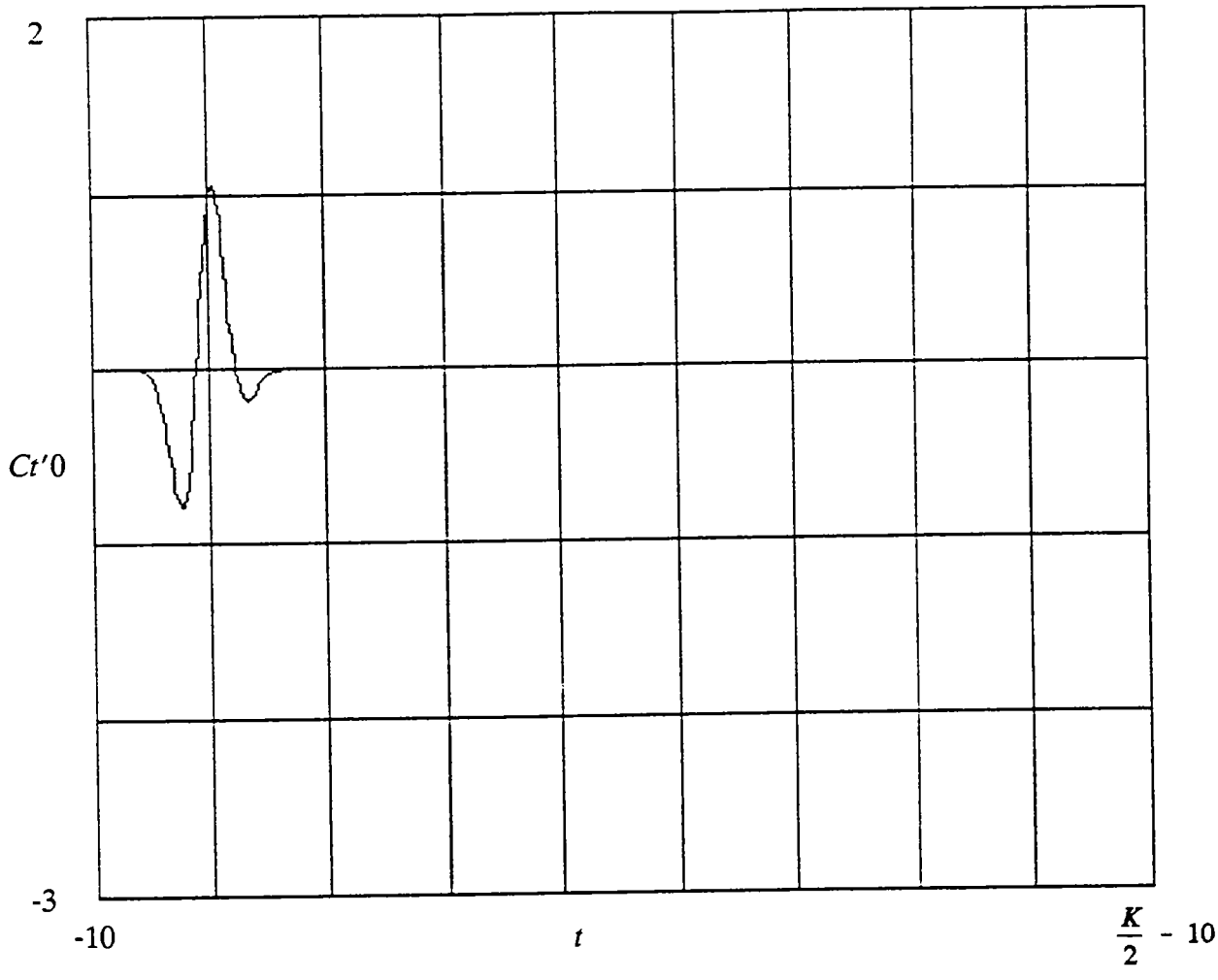

Time (nanoseconds, 0.5 nsec/division)

ϵ_1	= 6.14 + 0.1i	Portland cement concrete (PCC): thickness = 15 cm
ϵ_2	= 1	Air gap thickness = d_2 = 0.1 cm
ϵ_3	= 7.8 + 0.43i	Base layer: porosity = 25%, moisture content = 8%
R	= 0.132	Thin layer reflection coefficient
R_2	= 0.084	PCC-air gap-base reflection coefficient

Figure 3.12. Reflection at the concrete-base interface with a 0.1-cm void introduced. Note that the amplitude is decreased relative to the case of no void (figure 3.11); the amplitude scale has been reversed.

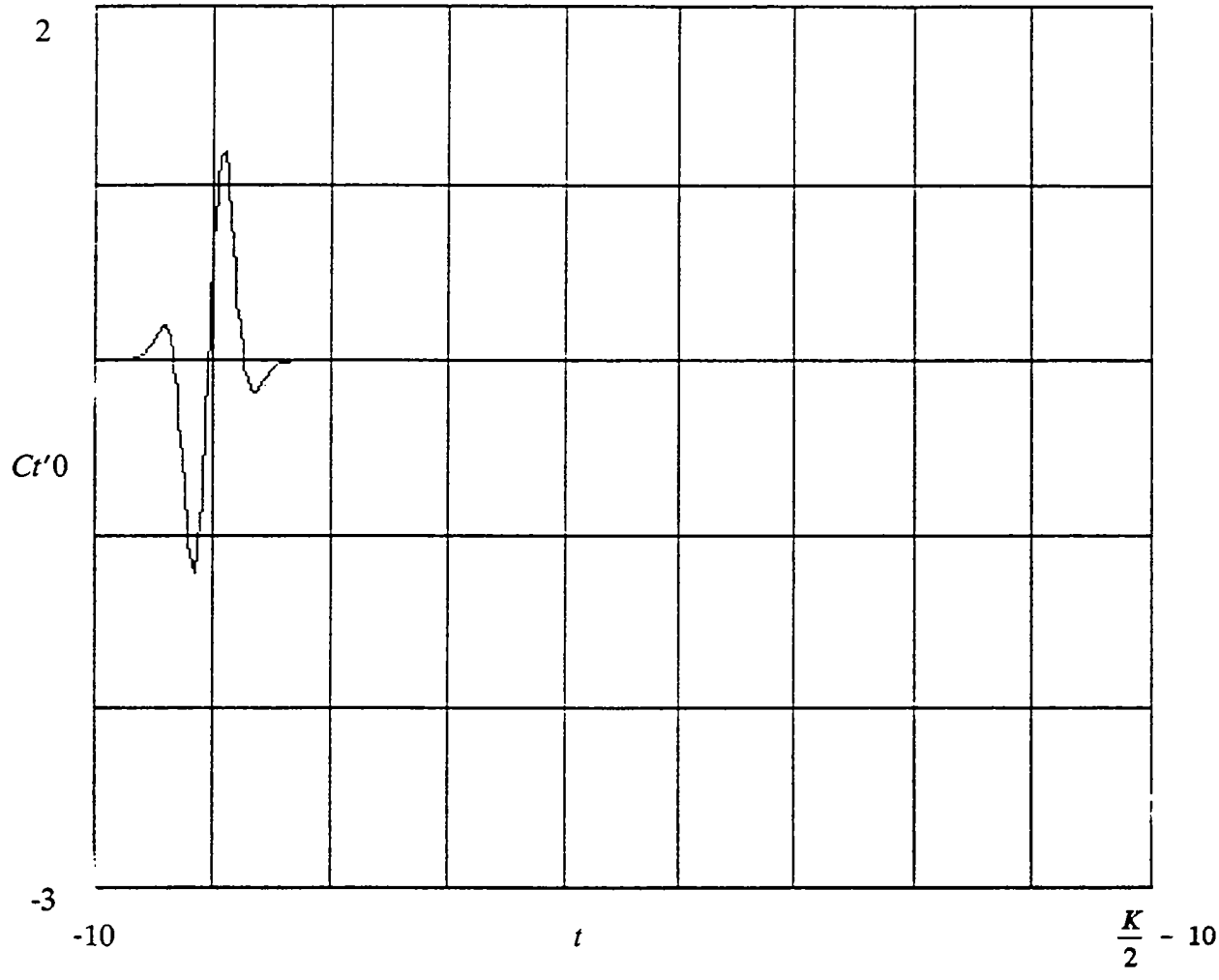

Time (nanoseconds, 0.5 nsec/division)

ϵ_1	= 6.14 + 0.1i	Portland cement concrete (PCC): thickness = 15 cm
ϵ_2	= 1	Air gap thickness = d_2 = 0.2 cm
ϵ_3	= 7.8 + 0.43i	Base layer: porosity = 25%, moisture content = 8%
R	= 0.171	Thin layer reflection coefficient
R_2	= 0.109	PCC-air gap-base reflection coefficient

Figure 3.13. Reflection at the concrete-base interface with a 0.2-cm void introduced. Note that the amplitude is increased relative to figure 3.12, and that the start of the pulse has the opposite polarity.

ϵ_1	= 6.14 + 0.1i	Portland cement concrete (PCC): thickness = 15 cm
ϵ_2	= 1	Air gap thickness = d_2 = 0.6 cm
ϵ_3	= 7.8 + 0.43i	Base layer: porosity = 25%, moisture content = 8%
R	= 0.387	Thin layer reflection coefficient
R_2	= 0.246	PCC-air gap-base reflection coefficient

Figure 3.14. Reflection at the concrete-base interface with a 0.6-cm void introduced. Note that the amplitude is increased relative to the previous cases; the amplitude scale has been increased.

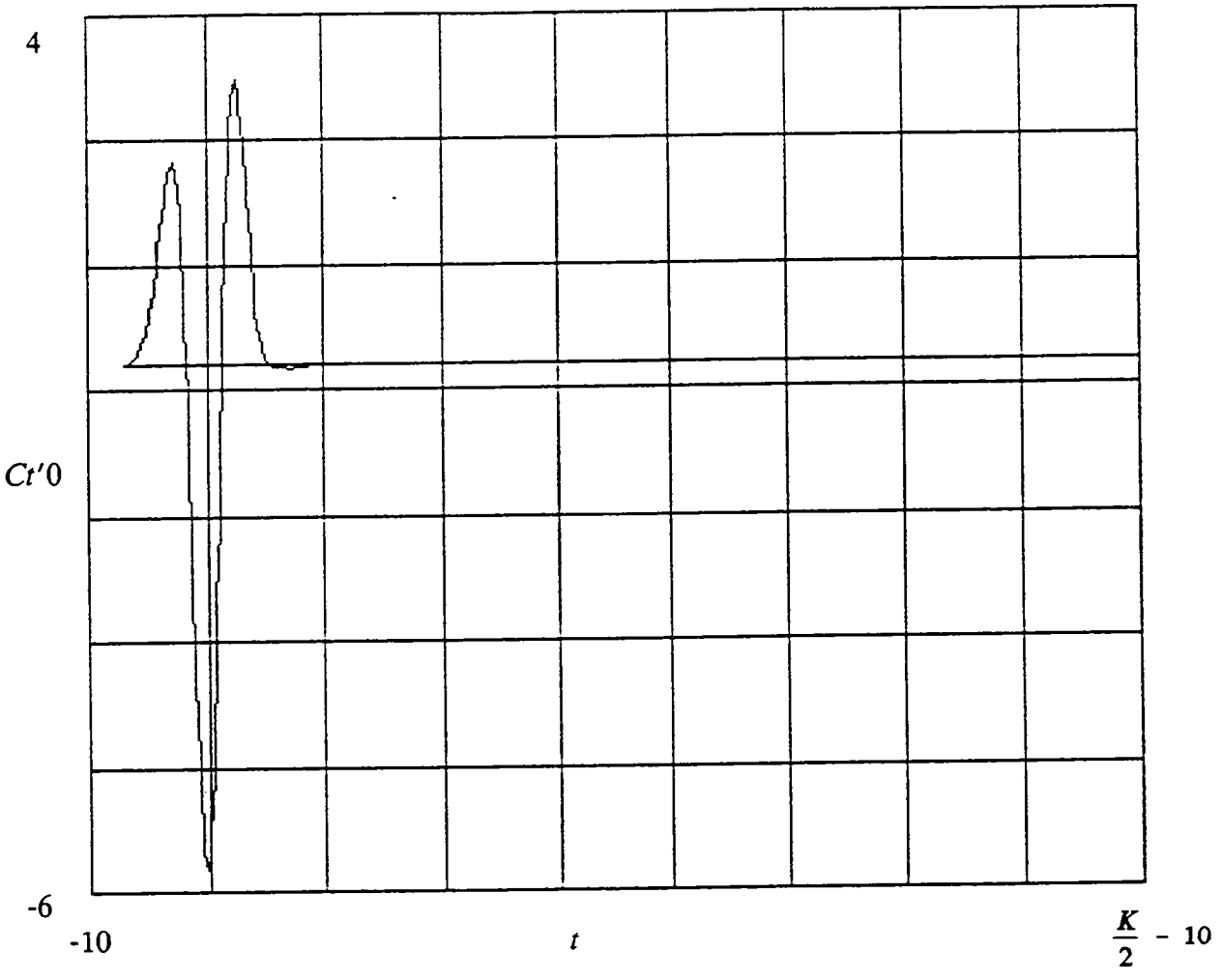

Time (nanoseconds, 0.5 nsec/division)

ϵ_1	= 6.14 + 0.1i	Portland cement concrete (PCC): thickness = 15 cm
ϵ_2	= 1	Air gap thickness = d_2 = 0.2 cm
ϵ_3	= 7.8 + 0.43i	Base layer: porosity = 25%, moisture content = 8%
R	= 0.644	Thin layer reflection coefficient
R_2	= 0.41	PCC-air gap-base reflection coefficient

Figure 3.15. Reflection at the concrete-base interface with a 2-cm void introduced.

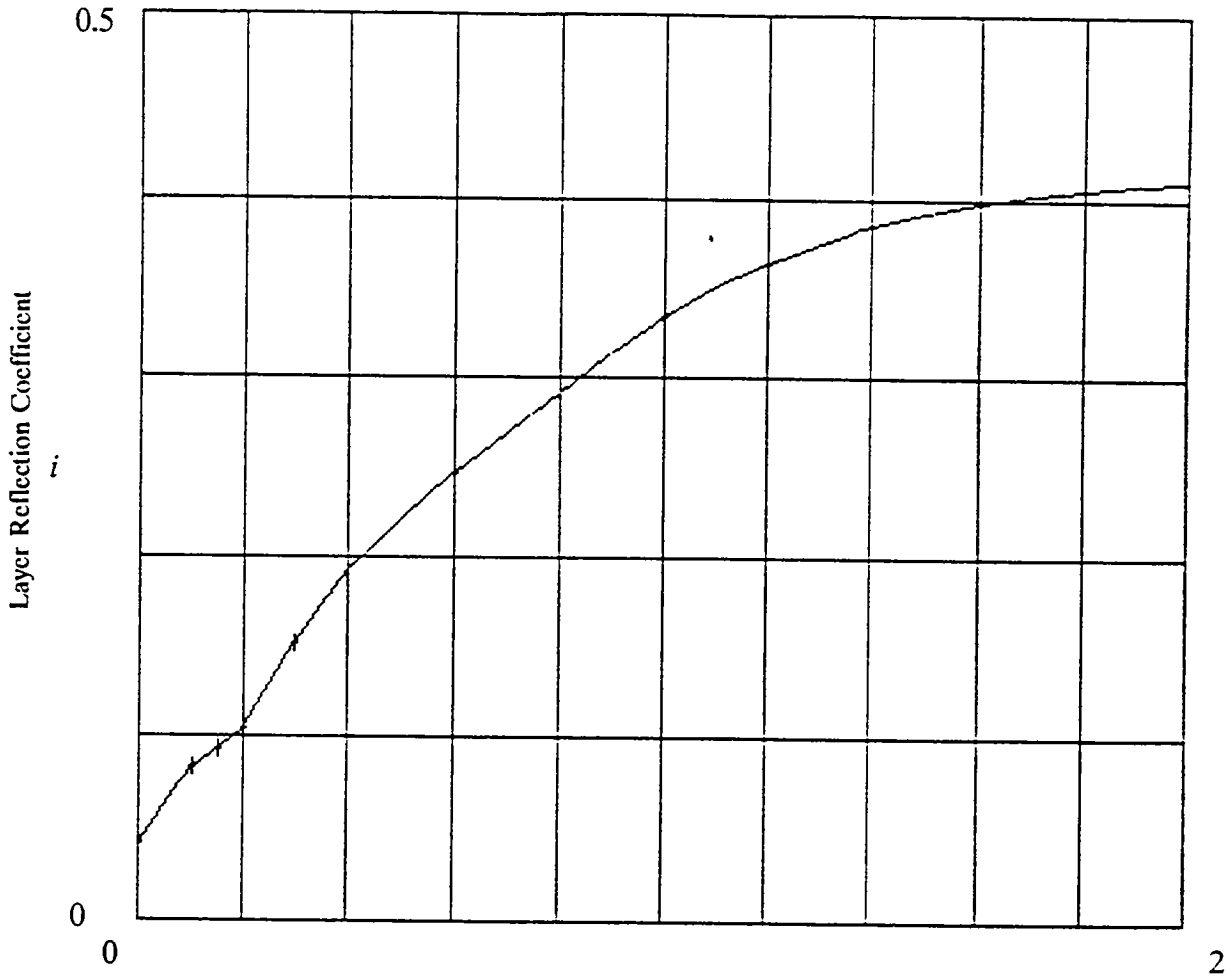

PCC pavements: thickness = 15 cm
Base layer: porosity = 25%
moisture content = 8%

Figure 3.16. Plot of the reflection coefficient of the concrete-base interface versus the air void thickness. The reflection is normalized to a metal reflector on the concrete surface.

3.5 Overlay Delaminations

Modeling delamination in asphalt in a manner similar to that used for voids under concrete slabs produced another set of radar traces (figures 3.17 through 3.20). The reflections from an air gap as the gap thickness is changed from 0.1 to 5.0 cm are presented. Figure 3.21 is a plot of reflection coefficient versus air gap thickness. Figures 3.2 through 3.25 illustrate similar changes, except that the gap is filled with water. Because of the high dielectric constant of water, dramatic changes in the signal occur as the gap thickness is varied from 0.02 to 2.0 cm. Figure 3.26 is a plot of reflection coefficient versus water gap thickness.

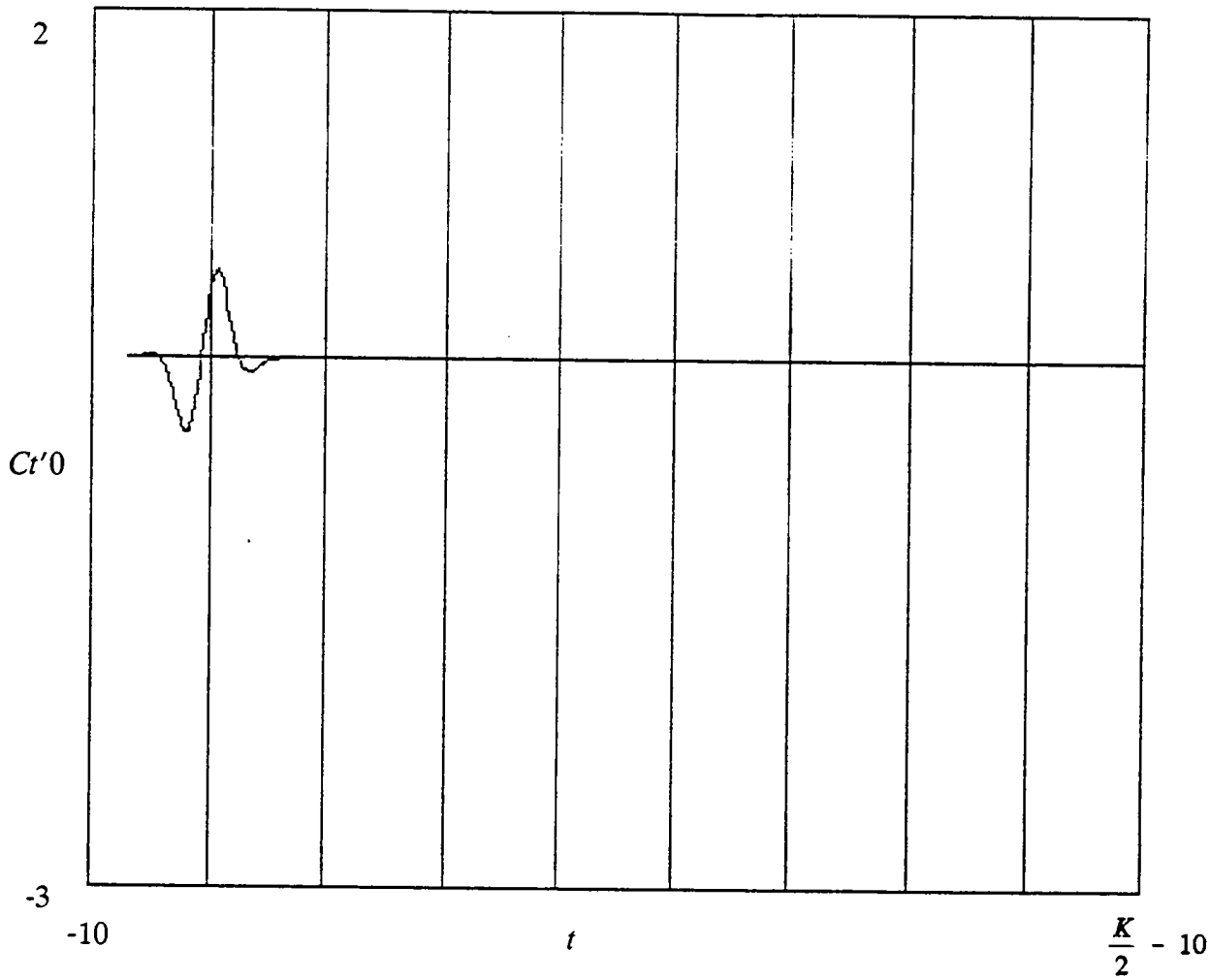

Time (nanoseconds, 0.5 nsec/division)

ϵ_1	= 5.13 + 0.11i	Asphalt layer: porosity = 10%, moisture content = 2%
ϵ_2	= 1	Air gap thickness = d_2 = 0.1 cm
ϵ_3	= 5.13 + 0.11i	Asphalt layer
R	= 0.067	Thin layer reflection coefficient

Figure 3.17. Reflection due to an air-filled delamination in asphalt—gap thickness, 0.1 cm.

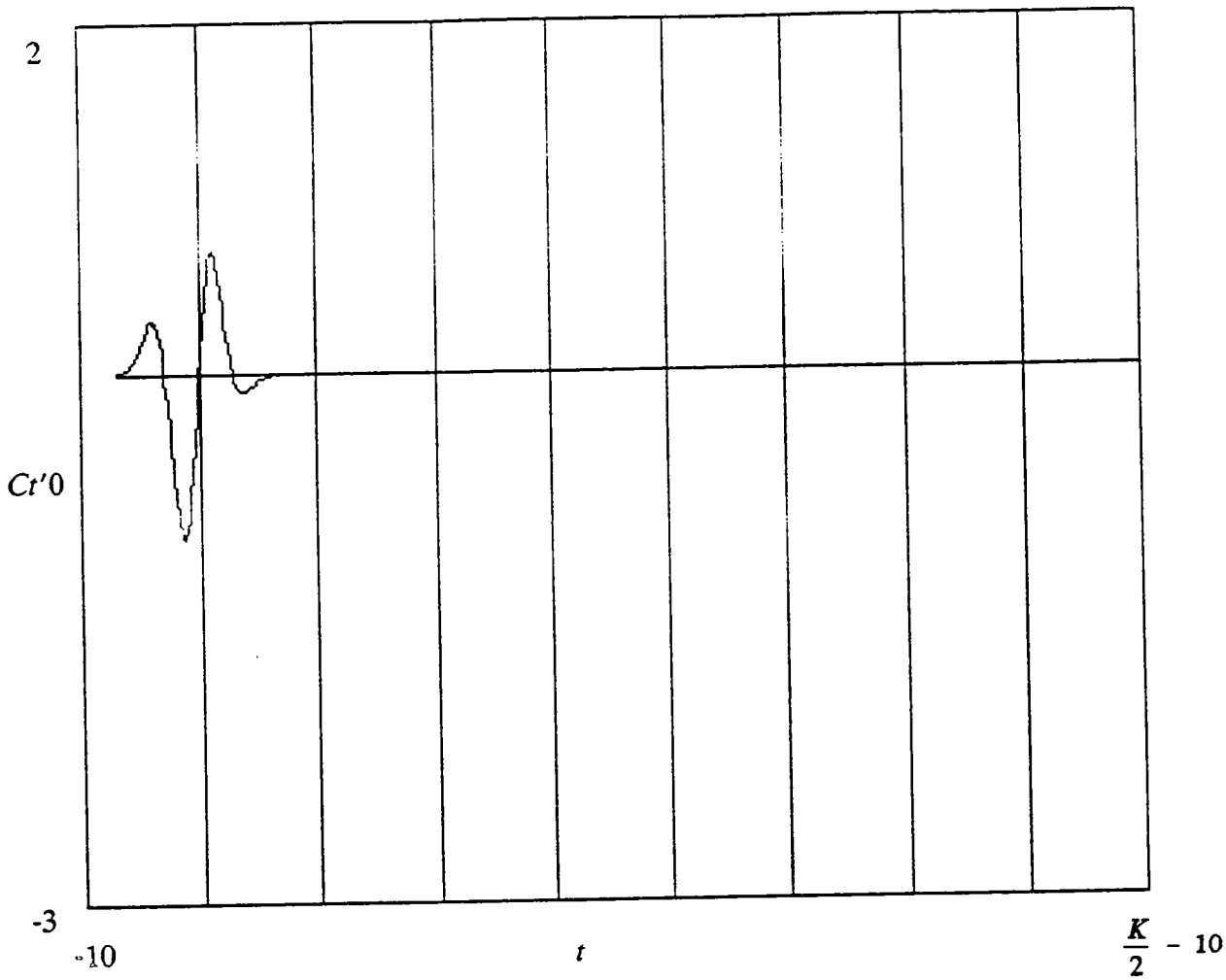

Time (nanoseconds, 0.5 nsec/division)

ϵ_1	= 5.13 + 0.11i	Asphalt layer: porosity = 10%, moisture content = 2%
ϵ_2	= 1	Air gap thickness = d_2 = 0.2 cm
ϵ_3	= 5.13 + 0.11i	Asphalt layer
R	= 0.118	Thin layer reflection coefficient

Figure 3.18. Reflection due to an air-filled delamination in asphalt—gap thickness, 0.2 cm. Note the phase reversal in the reflection.

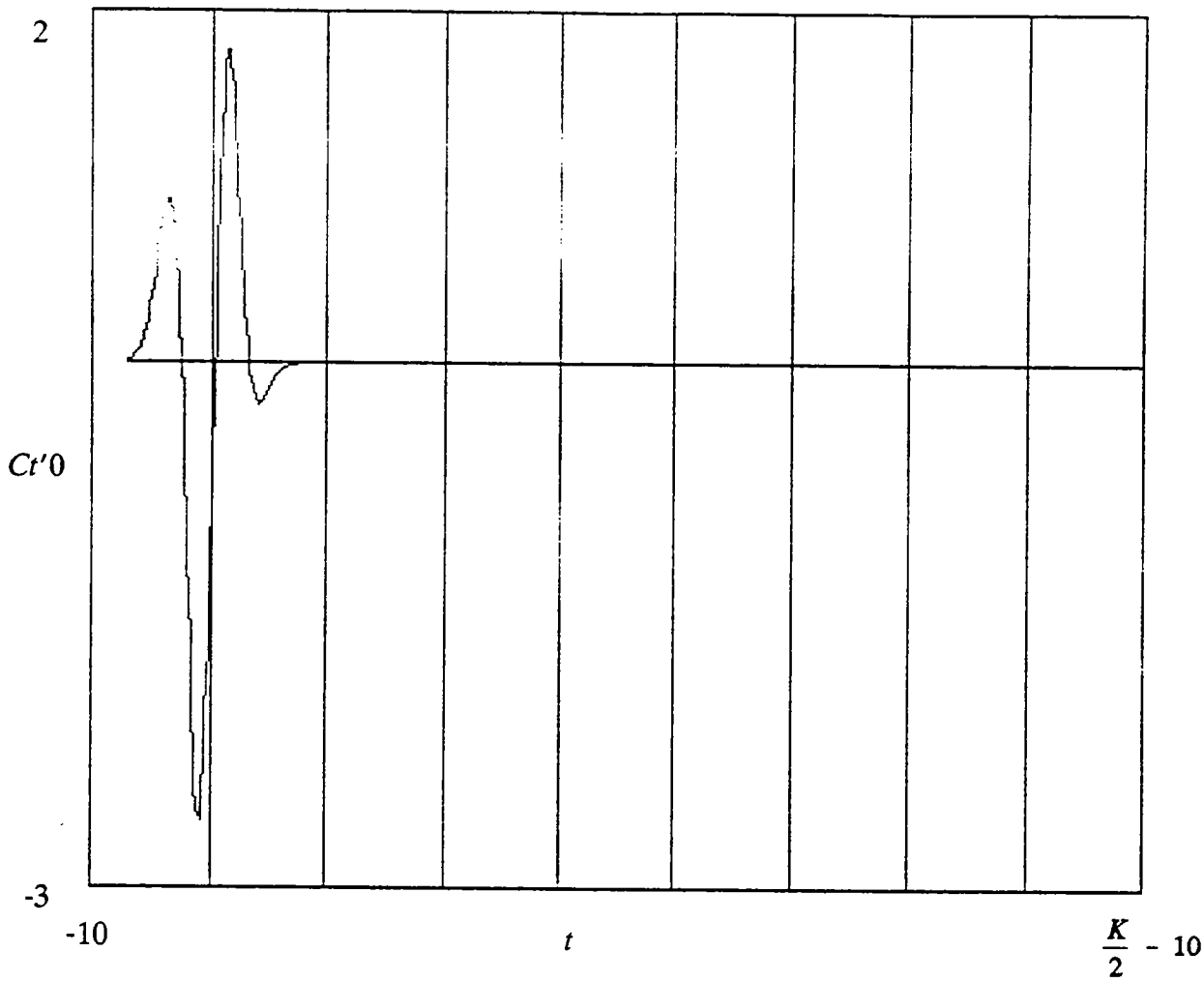

Time (nanoseconds, 0.5 nsec/division)

ϵ_1	= 5.13 + 0.11i	Asphalt layer: porosity = 10%, moisture content = 2%
ϵ_2	= 1	Air gap thickness = d_2 = 0.6 cm
ϵ_3	= 5.13 + 0.11i	Asphalt layer
R	= 0.314	Thin layer reflection coefficient

Figure 3.19. Reflection due to an air-filled delamination in asphalt—gap thickness, 0.6 cm. Note the phase reversal in the reflection.

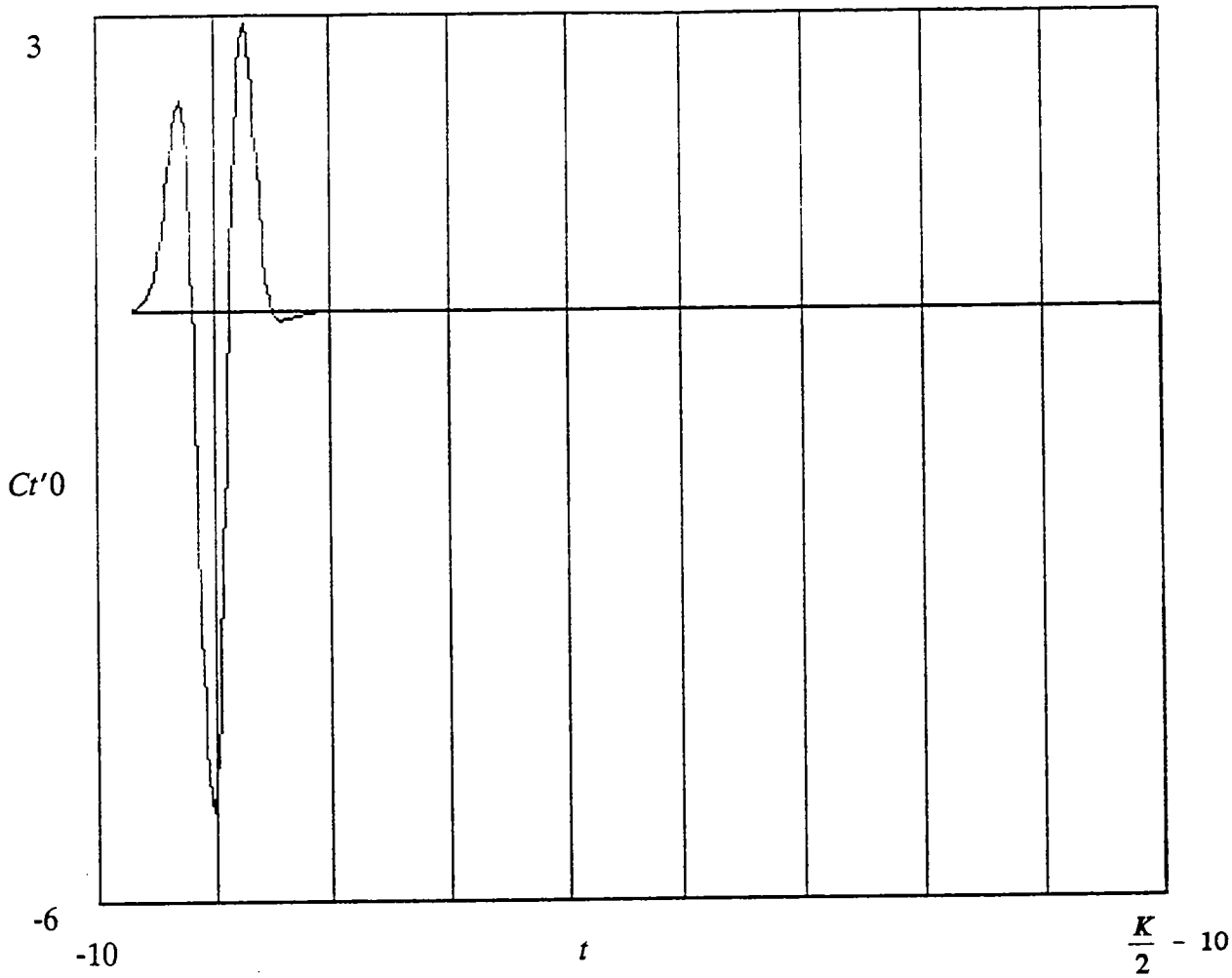

Time (nanoseconds, 0.5 nsec/division)

ϵ_1	= 5.13 + 0.11i	Asphalt layer: porosity = 10%, moisture content = 2%
ϵ_2	= 1	Air gap thickness = d_2 = 2 cm
ϵ_3	= 5.13 + 0.11i	Asphalt layer
R	= 0.573	Thin layer reflection coefficient

Figure 3.20. Reflection due to an air-filled delamination in asphalt—gap thickness, 2 cm. Note the phase reversal in the reflection.

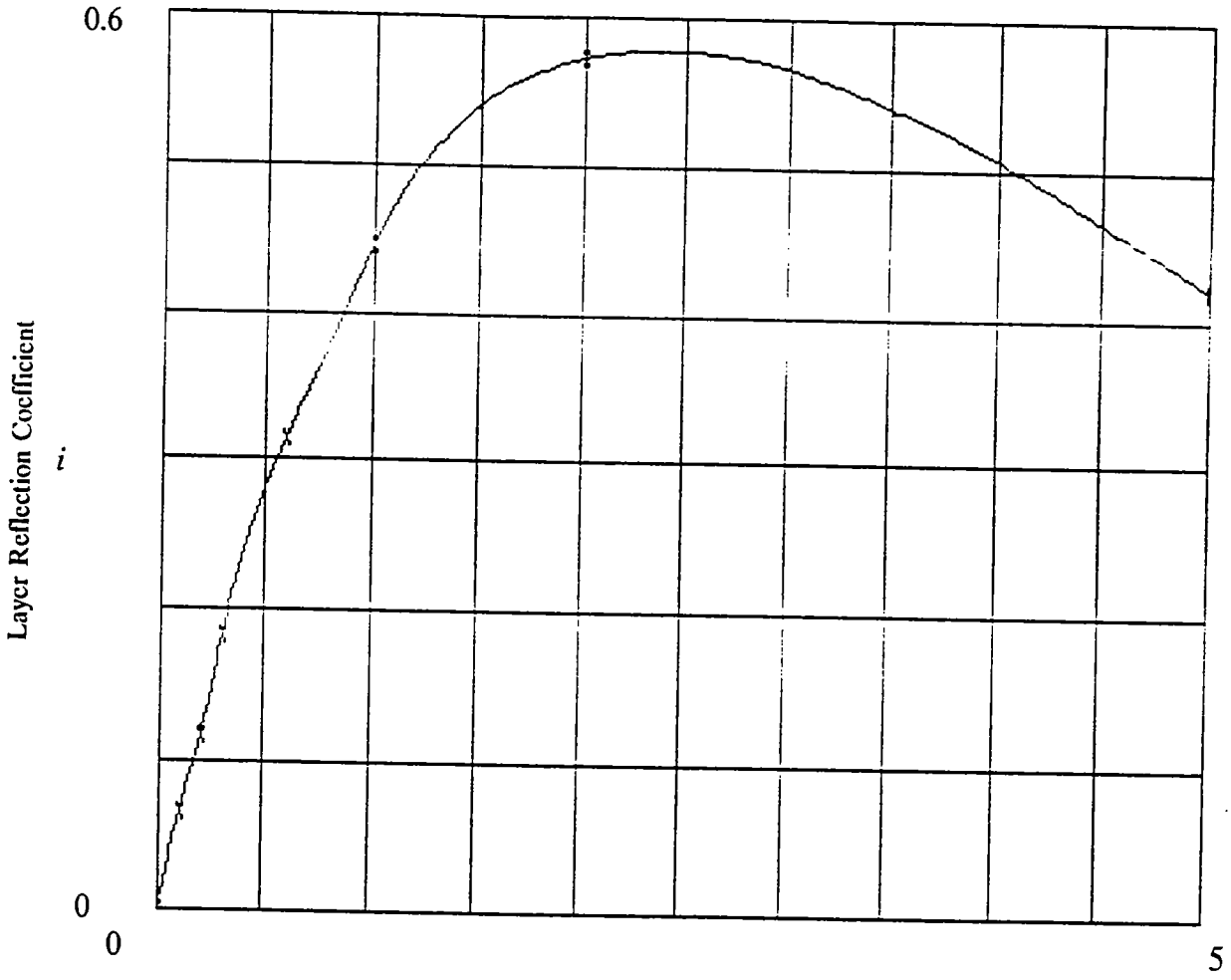

Asphalt porosity = 10%
Moisture Content = 2%

Figure 3.21. Plot of the reflection coefficient due to a air-filled delamination in asphalt versus the gap thickness

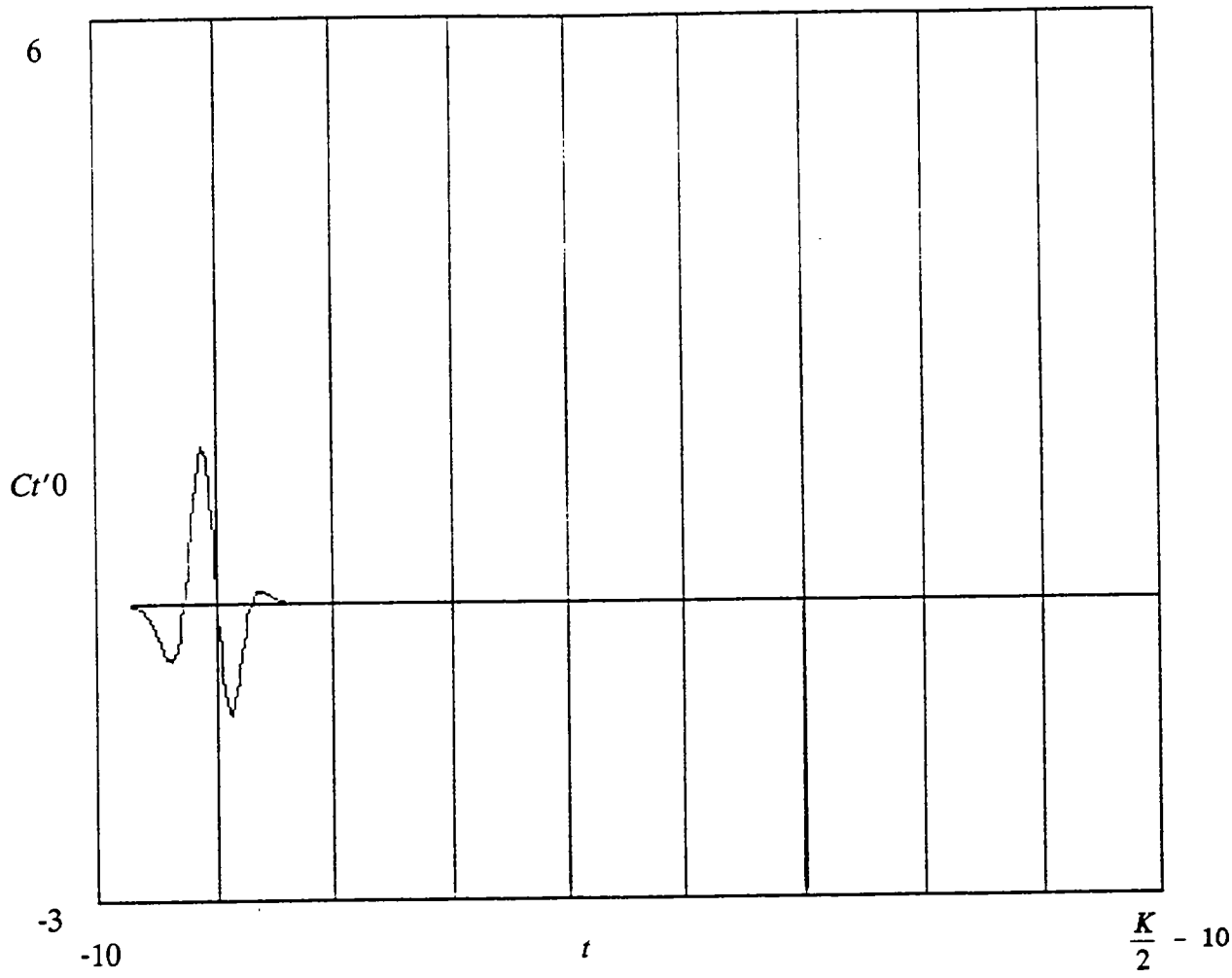

Time (nanoseconds, 0.5 nsec/division)

ϵ_1	= 5.13 + 0.11i	Asphalt layer: porosity = 10%, moisture content = 2%
ϵ_2	= 75.6 + 8.2i	Water gap thickness = d_2 = 0.02 cm
ϵ_3	= 5.13 + 0.11i	Asphalt layer
R	= 0.196	Thin layer reflection coefficient

Figure 3.22. Reflection due to an water-filled delamination in asphalt—gap thickness, 0.02 cm

ϵ_1	= 5.13 + 0.11i	Asphalt layer: porosity = 10%, moisture content = 2%
ϵ_2	= 75.6 + 8.2i	Water gap thickness = d_2 = 0.05 cm
ϵ_3	= 5.13 + 0.11i	Asphalt layer
R	= 0.429	Thin layer reflection coefficient

Figure 3.23. Reflection due to an water-filled delamination in asphalt—gap thickness, 0.05 cm. Note that there is no phase reversal in the reflection.

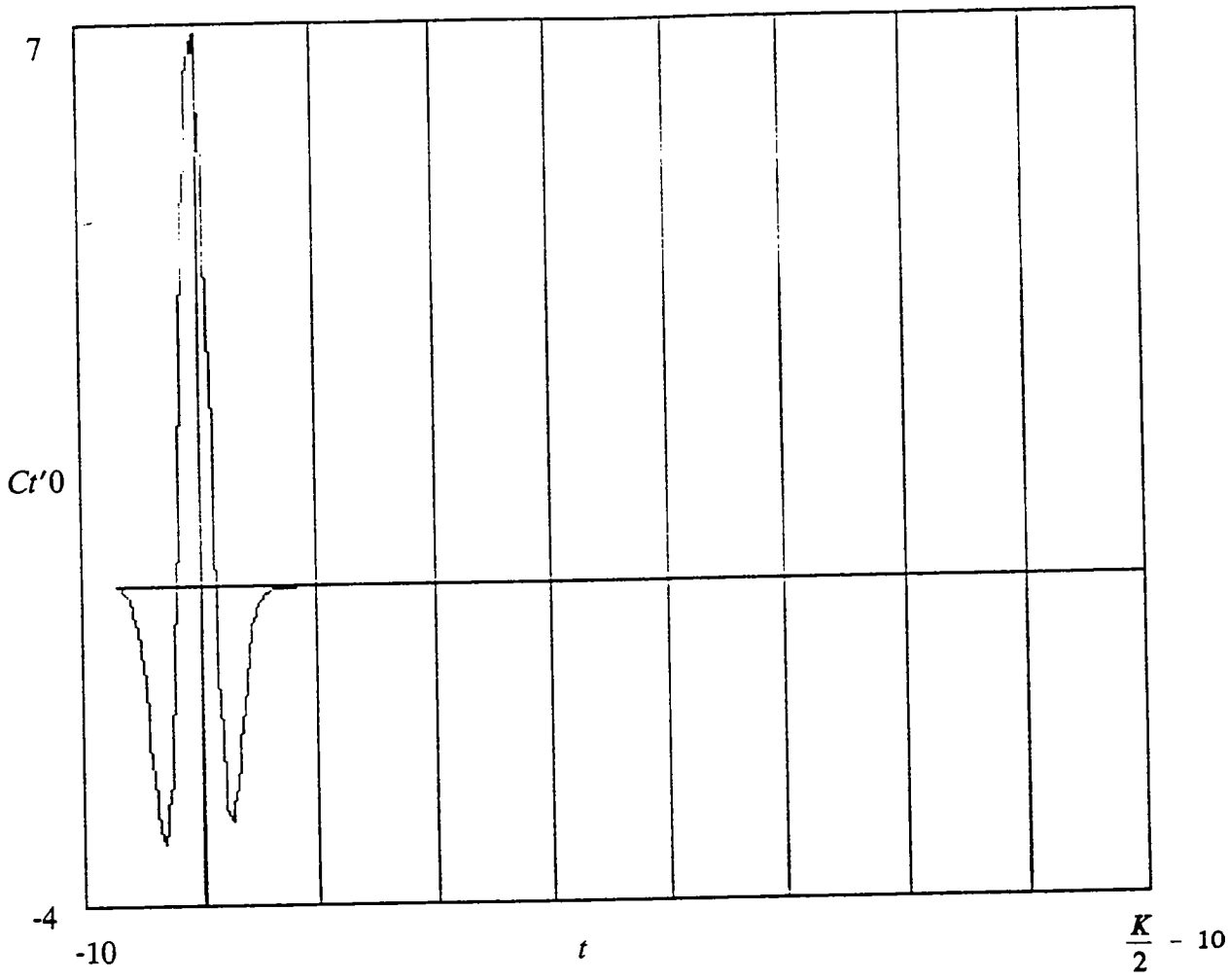

Time (nanoseconds, 0.5 nsec/division)

ϵ_1	= 5.13 + 0.11i	Asphalt layer: porosity = 10%, moisture content = 2%
ϵ_2	= 75.6 + 8.2i	Water gap thickness = d_2 = 0.2 cm
ϵ_3	= 5.13 + 0.11i	Asphalt layer
R	= 0.722	Thin layer reflection coefficient

Figure 3.24. Reflection due to an water-filled delamination in asphalt—gap thickness, 0.2 cm.

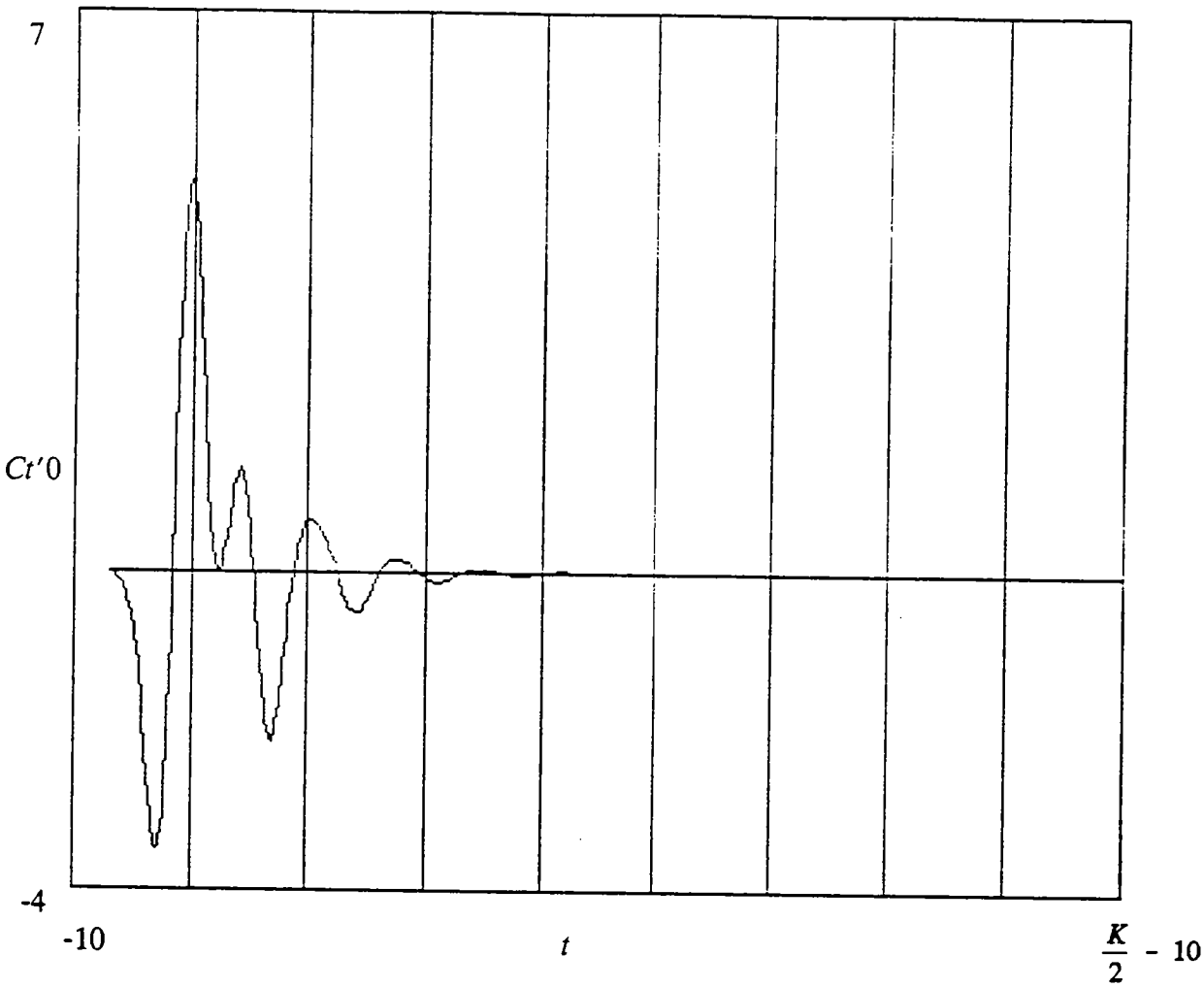

ϵ_1	= 5.13 + 0.11i	Asphalt layer: porosity = 10%, moisture content = 2%
ϵ_2	= 75.6 + 8.2i	Water gap thickness = d_2 = 0.6 cm
ϵ_3	= 5.13 + 0.11i	Asphalt layer
R	= 0.599	Thin layer reflection coefficient

Figure 3.25. Reflection due to an water-filled delamination in asphalt—gap thickness, 0.6 cm. Note that the reflections from the top and bottom of the gap are becoming distinct.

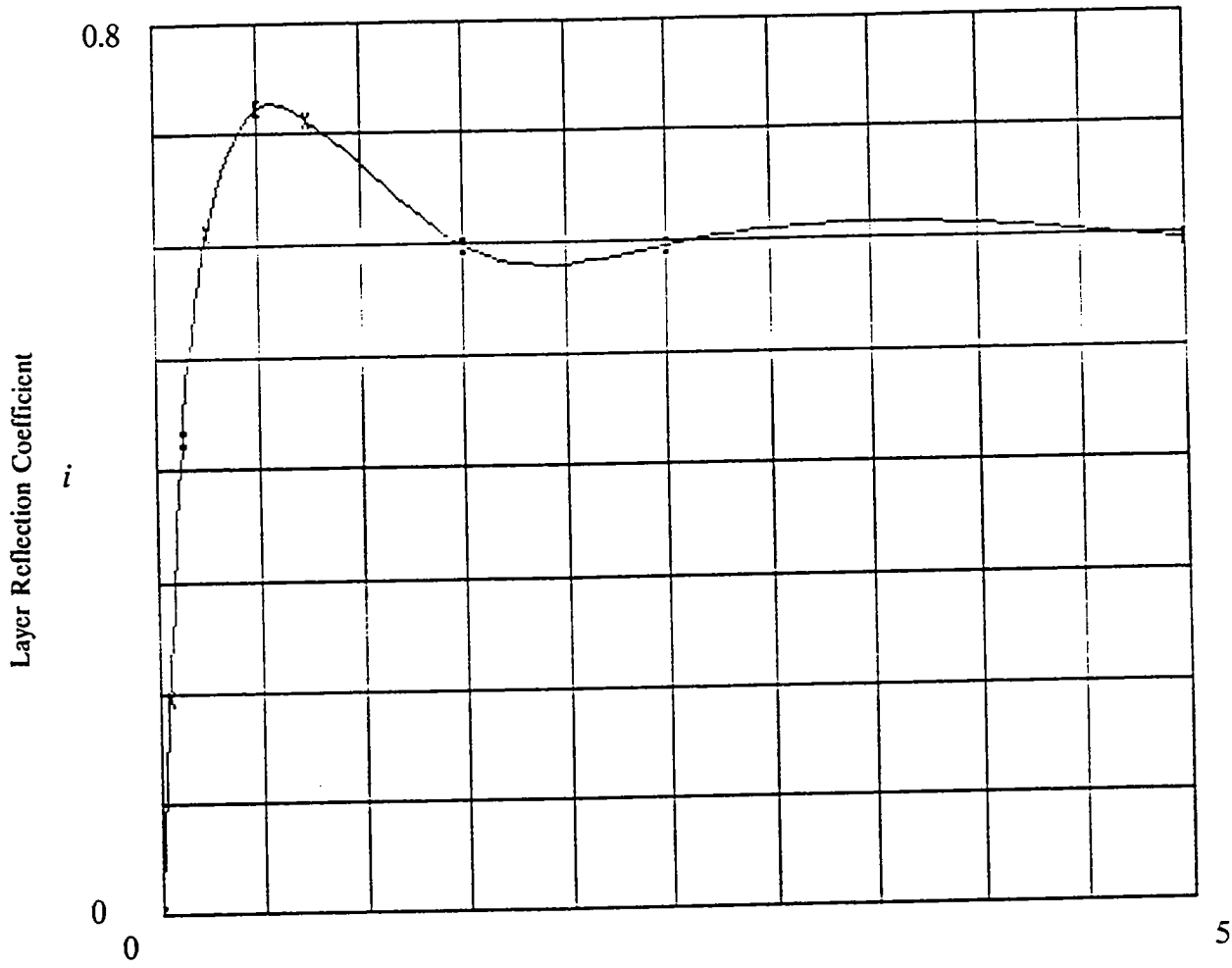

Asphalt porosity = 10%
Moisture Content = 2%

Figure 3.26. Plot of the reflection coefficient due to a water-filled delamination in asphalt versus the gap thickness

4

Equipment Description

The research team specified, designed, fabricated, and tested three successive ground-penetrating radar (GPR) systems in the course of the project. The first was the breadboard system, which could take stationary measurements to show proof of concept. The second system, known as the first-generation prototype, brought new technologies together around the Subsurface Interface Radar System-10 (SIR-10) was capable of stationary and moving measurements. The final system, or second-generation prototype, overcame many of the speed and noise limitations of the previous systems. Section 5 describes the development process of the GPR systems.

Each of these systems consisted of similar components. The major parts were the antennas, the transmitting and receiving electronics, and the control unit. The antennas transmitted and received the electromagnetic energy. The transmitting electronics determined the frequency of the pulse fed into the transmitting antenna. The receiving electronics sampled the signals returning from the receiving antenna. The control unit controlled the transmitting and receiving electronics, displayed the data, and stored the data for subsequent processing.

The final system had the antennas installed on a trailer. By using this setup it was possible to collect data on in-service highways in Texas and Georgia at close to highway speed. In addition, the prototype showed very good results in laboratory tests.

4.1 1.0- and 2.5-GHz Antennas

With any GPR system, there is a trade-off between resolution and depth of penetration. Higher-frequency antennas have higher resolution—that is, they can distinguish thin layers that lower-frequency antennas cannot. The 2.5-GHz antenna can resolve layers as thin as 2.5 cm (1 in.) without additional signal processing. For the 1-GHz antenna, the layer must be thicker than 7.5 cm (3 in.) for independent reflections to be observed. As a result, the 2.5-GHz antenna will be most effective in near-surface applications, such as measuring the thickness of the top layer or identifying stripping within the asphalt. The

1.0-GHz antenna will be more useful for deeper evaluations—for example, locating voids under rigid pavements—because lower-frequency signals are not attenuated as fast and therefore penetrate deeper.

4.2 Digital Acquisition System

The antennas and electronics were digitally controlled by a SIR-10 made by Geophysical Survey Systems, Inc. (GSSI). These digital systems allowed quantitative results for multichannel operation with digital tape storage. Interfacing the SIR-10 with a survey wheel provided distance control of the data, so that data could be collected at user-defined fixed distance intervals. These features made the SIR-10 an appropriate research tool.

However, at the high 2.5-GHz signals, problems were discovered that necessitated further development of the SIR system. The first-generation prototype used a standard SIR-10, which suffered from unacceptable jitter levels. This noise could be reduced by averaging successive radar traces, but only during stationary or very slow-moving measurements. Because this restriction was not acceptable, GSSI designed a new radar system, the SIR-10A, which was quieter and faster.

The laboratory and field testing indicated that to meet the requirements of the Strategic Highway Research Program, the SIR system would require improvement in two major areas:

1. The time jitter of the radar board must be reduced.

2. The transmit rate must be increased.

To those ends, the input data rate was increased approximately 16-fold by using two newly designed radar boards. The output data rate was increased from 20 to 100 scans/sec (for 4 channels, 256 samples/scan, 8-bit samples).

Accordingly, the performance of the second-generation prototype was found to be much improved. The jitter was reduced by a factor of 10 compared to the earlier SIR-10.

5

Equipment Development

5.1 Breadboard System

The breadboard system consisted of readily available components, except for the 2.5-GHz antennas, for which there was no source. No previous ground-penetrating radar (GPR) systems could operate above 1 GHz.

The 2.5-GHz transducer transmits and receives the radar signals through one or more antenna. The design goal for the antennas was to allow them to operate off the ground and pass the signals cleanly. It was important to maintain *pulse fidelity*—the ability of a device such as an antenna to allow signals to pass through unaffected. With the antenna design, the antenna's ability to radiate and receive the 2.5-GHz pulse was our design constraint. If the antenna had poor pulse fidelity, it would introduce spurious signals into the data, known as ringing, or clutter.

Antenna

To operate with the antenna off the pavement, it was desired to have the output impedance of the antenna match that of air. The impedance of air is 377 ohms. As a result, the design became a transverse electromagnetic horn. The design was characterized by varying impedance from the feed point at the top of the antenna to the end point. At the feed point, where the antenna connected to the system cable, the impedance was 50 Ohms. Therefore, the antenna should change in impedance from 50 to 377 ohms. The better this transition was accomplished, the less adverse affect these connections would have on signals passing through them.

Transmitter

The system required a 2.5-GHz monocycle generator, which was obtained from Avtech, Ltd. of Canada. The device specifications follow:

Pulse shape:	Monocycle
Pulse width:	0.4 nsec
Frequency:	2.5-GHz
Output signal amplitude:	16 V peak to peak
Pulse repetition rate:	10 MHz

Receiver

For the breadboard study, a Tektronix sampling oscilloscope was used for receiving the GPR return signal. A Model 7613 with a Model S-6 sampling head was used. Using this configuration, the receiver would sample frequencies as high as 11.5 GHz—more than adequate for the 2.5-GHz pulse. The design team from Geophysical Survey Systems, Inc. (GSSI) assumes that to maintain pulse fidelity, the actual prototype system would have a receiver able to sample up to 6 GHz.

Another consideration was the cables used to carry the 2.5-GHz signal to and from the antenna. The cable suitable for 1.0-GHz and lower signals would have too much signal loss to carry the 2.5-GHz signal adequately. Therefore, the breadboard tests were performed with low-loss cables.

Acquisition System

The research team was able to feed the signals from the sampling oscilloscope into a Subsurface Interface Radar (SIR-10) for digital storage. In addition, a second Tektronix scope, with analog-to-digital (A/D) capabilities, was used to digitize the GPR return signals for later processing. Figure 5.1 is a block diagram of the breadboard system.

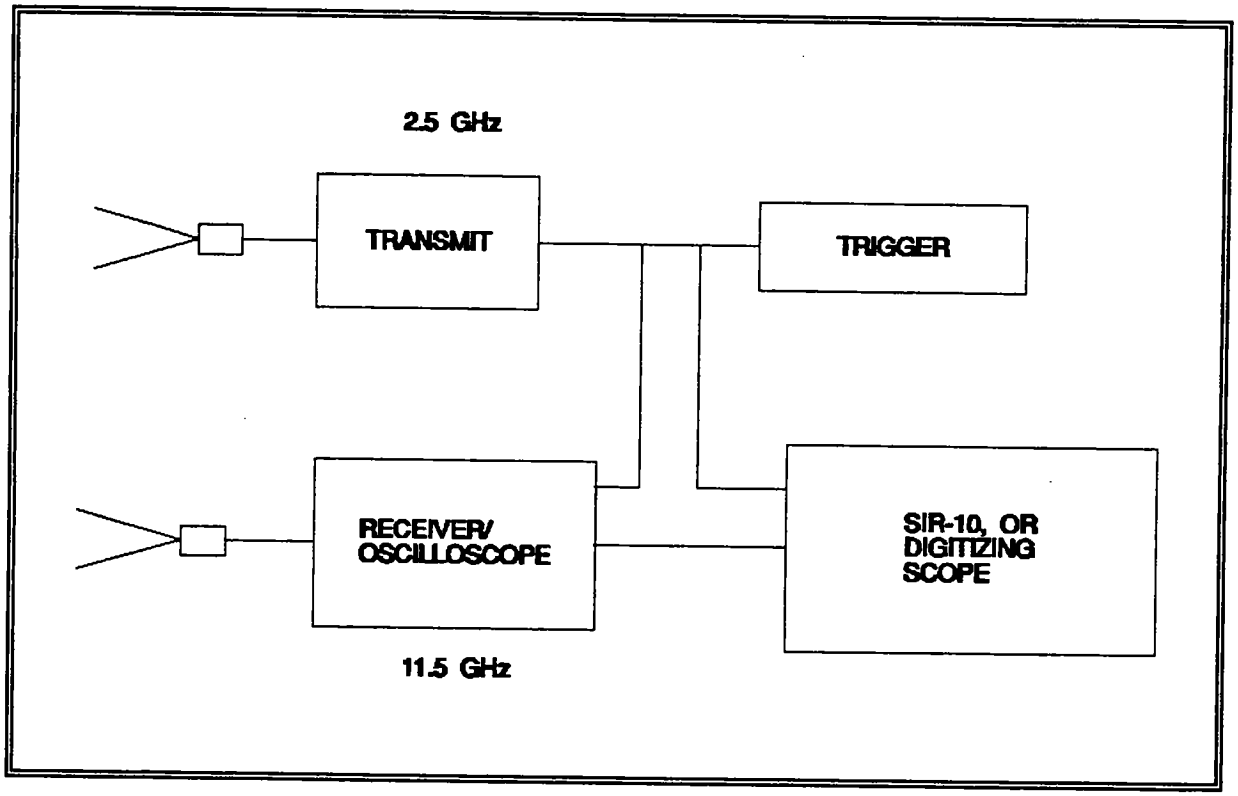

Figure 5.1. Block diagram of breadboard prototype

Breadboard System Performance

The breadboard system showed promise even though it suffered from noise problems. Two kinds of noise contributed to the problems: clutter and jitter.

Clutter is unwanted coherent signal. An unwanted signal that is always found at the same time is considered clutter. An example would be a reflection from the end of an antenna. The breadboard system did have clutter caused by electrical mismatches in its circuitry and cabling. This clutter would have to be reduced to make the prototype useful in field tests.

Jitter is random noise that significantly degrades signal quality. The jitter was generated in the sampling process. Variations in the timing of the transmitter and receiver electronics caused unpredictable changes in the signal amplitude. The jitter can be reduced by averaging successive traces, but the antennas should be stationary while the average is being taken, and the resultant trace will have a slightly lower frequency than the originals.

Although there was noise in the system, the study showed that there was potential for a prototype system to satisfy some of the project objectives.

5.2 First-Generation Prototype

The research team looked at the problems of the breadboard system, then specified the first-generation prototype.

Components

The antennas for the 2.5-GHz system were modified to reduce their contribution to the clutter. Also, a first attempt was made at building the 1.0-GHz antennas. They were a scaled-up version of the 2.5-GHz antennas.

The transmitting electronics for the 2.5- and 1.0-GHz systems were monocycle generators, again supplied by Avtech. The 1.0-GHz transmitter's specifications follow:

Pulse shape:	Monocycle
Pulse width:	1.0 nsec
Output signal amplitude:	20 V peak to peak
Pulse repetition rate:	Up to 1 MHz

The receiving electronics were to become a very important component of the prototype system. The receiver for the 2.5-GHz system was designed and built by Cambridge Consulting, Ltd. (CCL). It replaced the sampling oscilloscope. For the 1.0-GHz system, a standard GSSI sampler was used.

With these components, a GSSI SIR-10 could be used in place of the digital oscilloscope used in the breadboard testing of phase I. Figure 5.2 is a block diagram of the first-generation prototype. Figure 5.3 is a photograph of the SIR-10.

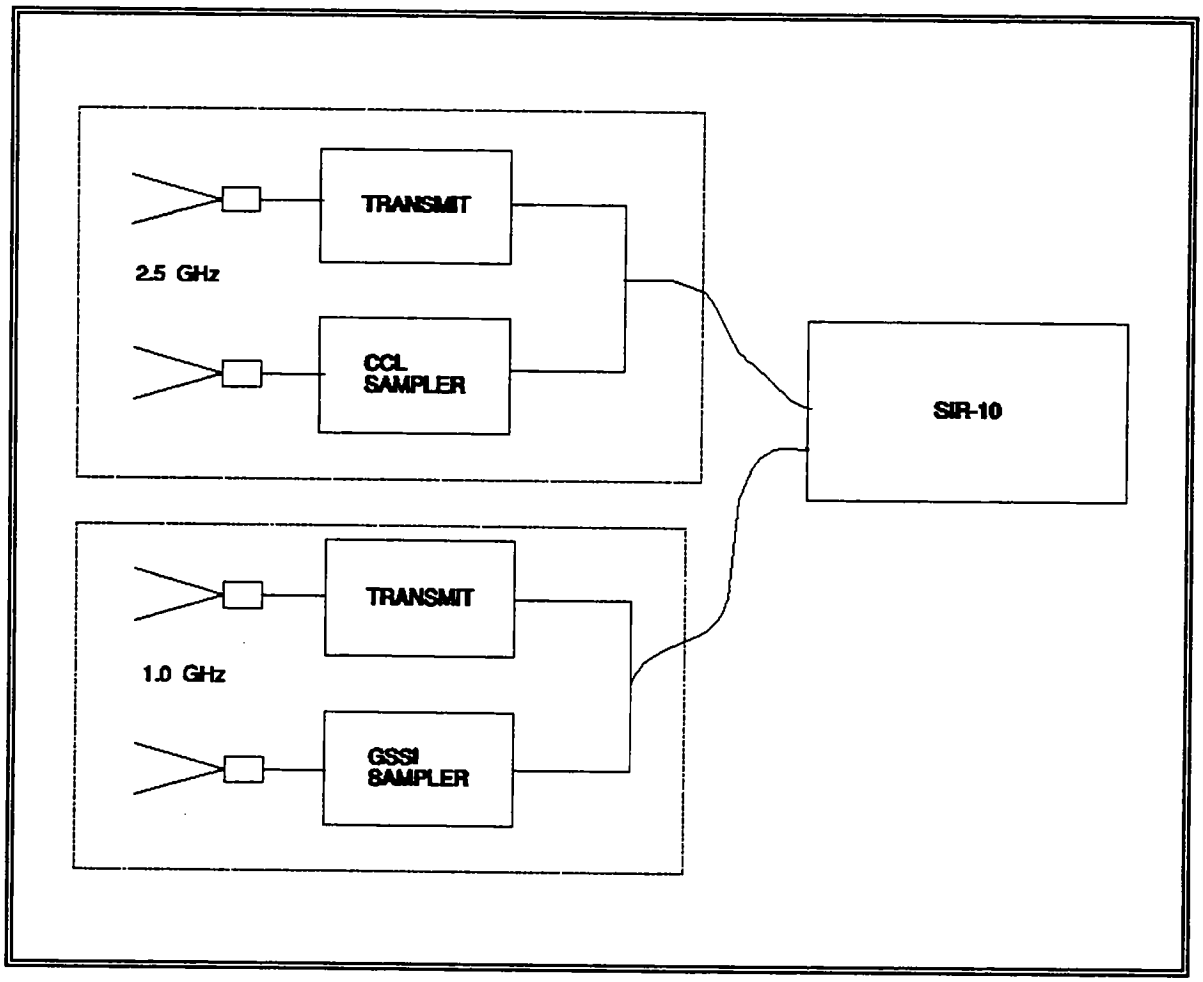

Figure 5.2. Block diagram of first-generation prototype

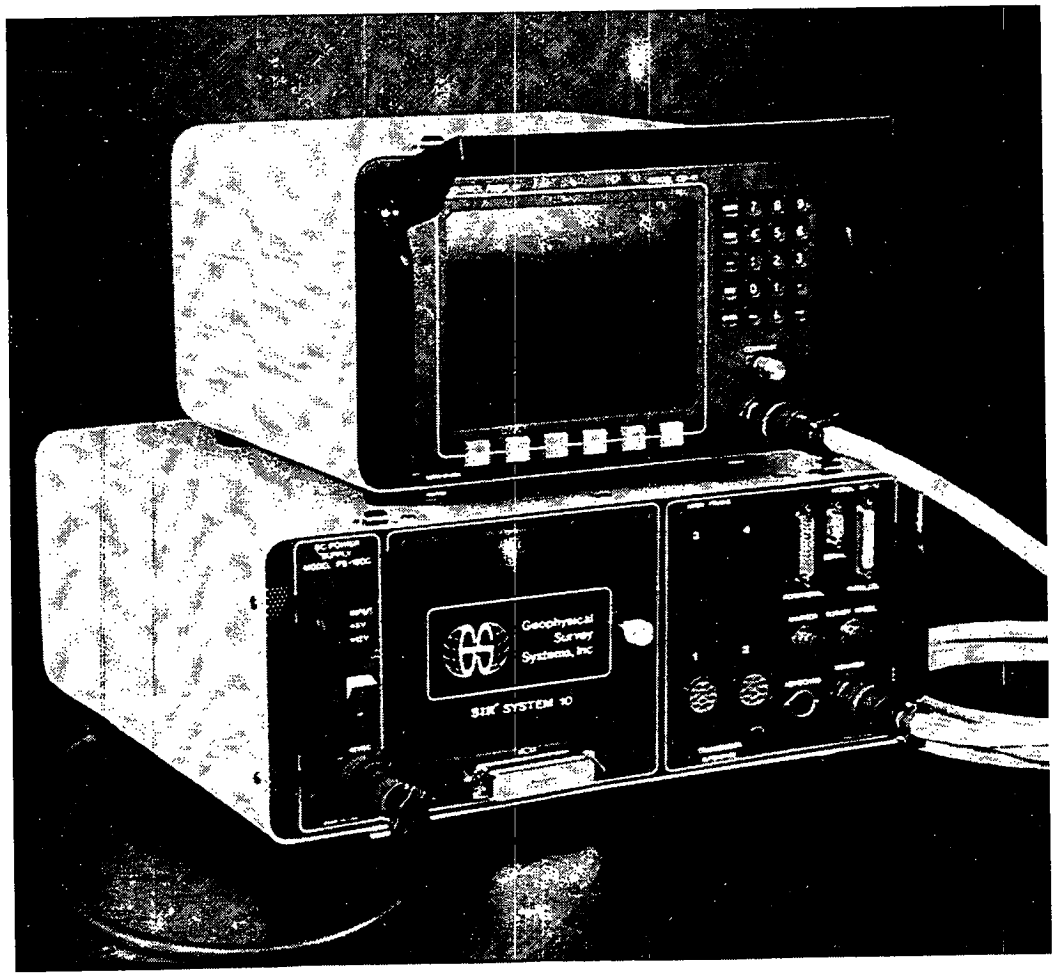

Figure 5.3. SIR-10 used to control the 1.0- and 2.5-GHz antennas and store the digital data for later analysis

Performance

The system performed better than the breadboard but was not without its own problems. At 2.5-GHz, the jitter was reduced, but still present. The source of this noise was found to be the SIR-10. There was clutter on the 1.0-GHz radar signal, which was found to be caused by the GSSI sampler and the antennas. The clutter was reduced by changing to the CCL sampler, but the antennas needed a little more work.

The first-generation prototype was subjected to stationary testing at the University of Texas at El Paso test facility and to moving tests on in-service roads in Texas. These tests were moderately successful. The 2.5-GHz transducer performed well, the 1.0-GHz transducer had problems. The jitter from the SIR-10 prevented the 2.5-GHz transducer from being used at highway speeds. The 1.0-GHz transducer still suffered from internal ringing.

5.3 Second-Generation Prototype

Components

The tests in Texas showed that the antennas needed minor changes. The research team agreed to reduce the level of the end reflection to below the level of a metal plate reflection. The antennas were given housings and mounted on a fiberglass and plastic trailer for the moving measurements. (Fiberglass and plastic affect radar signals less than metal would.)

Only minor changes were necessary to reduce jitter. In the transmitter, the sampler for the 2.5-GHz system was manufactured by GSSI, unlike the units employed in the first-generation prototype, which were delivered by CCL. A significant amount of jitter had been identified as coming from a direct current - direct current power converter in the electronics, which was eliminated. Additional jitter measurements were made on the electronics to verify that their jitter was less than that of the SIR-10.

Similar efforts were directed at the 1.0-GHz electronics. The phase II tests indicated the 1.0-GHz needed work. The sampler was a source of clutter on the 1.0-GHz signals. This noise was eliminated in the phase III prototype using the CCL sampler.

For convenient use in the field, we designed a trailer for deploying the antennas. A fifth wheel provided distance information to the SIR-10. The research team feels that with some minor changes the trailer will be a good platform for mounting the antennas. Figure 5.4 is a drawing of the antenna trailer.

Figure 5.5 is a block diagram of the second generation prototype.

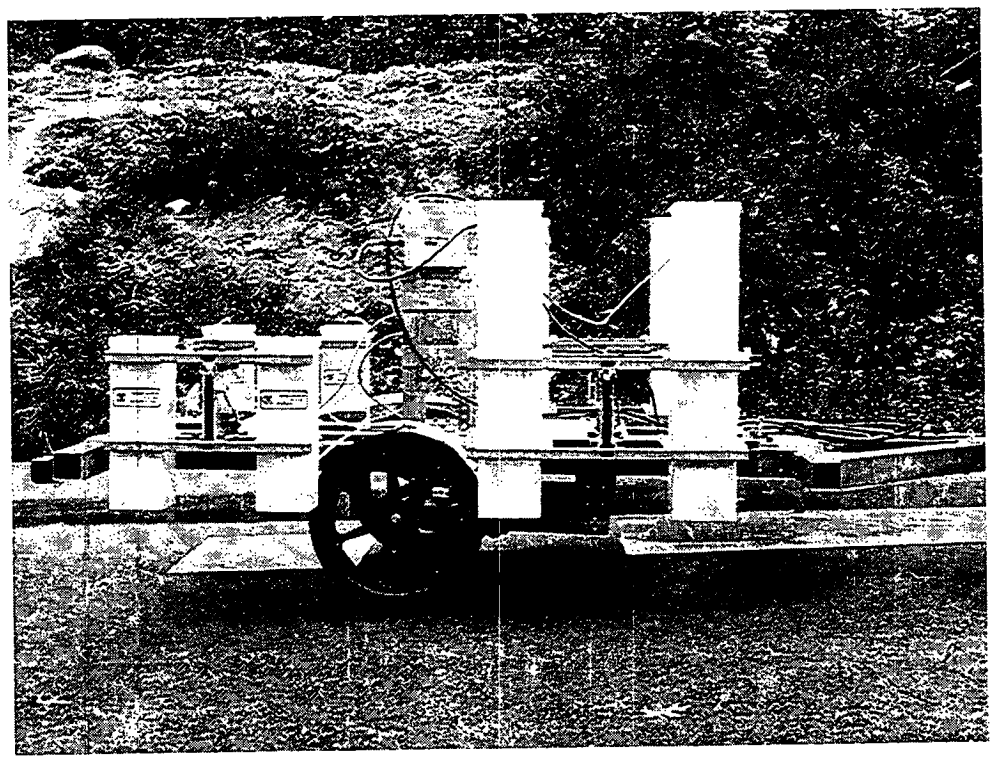

Figure 5.4. Antenna trailer carrying four sets of TEM horns. The larger antennas to the right are 1.0-GHz antennas. On the left are the smaller 2.5-GHz antennas. The transmitting and receiving electronics are on the tower in the center of the trailer.

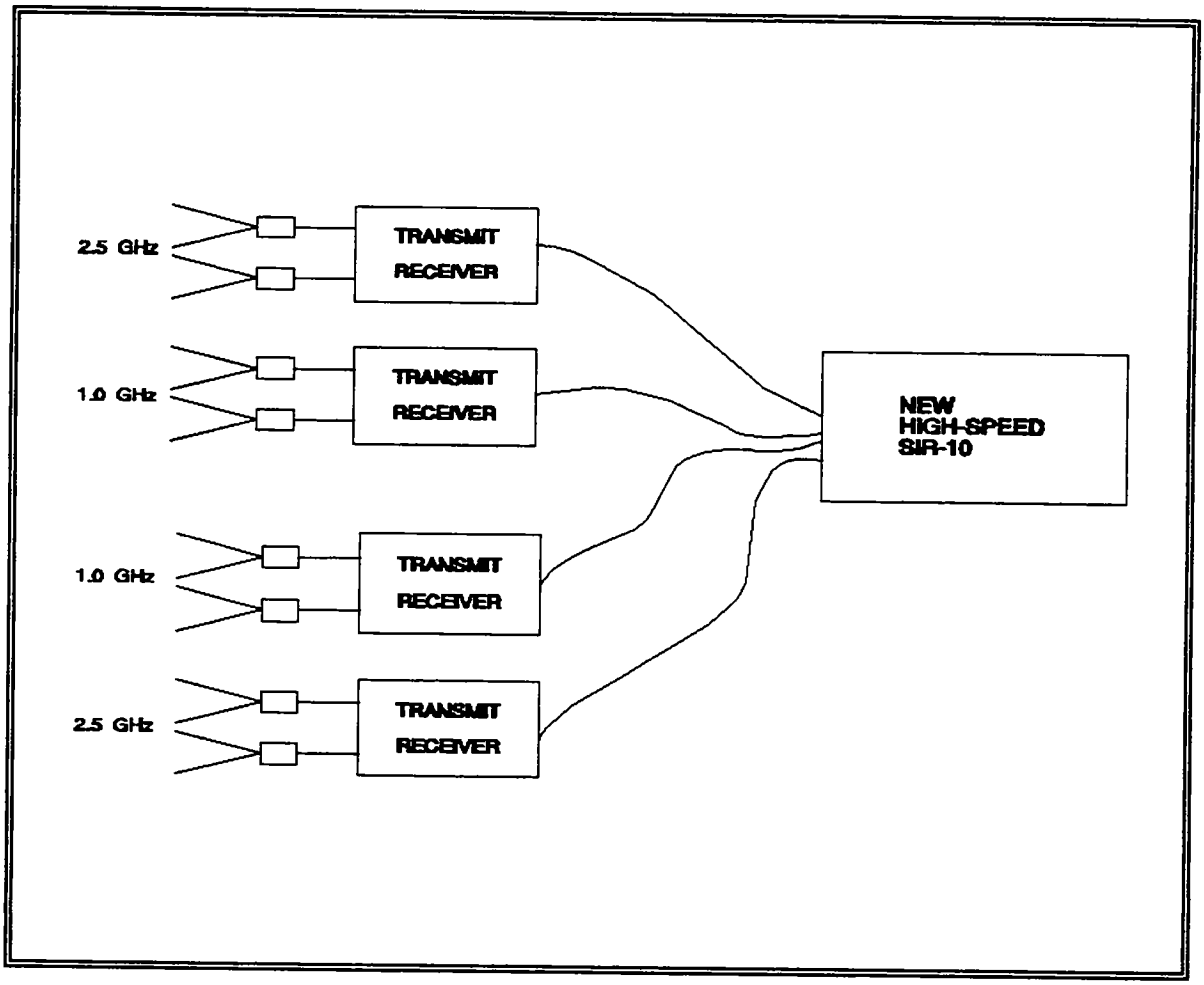

Figure 5.5. Block diagram of second-generation prototype

The final component was the SIR-10. The SIR system had to be redesigned to provide the measurement speed and accuracy associated with the 2.5-GHz transducer. In phase II, testing indicated that to meet the requirements of the Strategic Highway Research Program, the SIR system should be improved in two main areas:

1. The time jitter of the radar board must be reduced.
2. The transmit rate must be increased.

To those ends, the radar board was redesigned. The transmit rate was increased in the following ways:

1. By using a faster A/D converter.
2. By increasing the processing capability of the digital signal processor by
   a. raising its speed from 20 to 40 MHz and
   b. offloading some operations into hardware:

i. input stacking,
ii. first in-first out interface (faster than SKY interface), and
iii. some sampler control functions.

3. By using two radar boards in parallel. Dual-port memory must now eliminate the SKY array processor board, which will now be a bottleneck.

The input data rate of the system was increased by a factor of 8, from 50 kHz to 400 kHz, with one board. On the later two-board system, the data rate was 800 kHz. The output data rate was increased from 20 to 100 scans/sec (for 4 channels, 256 samples/scan, 8-bit samples).

The time jitter was reduced by

1. better isolating the critical timing circuits on the ground-plane islands,
2. locating all critical circuits together,
3. better regulating the local power supply,
4. eliminating noisy power buffers,
5. minimizing the number of crystals to minimize random noise,
6. eliminating sockets for the fast emitter-coupled logic chips, and
7. better locating circuit subsections.

Table 5.1 is a comparison of performance of the old SIR-10 with the newly developed SIR-10A.

Table 5.1
System Performance Comparison between the SIR-10 and the New SIR-10A.

	SIR-10A*	SIR-10	Units
Range	0-1000	0-32000	nsec
Hardware accumulator	1-256	N/A	steps
Transmit rate	2-800	2-78	kHz
Max input data word rate	800	78	kHz
Max output data word rate	100	20	kHz
Max A/D rate	1000	100	kHz
A/D resolution	12	16	bits
Pseudo-random transmit rate	hardware	software	
Delay control to 2nd board	0.5	N/A	μSec

* Assumes two radar boards
N/A = Not Applicable

Besides to the radar board changes, the system was modified as follows:

1. The EXB-8200 digital tape drive was replaced by the faster EXB-8500, and the maximum storage was increased from 2.5 gigabytes to 5 gigabytes.
2. The EGA monitor was replaced by a VGA monitor, which had higher resolution.
3. A built-in hard disk and Number Smasher were added to facilitate post processing.
4. There were some modifications to the transducer interface modules.

Performance

The performance of the second- generation prototype was much improved. The jitter as reduced by a factor of 10 compared to the old SIR-10. The antennas now had an acceptable clutter level. The sampler electronics produced some clutter, but it was eliminated.

6

Interpretation Software Development

A very important aspect of the development effort was the implementation of an automatic data-interpretation system to relieve the operator of the burden of data interpretation. The system could now give the maintenance engineer information on pavement condition instead of just radar signals.

The research team worked on forward modeling, neural networks (NNs) and signal-processing technology as methods of automatic data interpretation. The forward modeling provided synthetic radar traces to help the research team understand how the physical parameters of the pavement would affect radar signals. This modeling also provided simulated data for other processing requirements, saving the field expenses and time. The NNs and the signal-processing methodologies were two alternative approaches to automatic data interpretation.

6.1 Forward Modeling

Computer interpretation of ground penetrating radar (GPR) data was a key goal of the Strategic Highway Research Program (SHRP) highway maintenance measuring equipment program. An NN was trained for automatic GPR interpretation. During the prototype development of the computer software, it became evident that we could not collect enough real-world radar scans of various pavement conditions to properly train an NN. Therefore, we decided to use a combination of real radar scans and model radar scans. Model radar scans were generated that very closely approximated measured GPR scans. Figure 6.1 is an example of a measured scan from 30 cm (12 in.) of asphalt pavement; the Subsurface Interface Radar System-10 (SIR-10) GPR was used for the scan. Figure 6.2 is an example of model data superimposed on radar data; a digital storage oscilloscope was used for radar display.

Once an acceptable model scan was mathematically created, the desired pavement parameters were varied to generate a range of maintenance conditions—for example,

voids of different thickness under portland cement concrete (PCC) pavement or excessive moisture under asphalt pavement.

Model data was calculated for air voids under 15 cm (6 in.) of concrete, with the void thickness varying from 0 to 2.5 cm (0 to 1 in.) in 0.16 cm (1/16-in.) increments. Random noise (both high-frequency "impulsive" noise and low-frequency clutter) was added to the model data to more accurately simulate real GPR data (figure 6.3). The simulated radar data were used to train the NN, and additional simulated data were created to test it. The limited available real radar data were also used to test the network. These tests were successful, (figures 6.4 and 6.5).

Figure 6.4 represents a simulated radar profile of 15 cm (6 in.) of concrete over a base material where three voids have developed beneath the slab. The void thicknesses are 0.16, 0.95, and 2.2 cm (1/16, 3/8, and 7/8 in.). The void radar profile (figure 6.4) was processed in "real time" through the NN to produce the output in figure 6.5, showing the pavement thickness and the location, extent, and thickness of the voids.

The simulation process was repeated for variable moisture content in the base under an asphalt surfacing. The moisture content was varied from 4% (dry) to 12% (saturated) in 1% increments. A synthetic GPR profile is shown in figure 6.6 for asphalt over a 15 cm (6 in.) base on a sub-base. The base material on the left side of the profile is relatively dry, while the base material in the center of the profile is saturated. Figure 6.7 is the output of the NN, showing the variation in base moisture content and in pavement thickness. The NN output matches the simulated radar input. The NN was not trained on any specific scans used in the simulated profile.

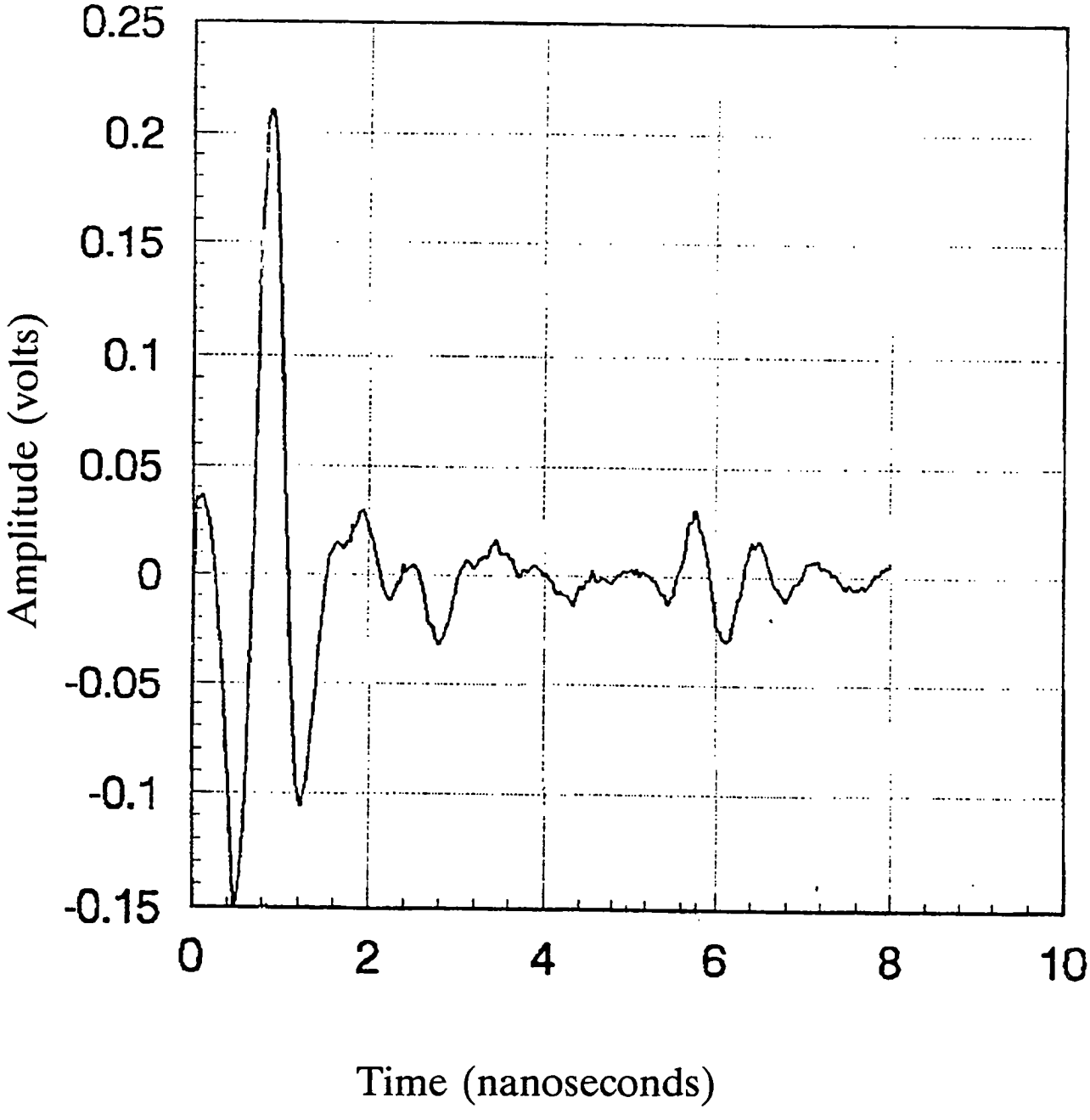

Figure 6.1. Example of a radar scan acquired with the SIR-10 and the 2.5-GHz antennas. The first strong reflection (0–1.6 nsec) is from the surface of the asphalt pavement. The pavement-base reflection is centered at 6 nsec. The other prominent reflection, at about 3 nsec is between asphalt layers.

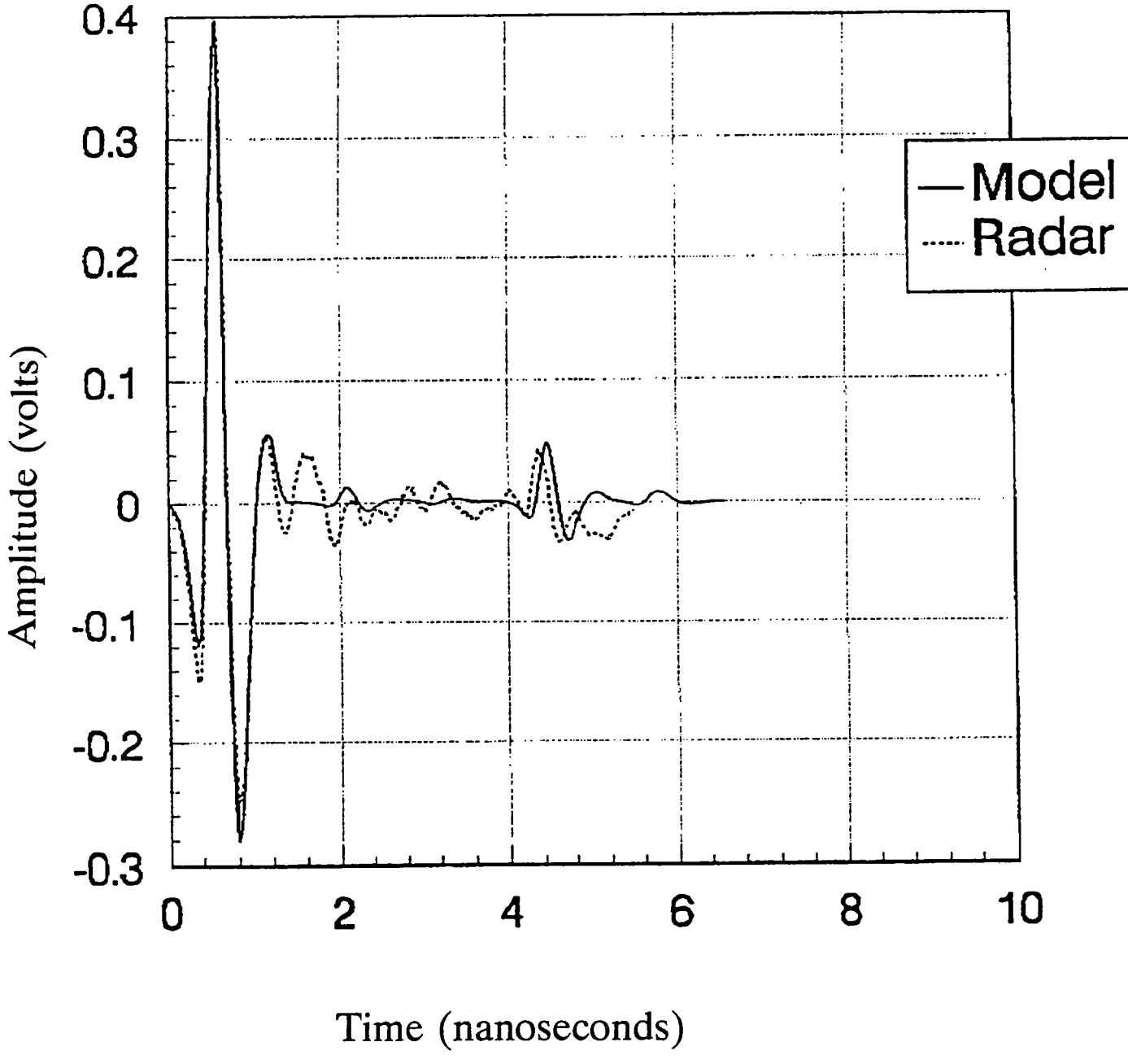

Figure 6.2. Example of model data overlaying a measured radar scan for 25 cm (10 in.) of asphalt. The asphalt-base reflection is centered at about 4.4 nsec.

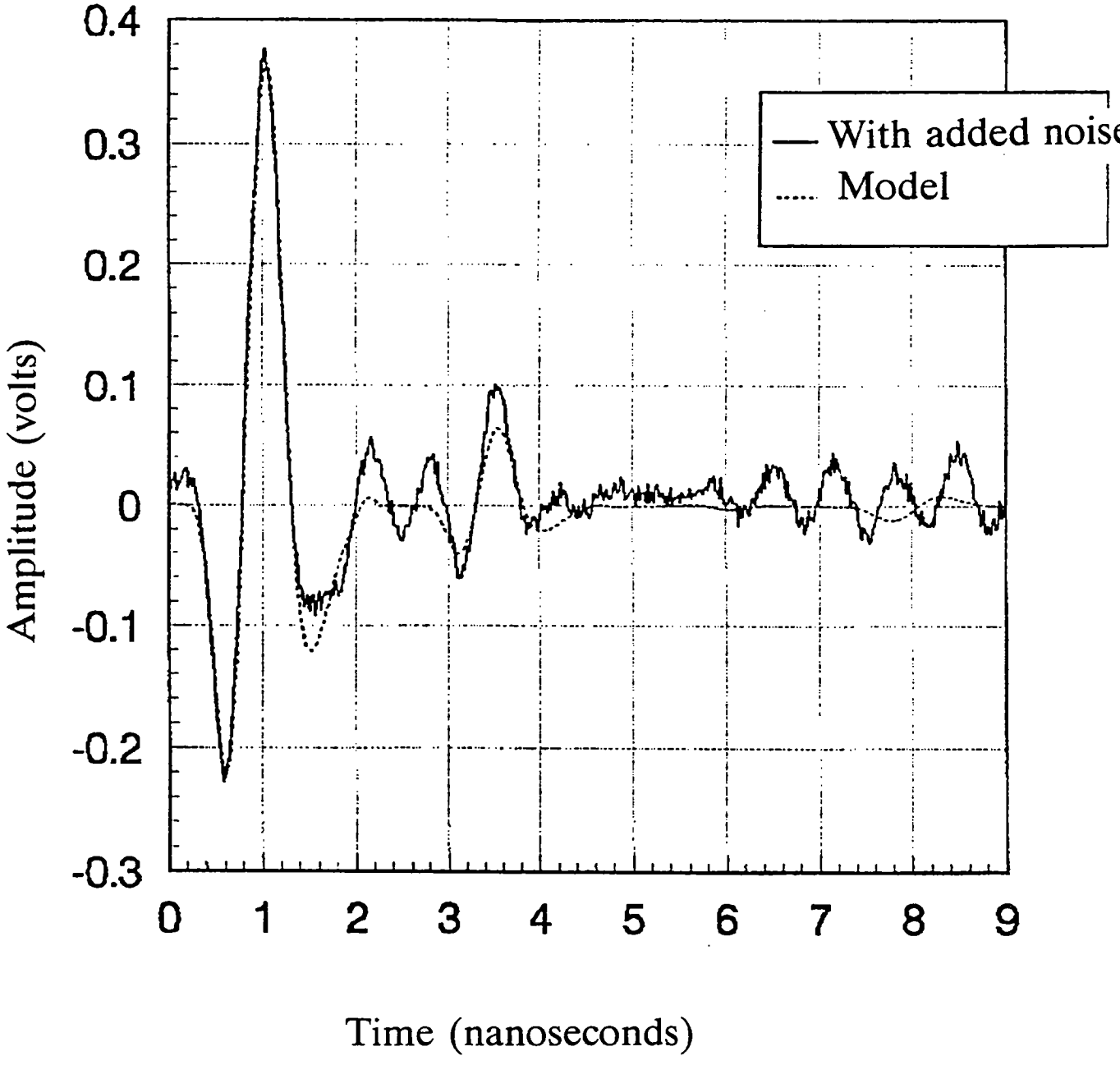

Figure 6.3. Example of model scan in which random noise and clutter have been added to the "clean" model data (dashed line) to create a noisy model scan (solid line). The pavement-void-base reflection is centered at about 3.4 nsec. The scan was calculated for a 0.16-cm (1/16-in._ air-filled void under 15 cm (6 in.) of concrete.

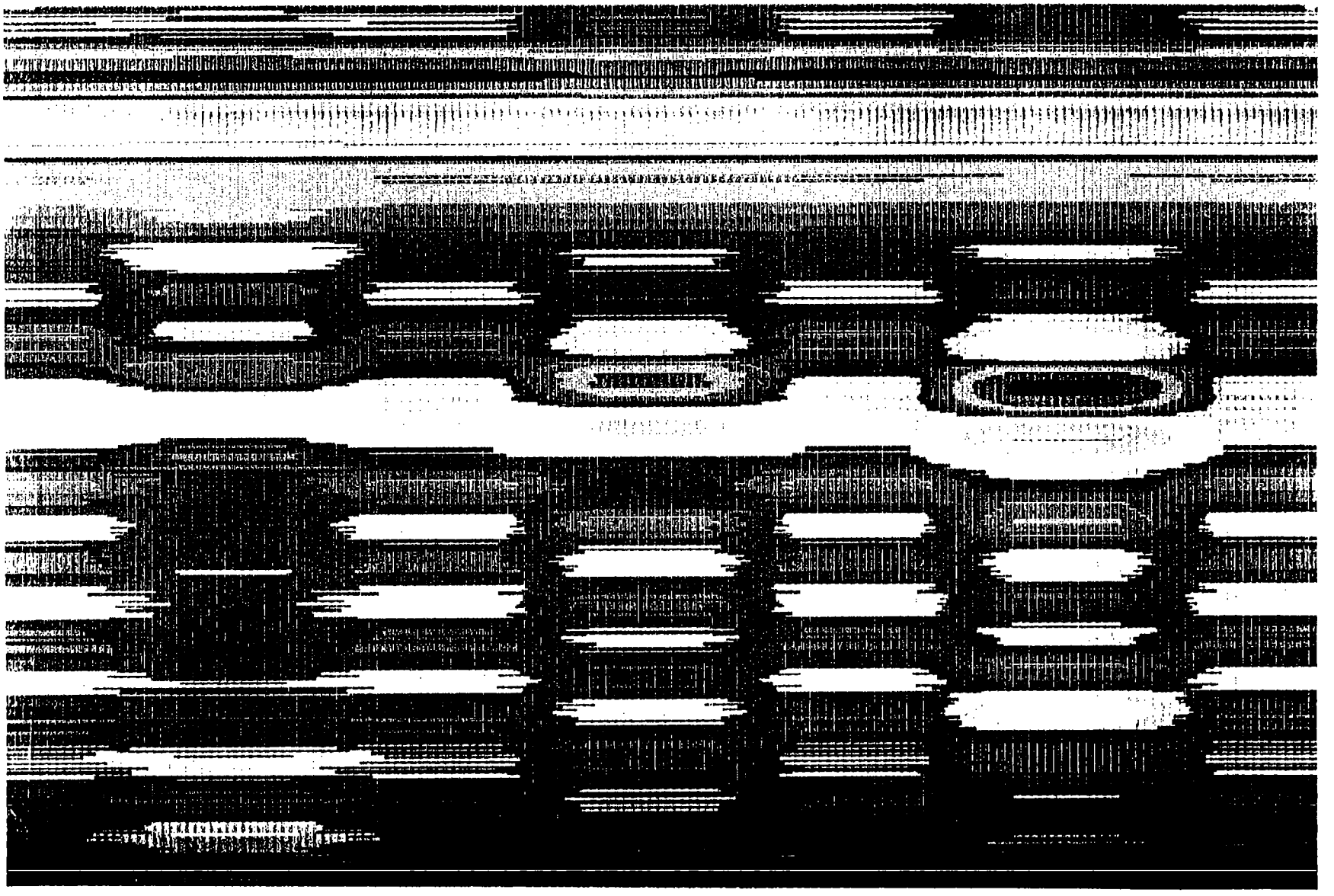

Figure 6.4. Simulated radar profile (1.0-GHz) for 15 cm (6 in.) of PCC pavement over three voids. The void thicknesses, from left to right are, 0.16, 0.95, and 2.2 cm (1/16, 3/8, and 7.8 in.).

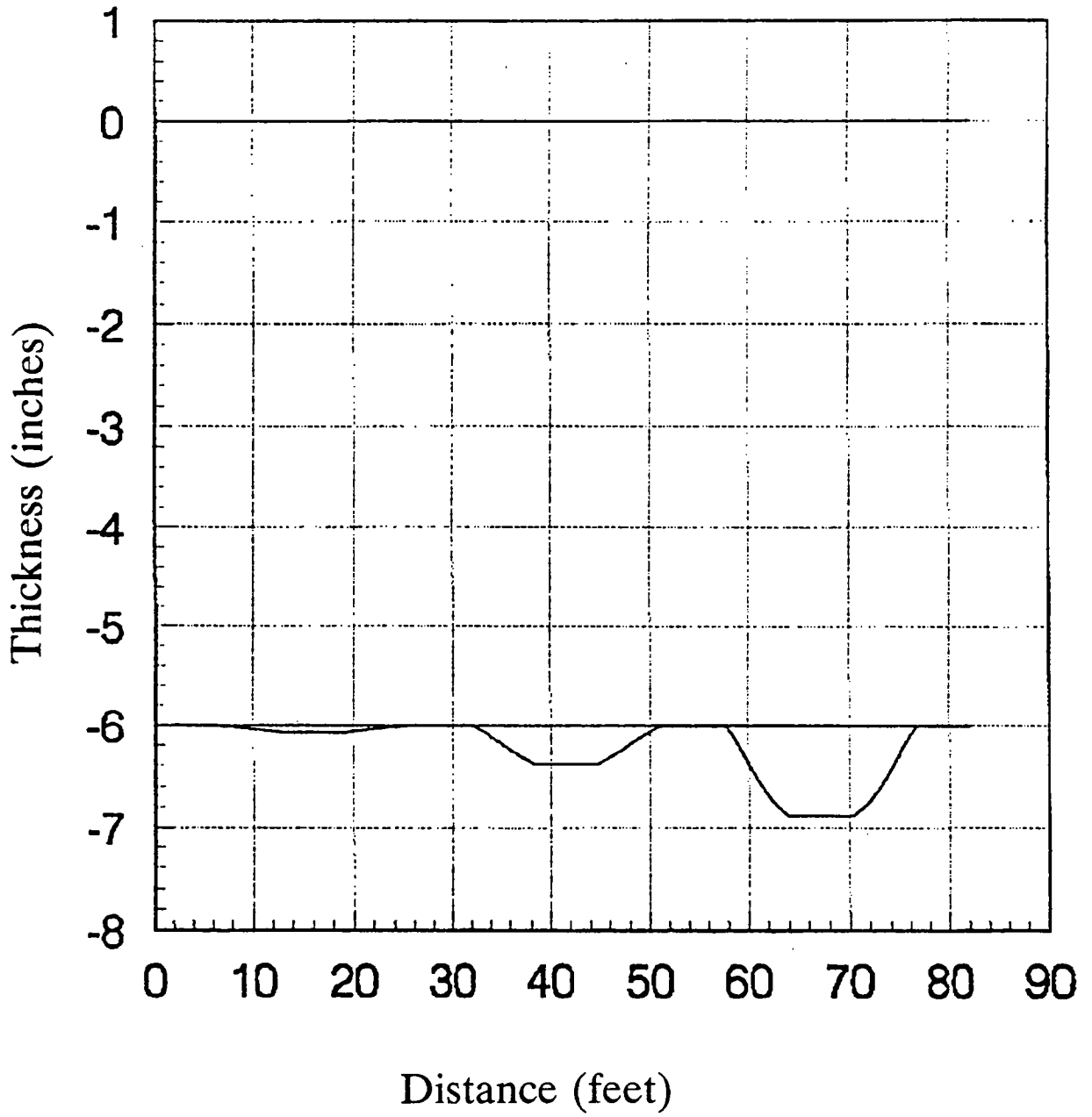

Figure 6.5. Neural network output showing the three voids (see figure 6.4) under 6 in. of pavement. The 1/16-inch void is centered at 16 ft, the 3/8-inch void is centered at 42 ft, and the 7/8-inch void is centered at 66 ft.

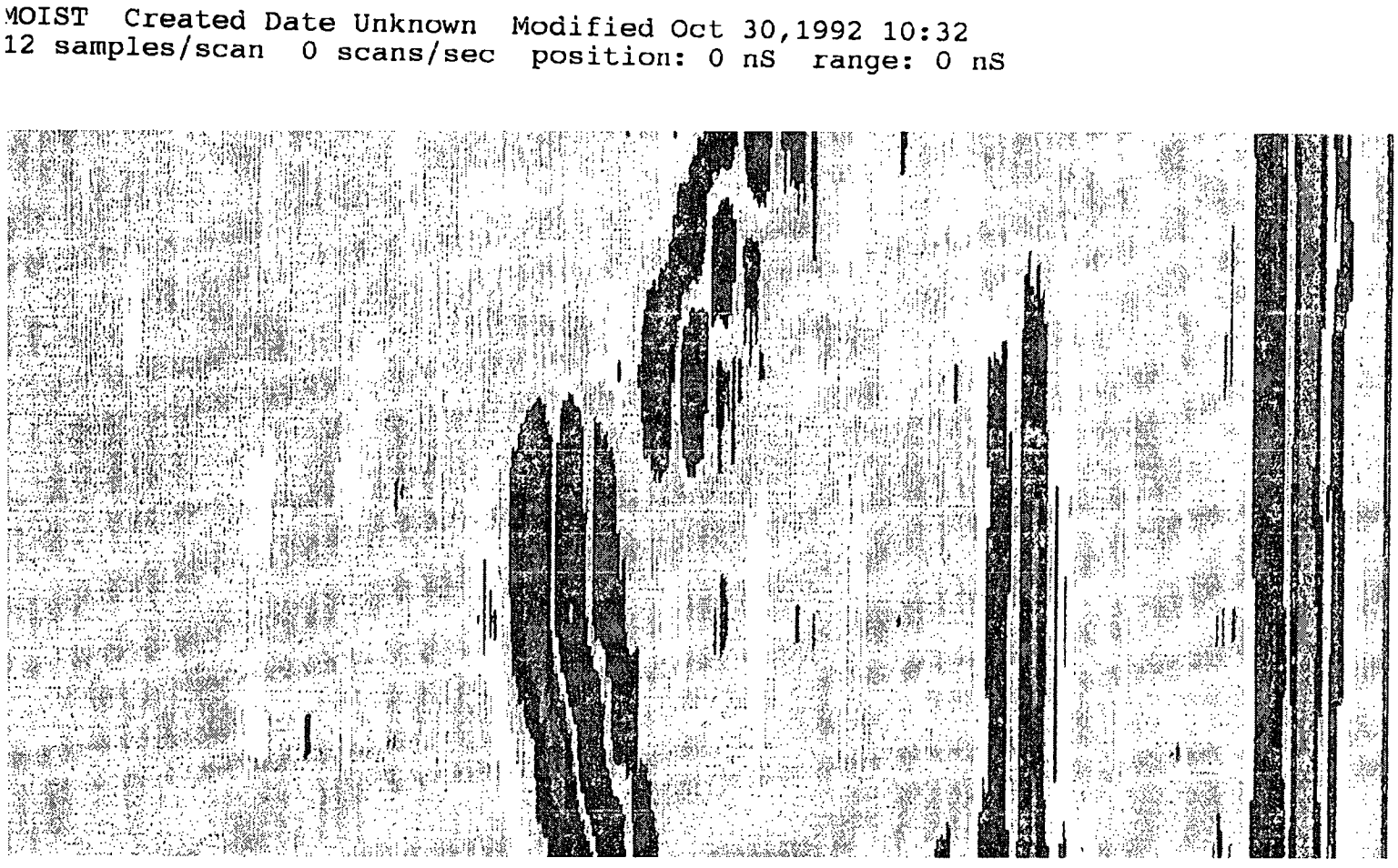

Figure 6.6. Simulated radar profile (2.5-GHz) for 15 cm (6 in) of asphalt pavement over 15 cm (6 in.) of base material. The moisture content of the base material is varied from dry at the left to saturated in the center of the profile.

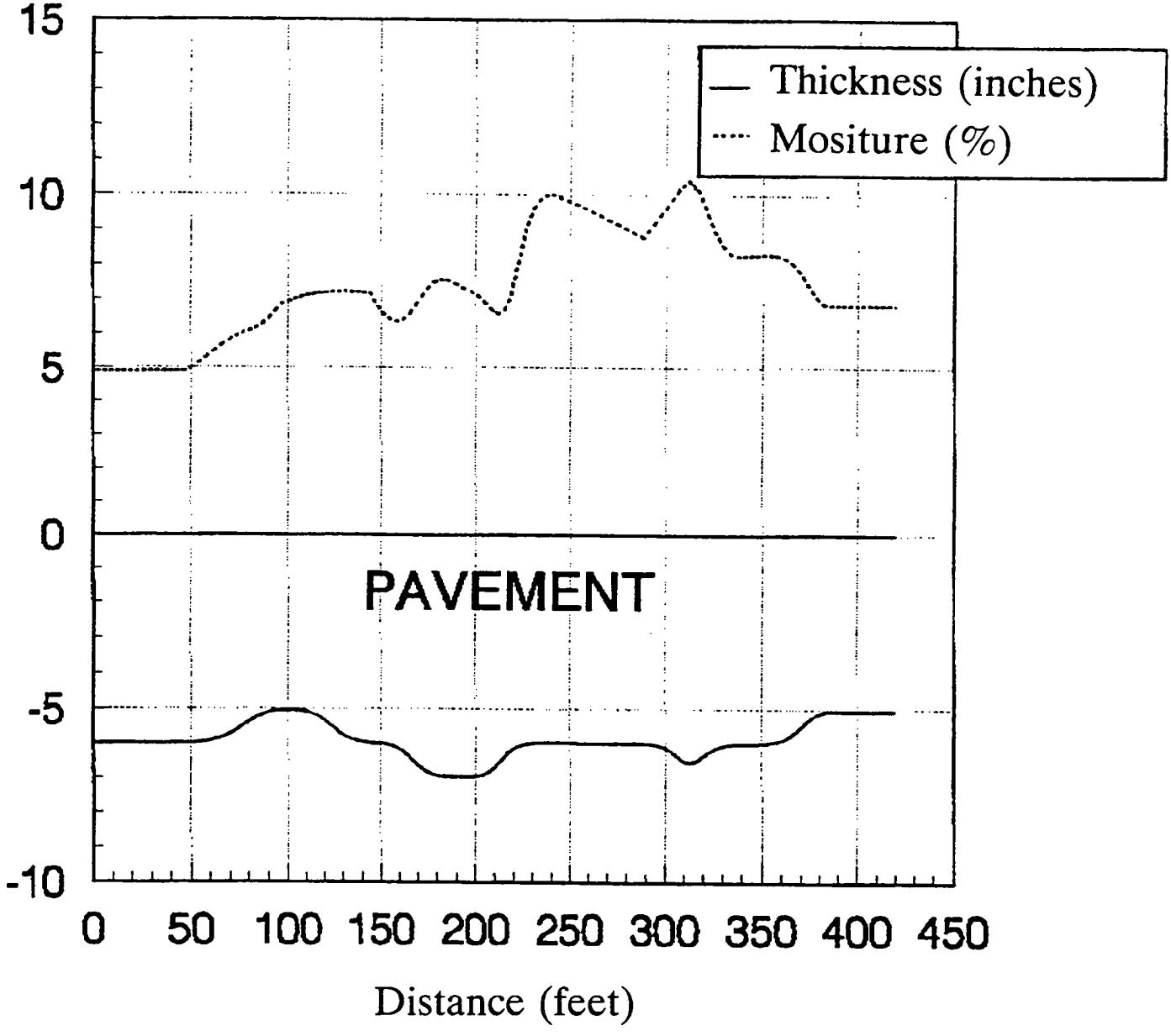

Figure 6.7. Neural network output for the input profile in figure 6.6

6.2 Neural Network Applications

For this project, we studied the feasibility of using an NN to identify anomalies in the pavement of a highway. We investigated various NN paradigms and architectures to arrive at an NN suitable for our application. Model data were created to simulate the various pavement conditions. We trained and tested the NNs on the model data and obtained encouraging results. NNs were then trained on model data and tested on real field data. These experiments showed that an NN can interpret radar data and therefore would be useful in pavement evaluation.

The final product was a prototype system that included input and output modules, a preprocessing module, and a run-time NN. We also created a library of various NNs to be run interchangeably in the system. Figure 6.8 shows the architecture of the system.

NNs are loosely based on the workings of the brain. Briefly, numbers are stored in layers of cells. Each cell is connected to cells in the succeeding layer, and the connections are weighted. Training the NN consists of modifying the weights until the output from the NN agrees with the desired output. Algorithms for modifying weights and for creating and running the NN vary with different NN architectures and are beyond the scope of the this report.

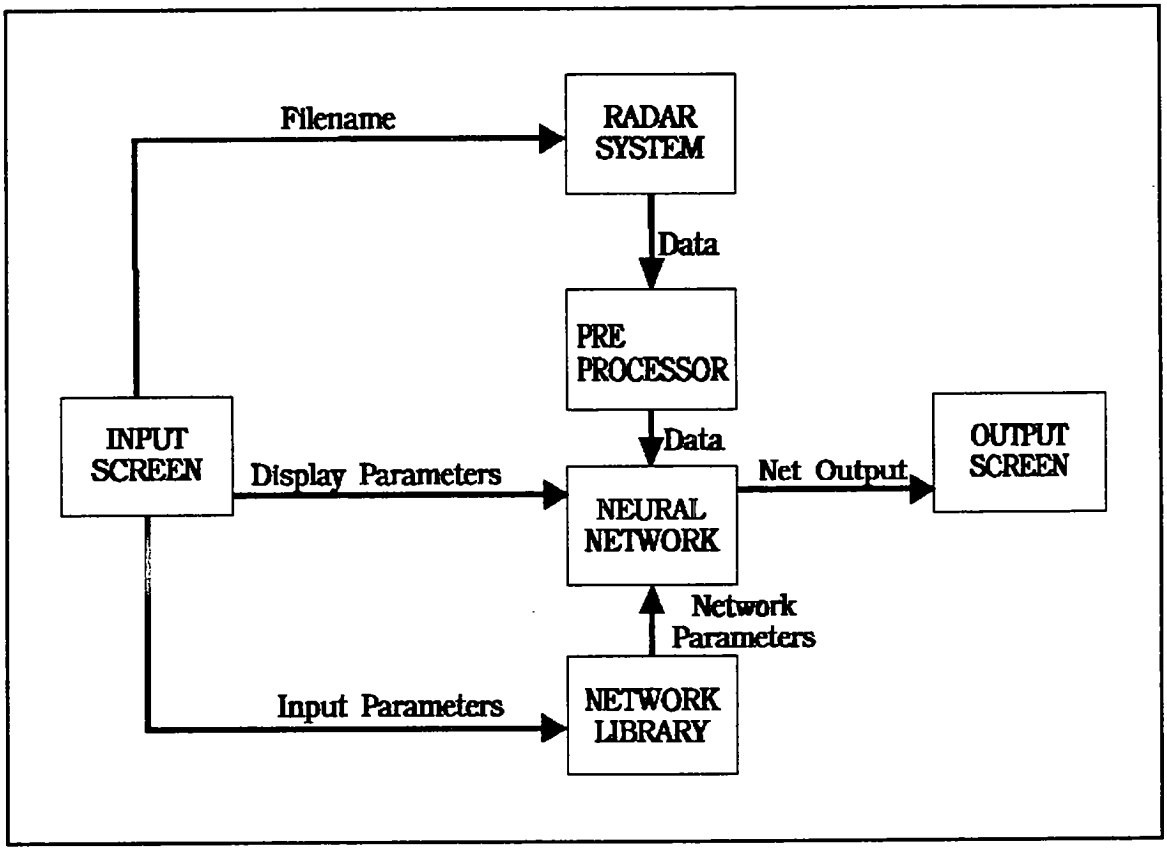

Figure 6.8. Block diagram of neural network processing

Throughout the project we tested various NN paradigms that had been found suitable for classification and data association. NNs that accepted only binary data were rejected. NNs that were studied in depth and tested with model data were back-propagation (Rumelhart, Hinton, and Williams 1986), counterpropagation (Hecht-Nielsen 1987), functional-link networks (Pao 1989), probabilistic NNs (Specht 1988), the cerebellar model arithmetic computer (Miller, Glanz, and Kraft 1990), and learning vector quantization (LVQ) (Kohonen et al 1988).

Initially we used LVQ because it produced NNs that were easy to train and had the greatest degree of accuracy and generalization. However, a drawback that became evident later in the project was the increasing number of output cells required for LVQ. LVQ, unlike back-propagation, produces a binary, "winner-take-all" output. A cell must be provided for each desired value of an output variable. For example, if the thickness of the pavement varies from 5 to 12 cm (2 to 5 in.) in 1- cm (0.4 in.) increments, eight output cells are needed. Although this limitation was acceptable for the original thickness studies, the number of output cells quickly proliferated when moisture content and voids were added to the desired output.

A second problem with LVQ was that the output had to be in discrete units, whereas the variables in the project were continuous data. For example, pavement thickness ranged from 5 to 12 cm. The LVQ network did not allow thicknesses between the 1-cm intervals specified as the output. We could not produce a thickness of 5.5 cm without creating an output value for 5.5.

With back-propagation, we could use one output cell for each variable. This cell could produce a continuous output within the range of the variable. Although the back-propagation networks are slower to train, this method better suited our needs for continuous outputs and multiple variables.

Neural Network Architecture

An NN can have a varying number of layers and cells. A layer for receiving data, called the *input layer*, and a layer for the results of the NN, called the *output layer*, are required. Between these two layers are the *hidden layers* which extract the important features of the input. Experiments showed that one hidden layer was sufficient and there were no advantages to adding more layers. More important, we found that decreasing the number of hidden cells to between two and six created NNs that were better able to generalize previous learning to previously unseen inputs.

Increasing the number of desired output parameters by adding more output cells increases the number of hidden cells needed. This approach forces the NN to extract significant differences in the input rather than using hidden cells to memorize certain patterns. A slight difference in a memorized pattern confused the NN, whereas forcing the NN to learn only gross feature differences enhanced performance on new data. The trade-off is that it takes longer to train the NN. The optimum number of hidden cells

varied with each NN created. Too few cells can prevent the NN from learning. Thus, each NN created required a series of training sessions to determine how many hidden cells to use.

Figure 6.9 shows an example of the architecture for an NN trained to detect moisture content. We were able to train this NN using only two hidden cells. The bias cell shown in the figure is a standard NN feature. This cell is added to the input layer. It outputs a constant value of 1 but has adjustable weights.

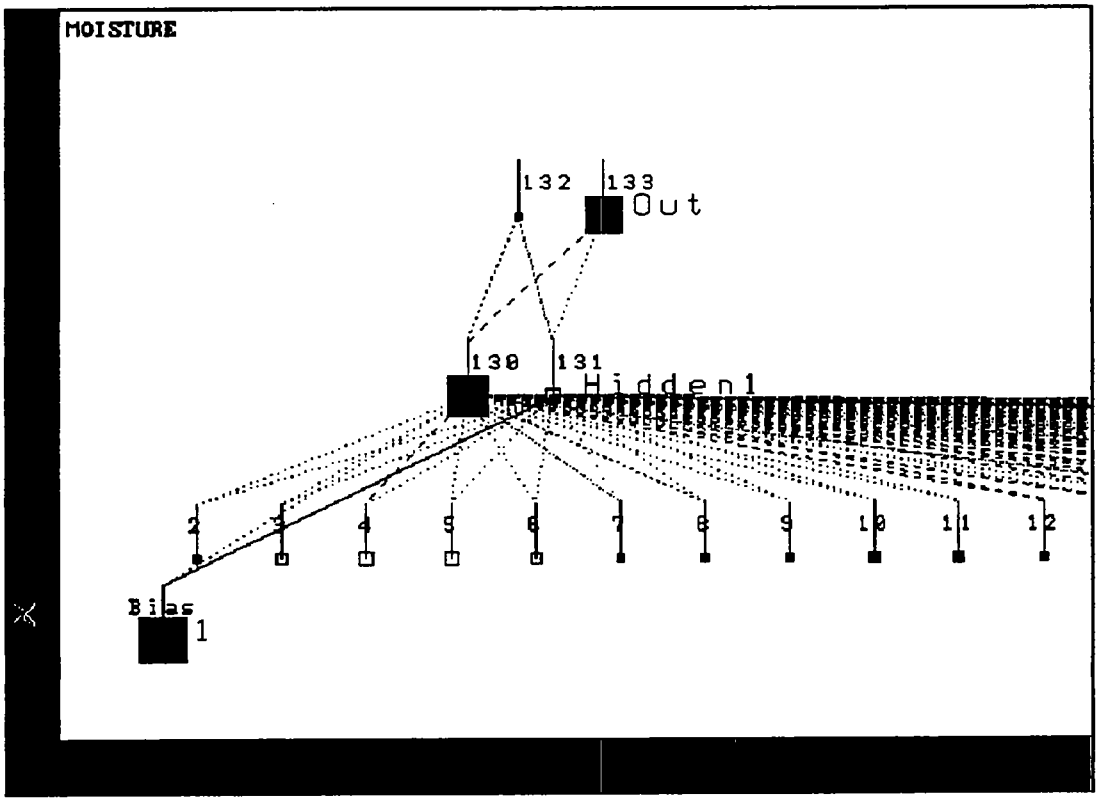

Figure 6.9. Example of an NN architecture. The first layer (2-129) is the input cells. The second layer (130 and 131) is the hidden cells, and the third layer (132 and 133) is the output cells. Cells in each layer are connected to all cells in the next layer.

Training the Neural Network

We trained the NN by presenting it with examples of data representing an input scan along with the desired output for that scan. The NN was originally assigned random weights connecting its layers. Experimentation showed that keeping the original random weights in the range of -0.3 to +0.3 produced the best NNs. The procedure in a back-propagation NN is to propagate the input through the layers to the output layer, determine the error at the output layer, and then propagate the errors back through the network from the output layer to the input layer. Thus training consists of minimizing the error, which is defined as the difference between desired and actual outputs. We

minimize the error by modifying the weights. Back-propagation employs a method called the gradient descent rule, which changes each weight according to the size and direction of negative gradient on the error surface.

NeuralWorks, the software used for training, picks examples randomly from the prepared set of input examples. Input consists of the first 128 numbers from the set. The last two numbers, in the input represent the desired output.

The software converts the data to the range -1 to +1, which is optimum for an NN. A minimum and maximum for each input and output must be provided for the normalization. We found that providing the NN with one minimum and one maximum for the entire set of learning and testing examples worked just as well as finding a minimum and maximum for each input and output cell. This simplification reduced the complexity of the run-time NN, which now stores only two numbers for all the inputs rather than two for each input (a total of 256 numbers).

The data must be properly aligned so that the same characteristic features are always presented to the same input cells. We did this by aligning the data at the second zero crossing of each scan, discarding data before this point. We began the input at the zero-crossing point. This method also reduced the size of the input by discarding data that provided no information. Every second number was written to the NN input file until 128 numbers had been written. Figure 6.10 shows an example of a trace of model data and the resulting input for the NN.

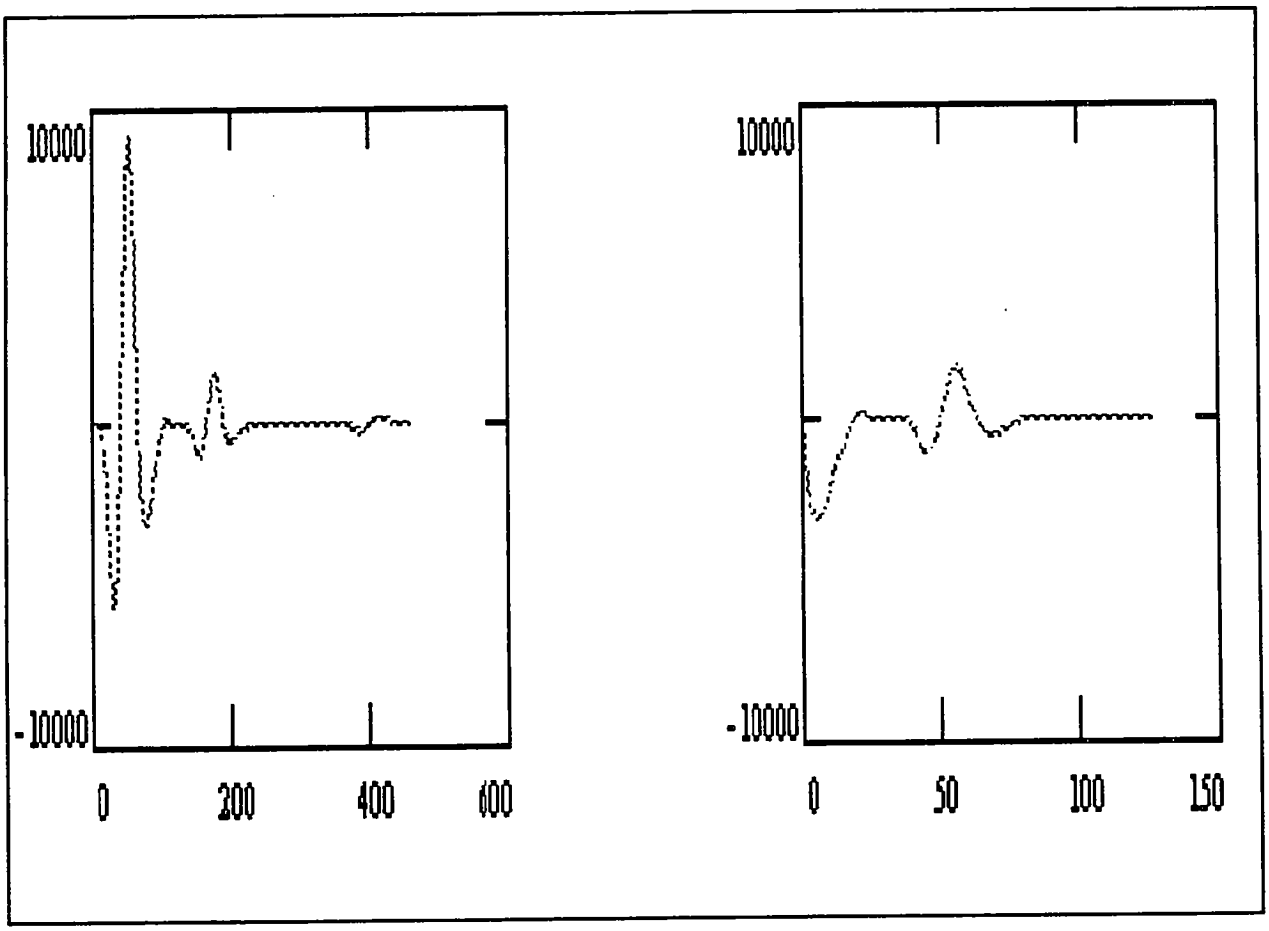

Figure 6.10. Original model data trace and resulting neural network input. The model data are reduced by discarding data before the zero crossing and by using only every second point.

Analysis of the Task

Thickness

We used the SHRP radar antennas and an oscilloscope to obtain tracings from a Geophysical Survey Systems, Inc. (GSSI), test bed that contained asphalt thickness steps ranging from 5 to 30 cm (2 to 12 in.). From these tracings, we created 1.0-GHz and 2.5-GHz model data representing the various thicknesses.

Figure 6.11 shows a scan from the oscilloscope superimposed on a model scan. Both scans are for a 15 cm (6 in.) thickness.

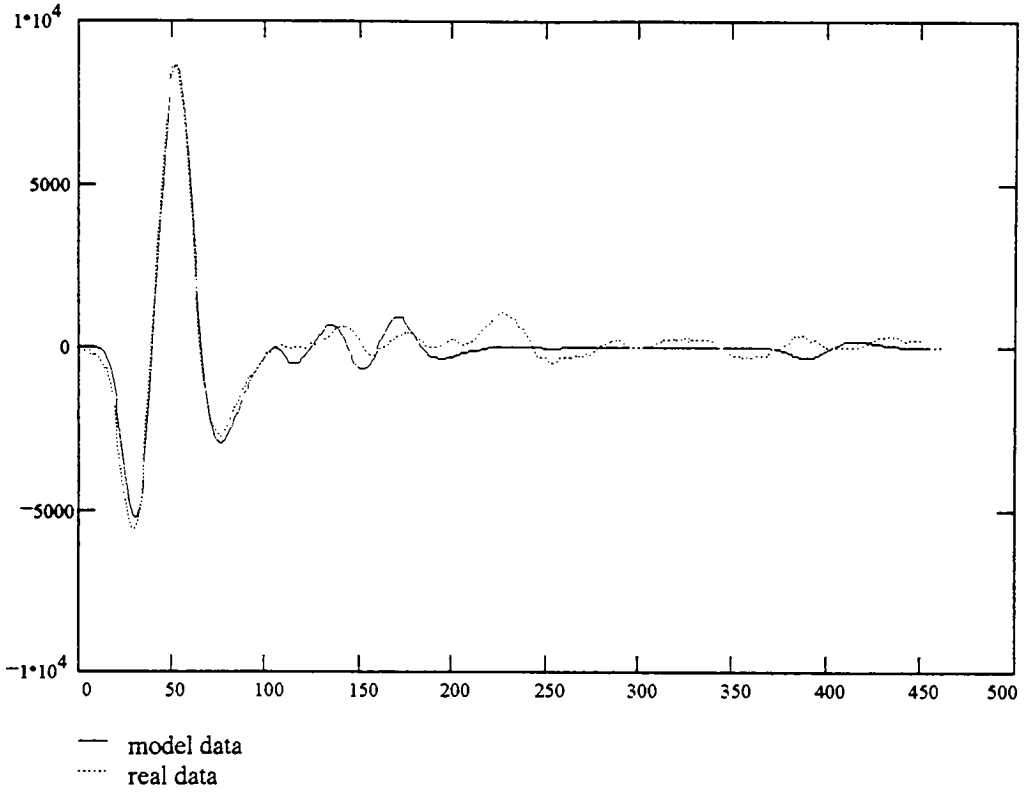

Figure 6.11. Model and real data for 15 cm (6 in.) thickness

Figure 6.12 shows the model data created for the different pavement thicknesses. The various thicknesses produce peaks at different distances from the zero crossing.

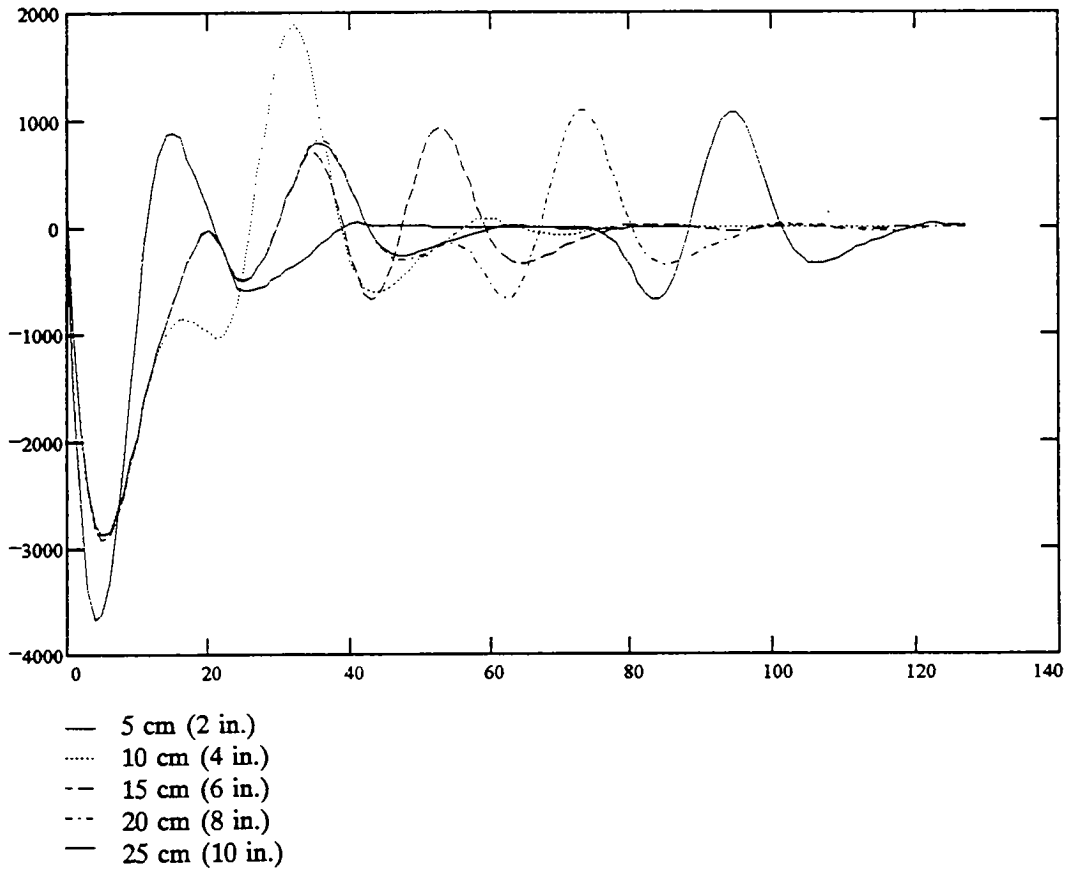

Figure 6.12. Model data for various pavement thicknesses

We created the training data for the NN from the model data. In this experiment we used only noiseless model data. We then tested the NN on data obtained from the oscilloscope. Table 6.1 shows the output from a trained NN.

Table 6.1
Results from Neural Network Trained on Model Thickness Data

Desired Output (cm)	Actual Output (cm)
5	4.906329
10	10.00219
15	15.06664
20	20.05681
25	24.96641
5	4.922163
10	10.13884
15	14.97889
25	25.03843

An interesting observation from these studies was how adding noise affected performance. Adding noisy data to the training examples greatly enhanced the performance of the NN. Since we had not created noisy files, we combined 1.0-GHz and 2.5-GHz model scans in a training file. Figure 6.13 shows both a 1.0-GHz and a 2.5-GHz scan for a 15 cm thickness (6 in.). Figure 6.14 shows 1.0- and 2.5-GHz model data and the real data for 15 cm (6 in.) asphalt pavement thickness.

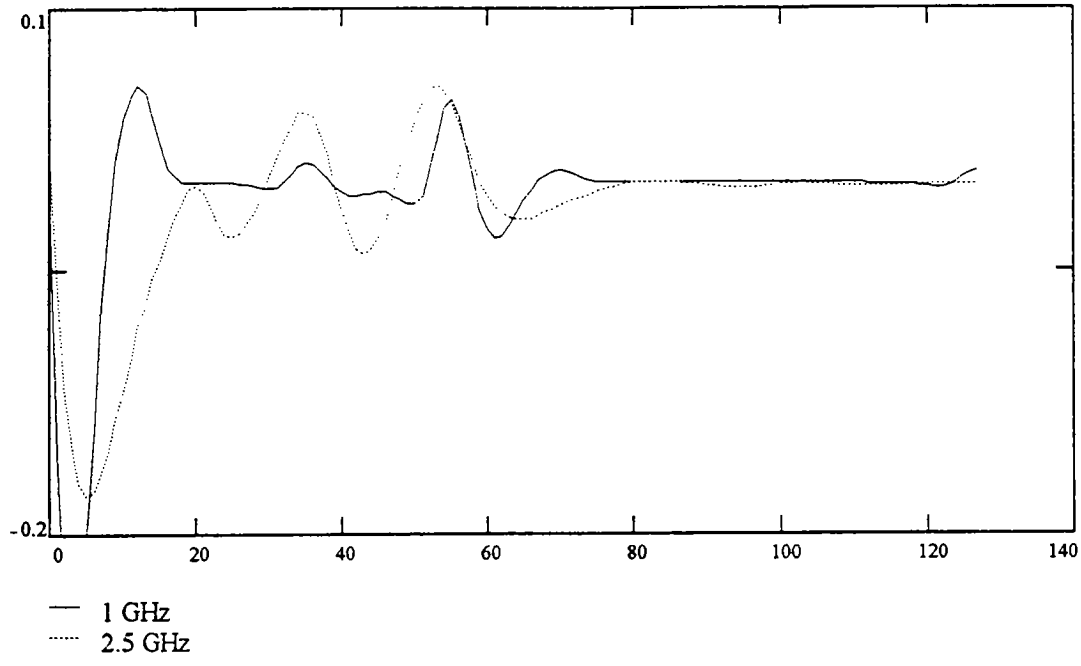

Figure 6.13. Scans of 15 cm (6 in.) pavement thickness from 1.0- and 2.5-GHz antennas

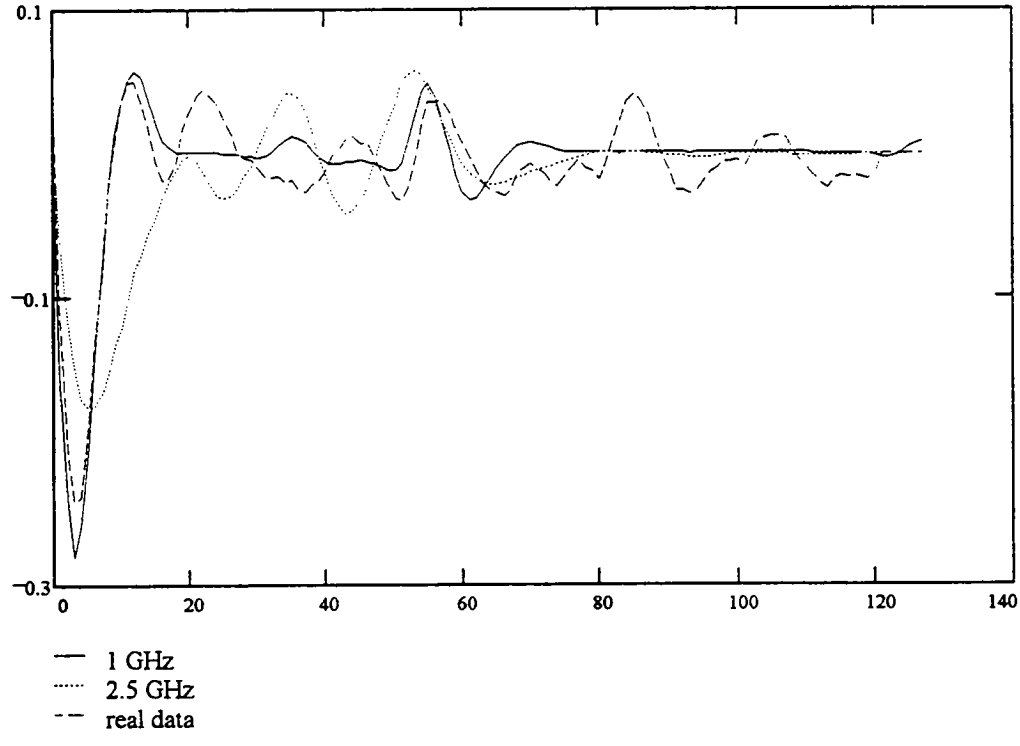

Figure 6.14. Real and model scans for 15 cm (6 in.) asphalt pavement thickness

The scans correspond at only one peak. The combination of the 1.0- GHz and 2.5-GHz model data forced the NN to concentrate the positive weights representing a 15 cm (6 in.) output at this feature. Otherwise, other extraneous peaks were positively weighted during training, causing less accurate networks. As figure 6.15 shows, the first peak is at the exact spot where the 5 cm (2 in.) peak appears. During the original training we found that these secondary peaks caused problems. The NN would positively weight both peaks, creating output between 5 and 15 cm (2 and 6 in.). Adding noise caused the NN to correctly distinguish between characteristic features and unimportant information.

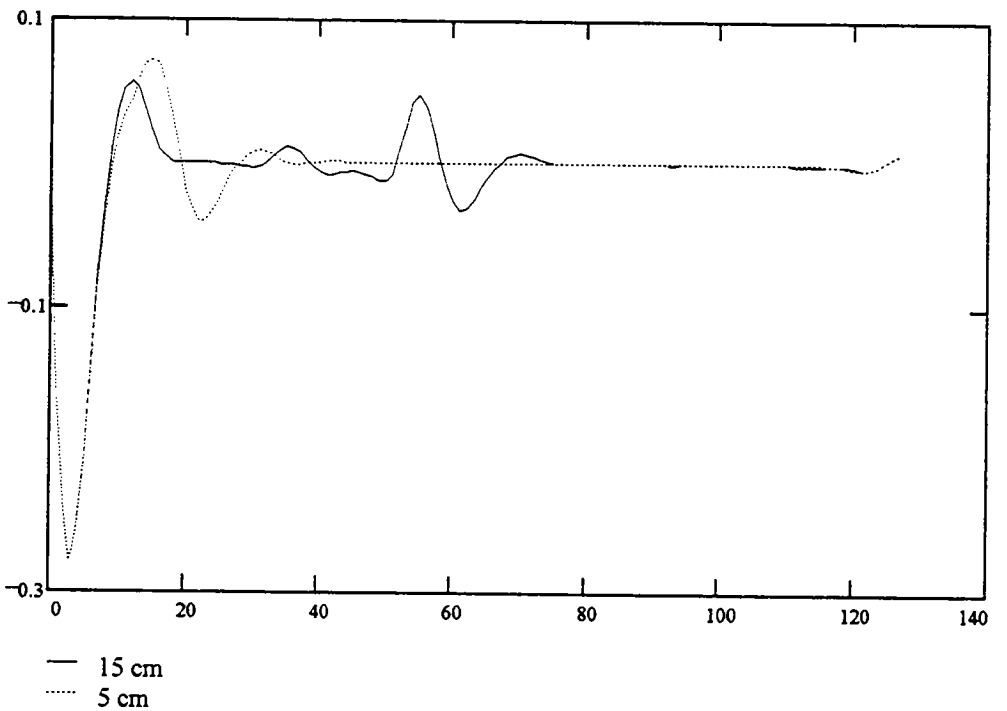

Figure 6.15. Model scans of 5 cm (2 in.) and 15 cm (6 in.) pavement thicknesses

Voids and Moisture

We trained NNs on simulated void and moisture content data created to replicate conditions at the test bed site in Texas. The simulated voids ranged from 0 to 2.9 cm (0 to 1⅛ in.). The moisture content varied from 4 to 12%. The thickness of the pavement was kept constant at 15 cm (6 in.), corresponding to the thickness of the test bed. An additional set of data was created that varied the thickness of the pavement and the moisture content. The thicknesses in these files ranged from 12.7 to 17.8 cm (5 to 7 in.).

Each data set consisted of a clean trace and four additional traces with varying degrees of noise added. Sample traces of a 1.3 cm (½ in.) void are shown in figure 6.16.

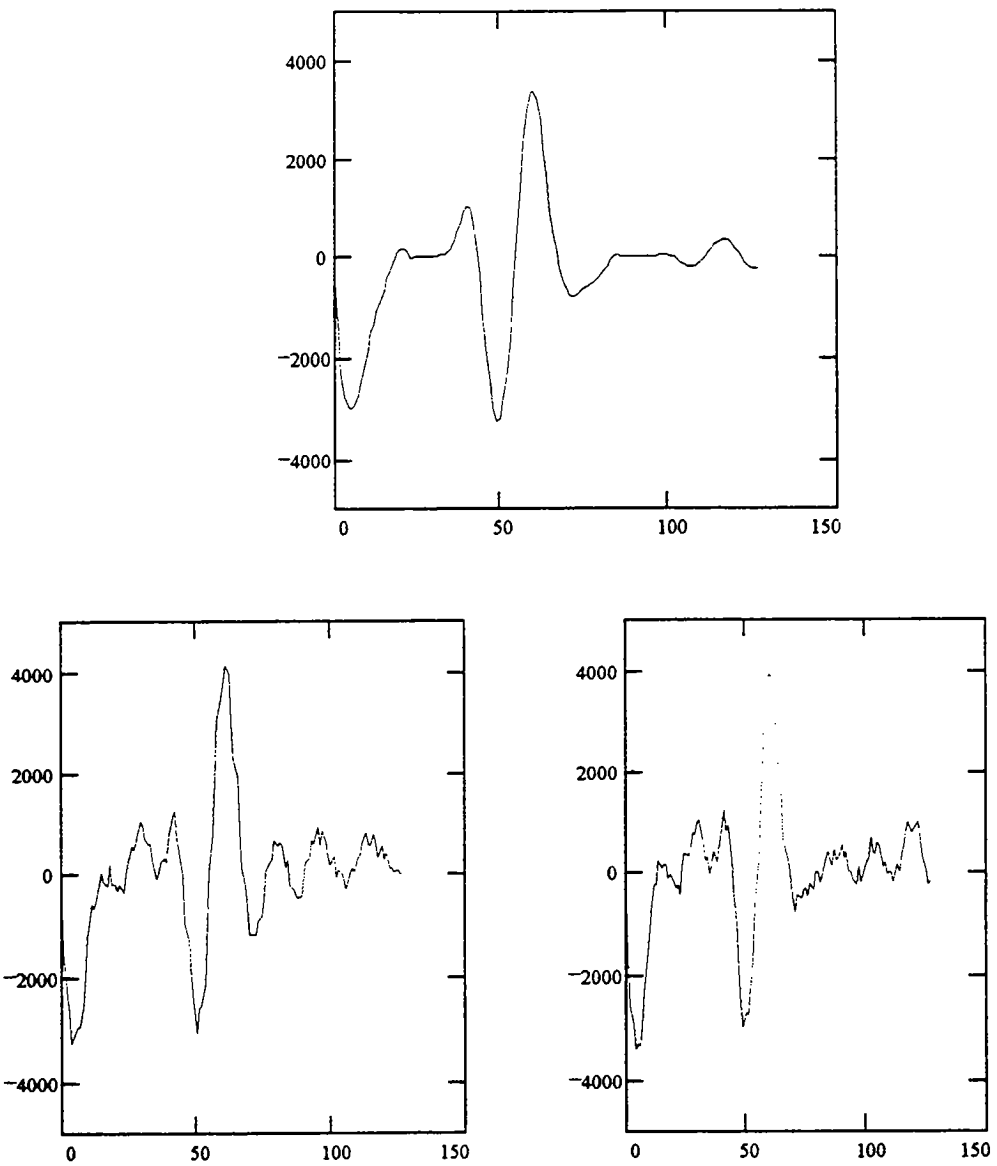

Figure 6.16. Clean and noisy data for a 1.3 cm (½ in.) void

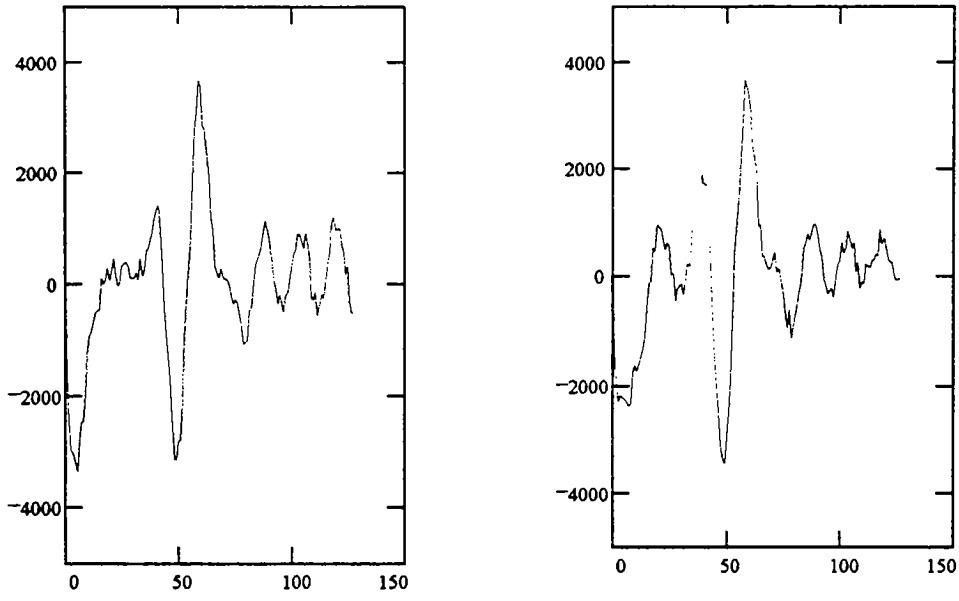

Figure 6.16. Clean and noisy data for a 1.3 cm (½ in.) void (Continued)

Adding noisy data to the training examples helped the NN learn only the distinguishing features and not extraneous information that is sometimes present in the training data. In figure 6.17 we superimpose two of the noisy traces on a clean trace. Note that the characteristic features of the data are constant throughout the traces, but the various other peaks and valleys differ in each scan.

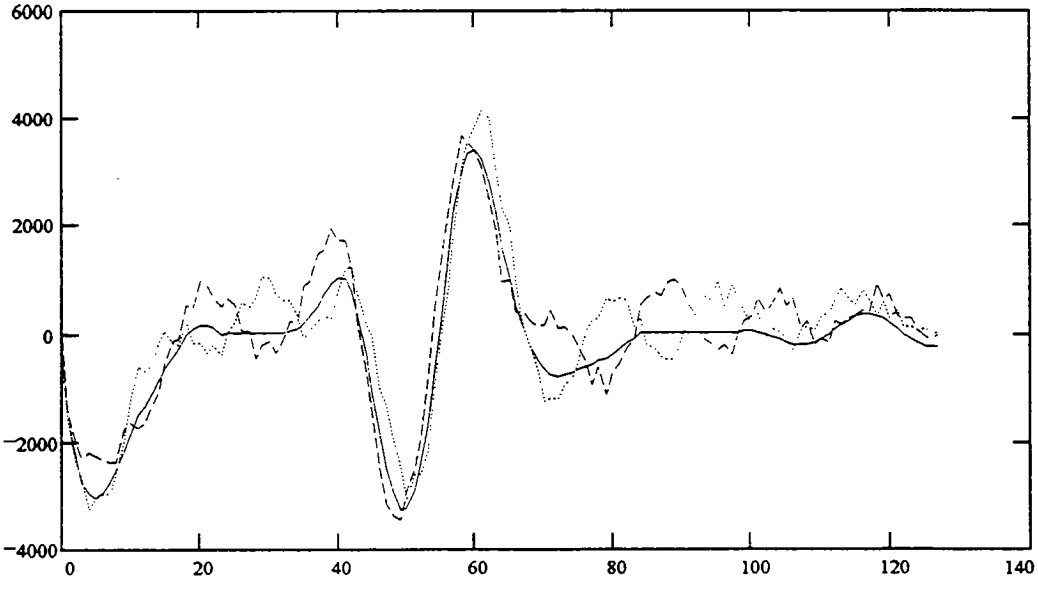

Figure 6.17. Superimposed clean and noisy data for a 1.3 cm (½ in.) void

We combined three data sets for the training examples in each of the NNs created. The training file consisted of one set of clean model data and two sets of noisy data. We then tested each of the trained NNs with the remaining two sets of noisy data not used for training. A sample output file from the NN trained to identify voids is shown in table 6.2.

Table 6.2
Output File for Neural Network Trained to Detect Voids

Desired Output:		Actual Output:	
Pavement Thickness (in)	Void Thickness (in)	Pavement Thickness (in)	Void Thickness (in)
6	0	6	0.007877
6	0.063	6	0.065796
6	0.125	6	0.111397
6	0.25	6	0.20887
6	0.375	6	0.33611
6	0.5	6	0.490972
6	0.625	6	0.606896
6	0.75	6	0.754507
6	0.875	6	0.87703
6	1	6	0.984438
6	1.125	6	1.107348
6	0.063	6	0.067282
6	0.125	6	0.132431
6	0.25	6	0.226254
6	0.375	6	0.38248
6	0.5	6	0.529554
6	0.625	6	0.657807
6	0.75	6	0.754458
6	0.875	6	0.87182
6	1	6	1.022679

The desired output shows a constant 15 cm (6 in.) pavement thickness with varying void thicknesses. The actual output shows that the network was able to identify voids to within approximately 0.25 cm (0.1 in.) on noisy test data that it had not been presented with previously.

A sample output file from an NN trained to detect moisture content is shown in table 6.3. The desired output has a constant 15 cm (6 in.) pavement thickness with a varying percentage of moisture in the pavement. Again, the actual output shows that the network was able to identify moisture content to approximately 0.1% on noisy data that it had not been trained on previously.

Table 6.3
Output File for Neural Network Trained to Detect Moisture Content

Desired Output:		Actual Output:	
Pavement Thickness (in)	Moisture Content (%)	Pavement Thickness (in)	Moisture Content (%)
6	4	6	3.921941
6	5	6	5.317132
6	6	6	6.275487
6	7	6	7.01514
6	8	6	8.692389
6	9	6	8.944772
6	10	6	9.469633
6	11	6	11.08505
6	12	6	12.03609
6	4	6	3.966606
6	5	6	4.559282
6	6	6	6.128095
6	7	6	7.88869
6	8	6	8.440479
6	9	6	8.958403
6	10	6	9.850467
6	11	6	11.42039
6	12	6	11.85126

We created an abbreviated version of the previous moisture content data that also varied the pavement thickness from 12.7 to 17.8 cm (5 to 7 in.). Results from this experiment are given in table 6.4. The actual output shows that the NN could identify the varying pavement thickness to within 0.25 cm (0.1 in.) along with the varying moisture content.

Table 6.4
Neural Network Output with Both Thickness and Moisture Content Varying

Desired Output:		Actual Output:	
Pavement Thickness (in)	Moisture Content (%)	Pavement Thickness (in)	Moisture Content (%)
6	5	6.000926	4.903785
5	6	5.039281	6.825517
6	7	5.983555	7.16013
7	7	6.993662	7.324593
6	10	5.975605	10.01689
6	9	6.003018	8.774427
6	8	6.019534	8.248093
5	6	5.039281	6.825517
5	5	5.040102	5.055578

We also conducted an experiment with both air and water voids included in the training data. An additional parameter was added to the output. The desired output now included a -1 if the void found was a water void or a +1 for an air void. Table 6.5 shows the results from a test run of this NN. The actual output shows that this NN is able to identify the thickness of the pavement and the thickness of the void and is also capable of correctly classifying the type of void.

Table 6.5
Neural Network Output Identifying Air and Moisture Voids

Desired Output:			Actual Output:		
Pavement Thickness (in)	Void Size (in)	-1 Moisture Filled or +1 Air Void	Pavement Thickness	Void Size	Void Contents -1 Moisture +1 Air
6	0.063	-1	6	0.050394	-0.99852
6	0.125	-1	6	0.099119	-1.00389
6	0.25	-1	6	0.269142	-1.00509
6	0.375	-1	6	0.405657	-1.00452
6	0.5	-1	6	0.506939	-1.004
6	0.625	-1	6	0.633968	-1.00316
6	0.75	-1	6	0.723103	-1.00241
6	0.875	-1	6	0.872807	-1.00104
6	1	-1	6	1.04849	-0.99882
6	1.125	-1	6	1.098422	-0.99791
6	0	-1	6	0.031758	-0.97213
6	0.031	1	6	0.03779	0.977271
6	0.063	1	6	0.054346	1.009613
6	0.125	1	6	0.121593	1.007582
6	0.25	1	6	0.239938	1.004735
6	0.375	1	6	0.380366	1.001858
6	0.5	1	6	0.497931	0.992182
6	0.625	1	6	0.61781	0.995354
6	0.75	1	6	0.767926	1.008107
6	0.875	1	6	0.869946	1.007333
6	1	1	6	1.00734	1.001625

The difference between an air void and water void is shown in the two traces of a 1.6 cm (⅝ in.) void shown in figure 6.18.

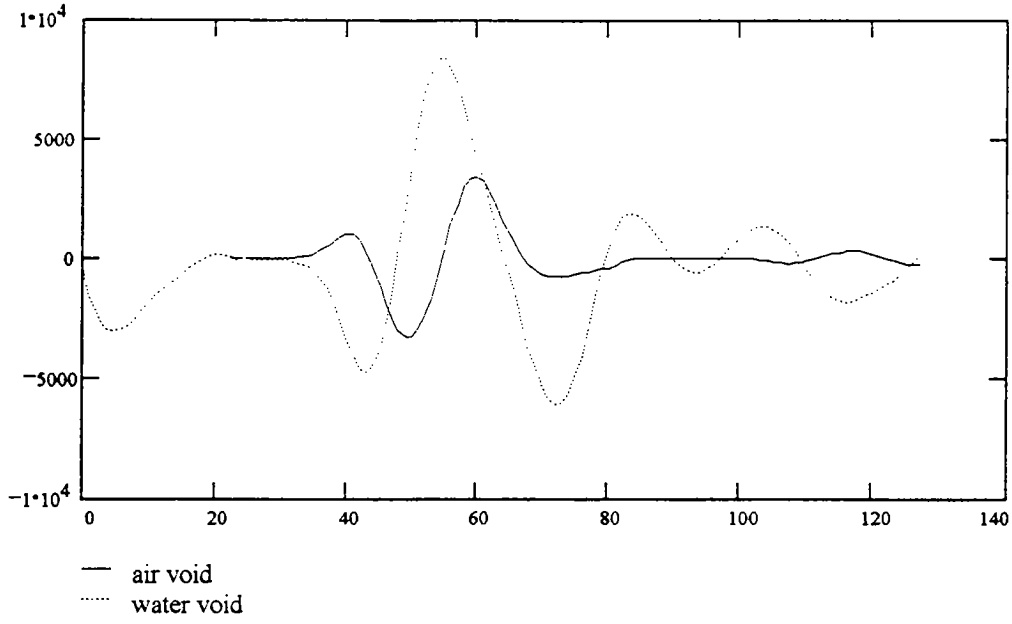

Figure 6.18. Air and water voids

Filtering

We investigated further preprocessing of the trace data to see whether we could improve NN accuracy, speed, or size. We used two filters common to seismic data analysis: the Fourier transform and the Hilbert transform (Yilmaz 1987). We expected the filtering to condense the information content of a scan, reducing the amount of input data necessary while making the NN more accurate. However, we found that the filtering was unable to achieve this purpose. We illustrate with the Hilbert transform. At first the results appear promising. Figure 6.19 shows four scans representing various moisture contents that have been filtered using the Hilbert transform.

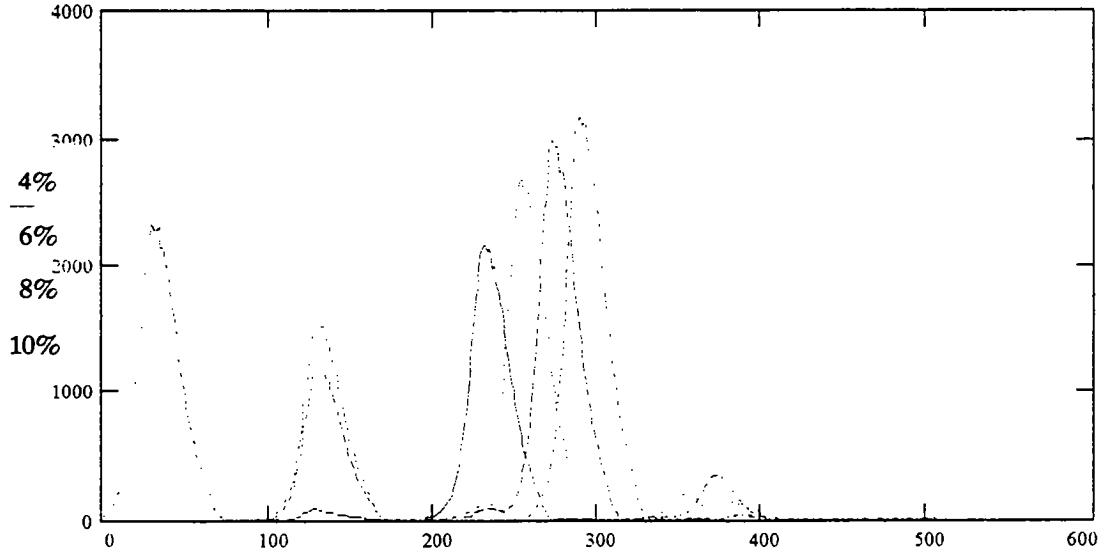

Figure 6.19. Hilbert transforms of scans with varying moisture content

The figure shows that almost all the information content is now in one peak. The height of the peak determines the moisture content. The problem is that the scans are the clean model scans. Noise, which is common with actual use of radar, has not been added. Figure 6.20 shows the Hilbert transforms of a noisy and a clean scan of a moisture content of 6%; figure 6.21 shows similar scans for a moisture content of 11%.

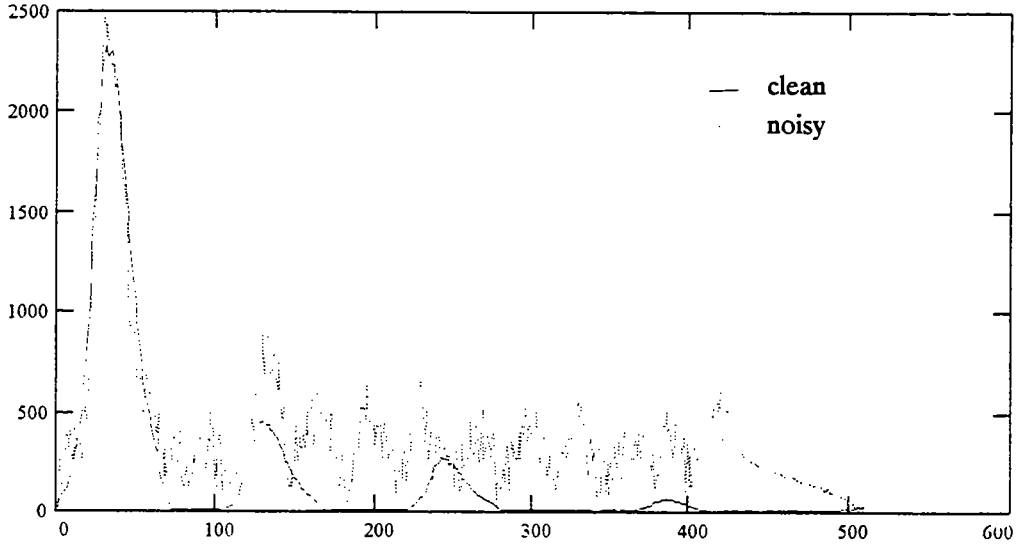

Figure 6.20. Hilbert transforms of clean and noisy data—moisture content 6%

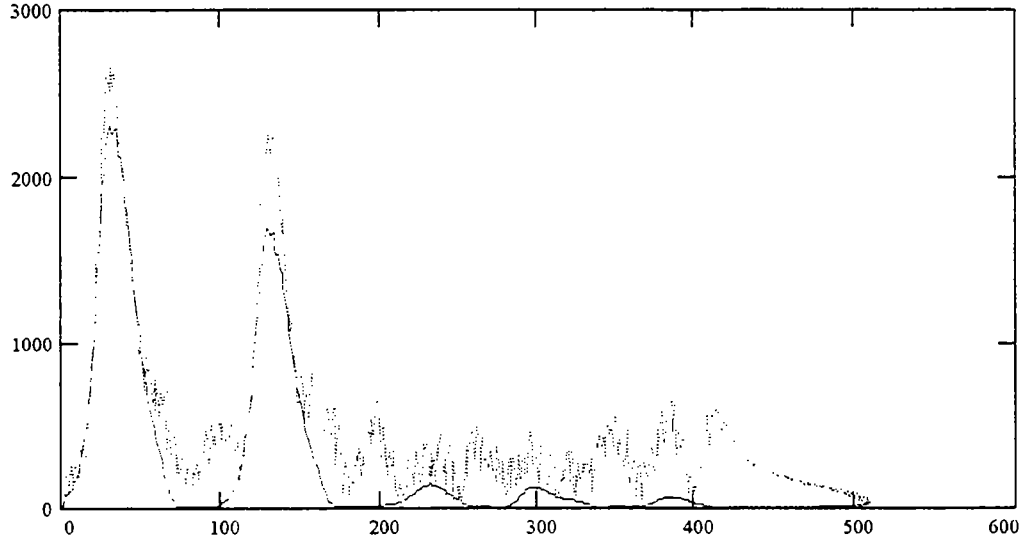

Figure 6.21. Hilbert transforms of clean and noisy data—moisture content, 11%

It is clearly evident from the two figures that noise causes the transform to increase the size of the peak for a particular moisture content. This increase will cause the NN to overreport the moisture content for a particular scan. Since noise is random and cannot be easily factored in as a constant, we have been unable to train an NN with prefiltered data.

6.3 Signal-Processing System

The Texas Transportation Institute's (TTI) software was used as a backup to the GSSI NN. This section describes the software and gives guidelines on how the information generated can be used in the maintenance environment. The software has been described elsewhere with case studies (Scullion, Lau, and Chen 1992), and a summary of the system will be presented in this section.

As discussed in section 2, the GPR transmitting antenna fires a radar pulse into the pavement. This pulse is reflected at layer interfaces where there are electrical discontinuities. The reflected pulse is captured by the system electronics and displayed as a plot of voltage versus time in nanoseconds. The amplitude of reflection at each layer interface is proportional to the electrical contrast between layers; the time between peaks is related to the thickness of the layers. The TTI software package processes every GPR trace collected on the highway. The user manually identifies peaks in the data and sets windows about these peaks. The software automatically locates and measures the amplitude of each peak within the window and calculates the time interval between them. From these amplitudes and time intervals the software calculates the relative dielectric constant and thickness of each layer.

Examples of selecting windows and performing the layer thickness calculation will be described later in this section. It must be remembered that a trace such as shown in figure 6.22 is collected at regular intervals along a highway. Therefore, amplitudes, time delays, dielectric constants, and thicknesses are computed at every location along the highway. The value of each and its variation along the highway are related to the precursors of distress as discussed in section 1, where tentative criteria are given for relating GPR measurements to these precursors.

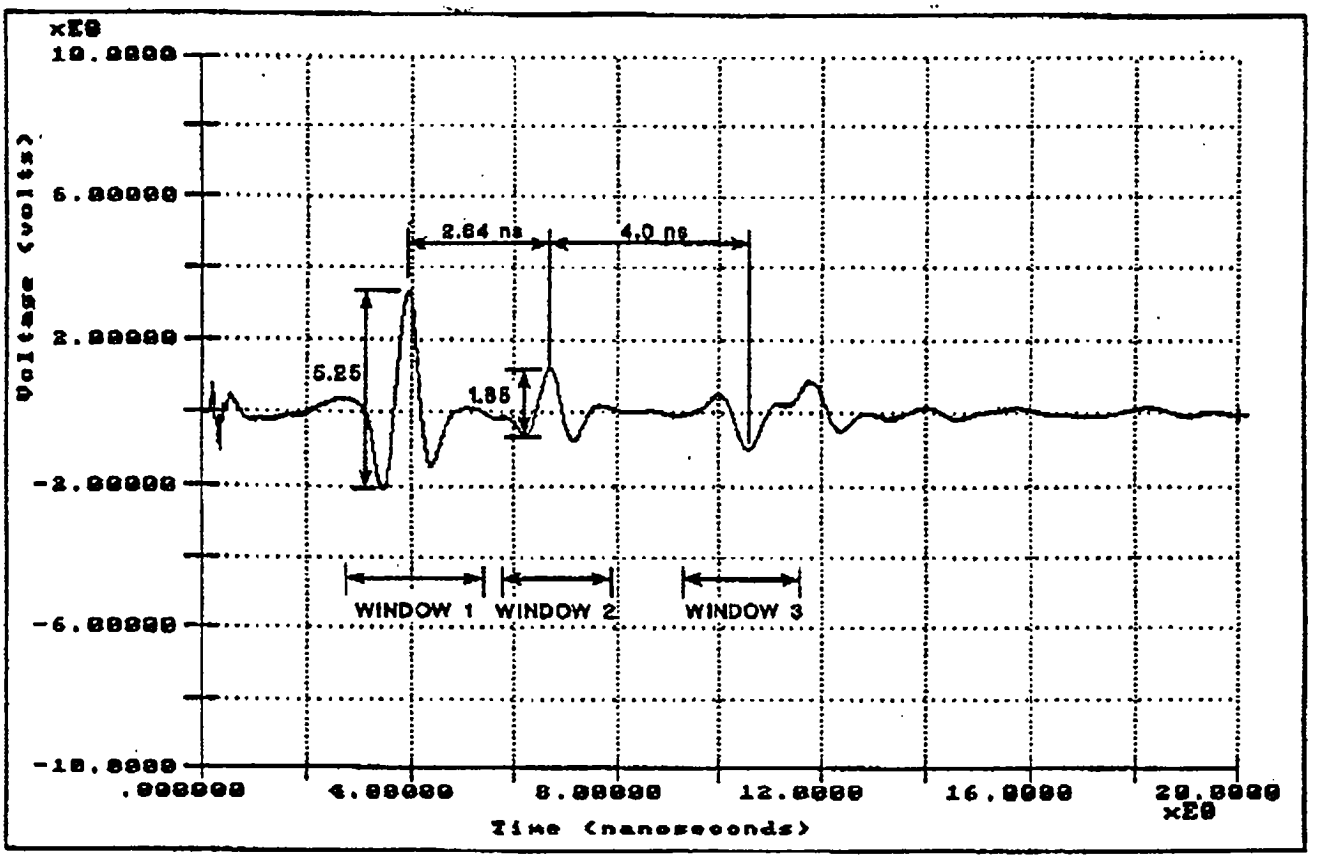

Figure 6.22. Example of layer thickness calculation procedure. The system automatically calculates amplitudes and time delays within user-specified windows.

Computer and Software Requirements

The TTI software is written using the ASYST data acquisition and analysis environment. To run the system the following computer system is required:

1. IBM-compatible microcomputer with 386/25-MHz microprocessor (or higher)
2. 4 megabyte combined conventional, extended memory
3. DOS 4.0 or higher
4. Hard disk with 400 megabyte available storage space and 17 msec or faster access time
5. VGA graphics adapter card with 256 kilobytes or more memory
6. Laser or dot-matrix printer

Input Files

A standard record format is used for files containing radar waveforms. Each record has 2,048 bytes (1,024 words). Words 1 through 1,022 contain digitized voltages (0 to 4,095) representing voltages from -10 to 10 V. Words 1,023 and 1,024 contain the distance-

measuring information. This package has been written to process data from any of the commercially available GPR systems. The GSSI system used in this study recorded 512 points per trace, so an interpolation scheme was used to convert it to the 1,024 points required.

Data-Processing Capabilities for Each GPR Trace

The software package has the following capabilities:

1. Automatic computation of amplitudes of peaks within user-specified windows and of time interval between adjacent peaks.
2. Ability to detect positive or negative peaks. Positive peaks indicate an increase in dielectric constant from one layer to the next, probably an increase in moisture content. Negative peaks indicate a dry, low-density layer or a void.
3. Automatic subtraction of end reflection to remove any antenna related noise (i.e., clutter), leaving only reflected information from the pavement layers.
4. Ability to ignore small peaks or peaks occurring at window edges.
5. Ability to use a fixed dielectric constant rather than a computed value in layer thickness calculation.
6. Ability to perform thin-layer analysis in which a template subtraction is applied to detect overlapping echoes near the surface. The template data file contains a GPR reflection trace from a thick homogeneous layer. By scaling, aligning, and removing the template from the field data trace, the properties of the second layer beneath the thin surface layer to be calculated.
7. Use of a height function to compensate for antenna bounce.

Output Information

For each GPR trace collected along the highway, the TTI software package calculates the following:

1. Amplitude of each peak in the trace (four maximum)
2. Dielectric constant of each layer (four maximum)
3. Time between peaks
4. Thickness of each layer (three maximum)

Equations Used

$$\sqrt{\epsilon_a} = \frac{A_m + A_0}{A_m - A_0} \tag{19}$$

$$\sqrt{\epsilon_b} = \sqrt{\epsilon_a}\left[\frac{1 - \left(\frac{A_0}{A_m}\right)^2 + \left(\frac{A_1}{A_m}\right)}{1 - \left(\frac{A_0}{A_m}\right)^2 - \left(\frac{A_1}{A_m}\right)}\right] \tag{20}$$

$$M = \frac{\sqrt{\epsilon_b} - \gamma\left(\sqrt{\epsilon_a} - 1\right)}{\sqrt{\epsilon_b} - \gamma\left(\sqrt{\epsilon_a} - 22.2\right)} \tag{21}$$

$$h_a = C\frac{\Delta t_1}{\sqrt{\epsilon_a}} \tag{22}$$

where

ϵ_a, ϵ_b	=	Dielectric constants of the asphalt and the base, respectively
ϵ_a	=	Dielectric constant of aggregate in base (4–6, typically)
A_m, A_0, A_1	=	Reflection amplitude from metal plate, top of surface, and top of base, respectively
γ	=	Ratio of dry density to density of solids
M	=	Moisture content of base (% by total weight)
h_a	=	Thickness of asphalt
Δt_1	=	Time between surface and base reflections
C	=	Calibration constant for GPR (theoretically 15 cm/nsec [5.9 in./nsec]) obtained experimentally from a height calibration procedure

Example of Layer Thickness Calculation

The basic operation of the data-processing procedure involves the user manually identifying peaks in a single GPR trace and setting windows about those peaks. The software then automatically locates peaks within the specified windows for every trace in the input data file and measures amplitudes and time delays. From these amplitudes and times, the calculation of (1) the relative dielectric constant of each layer and (2) the thickness of each layer is made by means of the equations 19, 20, and 22.

As an example of the layer thickness calculation, the GPR waveform from an asphalt test box is shown in figure 6.22 (see Scullion, Lau, and Chen 1992, for details of equipment used). The thickness of both the asphalt and granular base layer was 15 cm (6 in.); the

wooden box containing the sample was resting approximately 7.5 cm (3 in.) above the floor. The overall dimensions of each sample were 90 x 90 x 30 cm (36 x 36 x 12 in.). The end reflection has been automatically removed from the corresponding GPR waveform (figure 6.22). The large peak at 4 nsec is from the asphalt surface; the next is from the top of the granular base. The negative peak just after 10 nsec is where the GPR wave enters air at the bottom of the test box.

The figure also shows the three user-defined windows and the measured amplitudes and time delays. In the metal plate test, an amplitude of reflection of 12.92 V was recorded. The GPR calibration constant was determined to be 13.6 cm/nsec (5.36 in./sec). The computation of dielectric constants and layer thicknesses proceeds as follows:

Using equation 19,

$$\sqrt{\epsilon_a} = \frac{A_m + A_0}{A_m - A_0} = \frac{12.92 + 5.25}{12.92 - 5.25} = 2.369$$

Using equation 22,

$$h_a = 5.36 \frac{\Delta t}{\sqrt{\epsilon_a}} = 5.36 \frac{2.64}{2.369} = 5.98 \in.$$

Using equation 20,

$$\sqrt{\epsilon_b} = \sqrt{\epsilon_a} \left[\frac{1 - \left(\frac{A_o}{A_m}\right)^2 + \left(\frac{A_1}{A_m}\right)}{1 - \left(\frac{A_o}{A_m}\right)^2 - \left(\frac{A_1}{A_m}\right)} \right]$$

$$= 2.369 \left[\frac{1 - \left(\frac{5.25}{12.92}\right)^2 + \left(\frac{1.85}{12.92}\right)}{1 - \left(\frac{5.25}{12.92}\right)^2 - \left(\frac{1.85}{12.92}\right)} \right]$$

$$= 3.349$$

Using equation 22,

$$h_b = 5.36 \frac{\Delta t}{\sqrt{\epsilon_b}} = 5.36 \frac{4.0}{3.349} = 6.40 \text{ in.}$$

The calculated thickness of the base (h_b) includes the thickness of the wood at the bottom of the test box.

Output Formulas of TTI Software

The main outputs from the system are graphical displays of any of the calculated parameters (four amplitudes, three dielectric constants, three thicknesses, three time delays, and base moisture content) against distance traveled along the highway. An example of this display is shown in figure 6.23. The peaks in the data are associated with problem conditions; in this case, voids beneath the slab were associated with peaks above 0.5 V.

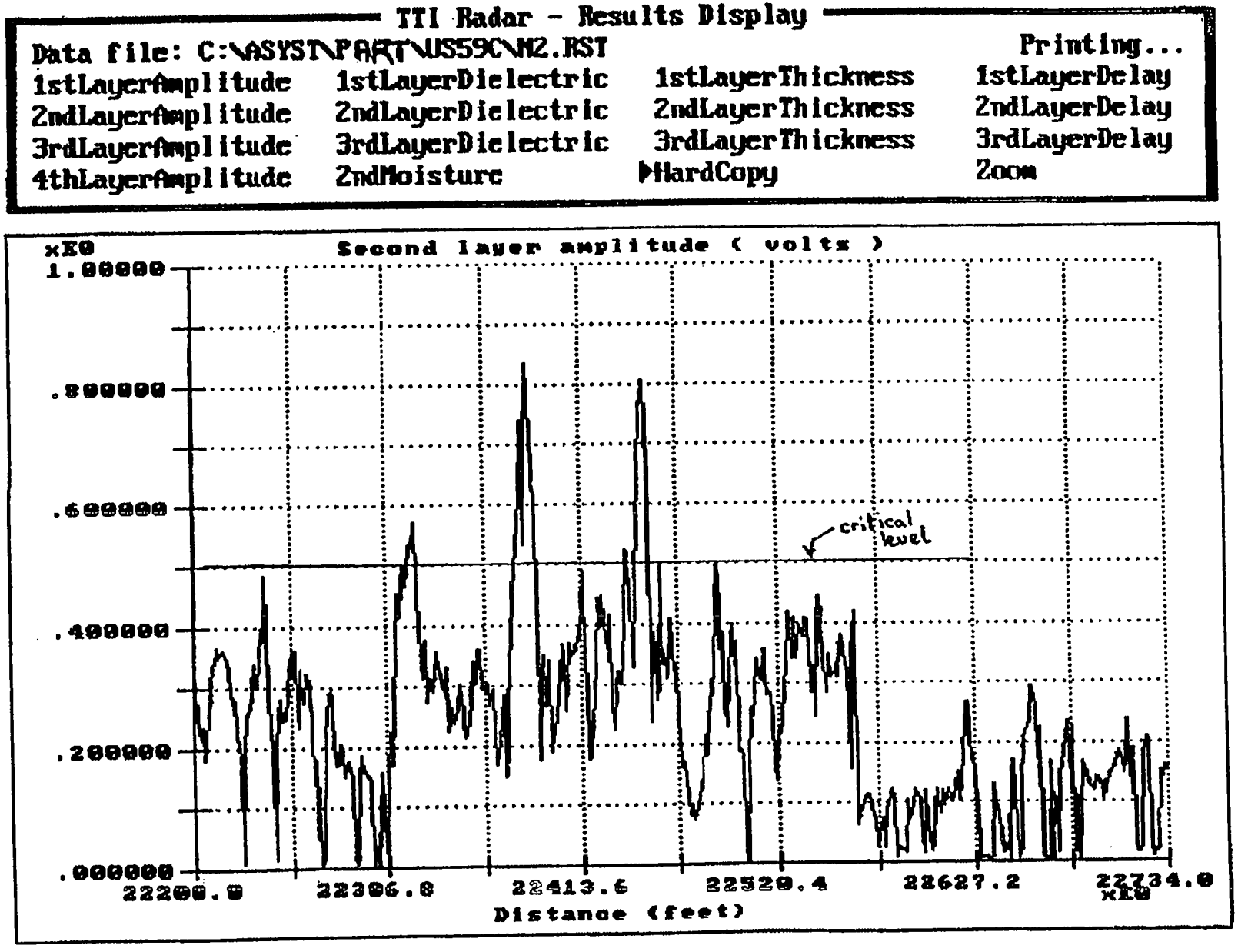

Figure 6.23. Graphical display from TTI data-processing system. In this case the amplitude of the second layer was used to indicate the presence of moisture-filled void beneath a concrete pavement.

7

Laboratory and Field Test Program

7.1 Specifications Testing

The first-generation prototype system had significant problems with clutter and jitter. Jitter is defined as excessive random variations in reflection amplitude from a fixed target, such as a metal plate. Clutter is undesirable perturbations in the tail of the radar trace that will superimpose themselves on the signals reflected from the pavement layer interfaces. To aid the system design process, a set of performance criteria were developed to ensure that the system supplies signals of sufficient quality for pavement applications.

Two approaches can be taken to set performance standards:

1. Base specifications on existing commercially available 1.0-GHz ground-penetrating radar (GPR) systems.
2. Base specifications on the accuracy required to meet the specified measurement criteria.

Both approaches have merit, although the second is clearly preferable. In establishing the criteria, the research team initially based them on their experience with other commercial radar units; the criteria were later modified by theoretical analysis of the accuracy required to meet the measurement criteria. The four criteria developed are listed below followed by the results obtained with the Geophysical Survey Systems, Inc. (GSSI) systems. In performing these tests, the equipment was mounted at the recommended test height above a metal plate or concrete slab.

Criterion A: Signal Jitter

The maximum change in amplitude for a reflection from a fixed object (large metal plate) should be less than 4% of the mean amplitude. The GPR is positioned above the

center of a 1.22 x 1.22 m (4 x 4 ft) metal plate, and 64 consecutive traces are taken at a data-acquisition rate of at least 25 traces per second. The amplitude of reflection for each trace is computed, and the difference between the high amplitude value and the low value should be less than 4% of the mean value. This specification is aimed at ensuring that the variations in the reflection amplitude are related not to problems with system noise but to changes in pavement condition.

Criterion B: Clutter Level

For an idealized GPR system, the metal plate reflection should consist of a symmetrical reflection from the surface of the metal plate plus a relatively flat tail. The tail is defined as that portion of the trace from 2 to 10 nsec after the surface reflection. It is in this area that the pavement information will be found. To ensure that peaks in the tail are related to subsurface pavement reflections, the following criterion was established: Using the same setup as Criterion A, measure the amplitude of reflection of any peak in the tail of the trace. This amplitude should be less than 5% of the amplitude of the metal plate reflection.

Criterion C: End Reflection

End reflection means internal system reflections that occur before the reflection from the pavement surface. To ensure that these reflections do not interfere with the pavement information, the following specification, which refers to the waveforms collected in Criterion A, was proposed: The end reflection, defined as any peak occurring before the metal plate reflection, should be less than 50% of the reflection from the metal plate.

The end reflection of interest is typically generated by the impedance mismatch at the end of the antenna as the wave enters air. The overlapping impact of this return can be minimized by raising the operating height of the antenna above the surface. There are then two conflicting requirements: (1) having the system close to the surface to get maximum focus of available power and (2) having the system far enough away to minimize end reflection overlap.

Both the 1.0- GHz and the 2.5-GHz systems are bistatic, consisting of both a transmitting and a receiving antenna. GSSI laboratory tests had concluded that the desired separation between these antennas was 18 cm (7 in.) for the 1.0-GHz system and 33 cm (13 in.) for the 2.5-GHz system. Tests at Texas Transportation Institute (TTI) concluded that the best height above the ground to operate these antenna to minimize end reflection problems was 46 to 51 cm (18 to 20 in.) for the 1.0-GHz antenna and 23 to 25 cm (9 to 10 in.) for the 2.5-GHz system. All the laboratory tests at TTI were conducted with this arrangement.

Criterion D: Penetration

The penetration capability of the systems was tested by resting a concrete slab 15 cm (6 in.) thick and 91 X 91 cm (36 X 36 in.) square on top of a large metal plate. The slab was of unreinforced concrete and at least 28 days old. The amplitude of reflection from the concrete surface and the plate was measured; the ratio of plate to concrete surface reflection should be greater than 30% for the 1.0-GHz system and greater than 20% for the 2.5-GHz system.

Test Results

Typical metal plate reflections from the GSSI 1.0- and 2.5-GHz systems are shown in figures 7.1 and 7.2. In figure 7.1, the end reflection is at approximately 7 nsec, the metal plate reflection is between 8 and 10 nsec, and the tail is relatively flat. In figure 7.2, the end reflection is just after 2 nsec, the surface echo at 5 nsec. For the 2.5-GHz system, a significant peak is observed in the tail at approximately 3.5 nsec.

The results obtained from the performance tests conducted at TTI are shown in table 7.1. The system met all the proposed specifications except the jitter criterion for the 2.5-GHz unit. The peak at approximately 3.5 nsec caused problems with quantifying the size of the reflections from subsurface layers. More work was needed to flatten the tail of the 2.5-GHz unit. This work involved changing the test setup, changing the antenna's end loading, or modifying the system pulser or sampler. Alternatively, the jitter needed to be accounted for in the signal-processing software.

Table 7.1
Results of Specification Test of the Second-Generation Prototype

Criterion	Test	Proposed Criterion	Performance	
			1.0-GHz	2.5-GHz
A	Clutter	< 4%	0.7%	1.4%
B	Jitter	< 5%	3.5%	14.5%
C	End Reflection	< 50%	34%	16.8%
D	Penetration	> 30% for 1.0-GHz > 20% for 2.5-GHz	86%	44%

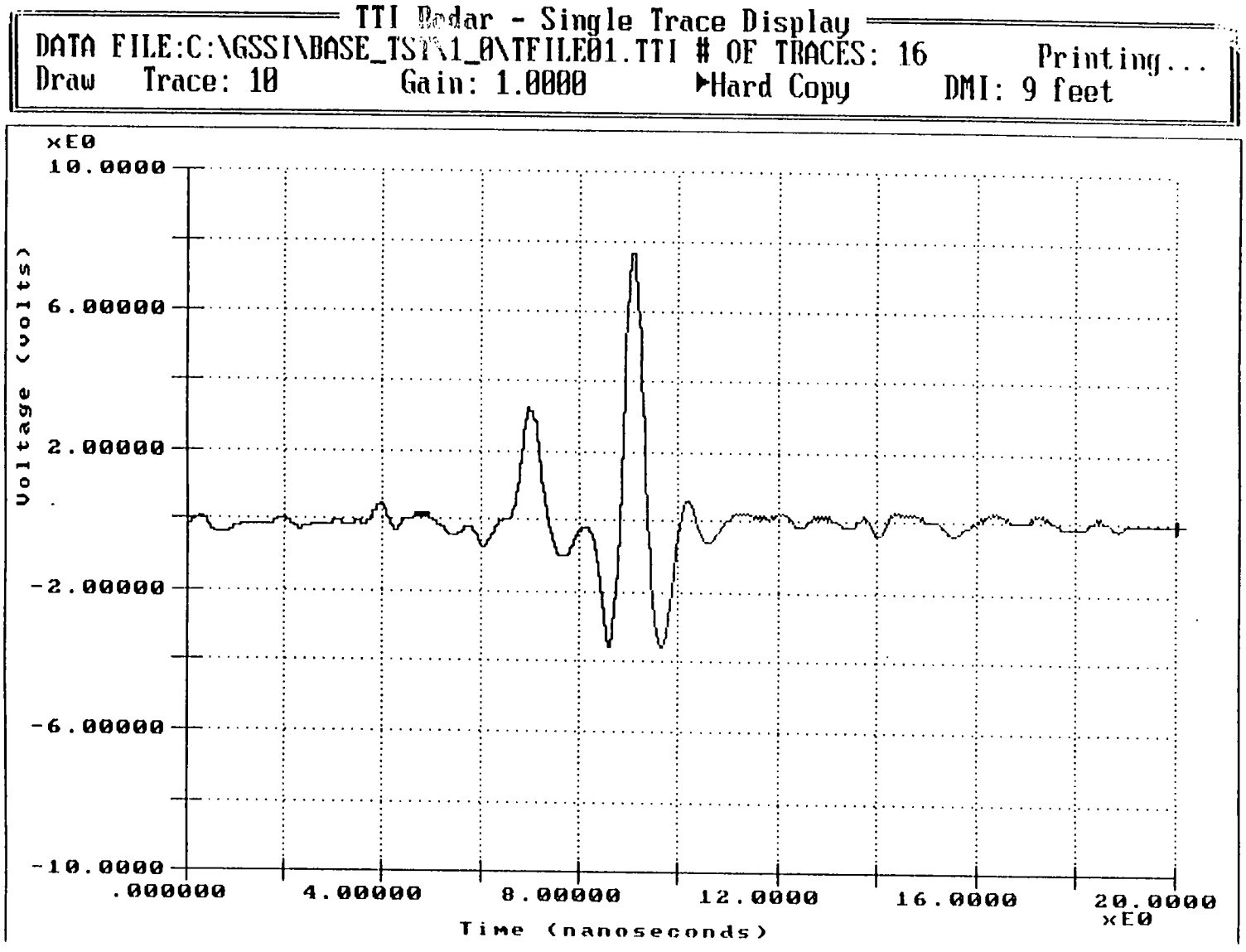

Figure 7.1. Metal plate reflection from 1.0-GHz antenna

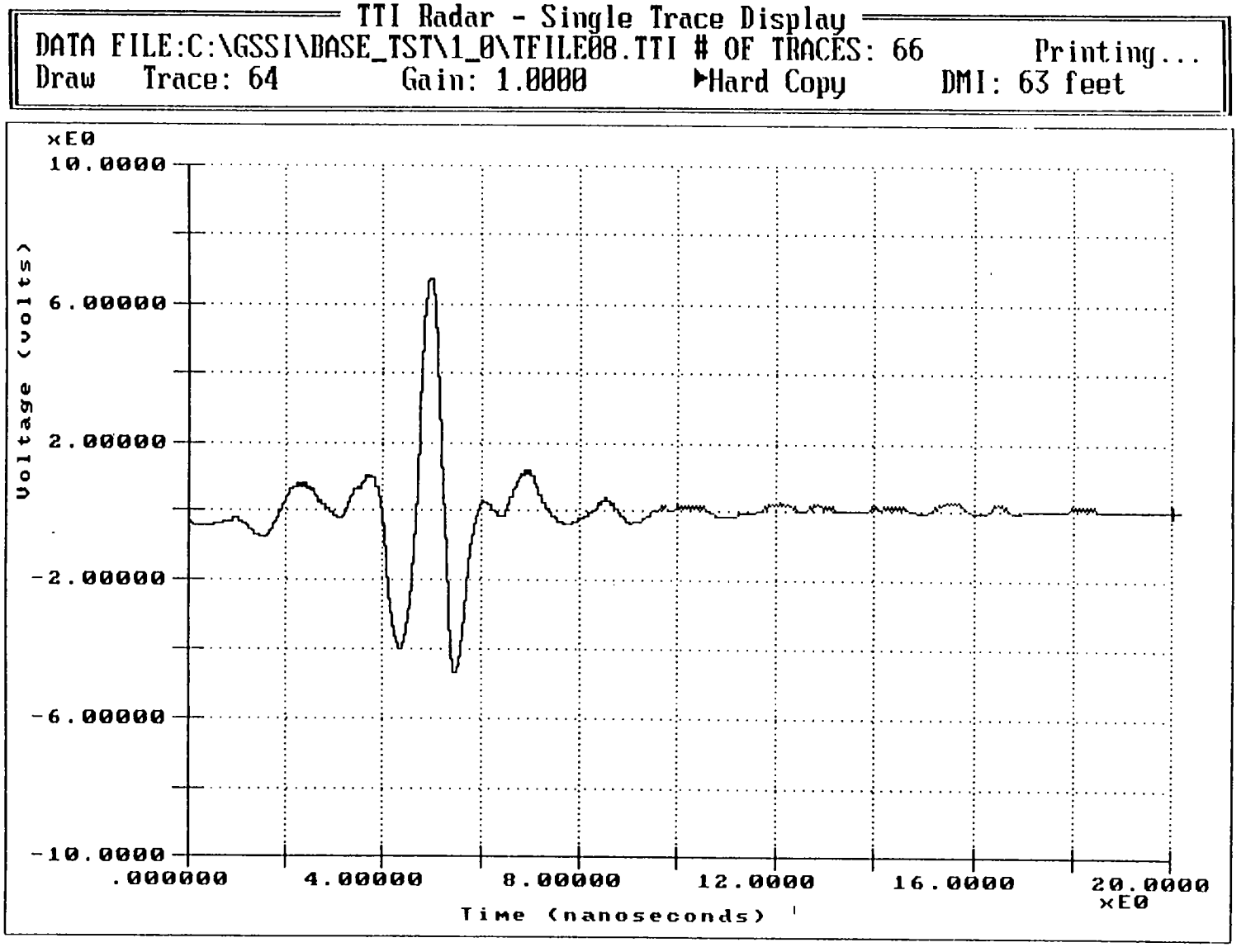

Figure 7.2. Metal plate reflection from 2.5-GHz antenna

7.2 Laboratory Test

A series of laboratory tests was conducted to evaluate GPR's potential for detecting changes in base moisture content and for identifying air-filled and moisture-filled voids beneath a concrete slab. The results of this evaluation are presented in this section.

Void Detection

The air void test consisted of a concrete slab 15 cm (6 in.) thick resting on wood dowels. Beneath the dowels was an asphalt slab. The dowel sizes were varied from 0.48 cm (3/16 in.) to 3.8 cm (1 ½ in.). The 1.0-GHz antennas were mounted approximately 48 cm (19 in.) above the concrete slab. Typical test results are shown in figure 7.3. With no void, a slight negative peak is observed at the concrete-asphalt interface because the concrete has a higher dielectric constant than the asphalt. The size of the negative peak increases with the size of the air void. A graph of air void size versus change in negative peak size is shown in figure 7.4. As reported in section 5, the noise in the system was low, less than 0.1 V. Therefore, under ideal conditions the 1.0-GHz GPR should be able to detect very small air voids. However, in the field the conditions are never ideal and the true baseline zero-void condition is difficult, if not impossible, to obtain. In most pavement applications, the slab thicknesses are substantially greater than 15 cm (6 in.), the steel reinforcing introduces more reflectors into the system, and the support conditions are extremely variable.

The water-filled void test results are shown in figure 7.5, in which the 0.48 cm (3/16 in.) and 3.8 cm (1 ½ in.) void GPR waveforms are presented. The amplitude of reflection at the water void was defined as the difference in voltage from the peak to the preceding minimum. In all cases, the amplitude was measured to be between 4.0 and 4.2 V. In figure 7.5, the only differences between the two reflectors at the water void are in the trailing leg of the reflection. With the smaller void, it appears that a negative peak is superimposed on the trailing leg of the water void reflection. The dielectric constant of the concrete was assumed to be 8 and that of the water to be 81, and the time intervals were measured between (1) the surface echo and the positive water void peak (3.05 nsec), and (2) the positive water void peak and the negative trailing leg peak (0.50 nsec). From these values, the thickness of the slab was calculated to be 16 cm (6.3 in) and the void to be 0.76 cm (0.3 in.); the actual sizes were 15 cm (6 inc.) and 0.5 cm (0.2 in). More sophisticated deconvolution of the thin water void reflection may produce better thickness estimates.

In the 3.8 cm (1 ½ in.) void trace, the negative peak (B) at 9 nsec indicates the top of the wooden box. The time delay between peaks A and B represents the travel time in water, 2.1 nsec. Assuming the dielectric constant of water is 81, the thickness is calculated as 3.7 cm (1.46 in.), versus the actual thickness of 3.8 cm (1 ½ in.). It appears that in this ideal case water-filled void is detected by the amplitude of the reflection. The thickness of the void can also be estimated reasonably accurately.

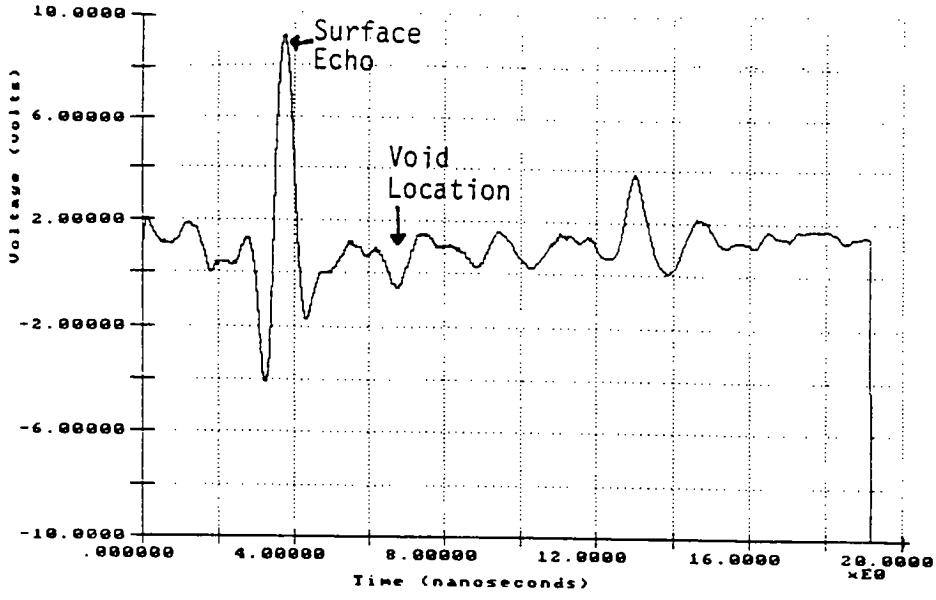

(a) No void

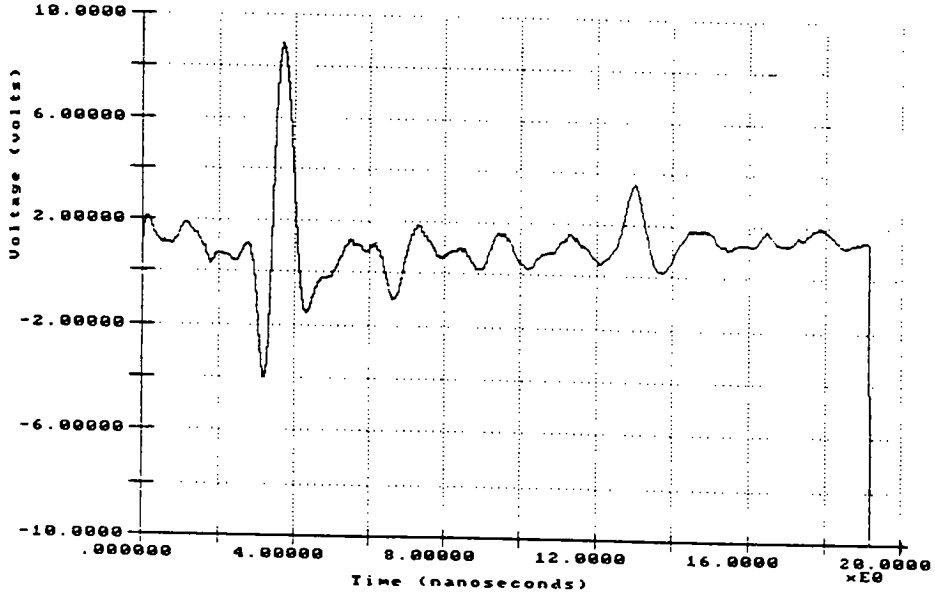

(b) 75 mm (5/16 in.) void

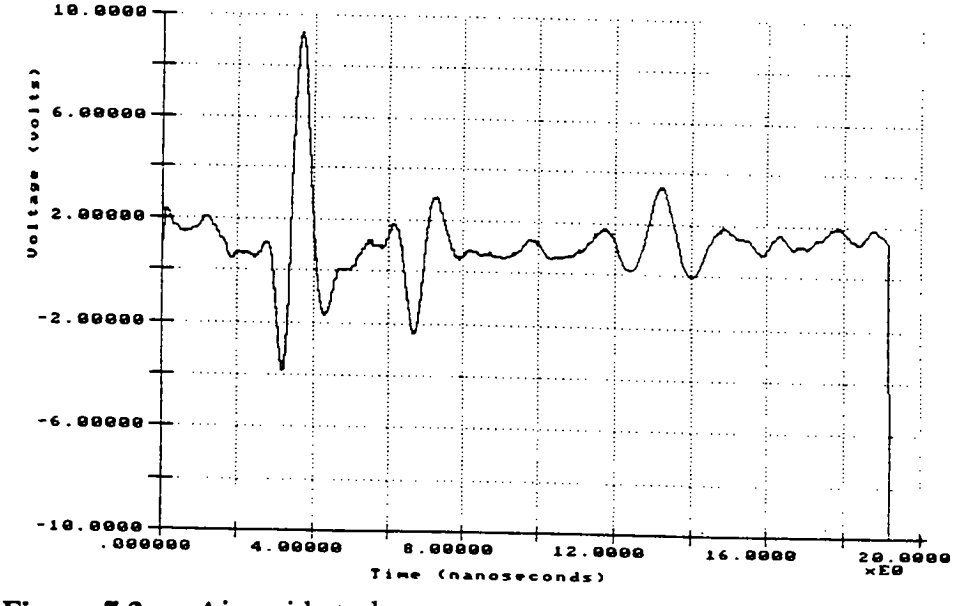

(c) 38 mm (1½ in.) void

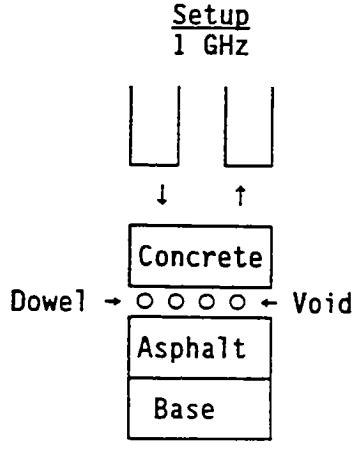

Figure 7.3. Air void study

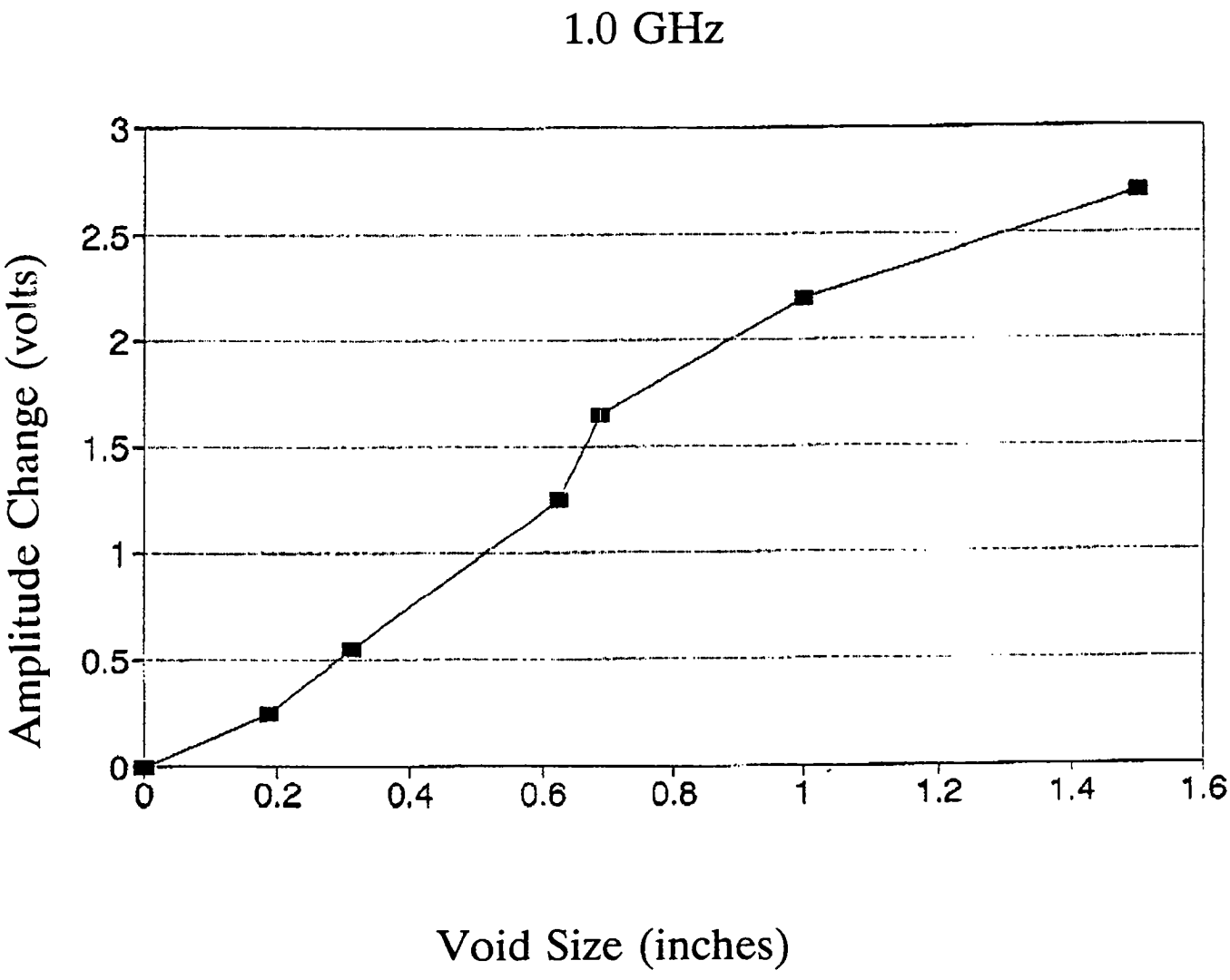

Figure 7.4. Air void test results

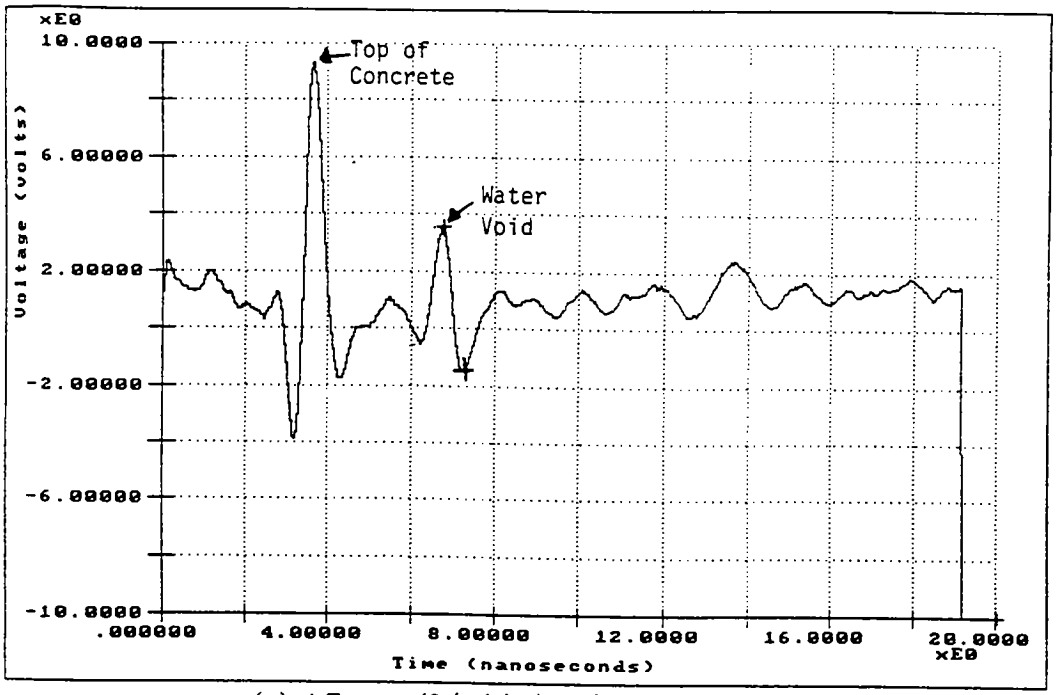

(a) 4.7-mm (3/16-in.) void

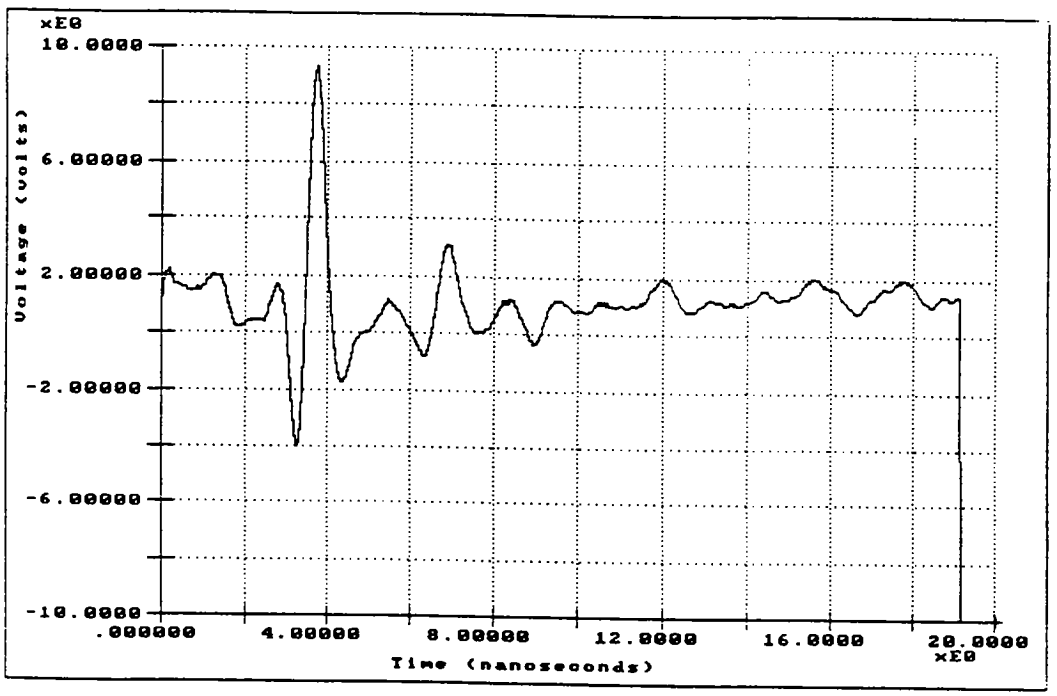

(b) 38-mm (1½-in.) void

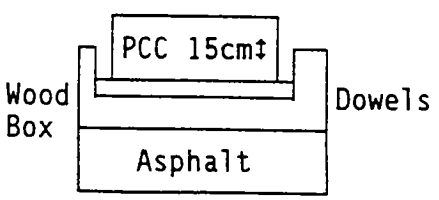

Figure 7.5. Moisture-filled void study

Studies of Moisture in the Base

A series of tests was conducted with crushed limestone granular base that was compacted to the same volume at different moisture contents. Tests were conducted at moisture contents of 6%, 8%, and 10% by weight. The 10% moisture content represents the fully saturated case for this material. GPR readings were taken with the 1.0-GHz unit directly above (1) the granular base (2) an asphalt slab 1.5 cm (6 in.) thick on top of the granular base, and (3) a portland cement concrete (PCC) slab 1.5 mm (6 in.) thick on top of the granular base. The collected GPR waveforms are shown in figures 7.6 through 7.8. A small metal plate was placed at the bottom of the granular base to ensure that the time of travel and corresponding base thickness could be calculated. The standard metal plate reflection was made at the same time, and that value was used in the TTI software package to calculate layer dielectric constants and thicknesses. The results of these calculations are shown in table 7.2. The results for the base only and for asphalt over base look promising. The base dielectric constant values increase with increasing moisture content, and the layer thicknesses are close to the actual thicknesses. In the calculation process, the metal plate and the surface reflections are used to calculate the dielectric constant of the top layer by means of equation 19 from section 6.3. The results from the test on the PCC slab are inconsistent; very small reflections were recorded beneath the slab. Also, the dielectric constant that was calculated from the surface reflection appears low.

It is possible to conclude that the GPR system can detect wet base conditions beneath asphalt layers. As discussed in earlier reports, the dielectric constant values calculated for the base layer appear consistent with those that would be calculated with the linear moisture model as described in section 2.4. With such a model, it should be possible to convert the measured dielectric constant to an in situ moisture content. However, it is doubtful that reasonable estimates can be made for base beneath PCC slabs. The dielectric constant for PCC is typically in the rang of 7 to 9 rather than the 5 to 6.5 calculated in these tests.

Table 7.2
Results from Signal Processing of Base Moisture Test Results

Test	%M	t_1	t_2	A_1	A_2	ϵ_1	ϵ_2	h_1	h_2
Base only	6	-	2.34	-	10.58	-	8.69	-	4.9
	8	-	2.89	-	12.51	-	14.46	-	4.7
	10	-	-	-	-	-	-	-	-
PCC over base	6	2.40	2.51	8.67	0.39	5.51	6.01	6.3	6.4
	8	3.04	3.04	9.29	0.78	6.30	7.51	7.5	6.9
	10	2.96	3.24	8.79	1.57	5.05	6.98	8.1	7.6
Asphalt over base	6	2.03	2.26	8.60	2.84	5.48	10.38	5.4	4.4
	8	2.42	2.85	9.04	4.92	5.32	15.09	6.5	4.6
	10	2.34	3.20	8.85	5.44	5.15	16.16	6.3	4.9

%M = Percentage moisture by weight
t_1, t_2 = Time of travel in top layer and base, respectively (nsec)
A_1, A_2 = Amplitude of reflection from top of surface and base, respectively (V)
ϵ_1, ϵ_2 = Calculated dielectrics for surface and base, respectively
h_1, h_2= Thickness of surface and base, respectively (in.) (h_1 = 6.0, h_2 = 4.8)

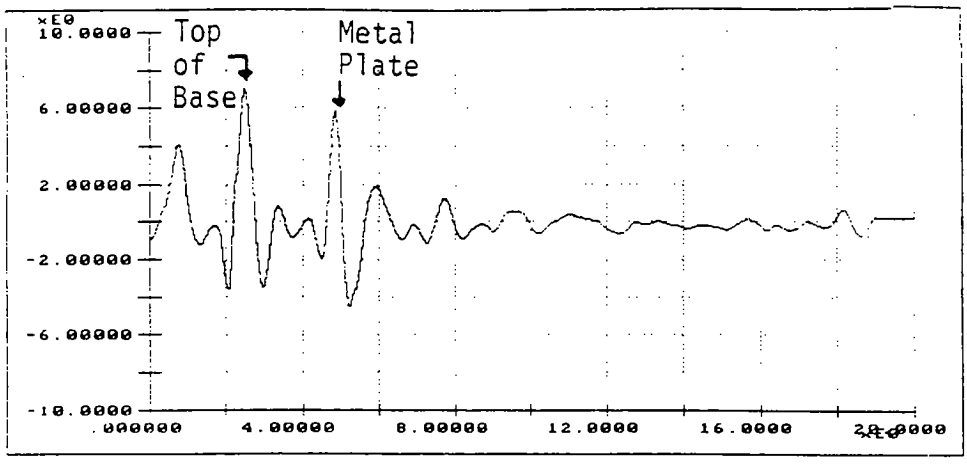

(a) 6% base

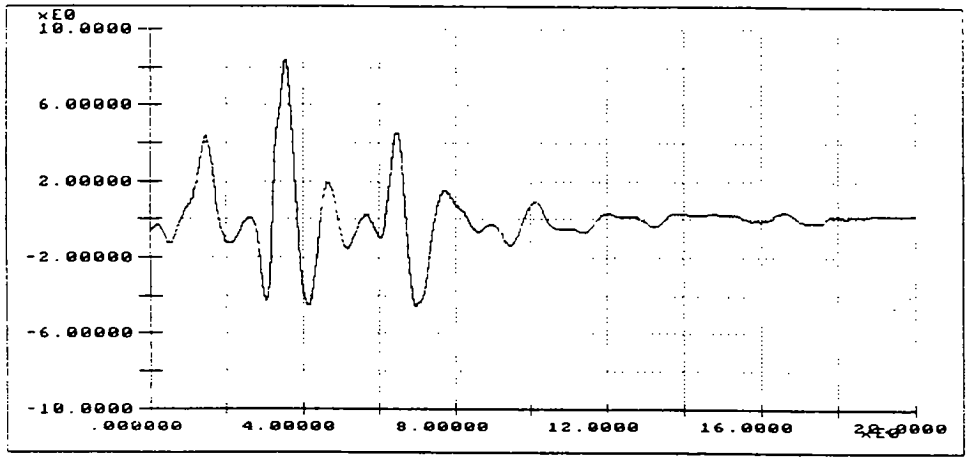

(b) 8% base moisture

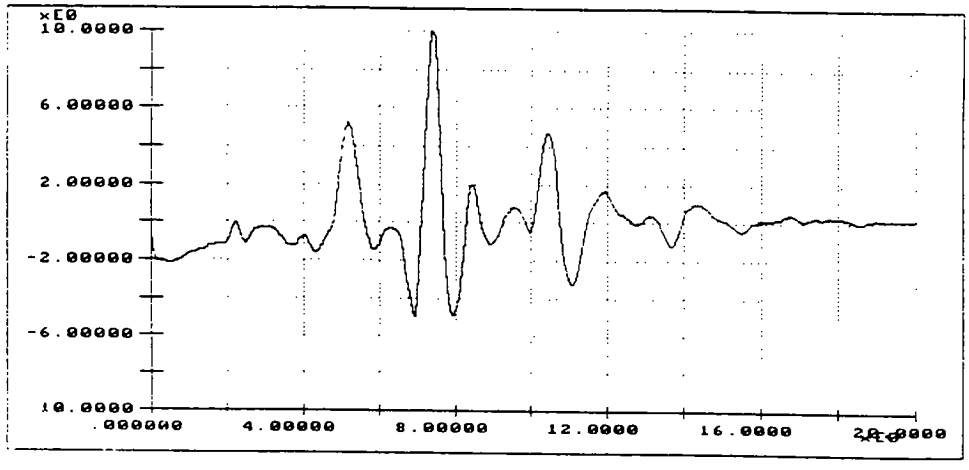

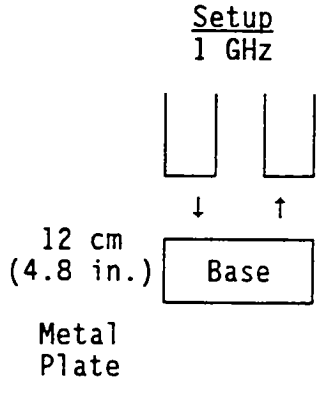

(c) 10% base moisture

Figure 7.6. Base moisture test results (volts versus time in nanoseconds)—granular base alone

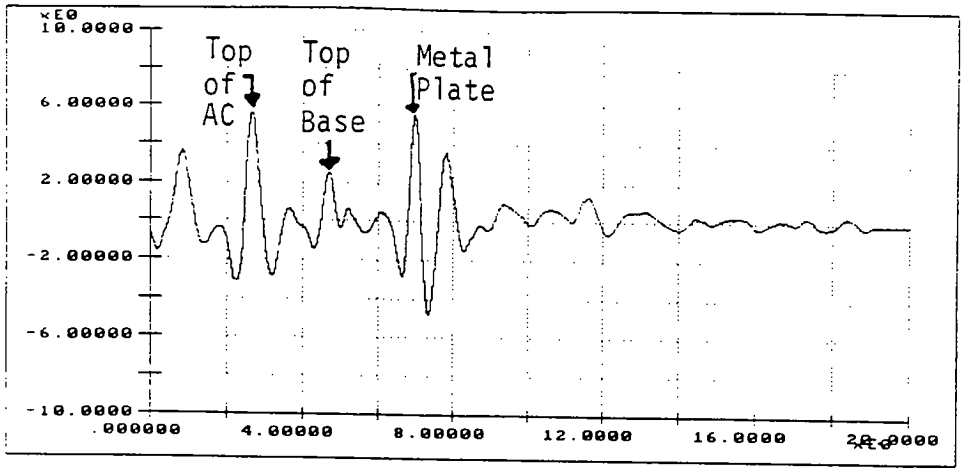

(a) 6% base moisture

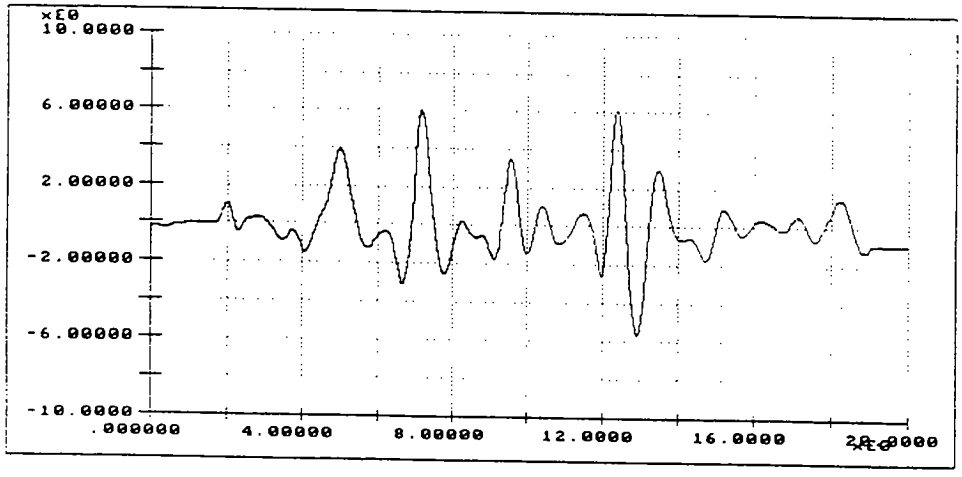

(b) 8% base moisture

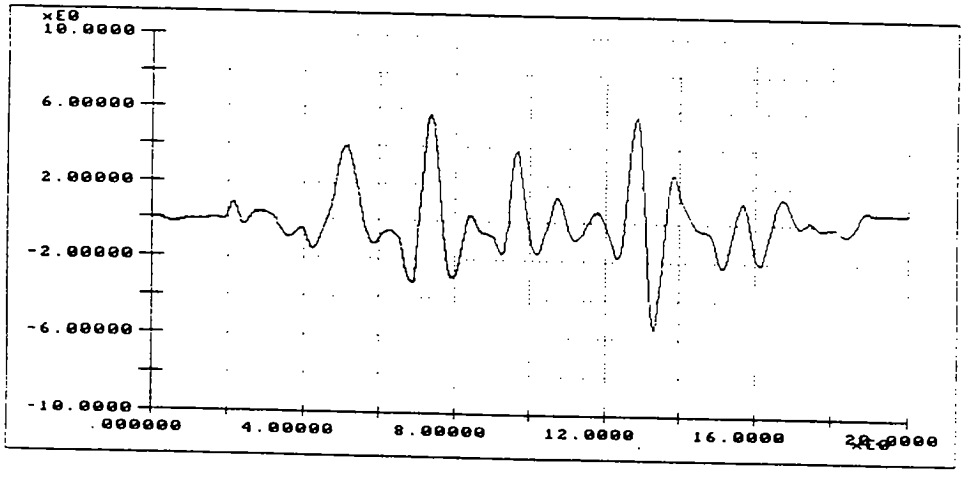

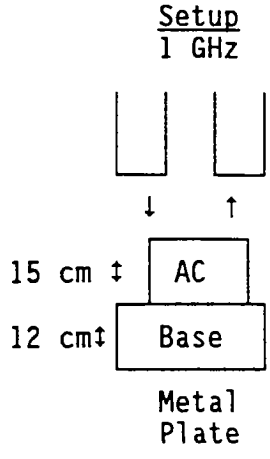

(c) 10% base moisture

Figure 7.7. Base moisture test results (volts versus time in nanoseconds)—asphalt slab over granular base

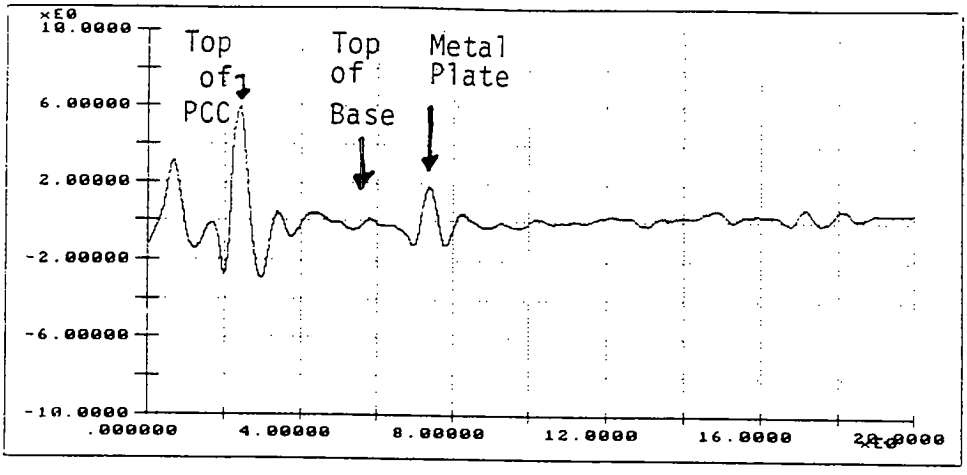

(a) 6% base moisture

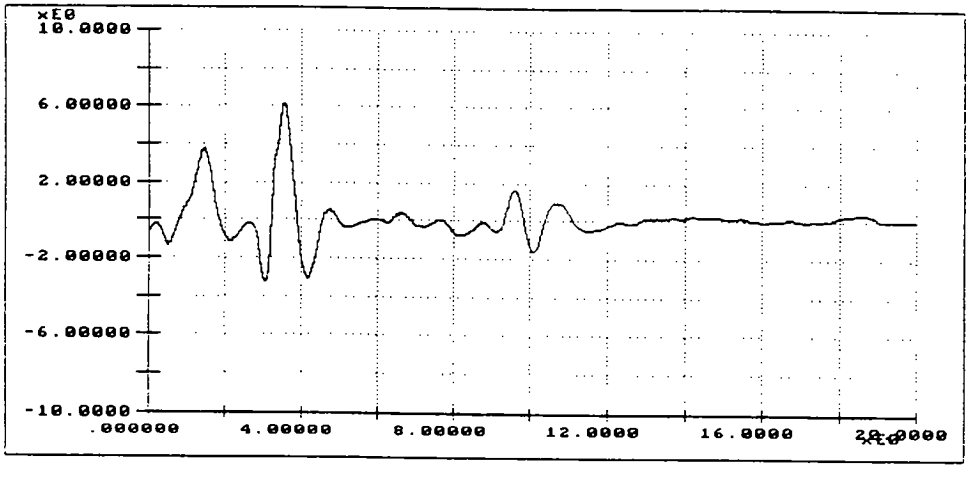

(b) 8% base moisture

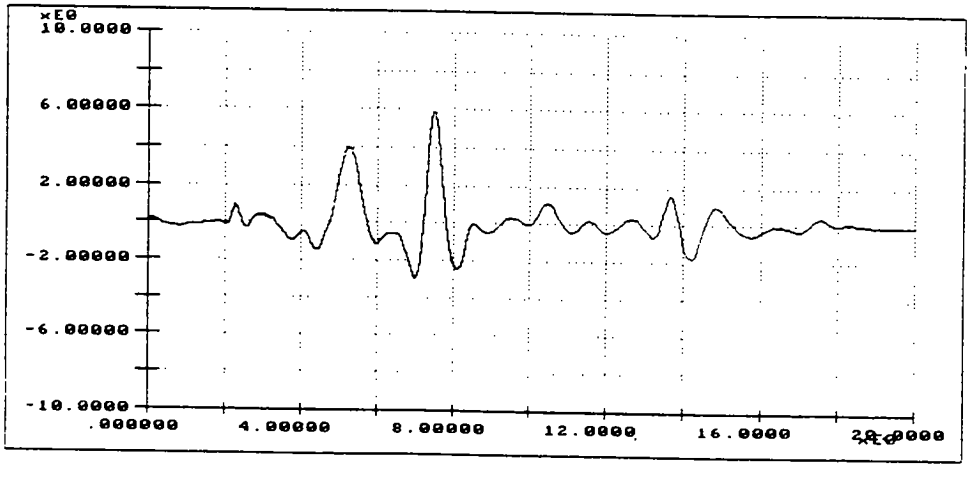

(c) 10% base moisture

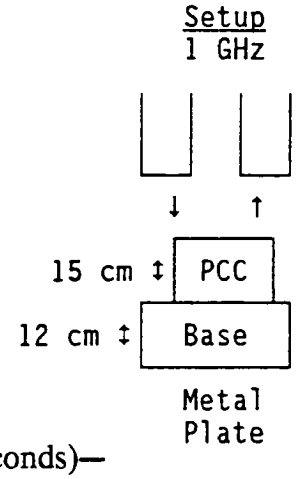

Figure 7.8. Base moisture test results (volts versus time in nanoseconds)—PCC slab over granular base

7.3 Pilot Scale Field Test Results

Asphalt Control Sections

As part of the field evaluation plan, a set of four small 1.8- x 1.8-m (6 ft x 6 ft) asphalt test sections was constructed. The composition of these test sections was verified to be the following:

Section 1: 17.8 cm (7 in.) of asphalt
5.0 cm (2 in.) of stripped asphalt
7.6 cm (3 in.) of flexible base

Section 2: 10.2 cm (4 in.) of asphalt
20.3 cm (8 in.) of flexible base

Section 3: 14.0 cm (5.5 in.) of asphalt
16.5 cm (6.5 in.) of flexible base

Section 4: 25.4 cm (10 in.) of asphalt
5.0 cm (2 in.) of flexible base

The stripped asphalt was simulated by using a single-sized aggregate lightly coated with asphalt. The result was a very low-density mix directly beneath the overlying asphalt layer. The GPR traces obtained are shown in figure 7.9 and 7.10. The trace for test section 1, which contains the simulated stripping, has the surface and base echoes at 3.7 and 6.8 nsec. However, just before the positive base return, there appears to be a negative echo at approximately 6.2 nsec, presumably from the thin stripping layer. The traces for test section 2 and 3 have clear surface and base echoes. The trace for test section 4 also shows a negative peak just before the base reflection (at 2.7 nsec). This peak was not intended but was possibly due to poor compaction of the bottom lift of the thick asphalt layer.

In processing these traces through the TTI software, two windows were set for test sections 2, 3, and 4, and the dielectric constants and asphalt thicknesses were calculated as shown in table 7.3. In processing the section containing the stripping, the asphalt was considered as two layers; the results shown in table 7.4.

Table 7.3
Results of TTI Software on Test Section with Varying Asphalt Thickness

Test Section	Dielectric Constants		Calculated Thickness (cm)	Actual Thickness (cm)
	Asphalt	Base		
2	6.1	12.8	9.4	10.2
3	5.9	13.2	13.5	14.0
4	5.6	10.3	26.0	25.4

Table 7.4
Results of TTI Software on Test Section with Asphalt Stripping

Test Section	Dielectric Constants		Calculated Thickness (cm)		Actual Thickness (cm)	
	Asphalt	Strip	AC	Strip	AC	Strip
1	5.4	3.2	18.1	4.1	17.8	5.0

The results from this analysis appear reasonable. The layer thickness estimates were accurate; the largest absolute error was 0.9 cm, and the average relative error was 6.7%. The stripping was identified as a low-dielectric-constant layer. This is reasonable because the layer was dry with a very low density. Typical asphalts have been measured to have dielectric constants of between 5 and 6. The stripped layer had a dielectric constant of 3.2.

Concrete Control Section

Further testing was performed on a concrete slab specifically designed for GPR calibration. The slab was resting on a cement-treated base (CTB). In one location, a metal plate was placed beneath the slab; in a corner location, a 2.5 cm (1 in.) air void was placed beneath the slab. The GPR waveforms collected with the 1.0-GHz unit are shown in figure 7.11. In the control location, it is very difficult to locate the interface between the concrete and the CTB. The reflections from the metal plate and air void are clearly shown. In calculating the thickness of the concrete above the metal plate, the TTI software was used. The dielectric constant of the concrete was calculated to be 9.7, with a concrete thickness of 17.7 cm (6.96 in.). The calculated concrete thickness compared very well with the actual verified thickness of 18.4 cm (6.8 in.). The air void, as expected, caused a negative peak in the trace at approximately 6.5 nsec.

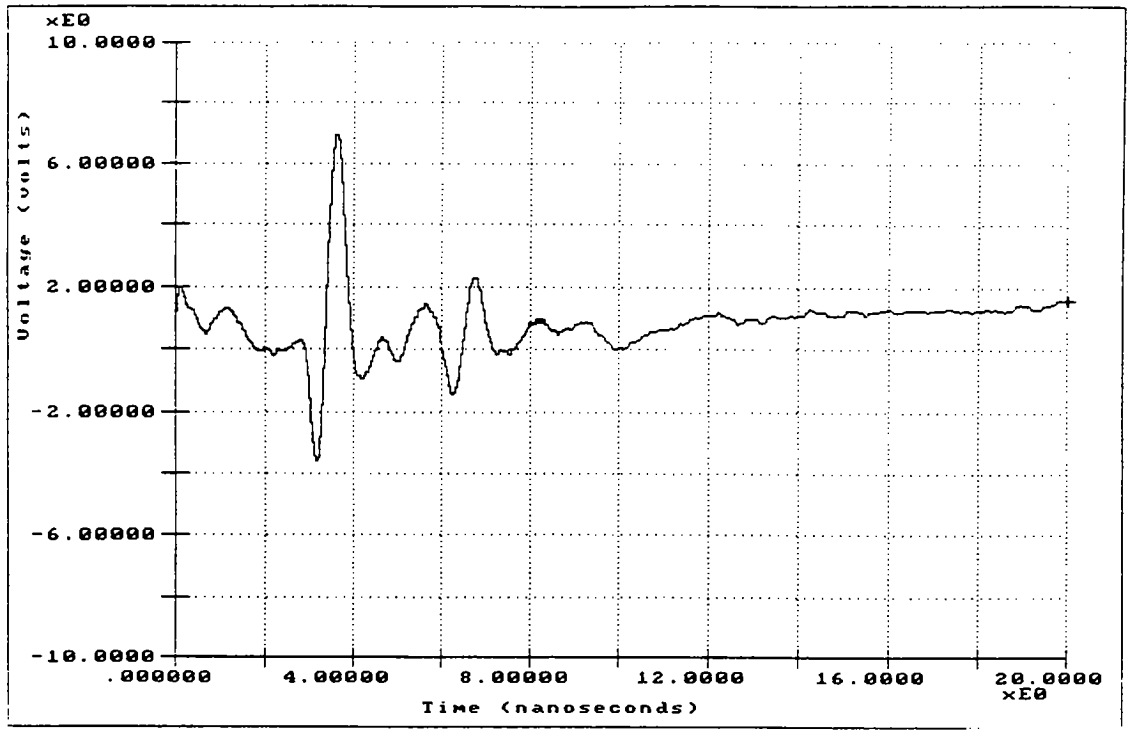

(a) Test section 1—17.8 cm (7 in.) of asphalt over 5.0 cm (2 in.) of stripping

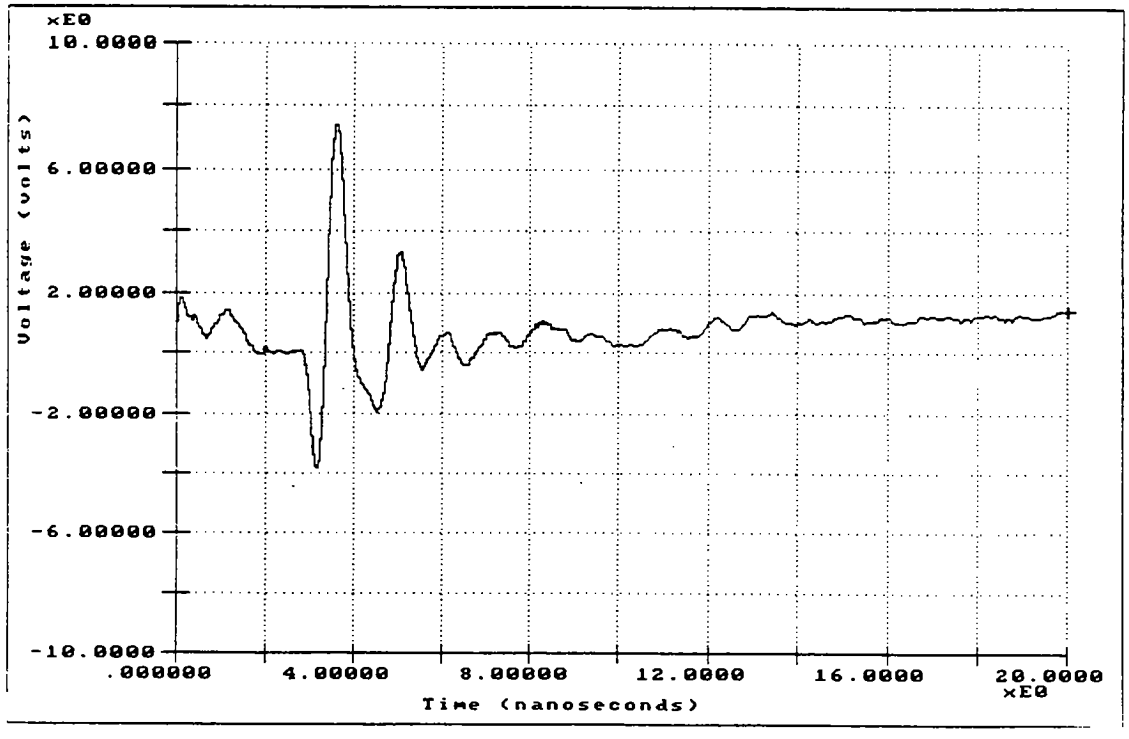

(b) Test section 2—10.2 cm (4 in.) of asphalt

Figure 7.9. Ground-penetrating radar traces from asphalt control test sections 1 and 2

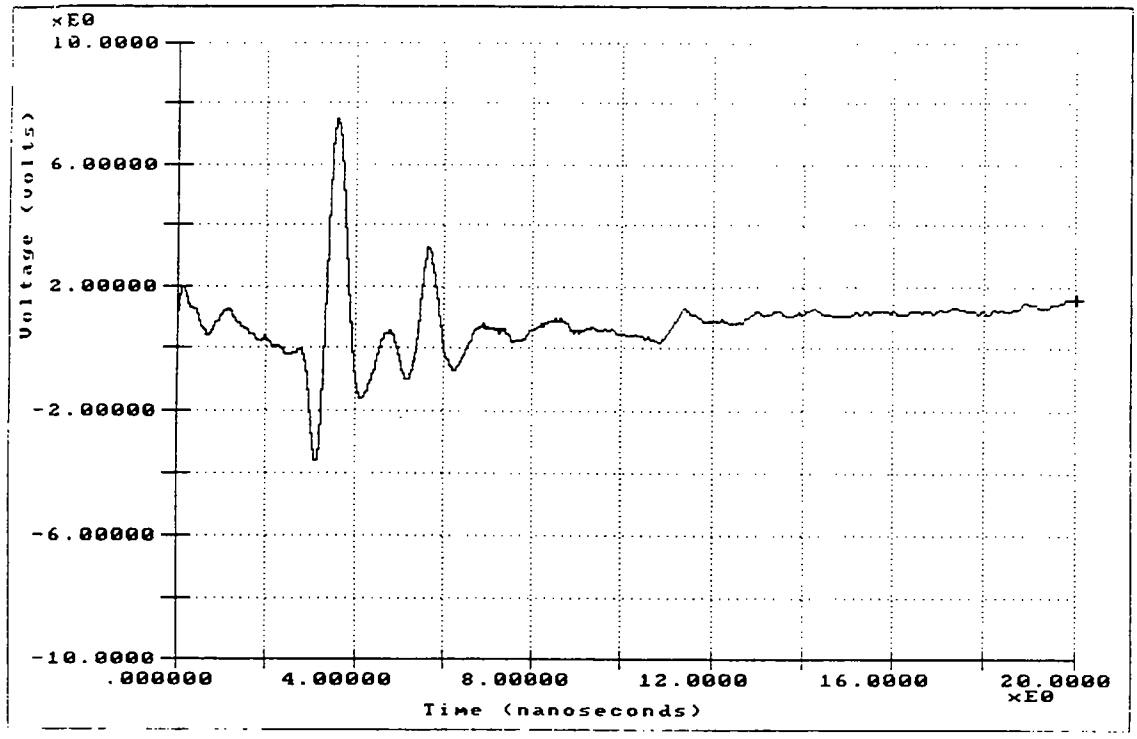

(a) Test section 3—14.0 cm (5.5 in.) of asphalt

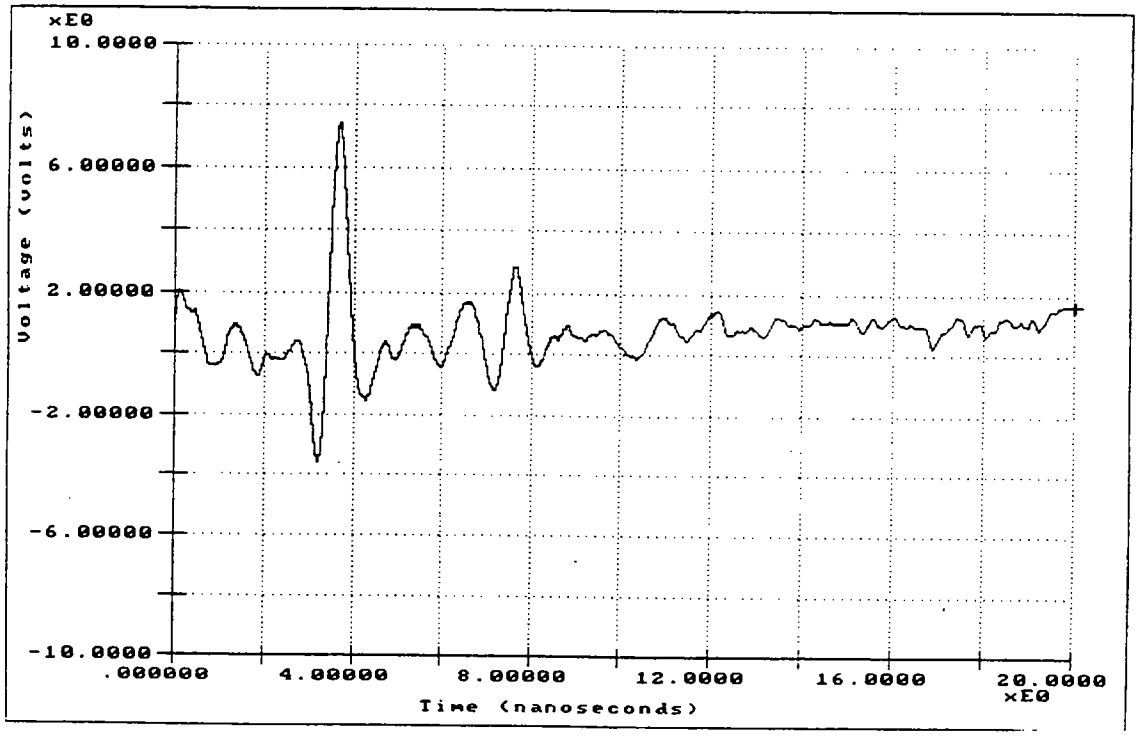

(b) Test section 4—25.4 cm (10 in.) of asphalt

Figure 7.10. Ground-penetrating radar traces from asphalt control test sections 3 and 4

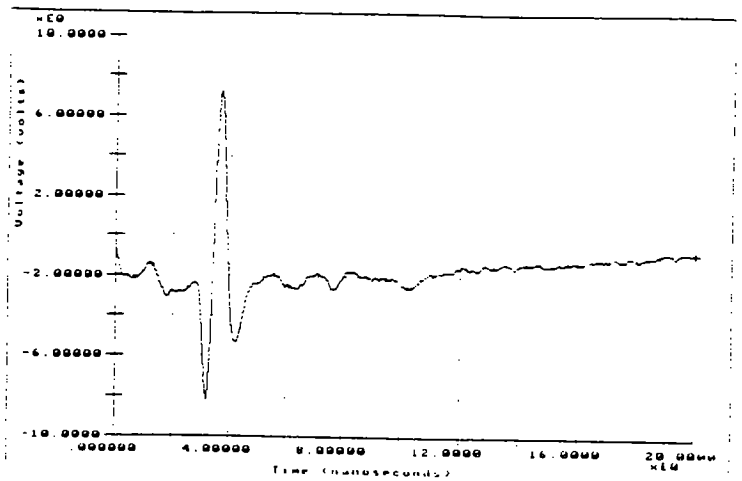

(a) Control location PCC over CTB

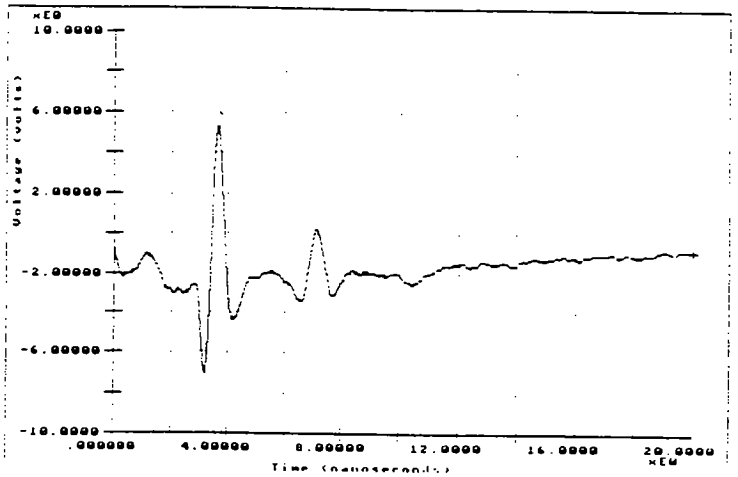

(b) Metal plate at bottom of PCC

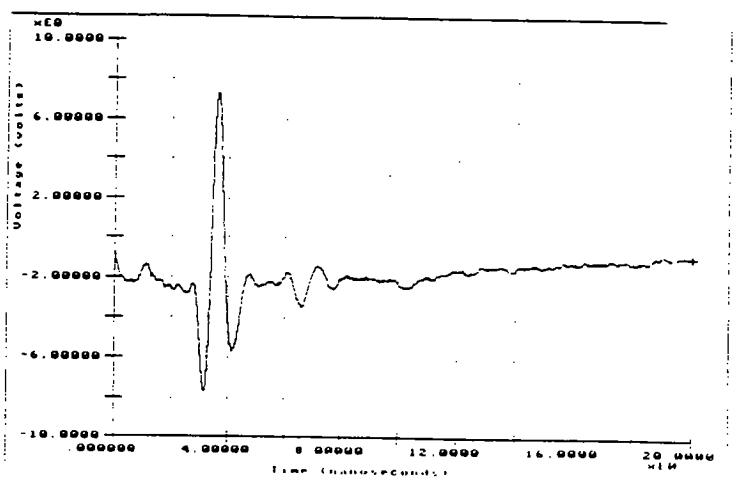

(c) Air void at bottom of PCC

Figure 7.11 Ground-penetrating radar waveforms from concrete test slab

8

Field Tests

8.1 Plan

A crucial phase of this study was the demonstration of the developed ground-penetrating radar (GPR) system to interested Departments of Transportation (DOTs). The plan was to ask the DOTs to nominate sections with one of the four conditions of interest (moisture in base, void, stripping, and delaminations), to test the section using the complete array of antennas from Geophysical Survey Systems, Inc. (GSSI) (both 1.0- and 2.5-GHz), and to perform data interpretation with a series of ground truth tests.

8.2 Site-Selection Plan

Both the Texas and Georgia DOTs had expressed interest in evaluating the new GSSI radar systems. From discussions with DOT officials, six sites were nominated for inclusion in the test program. These sites are described below.

Stripping Sites

Stripping is a problem in the asphalt layer. The bond between the asphalt and the aggregate breaks down, and the layer disintegrates. Stripping is frequently difficult to detect, because it often occurs in older asphalt layers buried beneath numerous overlays.

The following sections were nominated for testing:

Interstate Highway (IH) 45 Madisonville, Texas
19.0 cm (7.5 in.) of asphalt
23.0 cm (9.0 in.) of concrete

Localized slight alligator cracking had been reported in the wheel paths. The Texas DOT suspected that an older layer buried near the bottom of the 190 mm had stripped.

A rehabilitation was under consideration, and the DOT was trying to determine whether the existing asphalt should be completely removed.

U.S. 41 Jonesboro, Georgia

17.8 cm (7 in.) asphalt
10.0 cm (4 in.) macadam base
Soil base

The asphalt was composed of several thin overlays 2.5 to 5.0 cm (1 to 2 in.) thick. Some cores had been removed and broken in half. The Georgia DOT personnel had indicated that the lower portion of the core exhibited the beginning signs of stripping, identified by poor bond between aggregate and asphalt.

Moisture in the Base

Riverwatch Parkway, Georgia

20.3 cm (8 in.) asphalt
25.4 cm (10 in.) granular base

Moisture has been observed pumping through construction joints (figure 8.1). The problem appeared largely confined to a deep cut area. The DOT was interested in determining the extent of the problem area.

Farm-to-Market (FM) 2920, Tomball, Texas

10.2 cm (4 in.) asphalt
15.2 cm (6 in.) cement-treated base
15.2 cm (6 in.) lime-treated base

Moisture has been observed pumping through surface cracks (figure 8.2).

Voids Beneath Concrete Slabs

IH 20, near Augusta, Georgia

23.0 cm (9 in.) jointed concrete
stabilized soil-asphalt base

The joints were at 6.1-m (20-ft) spacings, and the shoulders were asphalt. Photographs of the section are shown in figure 8.3. Several concrete patches have already been placed on the section, and problems were noted with the concrete-asphalt shoulder joint.

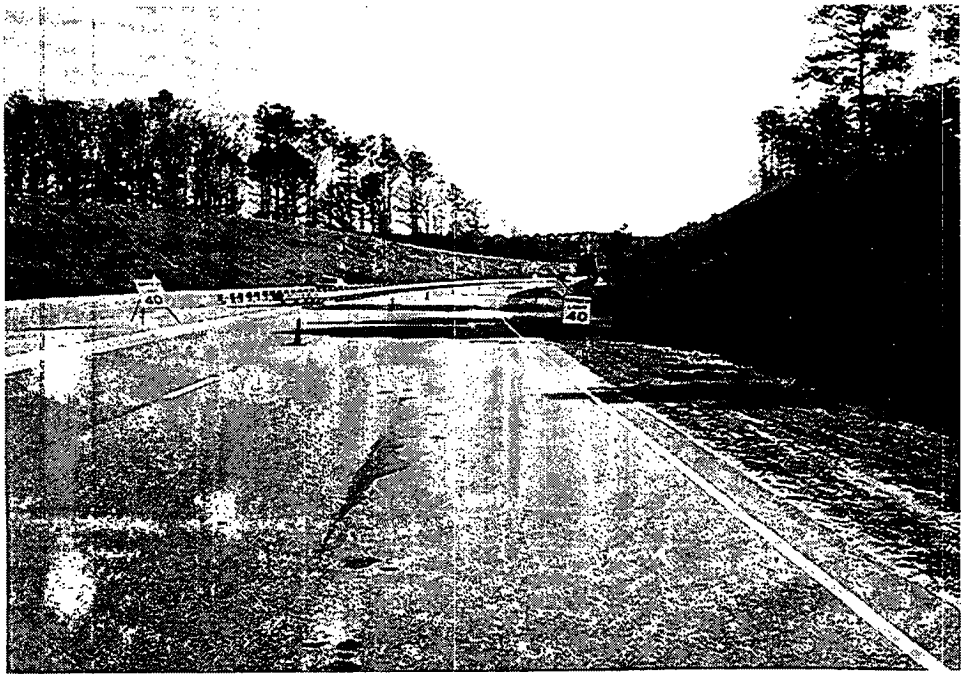

Figure 8.1. Riverwatch Parkway, Georgia—moisture seeping through construction joint

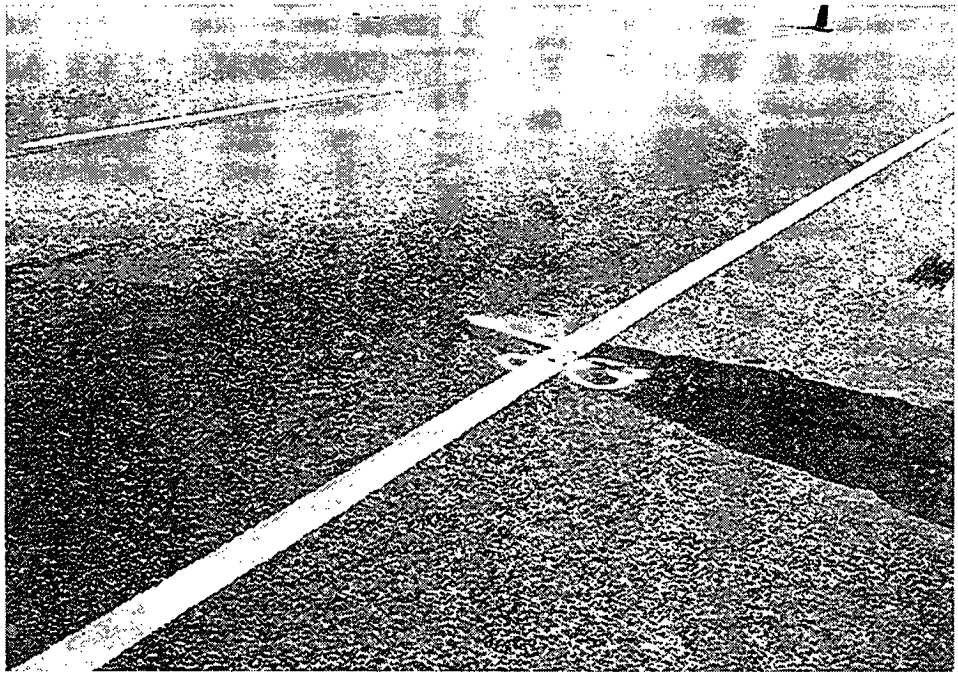

Figure 8.2. FM 2920, Tomball, Texas—moisture seeping through surface crack

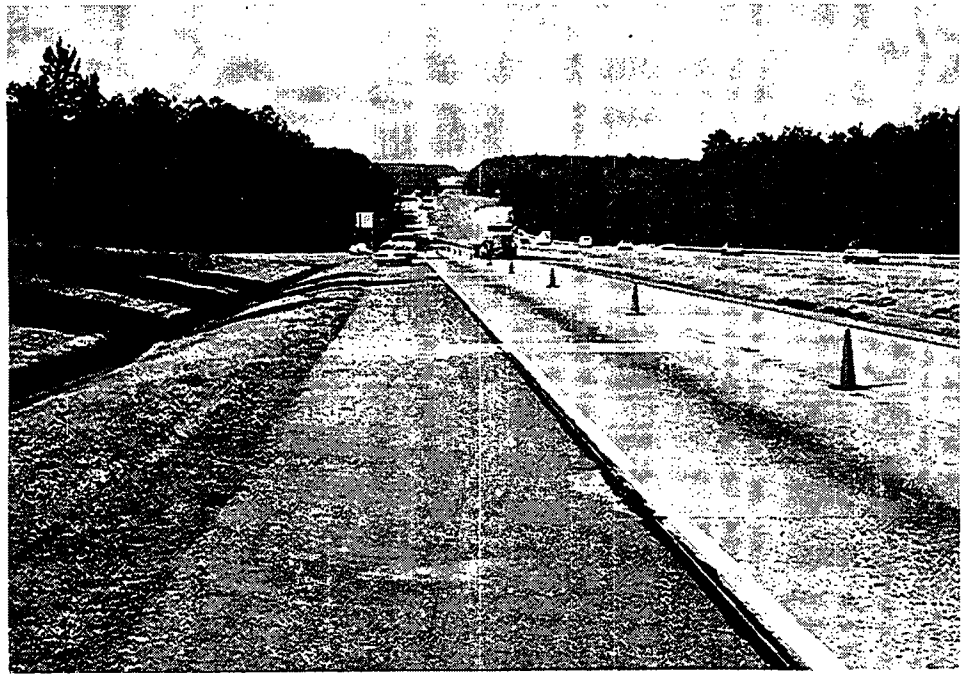

(a) GPR test section (note frequent patching)

(b) Problems with concrete-asphalt joint

Figure 8.3. IH 20, Near Augusta, Georgia

Overlay Debonding

IH 85, Gwinnett County, Georgia

10.2 to 17.8 cm (4 to 7 in.) concrete overlay
23.0 cm (9 in.) jointed concrete

The thin concrete overlays were approximately 10 years old. These overlays were intentionally debonded from the original concrete slab. The DOT was interested in evaluating whether GPR could detect the debonding between the layers.

8.3 Testing Sequence

To accommodate the needs of the DOTs, we requested that they select the limits of the sections. The minimum section length was set at 305 m (1,000 ft). The antennas were mounted on the test trailer as shown in figure 8.4. The system was turned on and left for about 10 minutes to warm up. Radar data were collected for the outer wheel path while the unit was moving at approximately 16 kph (10 mph). The return signals were displayed on the Subsurface Interface Radar System-10A color monitor. Notes were made of the location of any anomalous GPR signals during this first pass.

A second pass was made, and stationary GPR measurements were taken at locations where anomalous GPR return signals were observed. These locations were marked with paint spots. Ground truth testing was started immediately after the static GPR measurements. Typically, 8 to 10 locations per site were selected for ground truth testing. This testing consisted of the following:

1. Standard wet asphalt coring.
2. Dry augering (to obtain base and subgrade samples for moisture determination; see figure 8.5).
3. The epoxy core test (as developed under the Strategic Highway Research Program H-101 contract). This test was used on the test sites for voids and overlay delaminations. A dry hole is drilled through the slab and base layers (figure 8.6) and fluid, fast-setting epoxy is poured into the hole and allowed to harden. A standard 10.2-cm (4-in.) core is removed once the epoxy is hardened. Ideally, the epoxy will fill the void and hence determine its thickness.

8.4 Observations during Testing

During the actual GPR and ground truth testing, there were problems related to either equipment or pavement. These are described below.

It must be remembered that the GPR equipment was a prototype; therefore some minor problems are to be anticipated. The following problems were encountered:

1. The trailer design did not facilitate high-speed data acquisition. Strengthening of the axles is urgently required for future work. The maximum speed used with the current setup was 16 kph (10 mph).
2. The 2.5-GHz antenna traces continue to have a high level of background system noise. GSSI has since reduced this problem by redesigning the sampler, but the redesign was not ready in time for the field testing. The data analysis section therefore emphasizes processing the traces obtained with the 1.0-GHz antenna.
3. Early in the field testing, the distance-measuring instrument (DMI) broke. The intention was to let the operator collect data at whatever DMI interval was required. Without the DMI, it was possible to operate only at the data-acquisition speed of 50 traces per second.

Regarding pavements, the following observations were made:

1. FM 2920, Tomball, Texas. Although the intent of the testing was to find moisture in the base, in this section the moisture was located beneath the cement-treated base. In the ground truth testing only one very localized spot was found that had significant moisture problems.
2. U.S. 41, Jonesboro, Georgia. This section had a thick asphalt layer over a macadam base. The section was badly cracked, and there had been substantial rainfall the day before GPR testing. Large changes were observed in the GPR signals, but they were attributed to changes in the water content of the macadam layer. The section was supposed to be for detecting stripping, but no obvious stripping was detected in any of the removed cores.
3. Riverwatch Parkway, Georgia. This section was intended to evaluate GPR's ability to detect moisture variations in a granular base course. However, the actual moisture content of the base was found from coring to be relatively constant along the length of the highway.

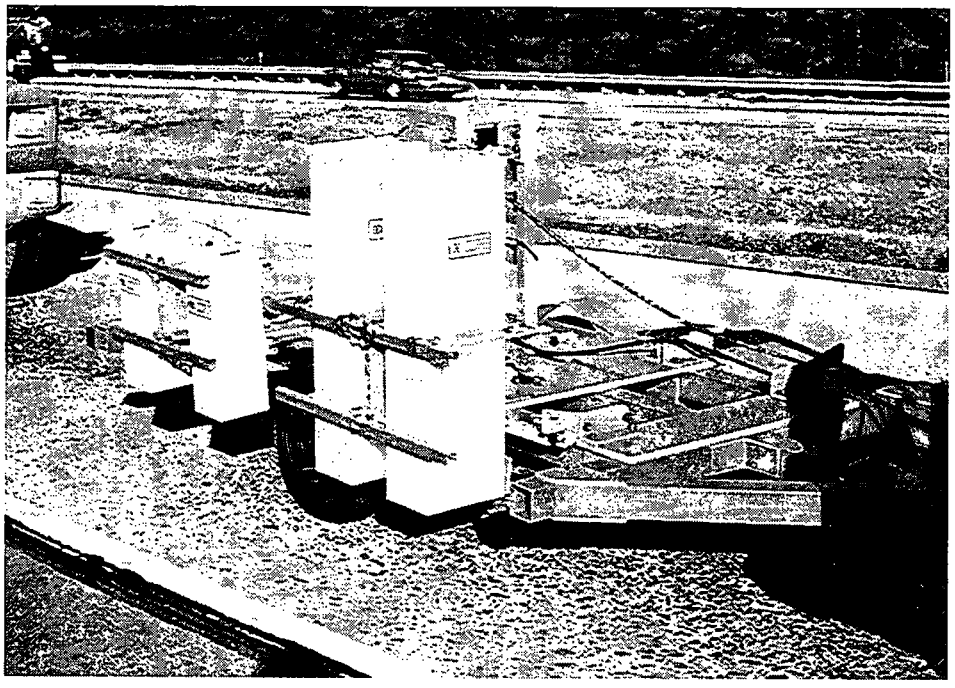

Figure 8.4. GSSI trailer with 1.0-GHz and 2.5-GHz antennas. The antennas are bistatic; one transmits and the other receives GPR signals.

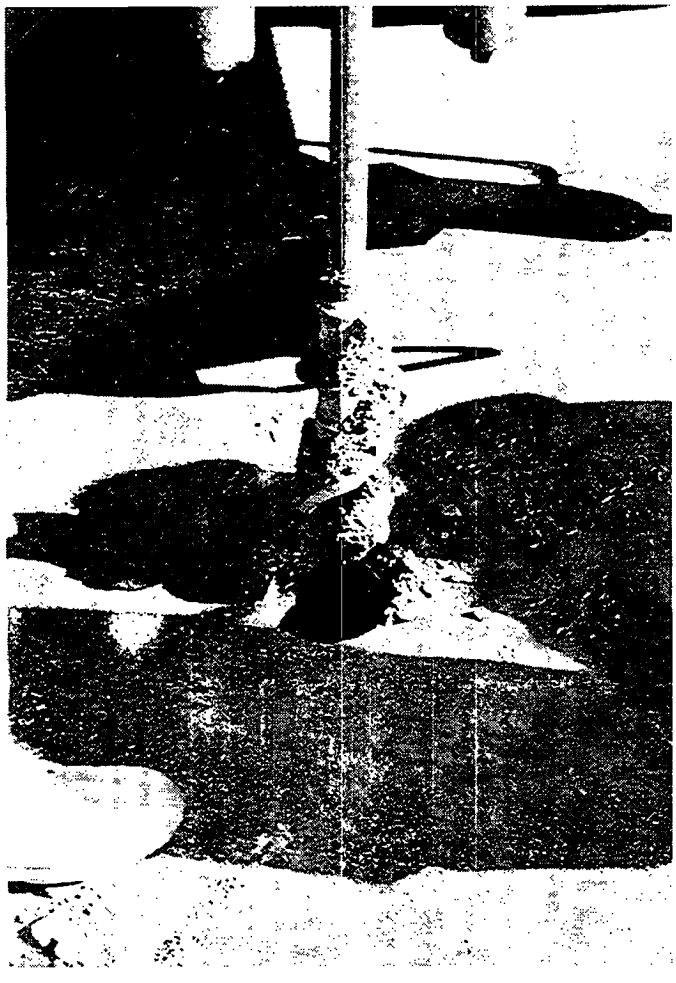

Figure 8.5. Dry augering of base samples

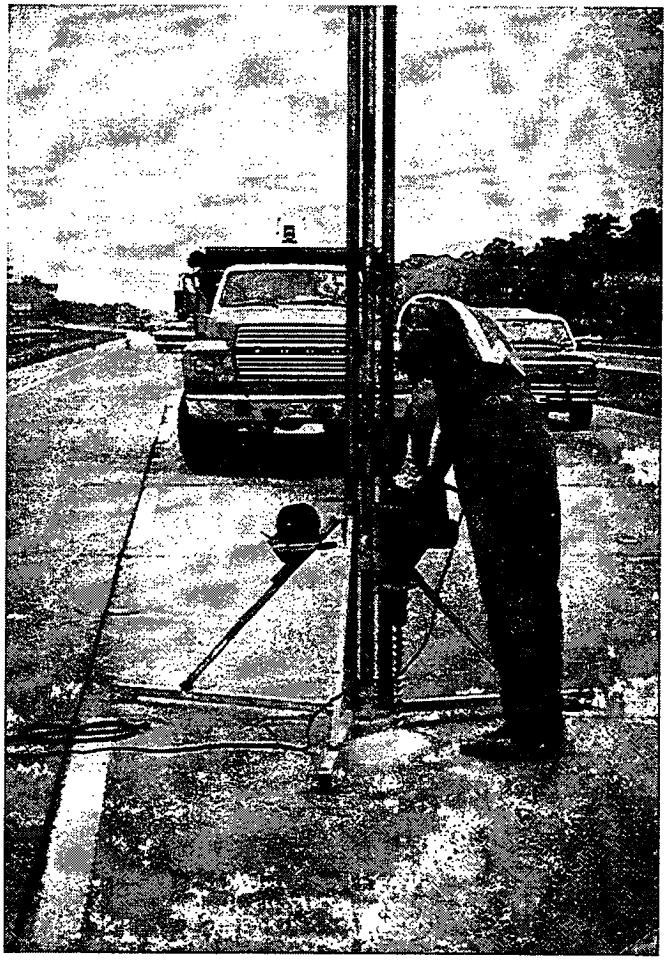

Figure 8.6. Drilling dry hole for epoxy core test

9

Results of Field Tests

The data acquired in Texas and Georgia were interpreted by means of the neural network (NN) from Geophysical Survey Systems, Inc. (GSSI), and the software package from Texas Transportation Institute (TTI). This section describes the results of those two efforts.

9.1 Neural Network Results

Stripping

Interstate Highway (IH) 45, Madisonville, Texas

Stripping of the asphalt was the pavement problem. Eight core samples were taken from the highway. We had only a qualitative description of the severity of the stripping, ranging from fair to severe. We used a ranking ranging from 0.2 for minor stripping to 1.0 for severe stripping. We trained an NN using five different files from five different core sites, to output the thickness of the asphalt, the thickness of the base, and the rank of the stripping. Table 9.1 shows the values for the training and testing files; Table 9.2 shows the output from the trained NN.

Table 9.1
Radar Files Used for Neural Network

	Asphalt Thickness (in.)	Base Thickness (in.)	Stripping
Training	3.0	2.5	1
Training	2.12	2.5	1
Training	2.5	2.5	1
Training	2.5	2.75	1
Training	2.75	2.75	0.2
Testing	3.0	2.5	1
Testing	2.25	2.5	1
Testing	2.75	2.75	0.2

We then tested the NN on a continuous scan of the highway. The network also provided the thickness of the asphalt and base, as well as severity of stripping. Graphs of results are shown in figures 9.1 through 9.3.

Table 9.2
Output from Trained Neural Network

	Asphalt Thickness (in.)	Base Thickness (in.)	Stripping
Actual	3.0	2.5	1
Net Output	3.002512	2.747628	0.975472
Actual	2.25	2.5	1
Net Output	2.114687	2.546146	0.956950
Actual	2.75	2.75	0.2
Net Output	2.646727	2.589562	0.204035

U.S. 41, Atlanta, Georgia

We tested the same NN with data we had obtained from ground truth testing on U.S. 41 in Georgia. The field notes stated that cores from the asphalt layers looked in reasonably good shape, and none of the cores showed appreciable stripping damage. The stripping was not as bad as that on IH 45 in Texas. Therefore, we predicted that

the NN should report stripping near the minor (0.2) stripping range if it could identify the new data. The results averaged 0.225 and confirmed that the NN was able to generalize to the Georgia data. The thickness of the pavement, which ranged from 15 to 20 cm (6 to 8 in.) of asphalt, was not similar to the thicknesses used in training this network, so the NN was not tested on pavement thickness.

We also trained an NN on laboratory stripping test sections. The test bed consisted of four sections of varying thicknesses of asphalt and base and two sections with simulated stripping in the asphalt. The stripping was 2.5 cm and 75 cm (1 in. and 3 in.) thick. Although we were able to train the NN to identify the thickness of the pavement and the thickness of the stripping in the laboratory data, we were unable to use this NN to generalize to field data. The problem is illustrated by the traces shown in figure 9.4. The artificial circumstances in the laboratory do not agree with those in the field. There are no characteristics in common that the NN can distinguish.

We concluded from these tests that laboratory simulated highway conditions were not effective for training an NN for subsequent field work. The conditions in the laboratory were too contrived and dissimilar to actual road conditions to create radar scans that resemble scans produced in the field. Previous experiments showed that we can use pure mathematical modeling of the road conditions to train NNs in the absence of real field data. We were able to produce simulated scans that correspond with field scans in key areas and also capture the characteristic features that the NN uses to distinguish the various road anomalies.

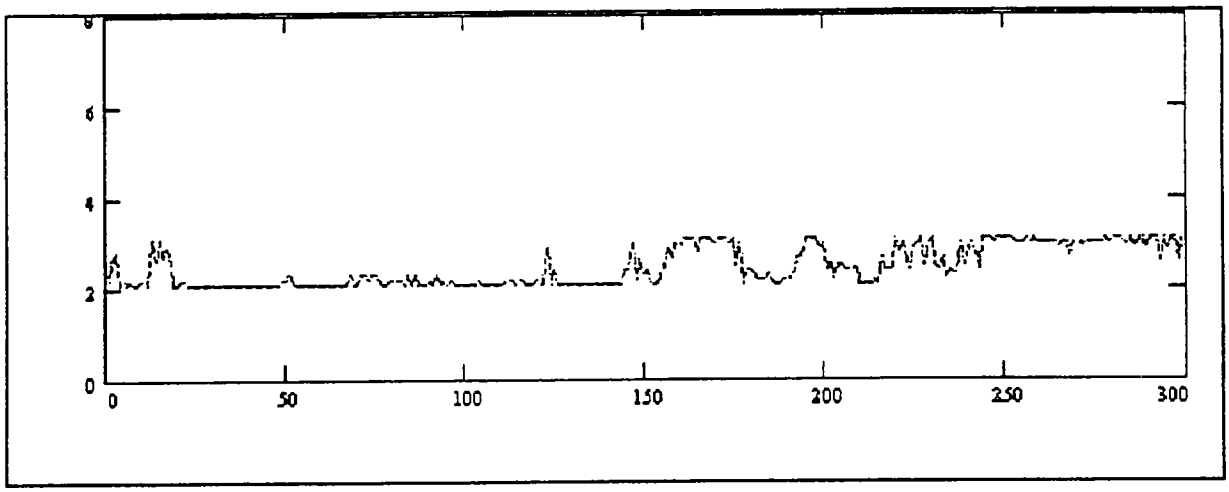

Figure 9.1. Asphalt thickness of IH 45

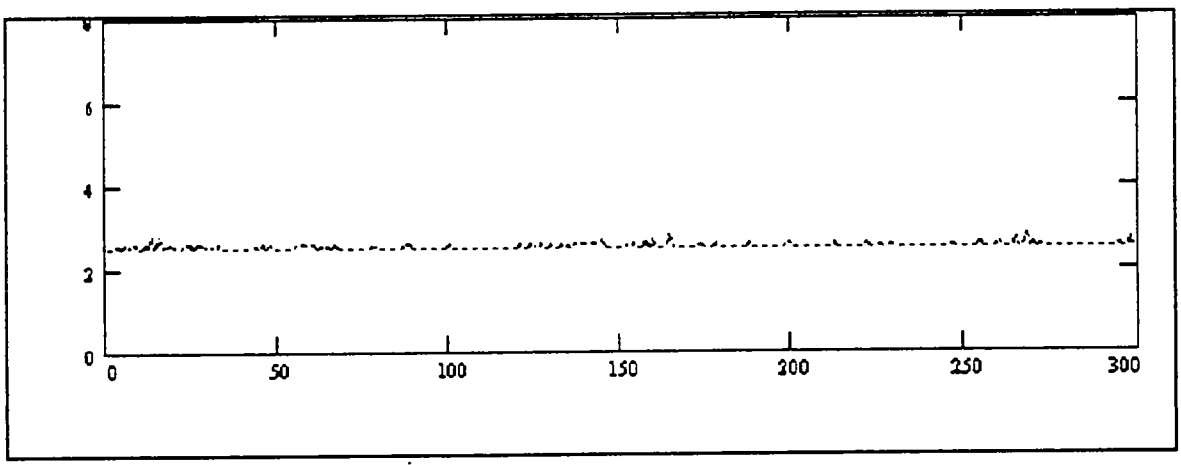

Figure 9.2. Pavement thickness of IH 45

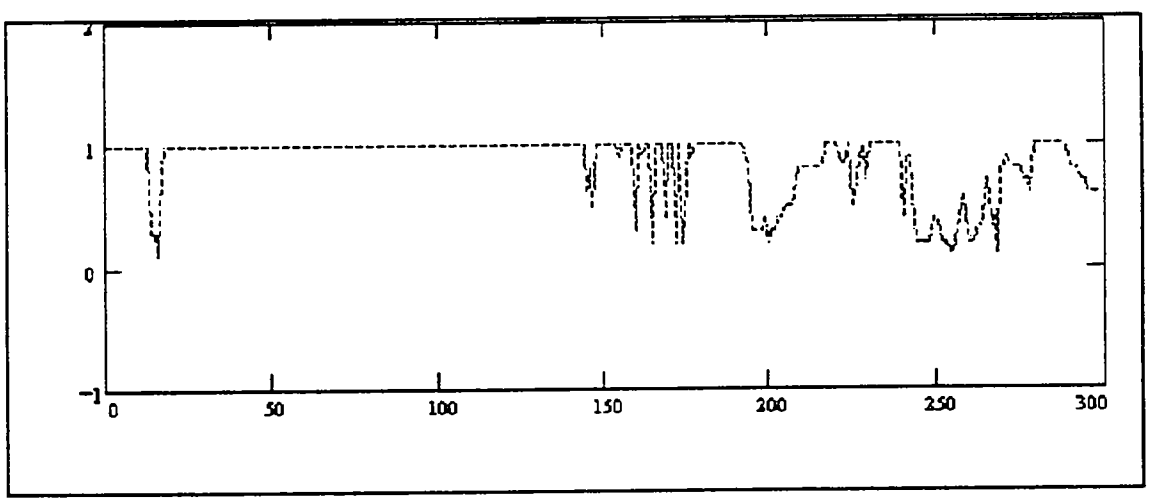

Figure 9.3. Severity of stripping on IH 45

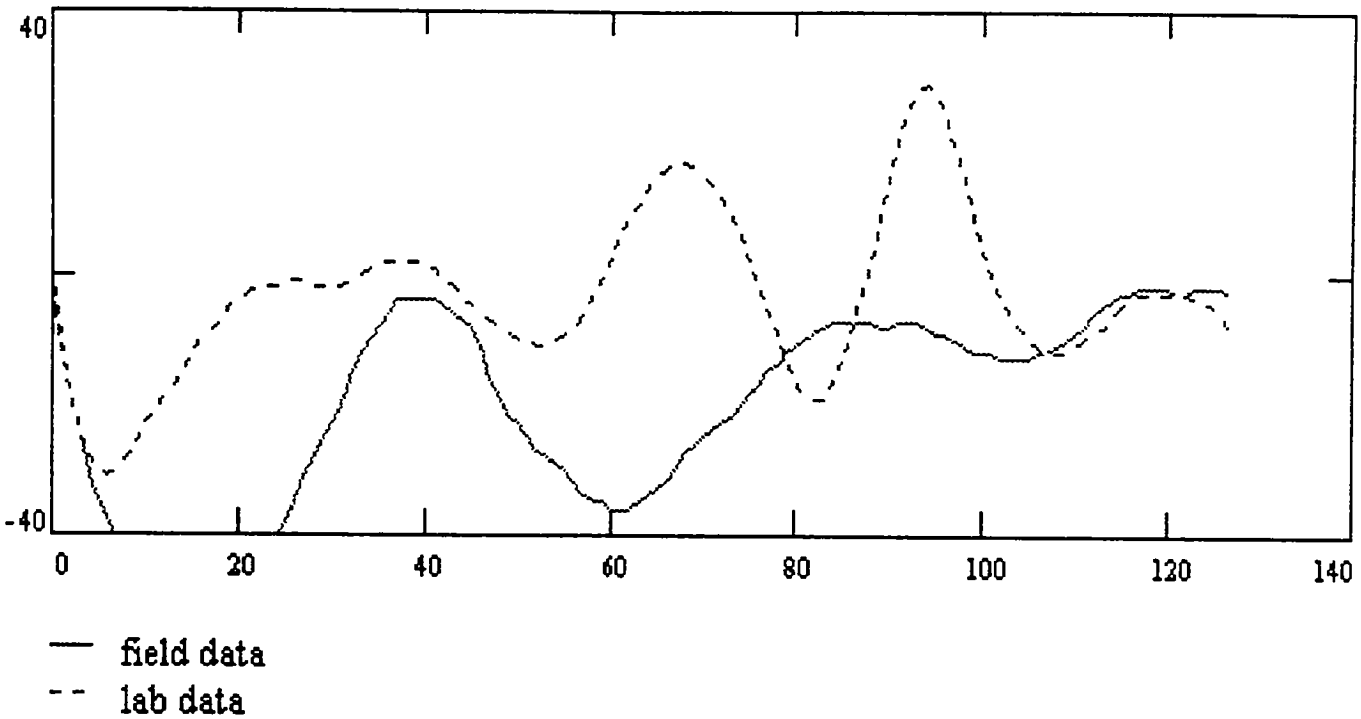

Figure 9.4. Sample laboratory and field traces

Moisture in the Base

Farm-to-Market (FM) 290, Tomball, Texas

The pavements in the Texas field test consisted of a layer of asphalt ranging from 7.8 to 12.0 cm (3.1 to 4.75 in.) and a layer of cement-treated base (CTB) ranging from 14.0 to 18.5 cm (5.5 to 7.3 in.). The pavement problem was moisture in the subgrade beneath the CTB. The moisture in the top of the base ranged from 4.7% to 6.4%. Moisture in the bottom base ranged from 4.2% to 6.3%. Moisture in the subgrade ranged from 8.4% to 11.3%. At one location, the subgrade was fully saturated; water rose in the core hole.

Five different files of varying thicknesses and moisture content were obtained. Three files were used to train an NN, which was then tested with the remaining two files. Five output parameters were used: asphalt thickness, CTB thickness, top base moisture, bottom base moisture, and subgrade moisture (table 9.3). The values used in testing were not values the NN had previously learned, so the NN had to generalize its learning during testing. Table 9.4 shows the output from a trained NN.

Table 9.3
Files Used for Neural Network

File Type	Asphalt Thickness (in.)	CTB Thickness (in.)	Top Base Moisture (%)	Bottom Base Moisture (%)	Subgrade Moisture (%)
Testing	3.5	7.0	-	-	Saturated
Training	4.5	5.5	4.8	6.3	11.3
Training	3.1	7.3	5.6	5.0	8.4
Training	4.75	6.0	5.6	-	8.6
Testing	3.2	5.9	4.7	4.2	9.2

Table 9.4
Sample Output of Texas Network

	Asphalt Thickness (in.)	CTB Thickness (in.)	Top Base Moisture (%)	Bottom Base Moisture (%)	Subgrade Moisture (%)
Actual	3.5	7.0	-	-	Saturated
Net Output	3.101315	7.288461	5.5937	4.985649	11.223761
Actual	3.5	7.0	-	-	Saturated
Net Output	3.099825	7.300335	5.600681	4.998768	11.297320
Actual	3.2	5.9	4.7	4.2	9.2
Net Output	3.311433	6.148523	4.838578	5.171460	9.817370
Actual	3.2	5.9	4.7	4.2	9.2
Net Output	3.102043	5.673534	4.852891	5.000435	8.821394

Riverwatch Parkway, Georgia

In this trial the pavement consisted of 21.0 to 22.9 cm (8.25 to 9.0 in.) of asphalt and 25.4 to 34.3 cm (10 to 13.5 in.) of granular base material. The pavement problem was again moisture in the base, which ranged from 3.3% to 6.2%; in the subgrade, moisture ranged from 11.8% to 16.8%.

Six different files were used; four to train the NN and two test it. Four output parameters were used: asphalt thickness, base thickness, base moisture content, and subgrade moisture content (table 9.5). As before, the values used in testing had not been previously learned by the NN. Table 9.6 shows the output of the trained NN.

Table 9.5
Files Used for Training and Testing Georgia Neural Network

File Type	Asphalt Thickness (in.)	Base Thickness (in.)	Base Moisture (%)	Subgrade Moisture (%)
Testing	8.5	10	5.7	-
Training	8.5	10.5	6.2	14.4
Testing	8.75	10.75	3.3	15.8
Training	8.5	13.5	6.0	14.1
Testing	8.25	11.5	4.1	15.7
Training	3.5	11.75	4.1	16.8

Table 9.6
Sample Output of Trained Neural Network

File Type	Asphalt Thickness (in.)	Base Thickness (in.)	Base Moisture (%)	Subgrade Moisture (%)
Actual	8.5	10.0	5.7	14.0
Net Output	8.510421	11.228883	6.03926	13.659081
Actual	8.5	10.0	5.7	14.0
Net Output	8.577479	11.419979	5.967682	14.206089
Actual	8.25	11.5	4.1	15.7
Net Output	8.467011	12.180161	4.376184	16.312422
Actual	8.25	11.5	4.1	15.7
Net Output	8.436436	12.140727	4.514038	16.414690

Texas and Georgia Data

We combined the data from the Georgia and Texas files and trained a new NN. The files shown in tables 9.3 and 9.5 were used in one network. Files used for training and testing remain the same. In the Georgia data, we added a zero for the desired output for bottom base moisture to maintain consistency. The output of this NN is shown in table 9.7.

Table 9.7
Results from Combined Neural Network

	Asphalt Thickness (in.)	Base Thickness (in.)	Top Base Moisture (%)	Bottom Base Moisture (%)	Subgrade Moisture (%)
Actual	8.5	10.0	5.7	0.0	14.0
Net Output	8.508083	10.013227	5.695247	0.0003595	13.986312
Actual	8.5	10.0	5.7	0.0	14.0
Net Output	8.509891	9.999255	5.690246	0.000075	13.988375
Actual	8.25	11.5	4.1	0.0	15.7
Net Output	8.490645	13.812532	5.087718	0.002535	16.212387
Actual	8.25	11.5	4.1	0.0	15.7
Net Output	8.490576	13.800926	5.077179	0.002283	16.261164
Actual	3.5	7.0	-	-	Saturated
Net Output	4.813037	6.269884	4.673773	6.329368	13.395400
Actual	3.5	7.0	-	-	Saturated
Net Output	4.953895	7.733304	4.681155	6.286990	13.297686
Actual	3.2	5.9	4.7	4.2	9.2
Net Output	3.269982	6.946465	5.529319	4.999324	8.747825
Actual	3.2	5.9	4.7	4.2	9.2
Net Output	3.164634	7.137173	5.557502	5.006194	8.577032

We tested a continuous file section of this Georgia highway where the problem was moisture in the base and subgrade. We used an NN that had been trained on a different section of the same highway. The results are shown in figure 9.5 and 9.6.

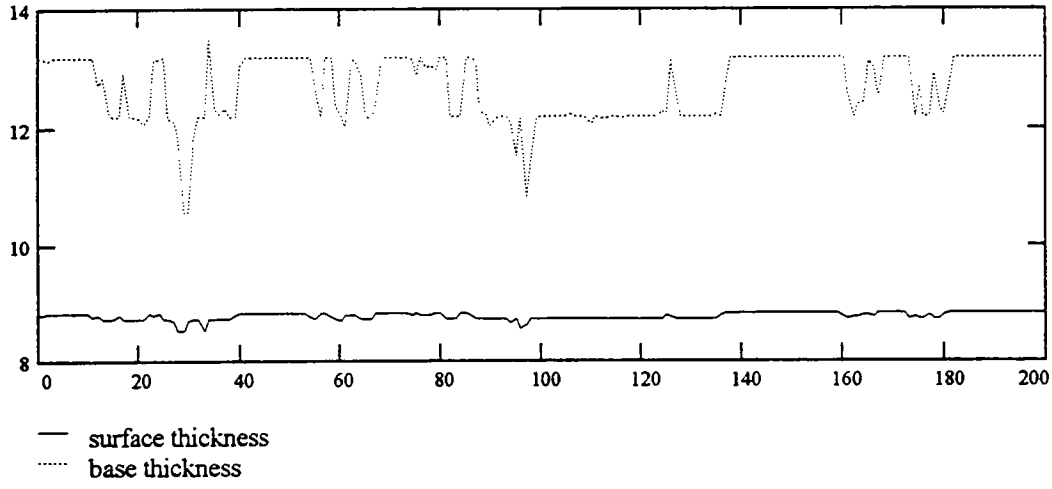

Figure 9.5. Pavement thickness of Riverwatch Parkway

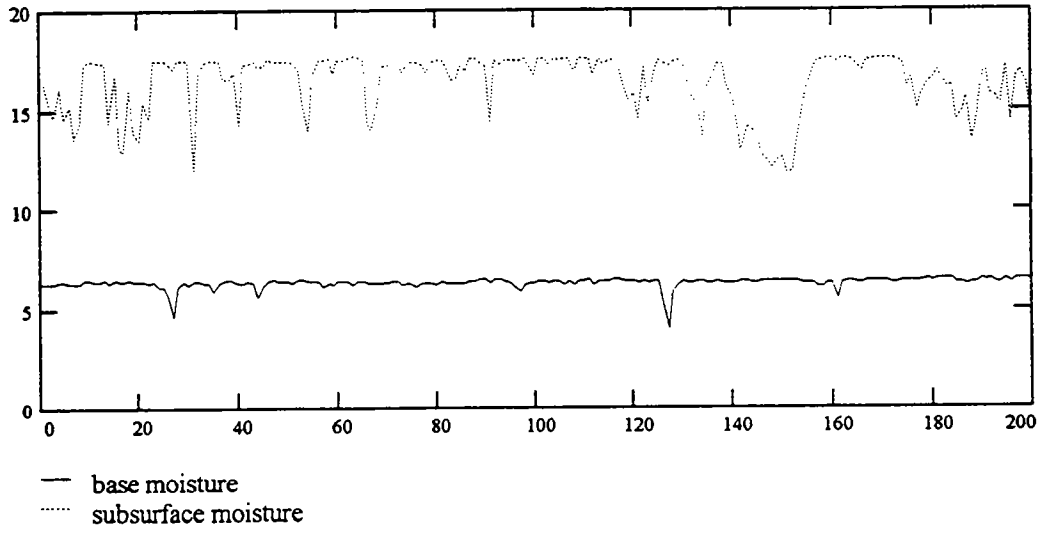

Figure 9.6. Moisture content of Riverwatch Parkway

Void Under Rigid Pavements

IH 20, near Augusta, Georgia

We used ground truth testing data from IH 20. The problem was identified as voids under the pavement. It had not been possible to determine the void thickness in the field. Core samples were only marked by a "void" or "no void" designation. Patches were also found along the highway, and areas with patches were identified on the field notes. Therefore, we set up the following for the NN to learn:

0 = Patch
1 = No Void
2 = Void

We selected core samples and patches from the end of the sample file to train the NN and scans from the beginning of the file to test the NN. Results of the testing are shown in table 9.8; the NN was able to correctly distinguish between patches, voids, and normal sections.

Table 9.8
Results of IH 20 Void Testing

Desired Output	Net Output
2.000000	1.999331
2.000000	1.999037
0.000000	0.000183
0.000000	-0.000177
1.000000	0.982018
1.000000	0.876110

In sum, we have shown in these experiments that an NN can be trained with field data to identify voids in a highway. We also have shown that an NN can be trained with mathematically modeled data to subsequently identify voids in a real situation.

We ran a continuous section of the highway file through the NN. A graph of the results is shown in figure 9.7. The output from the NN corresponds with the marked voids and patches that were obtained in the field. Additional voids are also indicated by the NN where no core samples had been taken.

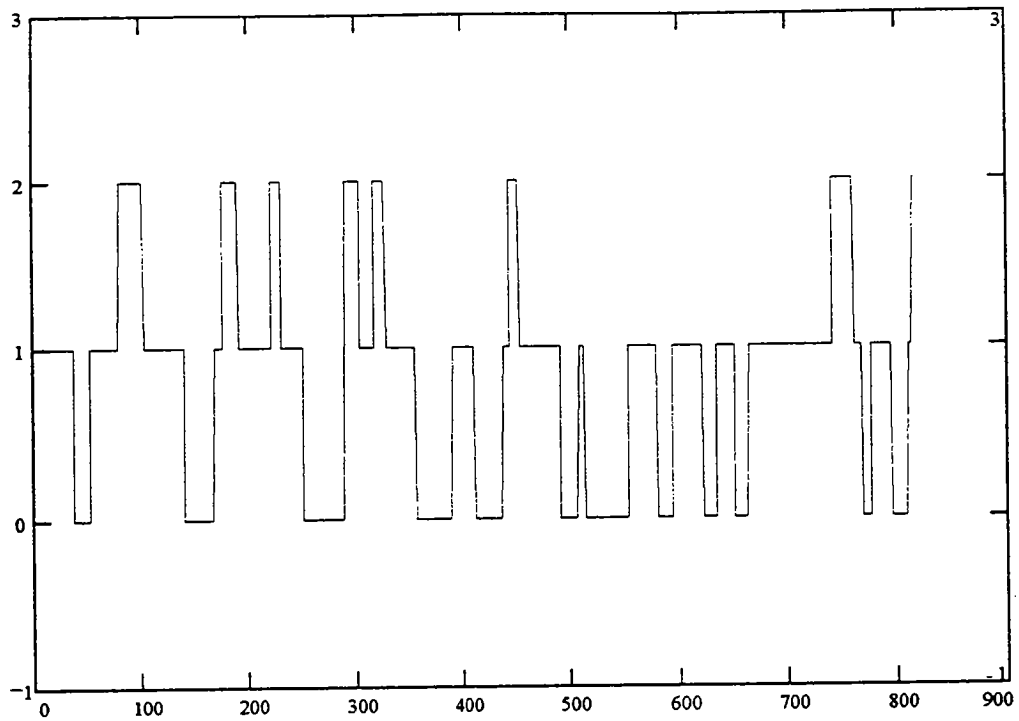

Figure 9.7. Neural network results from a section of Georgia IH 20, Georgia

9.2 TTI Software Results

Stripping

U.S. 41, Jonesboro, Georgia

The beginning stages of stripping have been reported by Georgia DOT engineers. The asphalt on this section has numerous overlays. A typical profile follows:

1.6 cm (0.625 in.) of friction course
5.1 cm (2 in.) overlay
5.1 cm (2 in.) overlay
5.1 cm (2 in.) original surface
6.4 cm (2.5 in.) of base asphalt
6.4 cm (2.5 in.) macadam base

Stripping was suspected in the lower layers.

Typical Traces

See figure 9.8 for typical traces obtained.

Discussion

The pavement section was badly cracked, and rain had fallen the day before the ground-penetrating radar (GPR) testing (see figure 9.9). The GPR is no doubt responding to the moisture content of the macadam layer. However, all the ground truth testing was done wet, and it was impossible to get any indication of the condition of the macadam which disintegrated during coring (see figure 9.10). No obvious stripping was observed in any of the cores obtained.

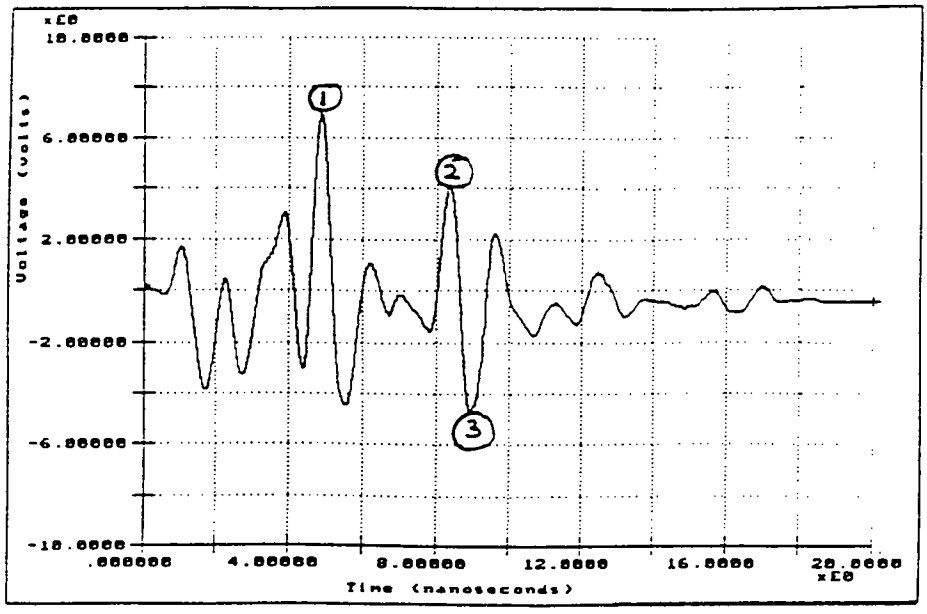

Core 1
5 3/4 in. C
3 1/2 in. McAdam

	A	ϵ	h	Δt
(1)	11.7	5.5	9.2	3.4
(2)	5.2	13.0	1.0	.5E
(3)	7.3	3.6		

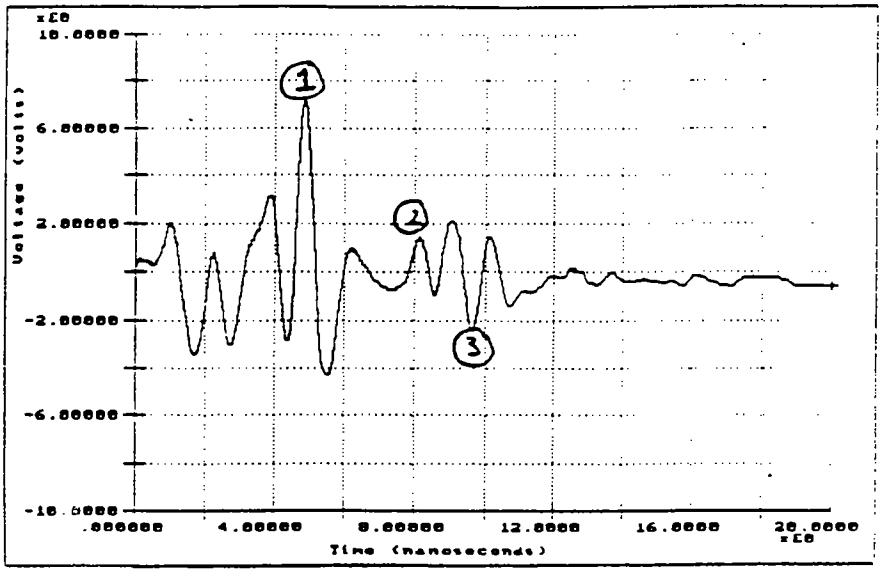

Core 5
9 1/4 in. AC
3 1/2 in. McAdam

	A	ϵ	h	Δt
(1)	11.9	5.6	8.6	3.3
(2)	1.8	7.6	3.3	1.5
(3)	4.3	3.7		

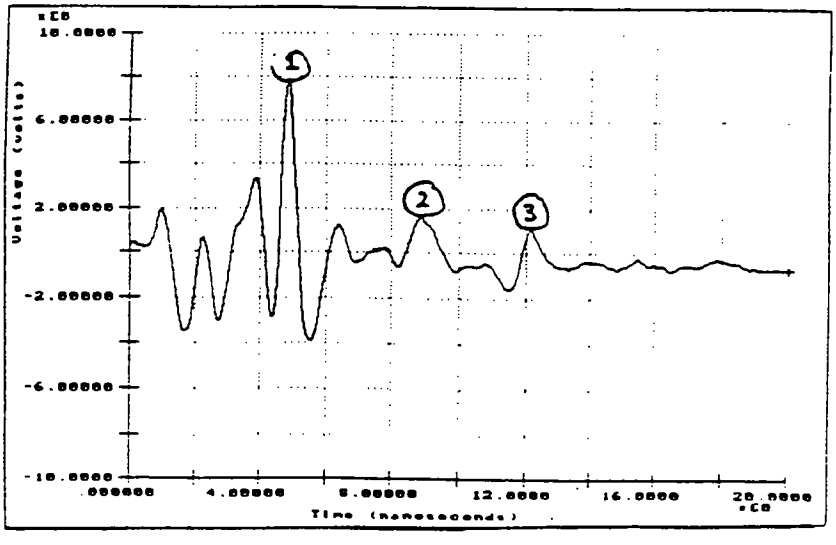

Core 7
6 1/2 in. AC
5 3/8 in. McAdam

	A	ϵ	h	Δt
(1)	12.3	6.1	10.1	4.0
(2)	1.9	8.4	7.1	3.3
(3)	1.4	10.6		

Figure 9.8. Ground-penetrating radar traces from U.S. 41, Georgia

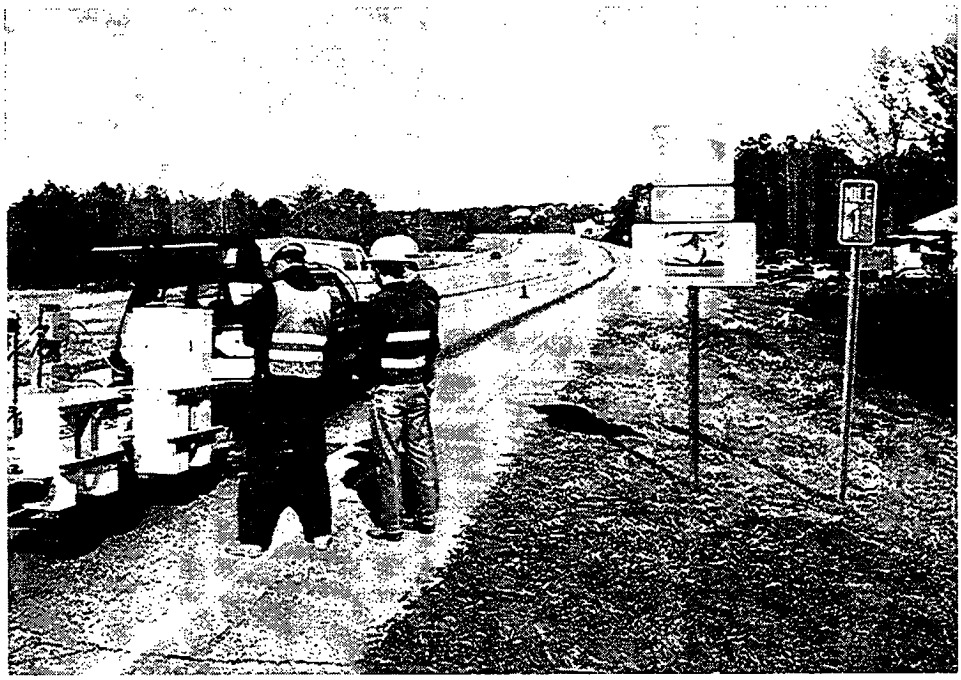

Figure 9.9. U.S. 41, Georgia

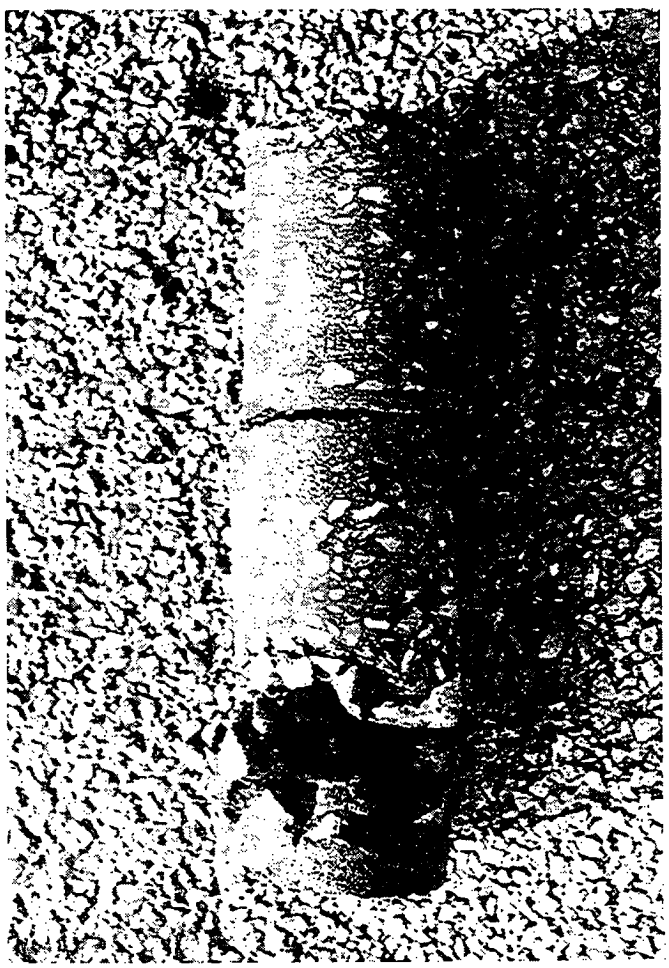

Figure 9.10. Extracted core—macadam layer at bottom of core

IH 45, Madisonville, Texas

Attached are a few samples of the GPR waveforms and cores we obtained from Madisonville. The only core with no stripping is core 8 (see figure 9.11). The other four have stripping at some depth below the surface (approximately 5 to 7.5 cm [2 to 3 in.]) (see figures 9.12 through 9.15). The TTI software could find no connection between the condition of the cores and the GPR traces.

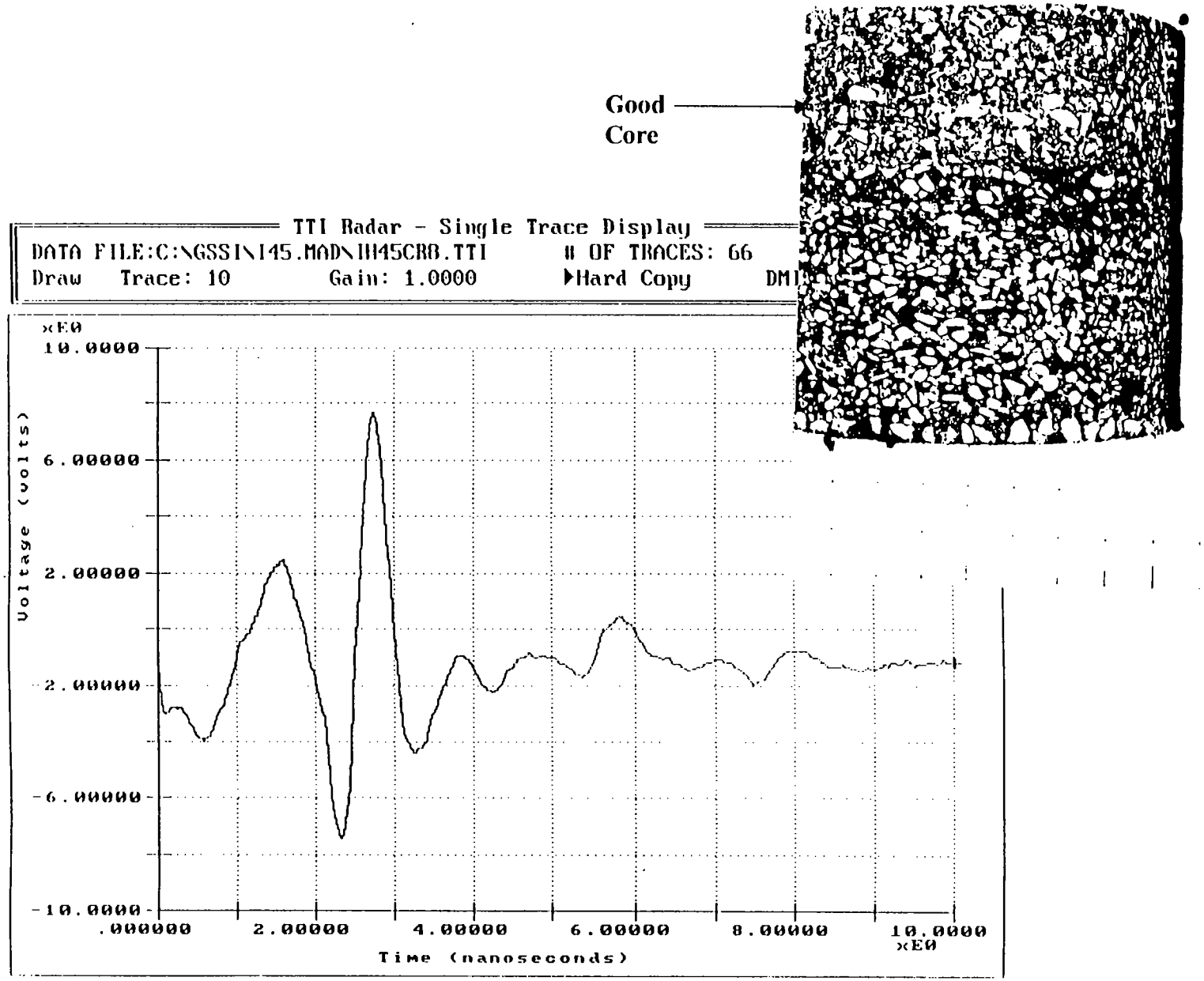

Figure 9.11. Radar trace and ground truth core 8, which contains no stripping

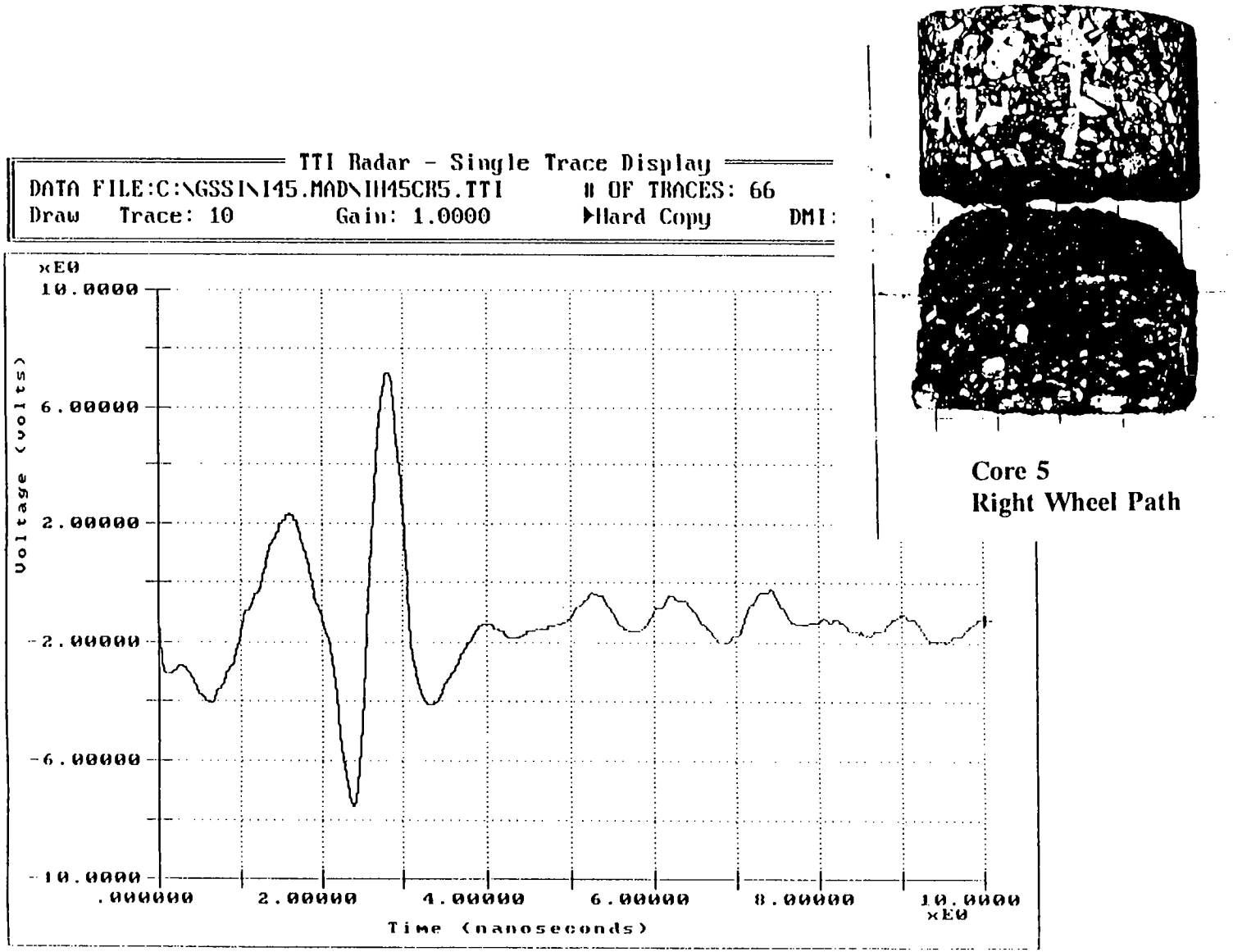

Figure 9.12. Radar trace and ground truth core 5, which contains a stripped layer

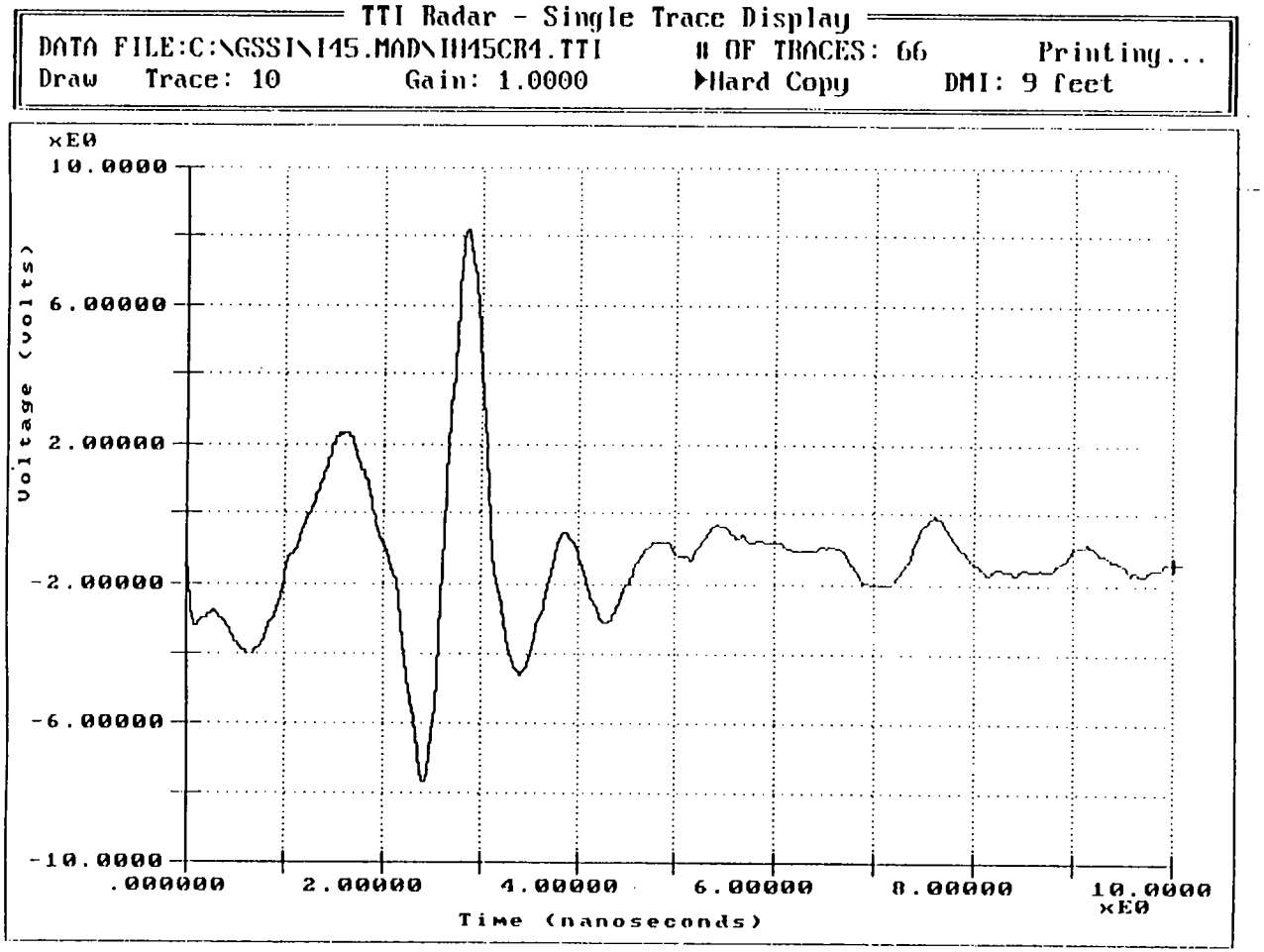

Core 4
Right Wheel Path

Figure 9.13. Radar trace and ground truth core 4, which contains stripping

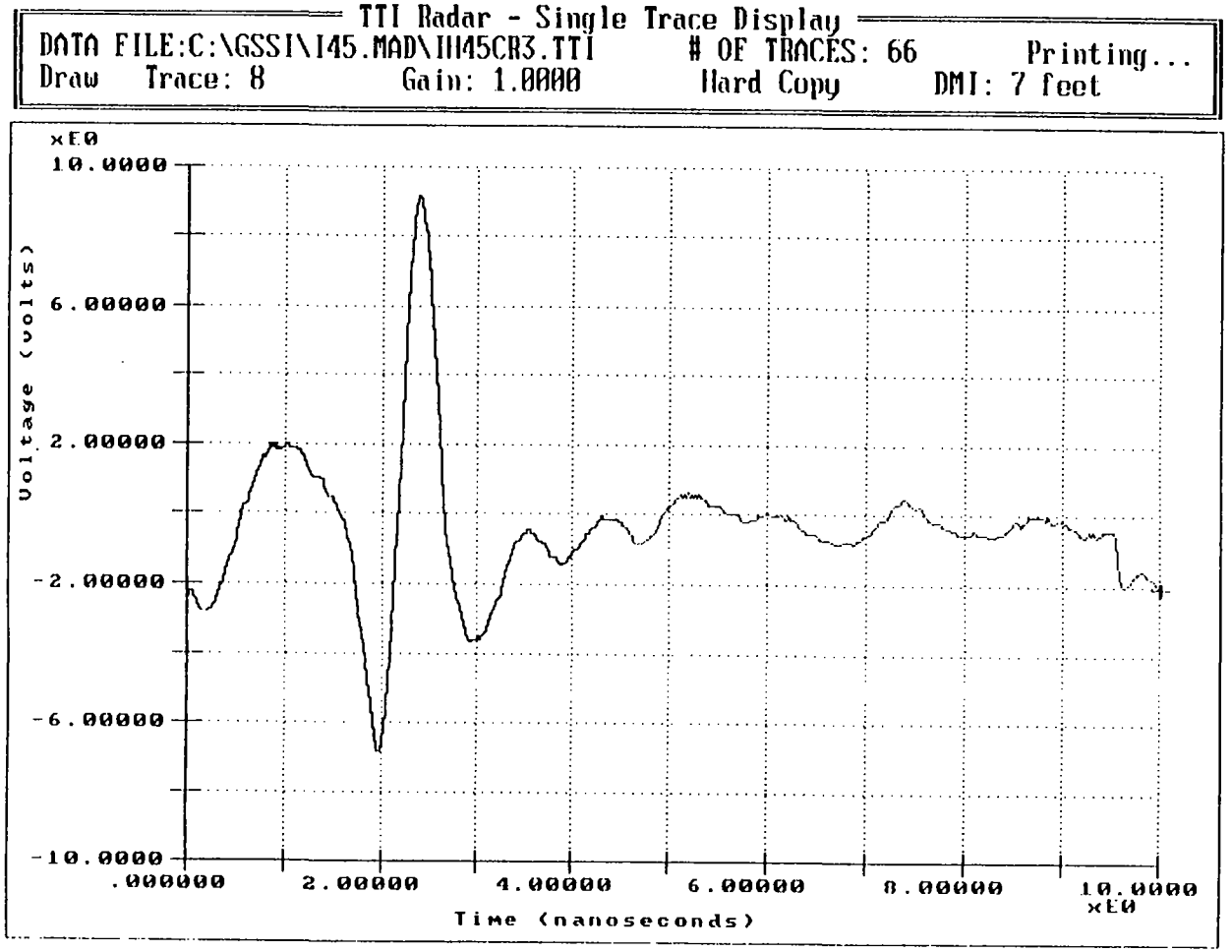

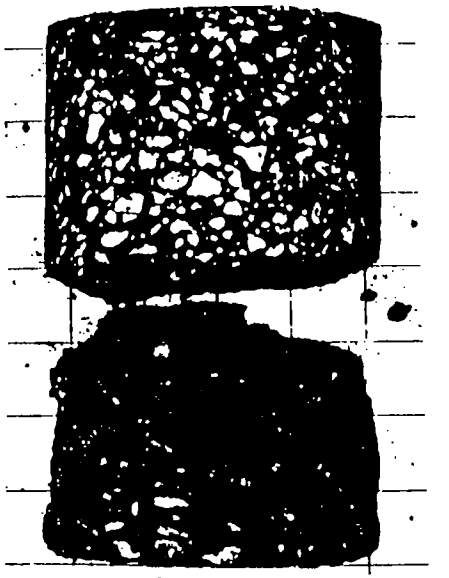

Core 3
Right Wheel Path

Figure 9.14. Radar trace and ground truth core 3, which contains stripping

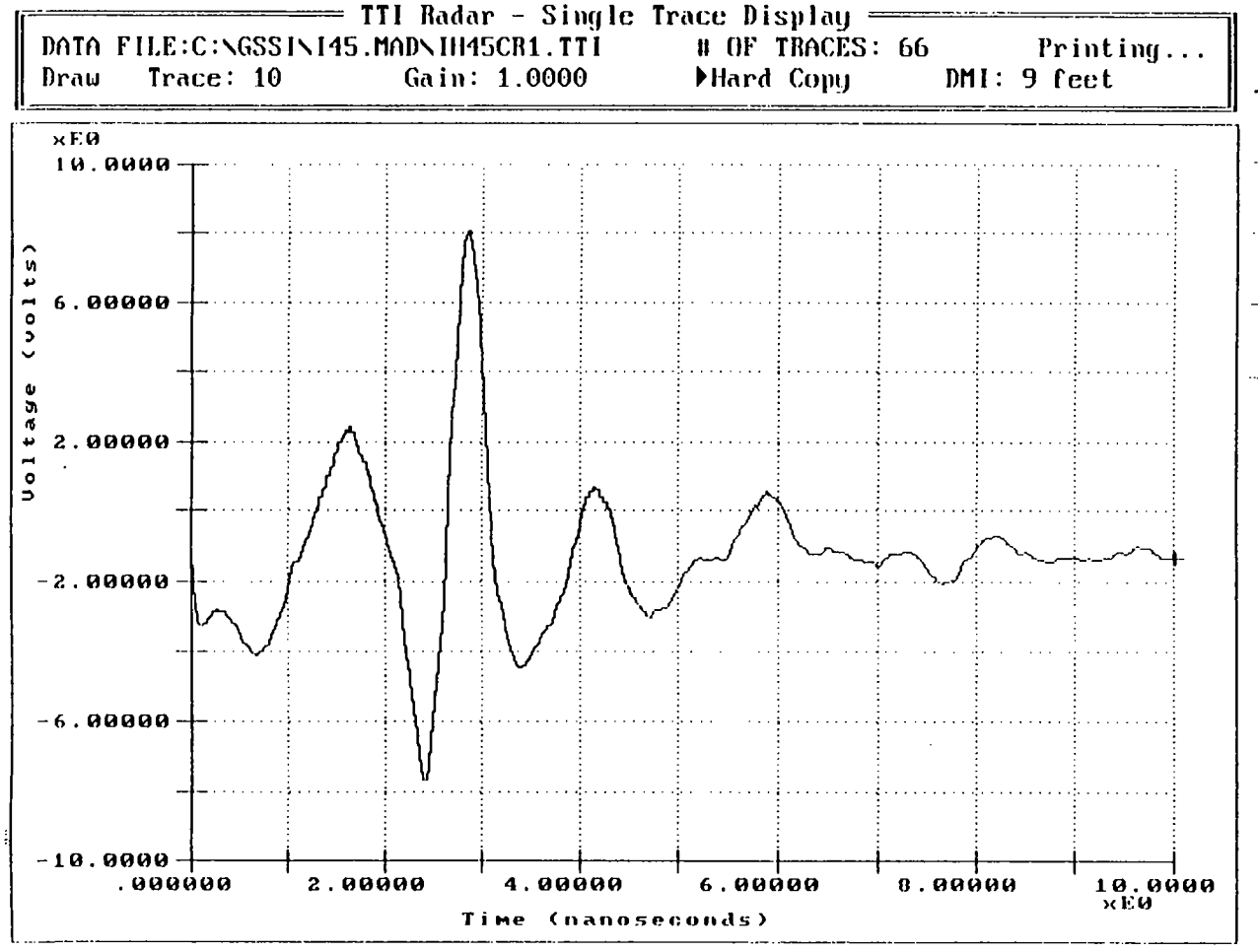

Core 1
Right Wheel Path

Figure 9.15. Radar trace and ground truth core 1, which contains stripping

Moisture in the Base

Riverwatch Parkway, Georgia

Typical Traces. See figure 9.16 for typical traces obtained. Core hole 1 has a good surface echo with no reflection from the top of subgrade. Core hole 3 has an adequate surface echo, although the lead leg is now shorter than the trail leg. The lead-leg-to-peak amplitude is used in the dielectric constant calculation. The surface dielectric constant has been reduced from 6.4 to 5.6. There is still no subgrade reflection. Core hole 6 has a poor surface echo, with signal drift to left that we should have noted in the field. Figure 9.17 shows the core hole 6. For this trace, the surface reflection could not be used to estimate the top layer dielectric constant; a value of 6.0 was assumed. The peak at 11 nsec was assumed to be from the top of the subgrade.

Table 9.9
Typical Results from Seven Core Holes

Core	Calculated from GPR						Measured			
	h_1	h_2	A_2	ϵ_1	ϵ_2	ϵ_3	h_1	h_2	M_1	M_2
1	8.3	-	2.9	6.5	11.1	-	8.5	10.0	5.7	-
2	8.5	-	2.9	6.4	10.9	-	8.5	10.5	6.2	14.4
3	9.2	-	2.9	5.6	9.5	-	9.0	13.5	4.0	11.8
4	9.0	-	3.0	5.5	9.3	-	8.5	13.5	6.0	14.1
5	8.4	11.6	3.6	6.0+	11.0	12.3	8.3	11.5	4.1	15.7
6	8.6	11.2	3.8	6.0+	11.5	13.7	8.5	11.7	4.0	16.8
7	8.6	11.5	3.9	6.0+	11.6	13.1	8.7	10.8	3.3	15.8

h_1 = Surface thickness (inches)
h_2 = Base thickness (inches) calculated only if a clear reflection was present
ϵ_1, ϵ_2, ϵ_3 = Dielectric constants of surface, base, and subgrade, respectively
M_1, M_2 = Measured moisture content in surface and base, respectively (% by weight)
A_2 = Amplitude of reflection from top of base (volts, peak to following minimum)

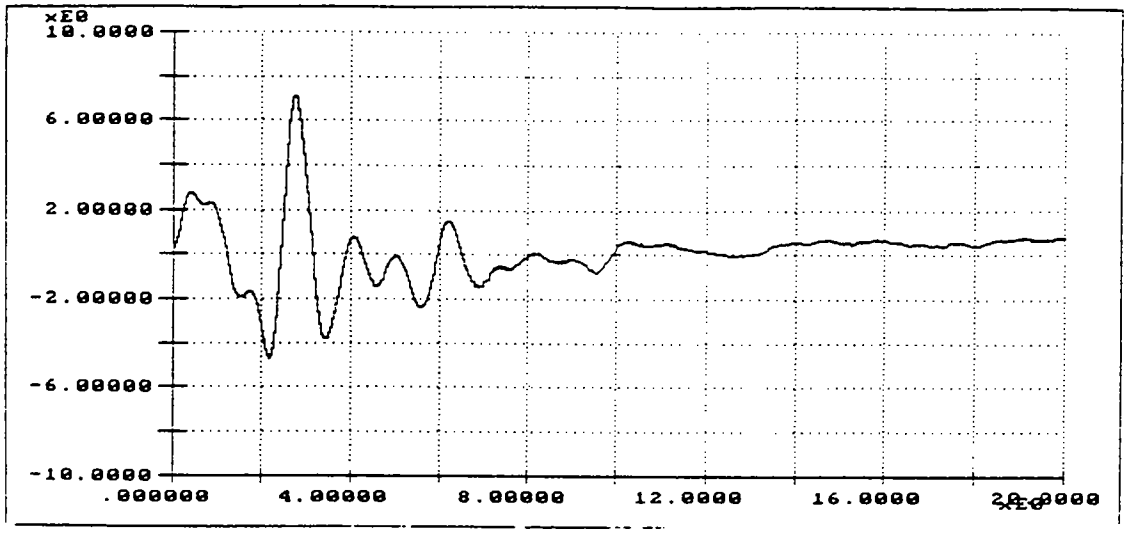

a) Core hole #1

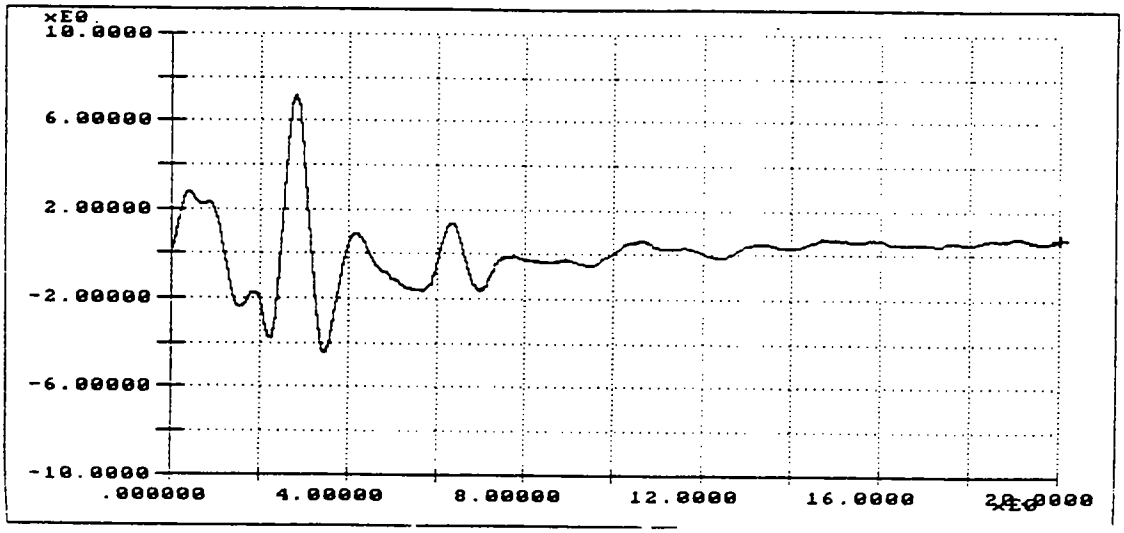

b) Core hole #3

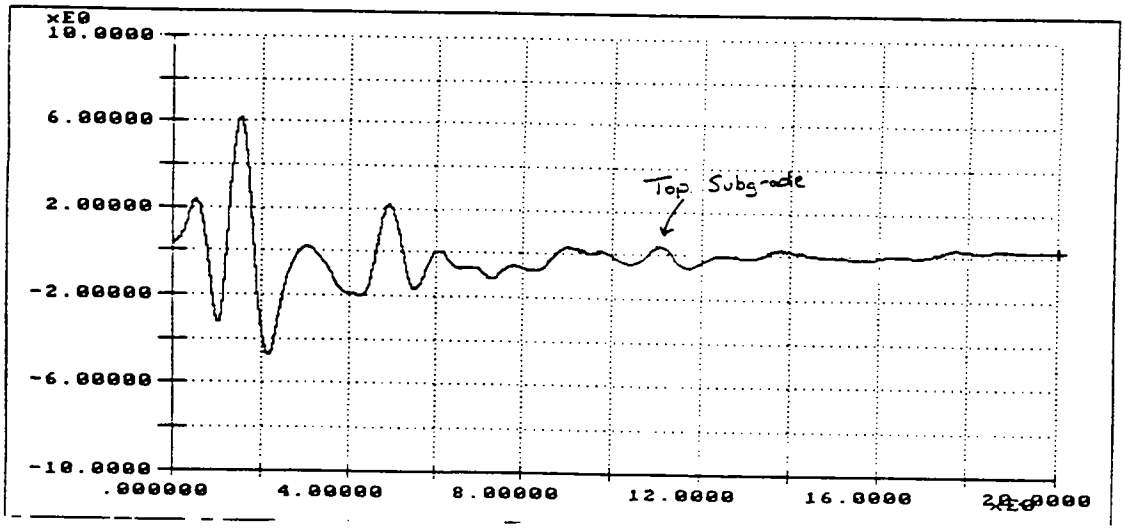

c) Core hole #6

Figure 9.16. Ground-penetrating radar traces (1.0-GHz) from Riverwatch Parkway, Georgia

Figure 9.17. Extracted core hole 6 from Riverwatch Parkway, Georgia

Results. The results of the GPR calculations are presented in table 9.9. The layer thicknesses correlate well. The largest error in calculating surface thickness was 0.13 cm (0.5 in.). The base thickness could not be calculated for all traces. When a reflection was present, the calculated base thickness predictions were accurate.

The moisture in the base does not correlate well with either the amplitude of reflection from the top of the base or the calculated base dielectric constant. The amplitude was measured from peak to trailing minimum. This finding contrasts with what we expected and what we observed in laboratory testing. One reason for the lack of correlation may be that the ground truth moisture content measurements were made at high speed in the field, and a gas flame was used to dry the sample. This method is the standard field test procedure in Georgia, but its accuracy is unknown.

Conclusion. Although moisture is seeping through construction joints, no significant changes in base moisture were found along the highway. The calculated layer thicknesses matched the measured ones well. The measured variations in base moisture content produced no significant change in radar waveform.

Void under Rigid Pavement

IH 20, near Augusta, Georgia

This highway consisted of 23 cm (9 in) of jointed concrete pavement over a granular base. The joint spacing was 6.1 m (20 ft), and the shoulder was asphalt. The pavement had received substantial maintenance in recent years, and several of the joints had been replaced (see figure 9.18). The suspected pavement problems were poor support conditions at joints, trapped moisture, and voids.

GPR Testing Program. Forty slabs were selected for GPR evaluation. The slabs were numbered, and a condition survey was made, noting all surface defects and the location of all patches. A single pass was made with the 1.0-GHz antenna. The testing was conducted in the outer wheel path of the outer lane, close to the asphalt shoulder. A GPR trace was collected approximately every 20 cm (8 in.); in total, 1,154 traces were recorded on the 40 slabs. Typical single traces are shown in figures 9.19 and 9.20, these being from the locations where subsequent ground truth testing was performed. Note in figure 9.19 that a significant peak is observed at approximately 7 nsec, which corresponds to the bottom of the slab. Substantial subslab moisture was found at this location. In figure 9.20, no peak is observed at 7 nsec. This was a no-void location. The variation in subslab reflection was observed as data was being collected. A later pass was made with the GPR to mark locations for ground truth testing; in total, six locations were chosen.

Ground Truth Testing. The purpose of the ground truth testing was to measure the size of the void beneath the slab. This testing was only partially successful. Of the six holes selected, four were in locations similar to figure 9.21 (suspected void locations), and the other two were in suspected no-void locations. A dry hole with a 3.8-cm (1.5-in.)

diameter was drilled to a depth of approximately 38 cm (15 in.) in each of the six locations. It was noted that in the four void locations the hole contained several inches of water after drilling; the other two locations were dry. This water was coming from beneath the slab.

To accommodate the Georgia DOT's need for minimum lane closures, it was necessary to remove the cores a maximum of 1 hour after pouring the epoxy. However, at the time of testing, the pavement temperature was below freezing. The temperature, along with the fact that the voids were filled with water, prevented the epoxy from curing adequately in the allotted time. Cores with a diameter of 100 mm (4 in.) were removed from each location; a typical example is shown in figure 9.21, which shows the bottom of the core. The red area shows the extent to which the epoxy had spread. It is clear that the red epoxy was able to work its way beneath the core, so a void must have been present.

At the four suspected void locations, cores similar to that shown in figure 9.21 were obtained. The existing water was bailed out of the core hole with a Shop-Vac suction pump. Water continued to flow back into the hole from beneath the slab even after 10 minutes of continuous pumping, indicating that substantial water flow occurred beneath the slab. The testing did confirm that the peaks in the GPR traces were caused by moisture trapped beneath the slab. The epoxy core test was not able to determine the thickness of the voids, although it did appear that a void was present in all suspected core holes. It appears that the epoxy test may be best suited to concrete pavements with stabilized base layers. Low temperature, saturated conditions, and permeable granular layers beneath the slab interfere with the test.

GPR Data Processing. The TTI data-processing program was used to analyze the GPR waveforms. A peak-tracking procedure was set up to measure the amplitude of the peak of the reflection from the bottom of the slab. A window was set between 6.4 and 8 nsec, and the peak was measured for all 1,154 waveforms. A typical plot for eight joints in the test location is shown in figure 9.22. The waveforms from joints 13, 15, 16, and 17 have large reflections from the bottom of the slab.

Criterion. The criterion previously recommended in the Task 6.0 report for detecting joint problems called for relating the amplitude of reflection at mid-slab to that measured at the joints. Furthermore, for the joint to be considered as potentially containing a void, the problem area should be at least 36 cm (14 in.) long. From figure 9.22, the mid-slab amplitudes ranged from 0.2 to 0.4 V. The recommended factor was 2 times the mid-slab reflection. Therefore the criterion would be to locate all joints where the reflection was greater than 0.8 V over a 36-cm (14-in.) length.

On this site we had the benefit of GPR traces taken directly before ground truth testing. The amplitudes obtained at the six locations are shown in table 9.10.

Table 9.10
Typical Results for Six Core Holes

Location	Case	Amplitude (V)
1	Moisture-filled void	1.7
2	Moisture-filled void	1.4
3	Moisture-filled void	1.5
4	Moisture-filled void	1.5
5	Dry hole, no void	0.3
6	Dry hole, no void	0.8

On the basis of these results, it was decided to use 1.2 V as the criterion for a moisture-filled void location and to search the data file for locations at which at least three consecutive traces have this condition. Three consecutive traces represent a test length of 61 cm (24 in.). In total, 14 out of the 40 joints met this criterion. Joints 13, 15, 16, and 17 from figure 9.22 met this criterion.

Alternative Graphical Display. In detecting moisture-filled voids, it is possible to use color graphics to highlight the problem locations. Such a color display is shown in figure 9.23. Each vertical line on this graph represents a single GPR waveform; the colors represent the voltage of the waveform, with red being the highest voltage. The red line at the top of the figure represents the surface. The scale on the right side is in inches. The green dots at approximately 10 in. represent moisture-filled voids beneath the pavement. For this particular application, color-graphics output may be desirable.

Conclusion. The 1.0-GHz system was successful in detecting trapped moisture beneath joints in this concrete pavement—23-cm (9-in.) thick. From this analysis, it seems feasible to modify the criterion for detecting moisture-related problems from 2 times the center slab reflection to 3 times. With granular base materials, it is impossible for GPR to distinguish between moisture-filled voids and saturated base conditions. In the saturated condition, there would still be contact between the slab and base, but some of the fine material may have been pumped out, leaving a highly permeable area. Water entering at the joints would saturate this low-density area. On highly permeable bases, it appears that GPR can detect moisture but not the existence of voids. It is proposed that GPR works best with stabilized bases—either cement-treated base or black bases—in which the stabilized layer can erode and leave distinct voids beneath the slab. When these voids become filled with moisture, they are readily detected by GPR.

Figure 9.18. IH 20, near Augusta, Georgia—jointed concrete pavement suspected of having voids and trapped moisture at joints

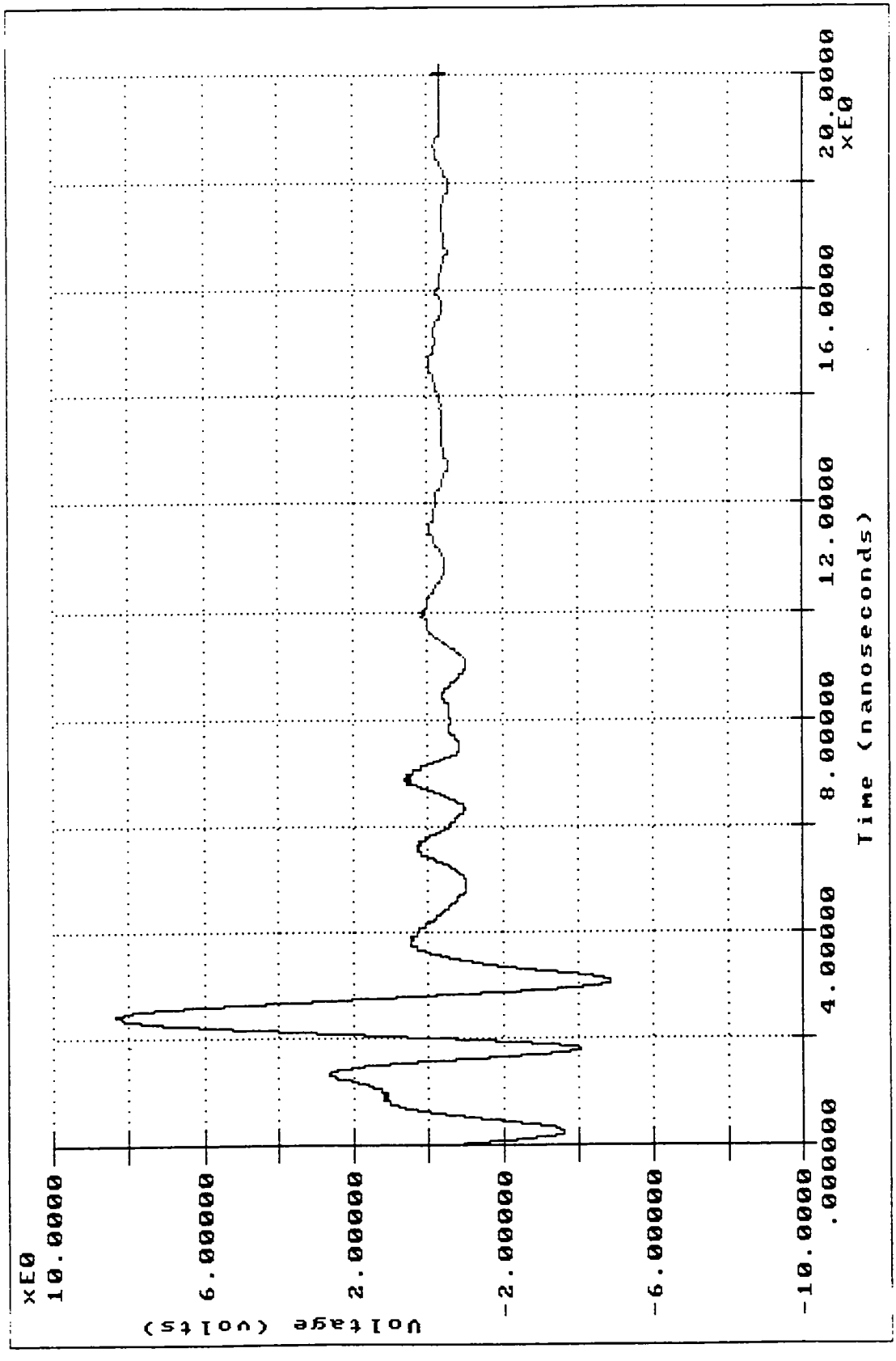

Figure 9.19. GSSI 1.0-GHz reflected waveform from IH 20 Georgia—moisture-filled void location

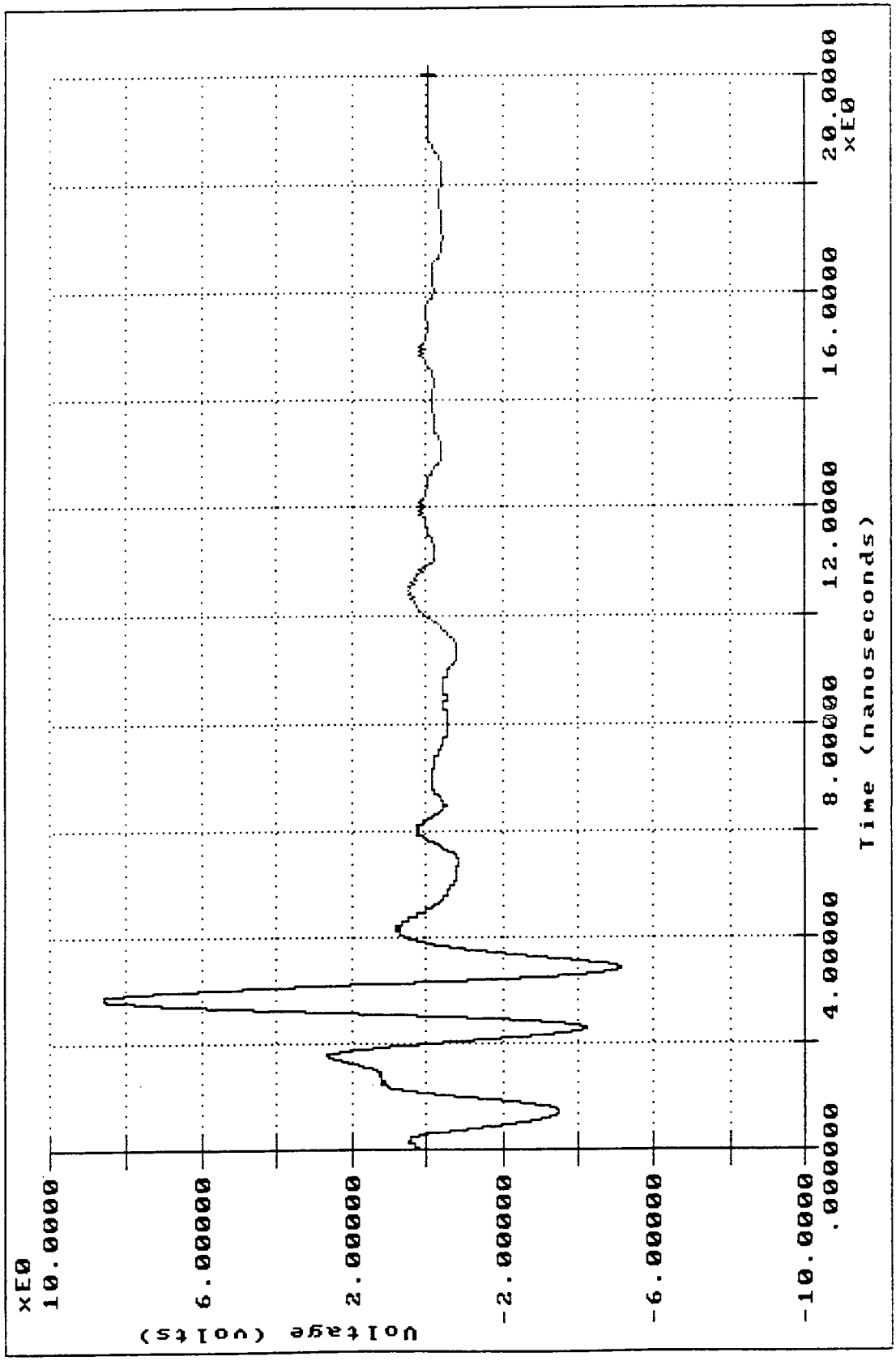

Figure 9.20. GSSI 1.0-GHz reflected waveform from IH 20, Georgia—no-void location

Figure 9.21 Core taken from IH 20, Georgia, after epoxy core test. The epoxy did not set up, but red area indicates that a void was present beneath the slab.

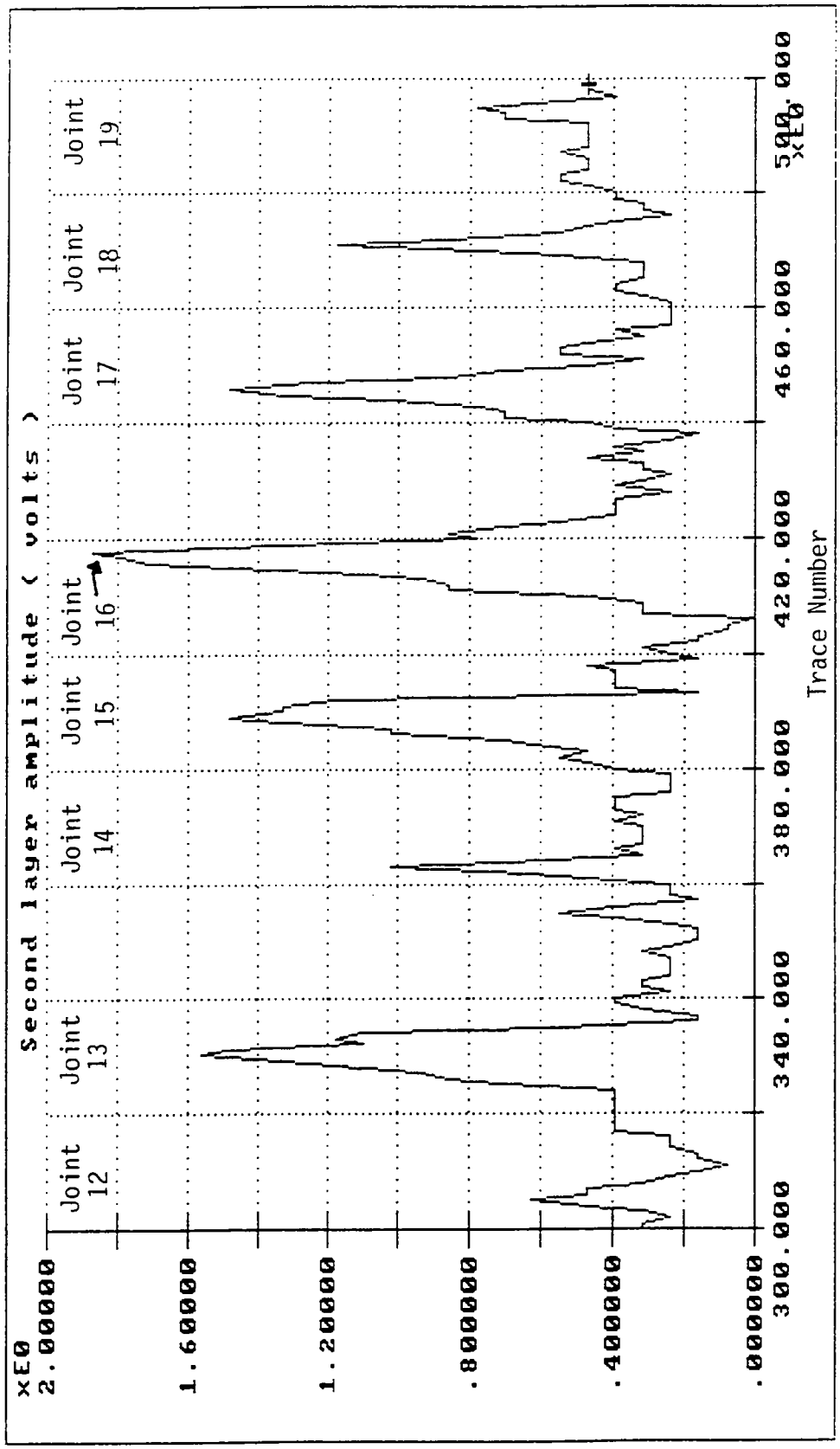

Figure 9.22. Amplitude of reflection from beneath the slab for eight joints on IH 20, Georgia. High values represent moisture-filled voids.

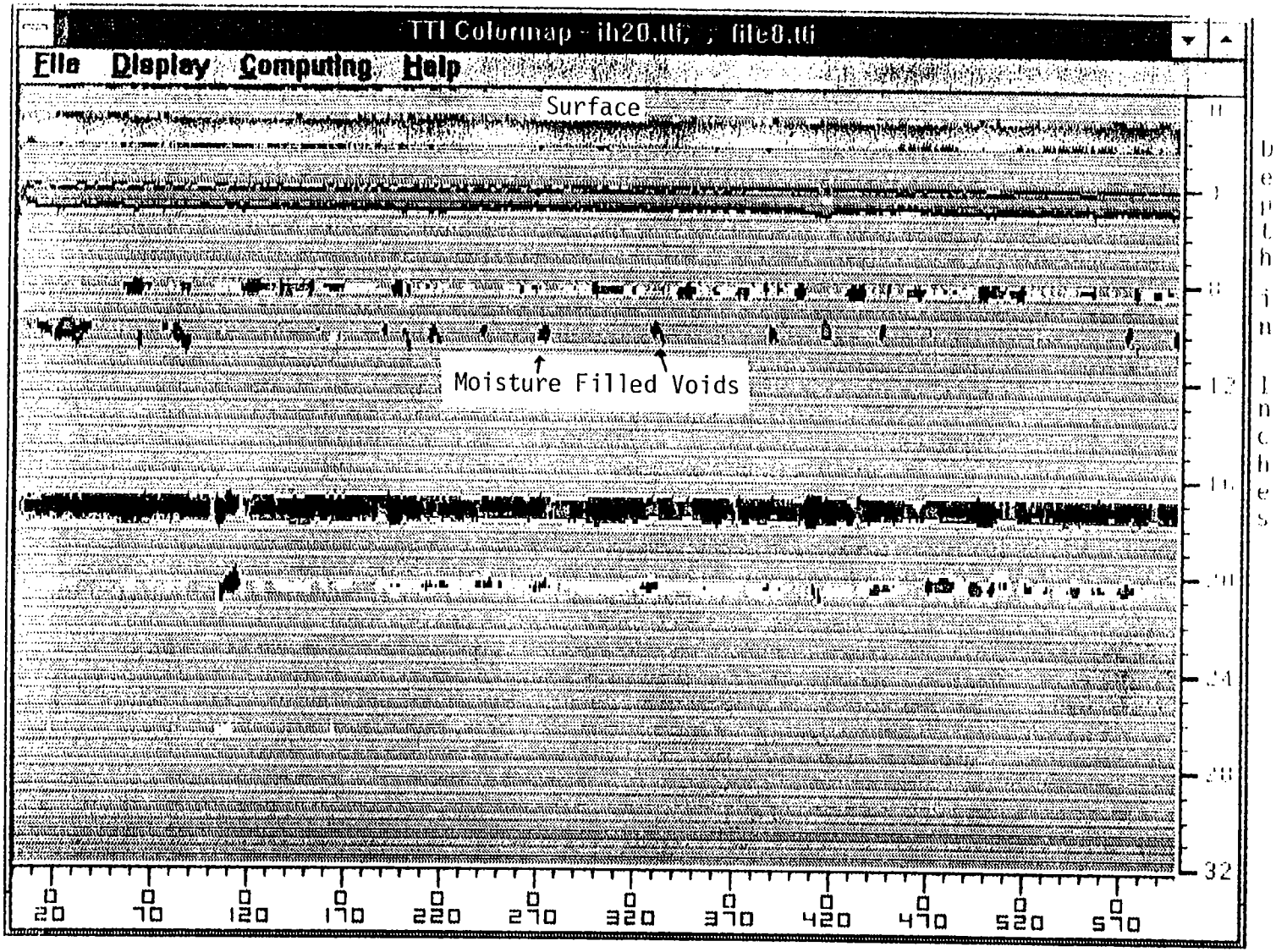

Figure 9.23. Color-coded display of ground-penetrating radar data collected on IH-20, Georgia

10

Conclusions and Recommendations

This project has developed a new high-frequency ground-penetrating radar (GPR) system and installed the Subsurface Interface Radar System-10A in a vehicle with antennas mounted on a trailer for highway testing. In producing a fieldworthy system, Geophysical Survey Systems, Inc. (GSSI), overcame major challenges in both the sampling hardware and the data-acquisition software. A limited number of tests were conducted with the final system. Up to the last month of the project, revisions were being made to the sampler electronics to reduce the noise level and improve the signal-to-noise ratio.

10.1 Conclusions

On the basis of our testing and demonstration of the prototype systems, the research team feels the equipment is close to meeting the needs of the maintenance divisions of state highway departments. If the research is continued as outlined in Recommendations for Future Research, the instrument could meet the goals of the program.

The first requirement is portability. The equipment as it is fills this intent. The trailer-mounted design allows the equipment to be very portable. The power requirements for the radar system can be satisfied by the 12 V direct current of the vehicle.

The cost of the entire system, including interpretation software, should be similar to that of other nondestructive testing equipment, such as the falling-weight deflectometer: approximately $125,000.

The system can be made easy to use, although we are not at that stage now. As the equipment stands now, it is suitable for a researcher or high-level technician. The research team believes that with further development and testing, the equipment can be made easy for almost anyone to use. The present system is almost completely self-calibrating. In the field, the only calibration required is to collect radar reflections from a metal plate, which is a simple procedure. The acquisition portion of the system can be

very easy to use with only minimal training, while the interpretation software needs more development, testing, and refinement.

As safety is an important factor, the system can be shown to be fieldworthy and capable of taking measurements at highway speeds, thus minimizing the need for lane closure. Also, the system's ability to collect data in two wheel paths of a lane at the same time minimizes the time spent in traffic, thus reducing danger to the work crew.

Although the prototype had some structural problems, these difficulties have been overcome to provide a rugged, fieldworthy system. Further refinements in the electronics should yield a very reliable instrument.

In conclusion, the system did attain some of the research goals, and with continued development and testing, all the goals can be met. Then the maintenance division will have a portable, fieldworthy inspection device that will be easy to use and cost-effective.

The laboratory and field tests did produce some promising results. The GPR return signals provide information that can be used to estimate the layer thicknesses, the moisture content of a flexible base course, and the existence of moisture-filled voids. In the field testing, the ability to detect air-filled voids and stripping in the asphalt was not fully evaluated. More testing of all of these conditions is urgently required.

10.2 Recommendations for Future Research

Our primary recommendation is for the continuation of field testing similar to the program conducted in Texas and Georgia. Test sites should be selected that have various levels of stripping, differing amounts of moisture in the base, and a range of void conditions. Only after further tests have been performed will the true potential of GPR for detecting maintenance problems be clearly defined.

Other recommendations can be made about the hardware and the software:

1. Further work is required on the 2.5-GHz system to reduce the clutter level.
2. Only limited work was performed with the neural network (NN) that automatically processes the GPR waveforms. If it can be shown that the NN system can interpret signals adequately by correctly identifying pavement problems, the system will be more useful to state Departments of Transportation (DOTs).

We built and trained NNs to identify pavement thickness, voids under pavement, stripping, and moisture content of pavement. We demonstrated the feasibility of training an NN with model data and having it extrapolate these results to real data. We built a prototype of a run-time NN and showed that it can identify various road impairments in close to real time. We developed techniques to preprocess the real and model data to

make it suitable for an NN. We identified parameters that improve the training of the NN and the accuracy and generalization of its recall.

The current run-time NN is a prototype showing proof of concept. The results of our research show that a fully developed version of the NN, with optimizations and improved interfaces, could be implemented for use on highways.

As we have been experimenting with various architectures and parameters, the data preprocessing and NN training have been done manually or with the aid of a variety of prototype tools. The development of a software system to automate these processes would allow an operator to train NNs in the field, so that they could be optimized for local conditions.

Currently, the NN produces only two outputs for each scan of radar data. Given the size of the radar files, these two outputs can produce large data files. Some of the data produced is not meaningful, because it represents normal road conditions. We believe that a fuzzy-logic-based expert system that (1) translates the results from the NN into commonsense terms and (2) alerts the operator to anomalies based on preprogrammed fuzzy rules would make the current system more efficient and easy to use. This automation also allows for future growth in the information obtained from the radar.

With additional rules, the fuzzy-logic system described above could also help the user set up the radar equipment. Expert knowledge available at GSSI could be used to create fuzzy rules for setting up the various parameters in the system on the basis of road conditions, desired results, and other parameter settings.

10.3 Recommendations for Implementation in State DOTs

If a state wishes to evaluate whether GPR can solve any of its pavement inspection problems, a first step would be to initiate a pilot test program such as those conducted in Texas and Georgia. The state would identify sections with potential problems, and would supply contact people, traffic control, and limited ground truth equipment (coring rig plus moisture content determination equipment). Typically, the sections could be up to 1.6 km (1 mile) long. Complete testing with GPR and ground truth, including traffic control, for a single section takes 1 day.

If the state is satisfied with the results, it must then decide whether to contract the services or purchase the system. A reasonable option would be to obtain GPR collection and interpretation services from a consultant. This option may well be the most cost-effective for many state DOT's. Prospective purchasers should understand that GPR is a sophisticated technology that will require a dedicated technician and data-collection vehicle. GPR should in fact be considered no different from other pavement inventory collection systems, such as skid, ride, and deflection testing. At its current stage of development, GPR is not ready for use by maintenance forces who want to keep it in the back of their truck. Future developments in automatic systems for measuring layer

thickness or moisture content may produce an instrument that can be used by anyone. However, such systems are a few years in the future.

Appendix: Software Development

Commercial Tools

Various neural network software packages for the IBM PC were investigated. NeuralWare, Inc.'s *NeuralWorks Professional II/Plus* was chosen because it was judged to be the most comprehensive of the available packages, with the largest number of preprogrammed network paradigms in an easy-to-use format.

MathCAD was used for developing the model data and for creating graphs.

Prototype

A prototype run-time version of a neural network was developed in *Microsoft C*. The program consisted of three modules: an input module, a module for the network, and an output module.

The input module was a series of pop-up menus. The user chose a file for processing from a list of **.DZT* files (files produced by *Radan*, the data-acquisition program) found in the current directory. In the next menu, the user selected the network of interest—either moisture content or voids under the pavement. Each network processed a second variable, the thickness of the pavement. The user then indicated how many points to plot on the x and y axes. The last screen allowed the user to select a point in the data at which to begin processing.

The main module of the program is the network. This module is subdivided into network, layer, and cell files. C classes represent each of the components of the neural network: network, layer, input cell, hidden cell, and output cell.

The chosen input file was opened. From the header of the file, the program determined the amount of data per scan, the data format, whether to display the data as scans per second or per meter, and the number of channels used. The network discarded all but the first data channel.

The network reads a previously created network definition file. The file is selected based on the user's choice of variable to test (void or moisture). This file defines the

various network parameters. As the file is being read, the layers and cells of the network are created dynamically. The number of layers and number of cells per layer are not predefined, so the user can build a network architecture specialized for a particular problem. In the tradition of object-oriented design, each class of the program stores all the information specific to its type. The network class stores the type of the network, the number of layers and inputs, a pointer to the first layer, and information about the data from the header of the input file. The layer class stores the transfer function for that layer, the number of cells in the layer, and a pointer to the first cell. All cell classes inherit some functionality from a base cell class that stores the layer number and the cell output. Input cells also store the minimum, maximum, divisors, and other data needed to scale the integer data from the input files to data ranging between -1 and +1. Non-input-layer cells store the number of weights going into the cell, the previous sum of weights times the inputs, and a pointer to the cell's weight vector. Output cells store the data necessary to descale the network output back to integers.

One scan at a time is now read from the input file. The data is converted from the *Radan* format to integers. Data before the first zero crossing of the scan is discarded. Every second point up to x points is used as the network input, x being the number of input cells in the network. The data is then scaled and fed to the input layer of the network. Each layer of the network, after the input layer, is run on the output of the previous layer.

The network produces two outputs: the thickness of the pavement and the variable selected by the user. This output is descaled, stored in two separate binary files, and plotted on the screen. The network continues processing the data from the input file, scan by scan, until the end of the file is reached. When the processing is done, the user is returned to the input screen. Another file can be chosen for processing, or the program can be terminated.

The output module plots output data as the network runs. The output screen is composed of two windows. One permanent window is painted when the program begins. This window contains the scales chosen by the user for the y axis, the legend for the plots, and a running total of the meters or seconds of data processed by the network. The second window, nested in the first window, plots the outputs as the data are received.

Auxiliary Tools Developed

We developed a variety of tools to create network files, to preprocess and format data for the network, and to convert data between various formats.

MAKENET reads a trained network file created from the *NeuralWorks* package. From this input file, the program creates the network definition file used by the network prototype. The file contains the specific network architecture: control strategy, number

of layers, number of units in each layer, transfer function, weights for each cell, and minimums and maximums used in scaling.

READOUT, READMOIS, and READVOID are data conversion programs that read the binary output files created by the neural network and create ASCII text files from the data. The programs store the data in a format suitable for the particular variable. Thickness is stored as an integer, moisture is stored as a percentage, and voids are stored as decimal values.

MAKEPRN converts data in *Radan* format to a format readable by *MathCAD*. We used *MathCAD* to create the model data. *Radan* was used to create an approximation of real data from the model data.

MAKEDZT converts *MathCAD* data files to the *Radan* format. We used this program to combine a few model scans into a simulated radar profile.

MINMAX is a program that finds the minimum and maximum in a training file.

B*p** is a set of programs that create the neural network learning or test files. These programs vary depending on the desired output. For example, BPVOID creates files for thickness and void outputs, BPMOIS creates files for thickness and moisture outputs, and BPWV creates files for thickness and water voids. The programs also vary depending on the format of the original files: model *MathCAD* data in floating point or integer format, or *Radan* format.

ZCROSS* is a set of programs developed to find the zero crossings of various file formats.

References

Birchak, J. R., Gardner, C. G., Hipp, J. E., and Victor, J. M., Jan. 1974. High Dielectric Constant Microwave Probes for Sensing Soil Moisture, *Proc. IEEE*, Vol. 62:93-98. (case for two components)

Bomar, L. C., Horne, W. F., Brown, D. R., and Smart, J. L., 1988. Determining Deterioration in Portland Cement Pavements using Radar and Video Imaging. *NCHRP* Report 304.

Carter, C. R., Chung, T., Holt, F. B., and Manning, D. G., 1986. An Automated Signal Processing System for Signature Analysis for Radar Waveforms from Bridge Decks, *Canadien Electrical Engineering Journal*, Vol. 11 No. 3.

Duke, S. K., 1990. Calibration of Ground Penetrating Radar and Calculation of Attenuation and Dielectric Permittivity Versus Depth. *Colorado School of Mines* Thesis T-3920.

Hecht-Nielsen, R., 1987. Counter-Propagation Networks, *IEEE First International Conference on Neural Networks*, Volume II:19-32.

Kohonen, T., et al, 1988. Statistical Pattern Recognition with Neural Networks: Benchmark Studies. *Proceedings of the Second Annual IEEE International Conference on Neural Networks.*

Maser, K. R., 1986. Detection of Progressive Deterioration in Bridge Decks Using Ground Penetrating Radar. *Proceedings of the Engineering Mechanics Division*, ASCE Convention, Boston, MA.

Maser, K. R., 1990. New Technology for Bridge Deck Evaluation, *Final Report New England Transportation Consortium*, MIT.

Maxwell-Garnett, J. C., 1904. Philos. Trans. Royal Society of London 203:385.

Miller, W, Glanz, F., and Kraft, G., 1990. CMAC: An Associative Neural Network Alternative to Backpropagation. *Proceedings of the IEEE.* Vol. 78, No. 10, October 1990:1561-1567.

Ozdogan Yilmaz, 1987. *Seismic Data Processing*, Society of Exploration Geophysicists.

Reynolds, J. A., and Hough, J. M., 1957. Formulas for Dielectric Constant Mixtures. *Proc. Phys. Soc. London*, Vol 70B, No. 452, Pt. 8:769-775.

Rumelhart, D. E., Hinton, G. E., and Williams, R. J., 1986. Learning internal representations by error propagation. In Rumelhart, D. E. and McClelland, J. L. (Eds.), *Parallel Distributed Processing: Explorations in the Microstructures of Cognition, Vol. 1: Foundations*. MIT Press, Cambridge, MA.

Sheriff, R. E., 1973. *Encyclopedia Dictionary of Exploration Geophysics*, Society of Exploration Geophysicists, Tulsa, OK.

Shutko, A. M., and Reutov, E. M., 1982. Mixture Formulas Applied in Estimation of Dielctric, *IEEE Transactions on Geoscience and Remote Sensing*, Vol. GE-20, No. 1:29-32.

Sihvola, 1989. Dielectric Mixing Model, *IEEE Transaction in Geoscience*, Vol 27, No. 4.

Specht, D. F., 1988. Probabilistic Neural Networks for Classification, Mapping or Associative Memory, *Proceedings of the Second Annual IEEE International Conference on Neural Networks*.

Steinway, W. J., Echard, J. D., and Luke, C. M., 1981. Locating Voids Beneath Pavement Using Pulsed Electromagnetic Waves, NCHRP 237.

Wright, D. L., Bradley, J. A., and Hodge, S. M., 1989. Use of a New High-Speed dIgital Data Acquisition System in Airborne Ice-Sounding, *IEEE Transaction on Geoscience and Remote Sensing*, Vol 27, No. 5.

Wright, D. L., Hodge, S. M., Bradley, J. A., and Jacobel, R. W., 1990. A Digital Low-Frequency, Surface Profiling Ice Radar System, *Journal of Glaciology*, Vol 36, No. 122.

Yoh-Han Pao, 1989. *Adaptive Pattern Recognition and Neural Networks*. Addison-Wesley Publishing Co., Inc. Reading, MA.

Highway Operations Advisory Committee

Dean M. Testa, *chairman*
Kansas Department of Transportation

Clayton L. Sullivan, *vice-chairman*
Idaho Transportation Department

Ross B. Dindio
The Commonwealth of Massachusetts Highway Department

Richard L. Hanneman
The Salt Institute

Rita Knorr
American Public Works Association

David A. Kuemmel
Marquette University

Magdalena M. Majesky
Ministry of Transportation of Ontario

Michael J. Markow
Cambridge Systematics, Inc.

Gerald M. (Jiggs) Miner
Consultant

Richard J. Nelson
Nevada Department of Transportation

Rodney A. Pletan
Minnesota Department of Transportation

Michel P. Ray
The World Bank

Michael M. Ryan
Pennsylvania Department of Transportation

Bo H. Simonsson
Swedish Road and Traffic Research Institute

Leland Smithson
Iowa Department of Transportation

Arlen T. Swenson
John Deere

Anwar E.Z. Wissa
Ardaman and Associates, Inc.

John P. Zaniewski
Arizona State University

Liaisons

Ted Ferragut
Federal Highway Administration

Joseph J. Lasek
Federal Highway Administration

Frank N. Lisle
Transportation Research Board

Byron N. Lord
Federal Highway Administration

Mohamed Y. Shahin
U.S. Army Corps of Engineers

Harry Siedentopf
Federal Aviation Administration

Jesse Story
Federal Highway Administration

8/16/93

Expert Task Group

Gerald M. (Jiggs) Miner, *chairman*
Consultant

Gary Demich
Washington State Department of Transportation

Wouter Gulden
Georgia Department of Transportation

Dwight Hixon
Oklahoma Department of Transportation

Rudy Hegmon
Federal Highway Administration

Frank N. Lisle
Transportation Research Board

Michael M. Ryan
Pennsylvania Department of Transportation

8/16/93